MODELING & SIMULATION FOR STABILITY AND FAILURE ANALYSIS OF FUNCTIONALLY GRADED PLATE UNDER MECHANICAL AND/OR THERMAL LOADING

Ph.D. Thesis

KANISHK SHARMA

(ID. No. 2013RME9036**)**

DEPARTMENT OF MECHANICAL ENGINEERING

MALAVIYA NATIONAL INSTITUTE OF TECHNOLOGY

JAIPUR-302017, INDIA

MARCH, 2018

MODELING & SIMULATION FOR STABILITY AND FAILURE ANALYSIS OF FUNCTIONALLY GRADED PLATE UNDER MECHANICAL AND/OR THERMAL LOADING

Submitted by

KANISHK SHARMA

(2013RME9036)

(Department of Mechanical Engineering)

Under the supervision of

DR. DINESH KUMAR

Assistant Professor

Department of Mechanical Engineering

M.N.I.T. Jaipur

Submitted in fulfillment of the requirements for the degree of

DOCTOR OF PHILOSOPHY

to

DEPARTMENT OF MECHANICAL ENGINEERING

MALAVIYA NATIONAL INSTITUTE OF TECHNOLOGY

JAIPUR

MARCH 2018

Dedicated to……

Almighty GOD

MALAVIYA NATIONAL INSTITUTE OF TECHNOLOGY JAIPUR
JAIPUR – 302017 (RAJASTHAN), INDIA

CERTIFICATE

This is to certify that the thesis entitled **"Modeling & Simulation for Stability and Failure Analysis of Functionally Graded Plate under Mechanical and/or Thermal Loading"** being submitted by **Mr. Kanishk Sharma (ID No. 2013RME9036)** to the **Malaviya National Institute of Technology Jaipur** for the award of the degree of **Doctor of Philosophy** in **Mechanical Engineering** is a bonafide record of original research work carried out by him. He has worked under my guidance and supervision and has fulfilled the requirement for the submission of this thesis, which has reached the requisite standard.

The results contained in this thesis have not been submitted in part or full, to any other University or Institute for the award of any other degree or diploma.

Dr. Dinesh Kumar
Assistant Professor
Department of Mechanical Engineering
M.N.I.T. Jaipur, INDIA

Date:

DECLARATION

I, **Kanishk Sharma**, declare that this thesis titled, **"Modeling & Simulation for Stability and Failure Analysis of Functionally Graded Plate under Mechanical and/or Thermal Loading"** and the work presented in it, are my own. I confirm that:

- This work was done wholly or mainly while in candidature for a research degree at this university.
- Where any part of this thesis has previously been submitted for a degree or any other qualification at this university or any other institution, this has been clearly stated.
- Where I consulted the published work of others, this is always clearly attributed.
- Where I have quoted from the work of others, the source is always given. With the expectations of such quotation, this thesis is entirely my own work.
- I have acknowledged all main sources of help.
- Where the thesis is based on work done by myself, jointly with others, I have made clear exactly what was done by others and what I have contributed myself.

Kanishk Sharma
(2013RME9036)

Date:

ACKNOWLEDGEMENTS

I would like to express my deepest gratitude to my supervisor, **Dr. Dinesh Kumar** for his guidance and support throughout this study. His extensive knowledge, serious research attitude, constructive suggestions and encouragement were extremely valuable to me. His influence on me is far beyond this thesis and will benefit me in my whole life.

I would also like to take this opportunity to thank the DREC members, **Dr. Himanshu Chaudhary, Dr. T.C. Gupta** and **Dr. Amit Singh** for their valuable suggestions during the progress of this work.

Also I would like to offer my sincerest gratitude to my Master supervisor **Prof. S. K. Rathore** for his continued blessings and supporting me to make the decision of being a PhD student. My special thanks are extended to my friends for their friendship, continuous support, understanding as well as encouragement.

I want to extend my sincere gratitude to my parents, brother, wife Kiran and son Vaibhav for their support in all the circumstances, help and love without which the thesis could not have reached the present form. Above all, I would like to thank almighty for all the blessings and for giving me the opportunity to follow my dreams.

Kanishk Sharma

Date:

ABSTRACT

Functionally graded materials (FGMs) are microscopically inhomogeneous advanced composite materials, which can efficiently avoid debonding, delamination, plastic deformation and cracking issues, generally present in the conventional composites, by continuous variations of material properties along any predefined direction(s). FGMs are usually made of ceramics and metals, and possess good thermal, wear and oxidation characteristics of ceramics, and at the same time contain good toughness, mechanical strength and machinability properties of metals. Owing to the favorable mechanical and thermal properties, the FGM structures in the various forms, such as beams, plates, shell etc., are used in a wide range of high-temperature applications, viz. rocket heat-shields, aircraft engines, thermal barrier coatings, heat exchanger tubes, etc. in various engineering fields requiring high thermal resistance combined with good mechanical response.

It is well known that many engineering structures used in various fields are in the form of thin plates that are susceptible to buckling, postbuckling and failure response under various in-plane loading conditions. Due to the inhomogenous nature of FGMs, studying the behavior of FGM plate under various mechanical and/or thermal loading conditions is quite complex. Therefore, it is imperative to understand response of FGM plates under various thermal and/or mechanical stimuli through theoretical modeling, numerical simulations, and/or experimental investigations that would, in turn, ensure the effective and efficient design of an overall structure involving FGM.

In this regard, the present work aims to explore the elastic and elastic-plastic buckling, postbuckling and failure analysis of perforated and imperforated FGM plate under thermal and/or mechanical loading conditions, considering the temperature-dependent and independent material properties of FGM. The actual non-homogeneous (only along thickness) FGM plate with continuously varying properties along thickness is modeled as a laminate composed of multiple perfectly-bonded layers made of isotropic and homogeneous material having layer-wise constant composition. At the mid of a particular layer, thermoelastic properties (i.e., elastic constants and thermal expansion coefficients) of FGM are calculated using theoretical and numerical micromechanics based models- Voigt's model, and Mori-Tanaka homogenization scheme. In accordance with the Tamura-Tomota-Ozawa model (TTO model), the ceramic phase of FGM is

considered to be elastic, whereas the metal phase is assumed to be elastic-plastic. Further, the elastic-plastic analysis of FGM is assumed to follow J_2-plasticity with isotropic hardening. The non-linear FEM formulation for plate analysis is based on the first-order shear deformation theory and the von-Karman's nonlinear kinematics. The incremental solution technique based on Newton-Raphson method is adopted for the solution of non-linear algebraic equations. Various verification studies have been carried out to verify the present numerical model by comparing the predicted results with the available results in the literatures. Thereafter, numerical studies are conducted on the buckling, postbuckling and failure responses of elastic and elastic-plastic FGM plates with and without perforation, considering the temperature-dependent as well as temperature-independent material properties, under thermal and/or mechanical loading condition to assess the effects of different material, geometrical and loading parameters on the structural integrity of FGM plates.

It is found that the FGM plate with elastic material properties exhibits only stable equilibrium path, whereas the elastic-plastic FGM plate shows destabilizing response at the ultimate failure point. The ultimate load capacity of FGM plate under thermomechanical loading conditions is found to be decreased with an increase in cutout size. It has been envisioned that the present study would provide an enhanced insight into the analysis and the design of FGM structures for real life applications.

CONTENTS

LIST OF FIGURES

LIST OF SYMBOLS

Most of the symbols are defined as they occur in the thesis. Some of the most common symbols, which are repeatedly used, are listed below:

x, *y*, *z*	=	Cartesian co-ordinate axes
u, *v* and *w*	=	Displacements corresponding to x , y and z direction, respectively
θ_x, θ_y	=	The rotations with respect to y and x direction
a, *b* and *h*	=	Length, width and thickness of the plate
E	=	Young's modulus of the FGM
E_c	=	Young's modulus of the ceramic
E_m	=	Young's modulus of the metal
α	=	Thermal expansion coefficient of the FGM
α_m	=	Thermal expansion coefficient of the metal
α_c	=	Thermal expansion coefficient of the ceramic
ν	=	Poisson's ratio of the metal, ceramic and FGM
V_m	=	Volume fraction of the metal
V_c	=	Volume fraction of the ceramic
n	=	Power law exponent
q	=	Stress transfer parameter
k_1 and k_2	=	Stress correction factors
$[D]$	=	Material property matrix
σ_{ym}	=	Yield strength of the metal material
σ_y	=	Yield strength of FGM
H_m	=	Tangent modulus of metal
H	=	Tangent modulus of FGM
$\{\epsilon\}^l$	=	Linear strain tensor
$\{\epsilon\}^{nl}$	=	Nonlinear strain tensor
$\{\epsilon_p^0\}$		Linear in-plane strain tensor
$\{\epsilon_b^0\}$	=	Bending strain tensor
$\{\epsilon_s^0\}$	=	Shear strain tensor
$\{\epsilon_p^{NL}\}$	=	Nonlinear in-plane strain tensor

$\{Q_{ij}\}$	=	Stiffness matrix tensor
$\{\sigma\}$	=	Stress tensor
κ	=	Strain hardening parameter
f	=	Yield surface
J_2	=	Second invariant of stress deviator tensor
$\{\varepsilon_p\}$	=	Plastic strain tensor
$\Delta\varepsilon_e, \Delta\varepsilon_T, \Delta\varepsilon_{TD}, and\ \Delta\varepsilon_p$	=	Incremental elastic strain, thermal strain , strain due to temperature-dependent material properties, and plastic strain
$\Delta\sigma$	=	Incremental stress
$d\lambda$	=	Plastic proportionality factor
ΔT	=	Temperature rise
$[D_{ep}]$	=	Elasto-plastic constitutive matrix
Δu^e	=	Incremental displacement vector
N	=	Interpolation functions
Δa	=	Incremental nodal displacement
B	=	Strain-displacement matrix
δW^e	=	Total virtual work in an element
δU^e	=	Virtual strain energy in an element
δV^e	=	Virtual external work in an element
$[K]$	=	Structural stiffness matrix
ΔR	=	Incremental external load
ΔR_T	=	Incremental thermal load
ΔR_M	=	Incremental mechanical load
ψ	=	Residual force
$[K_T]$	=	Tangent stiffness matrix
$N_{x\,(or\,y)}$	=	In-plane compressive force

Superscript

e	=	Element form
T	=	Transpose matrix

Subscript

c	=	Ceramic
m	=	Metal

max	=	Maximum

Abbreviation

FGMs	=	Functionally graded materials
TTO model	=	Tamura-Tomota-Ozawa model
TD	=	Temperature-dependent
TID	=	Temperature-independent
CPT	=	Classical plate theory
FSDT	=	First-order shear deformation theory
TSDT	=	Third-order shear deformation theory
HHM	=	Hencky–Huber–Mises

LIST OF TABLES

CHAPTER 1

INTRODUCTION

1.1 Overview

The advancement in materials has been associated with the man's evolution since ancient time. Yesterday it was the age of stone, bronze, and iron. Today it is the age of advanced materials such as advanced composites, smart materials and functionally graded materials (FGMs). The most lightweight composite materials with greater specific-strength and -weight have been used successfully in the aircraft industry and other engineering applications. However, due to strong mismatch of material properties at the interface, the structures made from traditional composites have several disadvantages like debonding, delamination, plastic deformation and cracking problems, especially at high temperatures and pressures. As a means of preparing thermal barrier materials and to eliminate such types of interface problems observed in the laminated composites, a concept of functionally graded materials (FGMs) was proposed in 1984 by Japanese material scientists in Sendai area. Functionally graded materials (FGMs), new generation composites, are inhomogeneous material with a smooth and gradual variation in its properties along some specified direction(s), obtained by varying the volume fractions of its constituents (Shiota and Miyamoto, 1997; Suresh and Mortensen, 1998).

Normally, there are two constituents of FGMs – ceramics and metals. Ceramic provides better thermal, wear and oxidation characteristics, whereas metal imparts high toughness, mechanical strength, and machinability properties to an FGM. Owing to the favorable mechanical and thermal properties, FGM offers a wide range of applications in various engineering fields requiring high temperature resistance combined with good mechnical strength. The promising advantages of using FGMs are decreasing the thermal stresses (Choules and Kokini, 1996), providing good bonding strength in between joints of dissimilar materials (Howard et al., 1994), and reducing the possibility of catastrophic failure of brittle ceramic materials (Bao and Wang, 1995). Further, FGMs are

also used in many other applications, for instance, in the rocket heat shields, heat engine components, heat exchanger tubes, plasma facings, fusion reactors, nuclear reactor plant, thermo-electric generators, and electrical insulating applications.

According to the gradient description the FGMs may be divided into two basic types namely continuous FGM and stepwise FGM. As shown in Fig. 1.1 (a), the continuous FGM exhibits a smooth change in material composition across the graded direction; whereas, the stepwise FGM consists of layered quasi-homogeneous material having layer-wise variation of compositions in the graded direction as shown in Fig. 1.1 (b). The continuous FGMs may eliminate the interfacial defects effectively; but, they are very difficult to produce. The stepwise FGMs, on the other hand, are easier to fabricate, at the same time, the interfacial defects in stepwise FGMs can also be controlled by design optimization (Shabana *et al.*, 2006).

Further, thin-walled members, such as plates and shells, used extensively in variety of engineering fields such as civil, aerospace, mechanical, naval, space engineering, and more recently, in micro-engineering, are more susceptible to buckling, large amplitude deflections, or excessive stresses under different in-plane mechanical and/or thermal loading conditions. Due to the fact that the membrane stiffness of plate like structures is significantly higher than their bending stiffness that causes these type of structures to absorb a large amount of membrane strain energy with less deformations. However, the deformations are much higher when these structures absorb the same amount of bending energy. If the plate is loaded in such a way that most of its strain energy is contributed by the membrane energy, and under some conditions, such as initial imperfection, eccentric loading, etc., if the stored membrane energy is converted into the equivalent bending energy at some critical load point (called buckling load), then the plate deforms dramatically in transverse direction producing excessive out-of-plane deflection in a destabilizing phenomenon known as buckling. It is well known that for the plate like structures, the buckling does not mean the ultimate failure, and these structures can carry extra load beyond the buckling point which is known as postbuckling strength (Singh and Kumar, 1999).

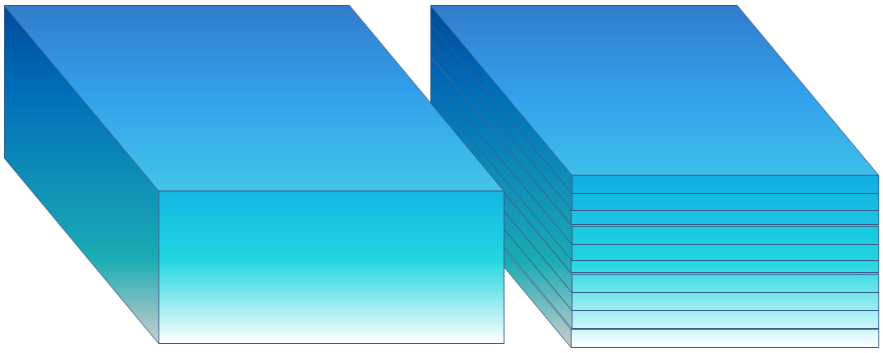

(i) Continuous FGM (ii) Stepwise FGM

Fig. 1.1: FGM models

In some applications, these structural elements are required primarily to resist buckling, and in others, they must carry a load well into the postbuckling range to yield weight savings. Thus, understanding their buckling and postbuckling behavior is needed for their efficient design.

Further, cutouts of various shapes and sizes are often inevitable in these plate-like structures to serve various practical needs, e.g., cutouts in wing spars and cover panels of commercial transport wings and military fighter wings are needed to provide access for hydraulic lines and damage inspection (Lal *et al.*, 2012). Besides, the presence of these cutouts introduces higher non-uniform stresses at the load-free boundary which may lead to premature failure of structures. FGM plates are usually subjected, in addition to mechanical load, to elevated temperatures, and at such a high temperature, the size and shape of cutouts would affect the buckling and postbuckling behavior of FGM plate prominently. Therefore, to make use of a new material, like FGM, in an efficient and economical manner, it is very essential to analyze and gain a thorough knowledge of responses, such as buckling and postbuckling behavior and failure, of various basic structural elements, such as thin plates with a hole, made of FGM under in-plane thermal and/or mechanical loads.

Moreover, it is also noteworthy to mention that the structure failure may be caused by material failure and/or instability. Before the material failure, the structure may show inelastic response producing plastic deformation which in turn causes a destabilizing effect on structures under in-plane compression and/or shear loads produced by mechanical and/or thermal conditions. Because of the safety reasons, structures, even those operating within elastic limit, are designed

to take overloads that can inevitably produce inelastic deformations (Bazant et al., 1991). Therefore, in the practical scenario wherein the stresses induced in the structures by in-plane mechanical and/or thermal loads overpass the elastic limit of the material, a proper elastic-plastic analysis is required for the reliable, accurate, and stable design of these structures under various loading conditions. Being an important design criterion, the elastic-plastic buckling and postbuckling behavior of isotropic and composite plates has been analyzed by many researchers (El-Sawy et al., 2004; Estefen et al., 2016; Ghavami and Khedmati, 2006; Narayanan and Chow, 1984; Paik, 2005; Shanmugam et al., 1999). However, comparatively very few investigations have been made for inelastic buckling and postbuckling analysis of FGM structures. Further, there are no works on elastic-plastic stability behavior of FGM plate under thermomechanical loading conditions, which is considered to be reasonable in the FGM under critical loading conditions because the ductility and good shear strength induced by the metal phase relax the stress concentrations induced around the inherited cracks and flaws of ceramics through the plastic deformation. Moreover, as the FGMs are intended to be used under critical temperature conditions, the possibility of plastic flow induced due to excessive heat flow is also inevitable.

1.2 Objectives and Scope of Present Research

The present work aims to explore the elastic and elastic-plastic buckling, postbuckling and failure analysis of imperforated and perforated FGM plate under thermal and/or mechanical loading conditions, with and without temperature-dependent material properties. Keeping in mind the aforementioned discussion, the main objectives of the present work are as follows:

- To develop a methodology for simulation of functionally graded materials to calculate their effective non-linear temperature-dependent thermoelastic material properties, and elastic-plastic stiffness and strength parameters.
- To incorporate material non-linearity, following J_2-plasticity with isotropic hardening, into the model of FGM plate, wherein the ceramic phase is considered to be elastic, and the metal is assumed to be elastic-plastic material in accordance with the Tamura-Tomota-Ozawa model

(TTO model), and to investigate the effects of plasticity on postbuckling and failure responses of FGM plates.

- To develop a computational technique for predicting the ultimate load capacity of FGM plate by extending an existing FEM based strategy used previously to predict the ultimate load capacity of isotropic homogeneous plates.
- To study the effects of geometric irregularities (i.e., cutout of various shapes and sizes) in the plate on the instability, postbuckling strength, and failure of FGM plate.
- Finally, to conduct parametric studies on buckling, postbuckling and failure responses of elastic and elastic-plastic FGM plates with temperature-dependent and -independent material properties under thermal and/or mechanical loading conditions to assess the effects of different material, geometrical and loading parameters on the overall structural integrity of FGM plates.

1.3 Thesis Outline

A general introduction to FGMs, motivation, and overview and consequently the main objectives of current research work are discussed in the present chapter. The remaining chapters of thesis are structured as follows

- Chapter 2 briefs the technical literature under the scope of the present research work and a systematic review of the previous research work on the analysis and design of FGM structures is furnished. The relevant review on the past research work carried out for thermal and/or mechanical buckling analysis of FGM plates is presented in the first section of this chapter. Consequently, the second section is devoted to discuss the past attempts on postbuckling analysis of FGM plate under thermal and/or mechanical loading conditions. The related literature and methodologies applied to simulate the elastic-plastic behavior of FGMs are discussed in the later section of the chapter. Based on the literature review the chapter finally concludes with outlining the major research gaps.

- The mathematical model based on the first-order shear deformation theory and the von Karman's nonlinear kinematics for thermomechanical buckling, postbuckling and failure analysis of elastic-plastic FGM plate is presented in chapter 3. The layerwise model of FGM plate in which the effective temperature-dependent thermoelastic and elastic-plastic material properties of FGM plate are calculated using Mori–Tanaka homogenization method and TTO model is discussed. Subsequently, the detailing regarding the solution methodology along with procedure of computer implementation is also furnished at the end of the chapter.
- Chapter 4 presents the elastic buckling and postbuckling analysis of imperforated and perforated FGM plate under mechanical loading conditions. The elastic failure analysis is also approached using 3-D failure criterion. After validating the results of the present formulation with the available results in the literature, the effects of material gradation, geometrical parameters, boundary conditions and loading conditions on non-linear buckling and postbuckling behavior, and failure of imperforated as well as perforated FGM plate are also discussed.
- In chapter 5, the thermal buckling and postbuckling analysis of imperforated and perforated FGM plate with temperature-dependent material properties is presented. The methodology of predicting the thermal buckling and postbuckling response is validated by comparing the results from the present formulation with that available in the literature. Various parametric studies are presented to examine the effects of temperature-dependent material properties, material gradation profile, size and shape of cutouts, boundary conditions and aspect and slenderness ratios on nonlinear thermal buckling and postbuckling response of FGM plate.
- The thermomechanical buckling and postbuckling analysis of imperforated and perforated FGM plate is performed in Chapter 6. The nonlinear temperature-dependent material properties are calculated across the thickness of FGM plate using Mori-Tanaka homogenization scheme, and numerical studies are conducted to assess the effects of different

material and geometric parameters on thermomechanical buckling and postbuckling responses of FGM plate.

- Chapter 7 aims to investigate the buckling, postbuckling and failure response of both imperforated and perforated elastic-plastic FGM plate under in-plane mechanical compressive loading. In accordance with the Tamura-Tomota-Ozawa model (TTO model), the ceramic phase of FGM is considered to be elastic whereas the metal phase is assumed to be elastic-plastic. Further, the elastic-plastic analysis of FGM is assumed to follow J_2-plasticity with isotropic hardening. After validating the present formulation with the results available in the literature, various numerical studies are conducted to examine the effects of material inhomogeneity, thermal loading, cutout shape and size on the elastic-plastic buckling, postbuckling and failure behavior of FGM plate.
- The thermal stability analysis of elastic-plastic FGM plate with temperature-dependent material properties is performed in Chapter 8. The nonlinear elastic-plastic analysis of FGM plate is carried out based on the J_2-plasticity with isotropic hardening, and the elastic-plastic strength parameters (i.e., yield strength and plastic tangent modulus) of FGM are calculated on the basis of TTO model. The effect of different material and geometric parameters on thermal buckling and postbuckling of imperforated and perforated FGM plate is investigated by conducting different numerical studies.
- In chapter 9, the elastic-plastic buckling postbuckling and failure analysis of imperforated and perforated FGM plate is carried out. The temperature-dependent thermoelastic material properties at a particular thickness of FGM plate are calculated with the aid of Mori-Tanaka method whereas the yield strength and tangent modulus across the thickness coordinate of FGM plate are calculated using TTO model. The chapter examines the effect of material inhomogeneity, thermal loading, cutout shape and size on the elastic-plastic buckling, postbuckling and failure behavior of FGM plate.
- Important conclusions derived from present research work and some areas for future research are summarized in Chapter 10.

CHAPTER 2

LITERATURE REVIEW

After having a general introduction to FGM, FGM structures and their applications in various fields in the last chapter, the present chapter is targeted to give comprehensive background of the research works done by the scientists and engineers in last few decades in the areas of structural analysis of FGM plates. As FGM plate like structures are designed to perform under critical mechanical and/or thermal loading conditions that may lead to excessive deflections due to buckling phenomenon caused by in-plane compression of the plate. Moreover, it is a well-known fact that under in-plane compression conditions, plate-like structures are designed efficiently and effectively by utilizing their postbuckling reserve strength possessed beyond buckling (Arbocz and Maggiori, 1987; Singh and Kumar, 1999). Therefore, being one of the major design criteria, there are numerous studies to-date on the buckling and postbuckling analysis of elastic FGM plates under mechanical and/or thermal loading conditions. In this regard, a number of reviews dealing with various aspects of the structural analysis of elastic FGM plates have been published over the years (Jha *et al.*, 2013; Swaminathan *et al.*, 2015; Thai and Kim, 2015).

The traditional elastic design consideration of FGM structures cannot estimate their true load capacity and therefore, requires an elastic-plastic analysis to predict the more realistic behavior, with a reasonable factor of safety against their ultimate failure point, of these FGM structures. However, due to the additionally required material parameters such as flow stress and the plastic strain-hardening modulus, which vary spatially, the modeling of elastic-plastic FGM is more complex than elastic FGM. Relatively few studies were devoted to the material characterization of elastic-plastic FGM and to the elastic-plastic analysis of FGM structures.

In order to give a complete perspective of present research, the extensive literature review on the buckling and postbuckling analysis of FGM plate and on the elastic-plastic analysis of FGMs is presented here.

2.1 Linear Buckling Analysis of FGM Plate

It is well known that occurrence of buckling leads to the reduction in the in-plane stiffness of the plate-like structures, which in turn increases the internal forces in structure by redistribution of internal forces in unbuckled members and causes buckling of the structure. In this regard, a number of investigations have been carried out to understand the buckling response of FGM plate under in-plane mechanical compression. For instance, the buckling analysis of simply-supported FGM plate under uniaxial compressive load was performed by Birman (1995). It was shown that the buckling load could be raised significantly using functionally graded hybrid composite plates. The mechanical buckling analysis of FGM plate was also carried out by Feldman and Abdoui (1997) by combining the micromechanics and continuum based approaches. Buckling analysis of FGM plate under in-plane compressive loading using classical plate theory (CPT) was carried out by Javaheri and Eslami (2002). Maa and Wang (2004) obtained a relationship in between buckling load solutions of third-order plate theory and CPT for a circular FGM plate under mechanical loading condition. The mesh-free method was applied by Chen and Liew (2004) to perform the buckling analysis of FGM plate under different type of non-uniform loading including pin loads, partial uniform loads and parabolic loads. Under the assumption of CPT, Shariat *et al.* (2005) obtained the closed-form solutions for critical buckling load of an imperfect FGM plate. Many researchers compared the buckling load solutions of FGM plate obtained through different plate theories. For instance, buckling analysis of sandwich FGM plate under the framework of sinusoidal shear deformation plate theory (SSDT) was performed by Zenkour (2005), and the corresponding results were compared with that obtained using CPT, first-order shear deformation theory (FSDT) and third-order shear deformation theory (TSDT). Naderi and Saidi (2010) examined the effect of bending-extensional coupling on bifurcational buckling of FGM plate and found that FGM plate may exhibit bifurcational buckling when the external in-plane load is applied on the physical neutral surface of the plate. The analytical formulation based on minimum potential energy principle and the Levy-type solution for buckling analysis of thin FGM plate under the assumption of CPT was presented by Mohammadi and Saidi (2010). Bodaghi and Saidi (2010) used the Levy-type

solution in conjunction of higher-order shear deformation theory (HSDT) to obtain the analytical solution for buckling load of thick functionally graded rectangular plates. Meiche *et al.* (2011) applied the HSDT for buckling analysis of FGM plate and compared the results of HSDT with CPT, FSDT, parabolic shear deformation theory, and 3-D elasticity theory. Thai and Choi (2012) calculated the buckling load of FGM plate under in-plane compression with the aid of refined plate theory, and compared the solutions with that obtained by CPT, FSDT, and TSDT.

The structures made by FGM are intended to be used under critical thermal conditions producing in-plane compression load to cause instability in the structure that may result in the excessive out-of-plane deflections and eventually leads to the failure of the structure. Hence being an important criterion to ensure the structural integrity of FGMs many research attempts have been made in the past to investigate the thermal buckling behavior of FGM plates. Lanhe (2004) analyzed the thermal buckling response of shear deformable FGM plate under uniform and non-uniform thermal loading conditions. The thermal buckling response of circular FGM plate based on TSDT was analyzed by Najafizadeh and Heydari (2004) using variational approach. Na and Kim (2004) adopted 18-noded solid element to perform three-dimensional thermal buckling analysis of FGM plate, incorporating the temperature-dependent material properties, under uniform and non-uniform thermal load distributions. The thermal buckling analysis of a simply-supported functionally graded skew plate was carried out by Ganapathi and Prakash (2006) using finite element formulation based on FSDT. Shariat and Eslami (2006) obtained a closed-form solution for thermal buckling load of imperfect FGM plate using CPT. The buckling analysis of simply-supported and clamped FGM plate under in-plane partial heating and uniform temperature rise was performed by Morimoto *et al.* (2006). A two-dimensional shear deformation theory was adopted by Matsunaga (2009) for thermal buckling analysis of FGM plate. Jalali *et al.* (2010) examined the thermal buckling behavior of circular FGM plates using a pseudo-spectral method that makes use of Chebyshev polynomials. While performing the thermal buckling analysis, Bouazza *et al.* (2010) found that the transverse shear deformation has a considerable effect on the thermal buckling load of FGM plate, especially for a thick plate or a plate with large aspect ratio. Zenkour and Sobhy (2010) obtained the thermal buckling

solutions based on sinusoidal shear deformation plate theory and compared the results with that calculated with CPT, FSDT, and TSDT. Thermal buckling response of simply-supported pre-stressed ceramic-FGM-metal hybrid composite plates was studied by Chen *et al.* (2011) using the average stress method, and they found that the critical buckling load of plate decreases due to initial compressive stress and increases with initial tensile stress. Tran *et al.* (2013) utilized an isogeometric FEM based on TSDT for thermal buckling analysis of FGM plates. The stability analysis of FGM isotropic and sandwich plates subjected to thermal loading was performed by Fazzolari and Carrera (2014) with the aid of a refined quasi-3-D equivalent single layer (ESL) and zig-zag (ZZ) plate models based on Carrera unified formulation and implemented within the hierarchical trigonometric Ritz formulation. The mechanical and thermal buckling behaviors of ceramic–metal functionally grade plates were studied by Zhang *et al.* (2014) using meshless method in which the shape functions were interpolated by the Kriging interpolation process. Atmane *et al.* (2016) provided the buckling solution of FGM plate graded with the sigmoid rule of mixtures, and subjected to uniform, linear, or sinusoidal temperature distribution across the plate thickness. Very recently, thermal buckling behavior of FGM, with a negative Poisson's ratio, plate resting on elastic Winkler-Pasternak elastic media is investigated by Mansouri and Shariyat (2017) using differential quadrature method.

2.2 Postbuckling Analysis of FGM Plate

It is well known that even after buckling, a thin plate is still capable of carrying a much increased load without failure caused by instability. Therefore, it is of practical importance to consider the load carrying capacity of FGM plate beyond buckling in the postbuckling regime to efficiently design of a FGM structures. There are numerous studies to-date on the postbuckling analysis of FGM plates under mechanical and/or thermal loading conditions. Researchers used different plate theories while studying the postbuckling response of FGM plates. Ma and Wang (2003) investigated the thermal postbuckling behavior of circular FGM plate based on classical plate theory and von Karman's nonlinearity. Using the same CPT theory, Yang and Shen (2003a, 2003b) (J Yang

and Shen, 2003) developed a semi-numerical approach using perturbation technique in conjunction with 1-D differential quadrature approximation and Galerkin procedure to study the large deflection and postbuckling responses of FGM rectangular plates under transverse and in-plane mechanical loads. Li *et al.* (2007) also studied the postbuckling response of circular FGM plate under mechanical and thermal loadings using CPT with von Karman assumptions.

Contrary to CPT, the FSDT considers the transverse shear effects and hence, provides accurate results as compared to CPT, especially for the plates made of composites and FGMs; therefore, it has been used by many researchers to perform the nonlinear stability analysis of FGM plates. Liew *et al.* (2004) examined the postbuckling response of FGM plate with temperature-dependent material properties under uniform thermal loading using FSDT. An analytical solution based on FSDT was presented by Woo *et al.* (2005) to study the postbuckling behavior of moderately thick FGM plates and shallow shells under edge compressive loads and a temperature field. Park and Kim (2006) presented thermal postbuckling and vibration studies of FGM plate with temperature-dependent material properties. They used FSDT along with von Karman nonlinearity to account for the large deflection of the FGM plate. Wu *et al.* (2007) also adopted FSDT to predict the postbuckling response of the alumina/aluminium FGM plate, subjected to thermal and mechanical loadings, using the fast converging finite double Chebyshev polynomials. Thermal postbuckling analysis of FGM skew plates using nonlinear finite element method based on the FSDT was presented by Prakash *et al.* (2008). Following the same theory, Lee *et al.* (2010) investigated the postbuckling behavior of FGM ceramic-metal plates under edge compression and temperature field using element free kp-Ritz method, and Duc and Tung (2010) considered the temperature-dependent material properties to conduct stability analysis of simply-supported rectangular FGM plates under in-plane thermomechanical loading. Kiani and Eslami (2012) studied the thermal postbuckling behavior of sandwich FGM plates resting on Pasternak-type elastic foundation under uniform temperature rise using FSDT.

In addition to CPT and FSDT, many researchers, Liew *et al.* (2003), Shen (2005), Yang *et al.* (2006), Shen (2007), Shen and Li (2008), Duc and Tung (2011), Kiani and Eslami (2012), and Zhang and Zhou (2015), have also employed higher-order theories to study postbuckling behavior of FGM plates.

Liew *et al.* (2003) examined the postbuckling behavior of functionally graded rectangular plates integrated with surface-bonded piezoelectric actuators using Reddy's HSDT, initially proposed for the analysis of composite plates (Reddy, 1984). Using the same theory but with thermo-piezoelectric effects, Shen (2005) performed the postbuckling analysis for a simply-supported FGM plate bonded with piezoelectric actuators under the combined action of mechanical, electrical and thermal loads. Considering the generic imperfection function that takes a form of the product of trigonometric and hyperbolic functions, Yang *et al.* (2006) examined the effect of initial geometrical imperfections on the postbuckling behavior of FGM plate. Shen (2007) performed the thermal postbuckling analysis of a simply-supported FGM plate with temperature-dependent properties. Employing the two-step perturbation technique, Shen and Li (2008) predicted the buckling load and postbuckling response of a simply-supported sandwich plate with FGM face sheets. Duc and Tung (2011) presented analytical formulations based on HSDT to study the buckling and postbuckling responses of thick FGM plates resting on elastic foundations and subjected to in-plane compressive, thermal and thermomechanical loads. Mechanical and thermal postbuckling analysis of FGM rectangular plates resting on nonlinear elastic foundations using the concept of physical neutral surface and HSDT was performed by Zhang and Zhou (2015).

Using 3-D finite element method, Na and Kim (2006) conducted thermal postbuckling analysis of FGM plates under uniform and non-uniform temperature rise along the thickness, considering the temperature-dependent material properties.

Furthermore, the cutouts of various shapes and sizes are often inevitable in plate-like structures to serve various practical needs (e.g., hardware to pass through, inspection hole, for windows and doors) or simply to reduce the weight of the structure. The presence of such cutouts introduces higher non-uniform stresses at its load-free boundary that may lead to premature failure of structures. Under thermal and/or mechanical load conditions, the size and shape of cutouts would prominently affect the buckling and postbuckling behavior of FGM plate. Relatively little efforts have been made in the past by the researchers and investigators to study the buckling and postbuckling behavior of FGM plate with geometric irregularities/discontinuities. For instance, Zhao *et al.* (2009) presented

results of thermal and mechanical buckling analysis of FGM plate with circular and square cutouts using the element-free kp-Ritz method. Lal *et al.* (2012) developed a FEM model for stochastic mechanical and thermal postbuckling response of functionally graded material plates with circular and square holes having material randomness. Natarajan *et al.* (2014) investigated the buckling behavior of FGM plate containing geometrical flaws in the form of crack and cutouts. Abolghasemi *et al.* (2014) examined the effect of the elliptical cutout on thermomechanical buckling response of FGM plate by drawing stability diagrams. Shaterzadeh *et al.* (2015) investigated the buckling behavior of FGM plate with multiple cutouts of various shapes under uniform temperature rise. The effect of internal defects (crack and cutout) on thermal buckling behavior of FGM plate was studied by Yu *et al.* (2016) using an extended isogeometric method, to capture the discontinuities in plate caused by internal defects without using any mesh refinement.

2.3 Elastic-Plastic Analysis of FGMs

Under the critical mechanical loadings and elevated temperature conditions, the FGM may show elastic-plastic response because the ductility and good shear strength induced by the metal phase can relax the stress concentration induced around the inherited cracks and flaws of ceramics through the plastic deformation. Furthermore, for the safety assessment of FGM structures it is very important and necessary to know the extreme loads acting on them and the overall structural response under these loading conditions. It requires to understand the elastic-plastic response of these FGM structures up to their ultimate strength point. Due to its significance in designing of FGMs under critical conditions, many researchers paid their attentions to characterization and structural analysis of elastic-plastic FGMs. For instance, Williamson *et al.* (1993) analyzed the effect of plasticity on thermal residual stresses at interfaces of FGM cylinders made of Ni/Al_2O_3 based on elastic-plastic finite element formulation. For calculating the elastic-plastic material properties of FGM, they used the modified rule-of-mixtures, basically proposed for metal alloys by Tamura et al. (1973) that is also termed as TTO model. By the proper calibration of a characteristic ‘stress transfer’ parameter, the TTO model governs the transition

from the Hencky–Huber–Mises (HHM) model, typically used for metals, to the Drucker–Prager constitutive model which is used for ceramics. A numerical study on the elastic-plastic deformation behavior of an FGM cylinder subjected to uniform internal heat generation was carried out by Ozturk and Gulgec (2011). Giannakopoulos *et al*. (1995) performed a FEM study to simulate the evolution of thermal stresses, the accumulation of plastic strains, and the development of monotonic and cyclic plastic zones during thermal cycling in the Ni/Al_2O_3 FGM layers. It was found that the accumulated plastic strain and residual stresses can be judiciously controlled by altering the compositional gradation of FGM. Carpenter *et al.* (1999) conducted experimental and numerical studies to examine the elastic-plastic fracture behavior of Ti/TiB FGM beam under 3-point bending. Shabana and Noda (2001) performed a thermo-elasto-plastic analysis of FGM subjected to residual thermal stresses produced by the fabrication process. The material characterization of elastic-plastic graded materials using micro-indention approach was performed by Gu et al. (2003). Jin et al. (2003) investigated the elastic-plastic crack growth in FGMs using cohesive zone model along with the extended TTO model, and it was found that the crack can be extended in FGMs at a much smaller rate than that for the metal. Eraslana and Akis (2006) obtained the plane strain analytical solutions for functionally graded elastic and elastic-plastic pressurized tube problems. A 3-dimensional FEM procedure was adopted by Nemat-alla *et al.* (2009) to perform the elastic-plastic stress analysis of bi-directional FGM plates with temperature-dependent material properties under transient thermal loading, and the authors could show that the residual thermal stresses are minimized effectively with the use of bi-directional FGMs. Meanwhile, the FEM simulations of low-velocity impact behavior of circular elastic-plastic FGM plate were performed by Gunes *et al.* (2011) assuming the ceramic phase to be elastic and the metal phase to be elastic-plastic, in accordance with the TTO model.

Moreover, in the practical scenario wherein the stresses induced in the structures by in-plane mechanical and/or thermal loads overpass the elastic limit of the material, a proper elastic-plastic stability analysis is required for the reliable, accurate and stable design of these structures under various loading conditions. The elastic-plastic buckling behavior of isotropic and composite plates have been analyzed by many researchers [e.g., (Bakker et al., 2009; Bi et

al., 2014; Durban and Zuckerman, 1999; Paley and Aboudi, 1991; Soh et al., 2000)]. However, there are very few investigations available in the literature on the inelastic buckling of FGM structures. For instance, Fu et al. (2014) presented the elastic-plastic buckling and postbuckling analysis of the functionally graded metal-metal sandwich plates with interfacial damage under mechanical loading conditions, and they concluded that the existence of the plastic deformation weakened the stiffness of the plate. The elastic-plastic stability analysis of FGM shells under various types of mechanical loads was carried out by Huang *et al.* (2014) and Zhang *et al.* (2015) to derive the expressions for elastic-plastic critical buckling loads.

Table 2.1 summarizes the existing research works on buckling and postbuckling analysis of elastic and elastic-plastic FGM plate with and without cutouts, and it can be observed that the stability and failure analysis of perforated elastic-plastic FGM plate has not been studied yet.

2.4 Observations

Based on the aforementioned detailed literature review, it is very clear that despite an overwhelming response for FGMs, very little work have addressed the stability and failure analysis of FGM plates with geometrical irregularity. Most of the relevant past studies have simplified the analysis by keeping the material properties unaffected by temperature, but such simplification does not hold good for FGM plate which is especially intended to be used under high-temperature conditions (Birman and Byrd, 2007).

Moreover, no literature has reported the effect of elastic-plastic material properties on the stability and failure response of imperforated and perforated FGM plates under thermal and/or mechanical loading conditions. Thus, it is imperative to examine the effects of cutouts of various shapes and sizes on buckling, postbuckling and failure responses of plate made of elastic-plastic FGM. In addition, a study on the sensitivity of the thermomechanical buckling and postbuckling behavior of elastic-plastic perforated FGM plates to various parameters, such as material gradation profile, geometrical parameters, and loading conditions, is also required.

Hence, it is aimed in present work to study the elastic-plastic buckling, postbuckling, and failure behaviour of FGM plate with a central cutout under thermomechanical conditions, considering material properties of FGM to be temperature-dependent. The actual non-homogeneous FGM plate with continuously varying properties along thickness is modeled as a laminate composed of multiple perfectly-bonded layers of isotropic material having layer-wise constant composition. A nonlinear FEM formulation based on the first-order shear deformation theory and the von Karman's nonlinear kinematics is utilized. The elastic-plastic behavior of FGM plate is assumed to follow J_2-plasticity and isotropic hardening in which the ceramic phase was considered to be elastic whereas the metal is taken to be elastic-plastic material in accordance with the TTO model. Subsequently, a parametric study is conducted to investigate the effects of various material, geometrical and loading parameters on the elastic-plastic buckling and postbuckling behavior, and the failure response of FGM plate under thermal and/or mechanical loading conditions.

Table 2.1: Summary of literature review on buckling, postbuckling and elastic-plastic analysis of FGM plates.

S. No.	Author(s)	Elastic/ Elastic-plastic	Failure analysis performed, Yes/No	Linear/ Nonlinear analysis	With cutout/ without cutout	Analysis techniques/ methods	Research focus
1.	Birman (1995), Feldman and Aboudi (1997), Javaheri and Eslami (2002), Ma and Wang (2004), Zenkour (2005), Naderi and Saidi (2010), Mohammadi and Saidi (2010), Bodaghi and Saidi (2010), Meiche *et al.* (2011), Thai and Choi (2012).	Elastic	No	Linear analysis	Without cutout	Galerkin method	Mechanical buckling analysis of FGM plate
2.	Chen and Liew (2004), Zhang *et al.* (2014).	Elastic	No	Linear analysis	Without cutout	Mesh-free method	Buckling analysis of FGM plate under non-uniform mechanical loading, Thermomechanical stability of FGM plate
3.	Lanhe (2004), Najafizadeh and Heydari (2004), Morimoto *et al.* (2006), Bouazza *et al.* (2010), Zenkour and Sobhy (2010), Matsunaga (2009), Atmane *et al.* (2016).	Elastic	No	Linear analysis	Without cutout	Analytical method	Thermal buckling analysis of FGM plate
4.	Shariat and Eslami (2006).	Elastic	No	Nonlinear analysis	Without cutout	Analytical method	Thermal buckling analysis imperfect FGM plate

S. No.	Author(s)	Elastic/ Elastic-plastic	Failure analysis performed, Yes/No	Linear/ Nonlinear analysis	With cutout/ without cutout	Analysis techniques/ methods	Research focus
5.	Na and Kim (2004), Ganapathi and Prakash (2006), Tran *et al.* (2013).	Elastic	No	Linear analysis	Without cutout	Finite element method	Thermal buckling of FGM plate with temperature-dependent material properties.
6.	Zhao *et al.* (2009), Natarajan *et al.* (2014), Abolghasemi *et al.* (2014), Shaterzadeh *et al.* (2015), Yu *et al.* (2016).	Elastic	No	Linear analysis	With cutout	Element-free kp-Ritz method, extended isogeometric analysis, Finite element method	Thermomechanical Buckling behavior of FGM plate with cutouts, thermal buckling of FGM plate with internal defects.
7.	Yang and Shen (2003a, 2003b), Yang *et al.* (2006), Shen and Li (2008).	Elastic	No	Nonlinear analysis	Without cutout	differential quadrature approximation, perturbation technique	Mechanical postbuckling analysis.
8	Ma and Wang (2003), Liew *et al.* (2004), Park and Kim (2006), Na and Kim (2006), Shen (2007).	Elastic	No	Nonlinear analysis	Without cutout	shooting method, differential quadrature method,	Thermal postbuckling analysis of FGM plates.

S. No.	Author(s)	Elastic/ Elastic-plastic	Failure analysis performed, Yes/No	Linear/ Nonlinear analysis	With cutout/ without cutout	Analysis techniques/ methods	Research focus
9	Shen (2005), Woo *et al.* (2005), Wu *et al.* (2007), Duc and Tung (2010), Lee *et al.* (2010), Zhang and Zhou (2015).	Elastic	No	Nonlinear analysis	Without cutout	Analytical method, Chebyshev polynomials, Analytical method, kp-Ritz method	Thermomechanical postbuckling analysis of FGM plate.
10	Lal *et al.* (2012).	Elastic	No	Nonlinear analysis	With cutout	First order perturbation technique	Thermal and mechanical postbuckling of FGM plate with cutouts.
11	Fu *et al.* (2014).	Elastic-plastic	No	Nonlinear analysis	Without cutout	Finite difference method	Mechanical buckling and postbuckling of FGM plate with interfacial damage.

CHAPTER 3

MATHEMATICAL FORMULATION AND COMPUTER IMPLEMENTATION

3.1 Introduction

The research gaps pertaining to the stability and failure analysis of FGM plate, and the necessity to include the material and geometrical nonlinearities in the respective analysis of FGM plate have already been discussed in the previous chapter. This chapter presents a mathematical model based on the first-order shear deformation theory and the von Karman's nonlinear kinematics for buckling, postbuckling and failure analysis of elastic-plastic FGM plate under mechanical and/or thermal loading conditions. The layerwise model of FGM plate is discussed in Section 3.2, in which the effective temperature-dependent thermoelastic and elastic-plastic material properties of FGM plate are calculated using Mori–Tanaka homogenization method and TTO model. The nonlinear FEM model of FGM plate is detailed in Section 3.3, wherein the geometrical nonlinearity in strain-displacement relationship is included in von Karman sense. The details of thermo-elastic-plastic constitutive relationship with J_2 –theory of plasticity are also furnished in the same section. Incremental procedure based on Newton-Raphson method adopted for the solution of the nonlinear algebraic equations is also discussed. Section 3.4 presents the methodology of ultimate failure prediction of FGM plate. Before the summery of the chapter, the computer implementation for nonlinear FEM analysis of FGM plate is discussed in Section 3.5.

3.2 Modeling of FGM Plate

Fig. 3.1 shows an FGM plate, consisting of two constituent materials (ceramic and metal), measuring a, b and h as length, width, and thickness, respectively. A coordinate system (x, y, z) is established on the middle plane of the plate. The volume fraction of the material constituents is assumed to follow a simple power law distribution in the thickness direction. In the present study, the

actual non-homogeneous FGM plate with continuously varying properties along thickness direction is modeled as a laminated plate composed of multiple perfectly-bonded layers of isotropic material having layer-wise constant composition, as used in earlier studies (Cinefra et al., 2010; Cinefra and Soave, 2011; Jin, 2002; Shakeri et al., 2006; Shakeri and Mirzaeifar, 2009; Shao, 2005; Yaghoobi et al., 2015).

In the present study, the temperature-dependent thermal (i.e., thermal expansion coefficient α) and mechanical material properties (i.e., Young's modulus *E*) of FGM plate are evaluated using below equation (Touloukian and Center, 1967).

$$P_j(T) = P_0(P_{-1}T^{-1} + 1 + P_1T + P_2T^2 + P_3T^3), \quad (3.1)$$

where, P(T) represents material property (E or α) evaluated at temperature T, and P_0, P_{-1}, P_1, P_2, and P_3 are the coefficients to calculate these temperature-dependent material properties for Al_2O_3 and Ni. The values of these coefficients for Al_2O_3 and Ni are given in Table 3.1. The variations of the material properties of Al_2O_3 and Ni with temperature are shown in Fig. 3.2.

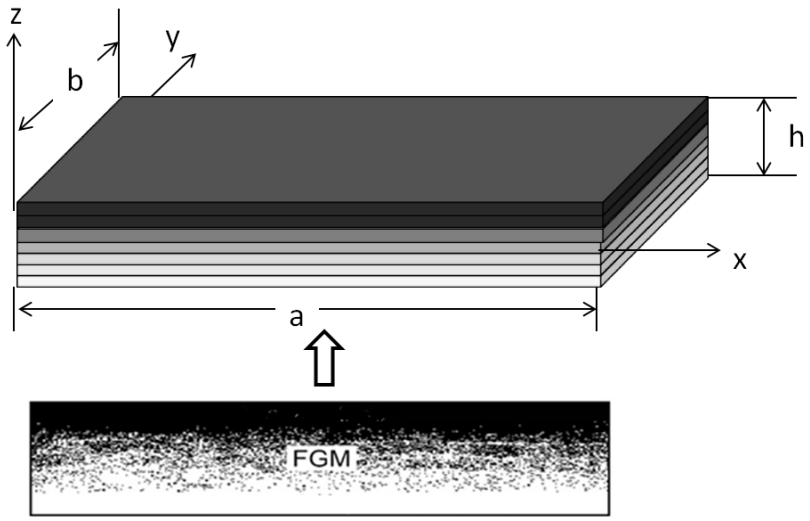

Fig. 3.1: Modeling of actual non-homogeneous FGM plate into a laminate composed of multiple perfectly-bonded homogeneous layers.

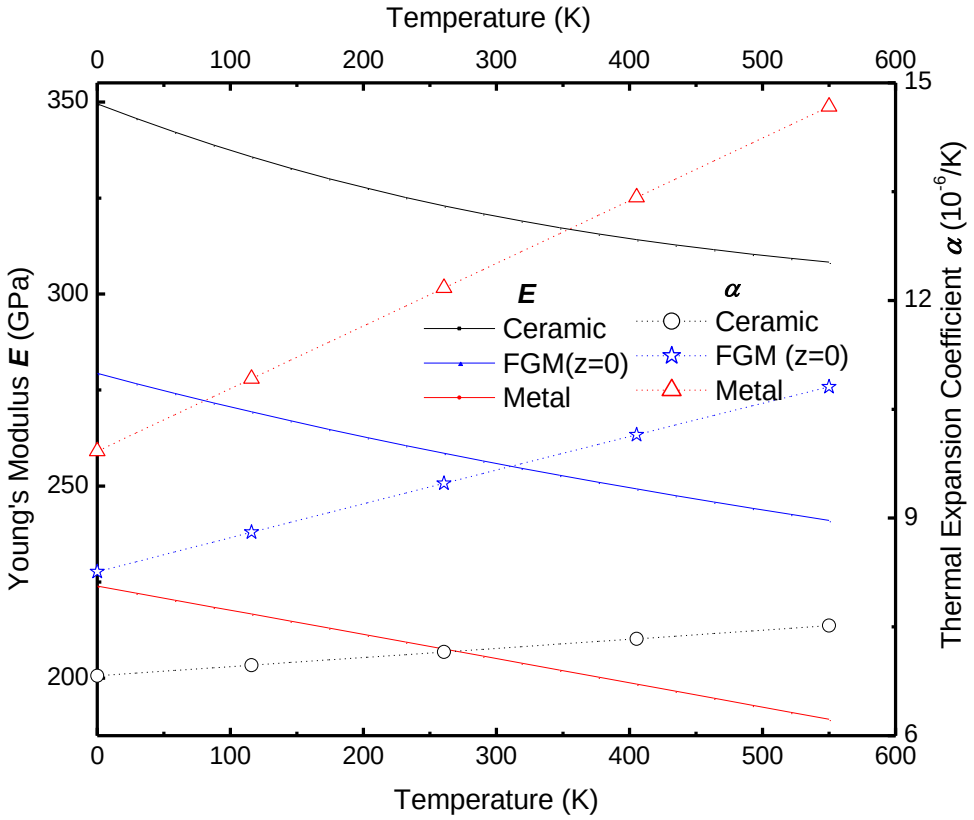

Fig. 3.2: Temperature-dependent Young's modulus (E) and thermal expansion coefficient (α).

Table 3.1:Temperature-dependent coefficients for Al_2O_3 and Ni [Reddy and Chin (1998)].

Property to be evaluated	Material	Coefficients				
		P_0	P_{-1}	P_1	P_2	P_3
E (in Pa)	Al_2O_3	349.55e9	0.0	-3.853e-4	4.027e-7	-1.673e-10
	Ni	223.95e9	0.0	-2.794e-4	-3.998e-9	0.0
α (in 1/K)	Al_2O_3	6.8260e-6	0.0	1.838e-4	0.0	0.0
	Ni	9.9209e-6	0.0	8.705e-4	0.0	0.0

3.2.1 Effective Thermoelastic Material Properties of FGM Plate

The volume fractions of ceramic and metallic constituents are assumed to follow, along the thickness of FGM plate, the power law distribution as given below:

$$V_m(z) = \left(\frac{z}{h} + \frac{1}{2}\right)^n; \; V_c(z) = 1 - V_m(z), \tag{3.2}$$

where, V denotes the volume fraction of constituents. The subscripts c and m, respectively, correspond to the ceramic and the metallic constituents. n is a

variable, called power law exponent, that determines the material variation profile through the plate thickness-coordinate, z varying from$-h/2\ to\ h/2$.

In the present study the effective thermoelastic material properties of two-phase FGM are calculated using two homogenization schemes: TTO model (i.e., also called modified rule-of-mixtures) and Mori-Tanaka method. These two approaches, used extensively in the literature (Asemi et al., 2013; Giannakopoulos et al., 1995; Gunes et al., 2011; Prakash et al., 2008; Swaminathan and Sangeetha, 2017) for accurately predicting the thermo-elastic constants of FGM, are discussed in the following paragraphs.

3.2.1.1 TTO model

The continuously varying mechanical properties of FGMs can be depicted by a homogenized rule-of-mixtures, so-called TTO model (also called the modified rule-of-mixtures). In TTO model effective Young's modulus of two-phase materials, like FGM, is given in terms of Young's moduli (i.e., E_c and E_m) and volume fractions (i.e., V_c and V_m) of respective phases (i.e., ceramic and metallic phases), and it is given as under:

$$E(z) = \left\{V_m(z)E_m\frac{q+E_c}{q+E_m} + (1 - V_m(z))E_c\right\}/\left\{V_m(z)\frac{q+E_c}{q+E_m} + (1 - V_m(z))\right\}, \quad (3.3)$$

where, the subscripts *c* and *m* correspond to the material phases ceramic and metal, respectively. The value of *q*, the stress transfer parameter or stress-to-strain transfer ratio, is basically determined experimentally that would depend upon the properties of constituent materials, the microstructure interaction and the applied loading conditions. It's value ranges from 0 to ∞, with $q \to \infty$ represents the case when the constituent materials deform identically in the loading direction (i.e., Voigt model), while $q = 0$ corresponds to the case wherein the constituent materials experience the same stress level (i.e., Reuss model). Due to the complicated microstructure of FGM, the constituting elements in FGM neither experience equal deformation nor equal stress. Generally, a nonzero finite value of q is assumed to approximately reflect the actual effects of micro-structural interaction and loading conditions in FGM. By performing experiments on dual-phase steels, over a wide range of volume fractions and applied strains, a value of q = 4.5 GPa was found by Fischmeister and Karlssor (1977). Subsequently, this value of q has been shown to yield a reasonable agreement with experimental and

numerical results for Ni-Al_2O_3 FGM by many researchers (Bhattacharyya *et al.*, 2007; Cho and Ha, 2001; Cho and Oden, 2000; Choi *et al.*, 2008; Finot *et al.*, 1996; Giannakopoulos *et al.*, 1995; Kapuria *et al.*, 2008; Kesler *et al.*, 1997). Therefore, based on these past studies, the value of q = 4.5 GPa is considered in the present work to simulate the response of Ni-Al_2O_3 FGM.

Further, the Poisson's ratio is assumed to be constant along the thickness of the FGM plate. Using the volume fractions of constituents at a particular value of thickness coordinate [calculated from Eq. (3.2)], the thermal expansion coefficient at particular thickness of FGM plate is calculated by using simple rule-of-mixtures as follows:

$$\alpha(z) = \alpha_c V_c + \alpha_m V_m. \tag{3.4}$$

3.2.1.2 Mori–Tanaka homogenization method

The graded thermo-elastic material properties across the thickness of FGM plate can also be calculated using Mori-Tanaka scheme (Benveniste, 1987; Mori and Tanaka, 1973). According to the Mori–Tanaka homogenization method, the effective bulk modulus $K(z,T)$, the thermal expansion coefficient $\alpha(z,T)$, and the effective shear modulus $G(z,T)$ of the FGM are calculated using the following expressions:

$$\frac{K(z,T) - K_m(T)}{K_c(T) - K_m(T)} = \frac{V_c(z)}{\left[1 + (1 - V_c(z))3\frac{(K_c(T) - K_m(T))}{3K_m(T) + 4G_m(T)}\right]} \tag{3.5}$$

$$\frac{G(z,T) - G_m(T)}{G_c(T) - G_m(T)} = \frac{V_c(\mathrm{z})}{\left[1 + (1 - V_c(\mathrm{z}))\frac{(G_c(T) - G_m(T))}{G_m(T) + f(T)}\right]} \tag{3.6}$$

$$\frac{\alpha(z,T) - \alpha_m(T)}{\alpha_c(T) - \alpha_m(T)} = \frac{(1/K(z,T)) - (1/K_m(T))}{(1/K_c(T)) - (1/K_m(T))} \tag{3.7}$$

$$f(T) = \frac{G_m(T)(9K_m(T) + 8G_m(T))}{6(K_m(T) + 2G_m(T))} \tag{3.8}$$

Thereafter, the effective values of Young's modulus $E(z,T)$ over the thickness of FGM plate can be determined using following equations:

$$E(z,T) = \frac{9K(z,T)G(z,T)}{(3K(z,T) + G(z,T))} \tag{3.9}$$

3.2.2 Effective Elastic-Plastic Material Properties of FGM Plate

The plastic behavior of FGM plate (i.e., yield strength and plastic tangent modulus of FGM) can be depicted by the same TTO model described in Section

3.2.1.1. It is to be noticed that the TTO model assumes that the overall failure behavior of two-phase composite containing both brittle and ductile phases is governed by the ductile constituent (Jin et al., 2003). This assumption is also considered to be reasonable in the case of FGMs (containing ceramic- a brittle phase, and metal- a ductile phase) because the ductility and good shear strength induced in the FGM by the metal phase relax the stress concentration induced around the inherited cracks and flaws of ceramics through the plastic deformation and hence, eliminate the possibility of brittle failure of FGM *(*Bandyopadhyay *et al.*,2000 ; Soh *et al.*, 2000) .

Based on the assumption that the FGM yields once the metal constituent yields, the TTO model uses q (stress transfer parameter), σ_{ym}(yield strength of metal) and H_m(tangent modulus of metal) to give the overall yield strength and tangent modulus of FGM, as given below, for predicting its elastic-plastic response.

$$\sigma_y(z,T) = \sigma_{ym}(T)\left[V_m(z) + \left(\frac{q+E_m(T)}{q+E_c(T)}\right)\frac{E_c(T)}{E_m(T)}(1-V_m(z))\right], \tag{3.10}$$

$$H(z,T) = \left\{V_m(z)H_m(T)\frac{q+E_c(T)}{q+H_m(T)} + (1-V_m(z))E_c(T)\right\} \times \left\{V_m(z)\frac{q+E_c(T)}{q+H_m(T)} + (1-V_m(z))\right\}^{-1}, \tag{3.11}$$

where, the subscripts c and m correspond to the ceramic and metal phases, respectively, and q represents the stress transfer parameter, also called stress-to-strain transfer ratio. Using the volume fractions of the constituents at a particular thickness coordinate [calculated from Eq. (3.2)], the temperature-dependent yield strength and tangent modulus of FGM plate are calculated at that thickness coordinate using Eqs. (3.10)-(3.11), respectively. It is assumed that under the assumption of idealized bilinear hardening behavior of metal, the FGM also follows bilinear plastic response [(Williamson et al., 1995)), Giannakopoulos *et al.* (1995)]. The values of temperature-dependent coefficients to calculate yield strength σ_{ym} and tangent modulus H_m of Ni phase of Ni-Al_2O_3 FGM are given in Table 3.2 (Williamson et al., 1995).

Table 3.2. Temperature-dependent strength coefficients for Ni (Williamson et al., 1995).

Property to be evaluated	Coefficients				
	P_0	P_{-1}	P_1	P_2	P_3
σ_{ym}(in Pa)	2.81e6	0.0	516.68e3	-8.79e2	-3.56e-1
H_m(in Pa)	91.75e7	0.0	930.64e4	-15.88e3	75.72e-1

3.3 Nonlinear Finite Element Formulation for Postbuckling Analysis of FGM Plate

3.3.1 Displacement Field

As observed by many researchers (Bellifa et al., 2016; Bouderba et al., 2013; Chi and Chung, 2006; Prakash et al., 2009; Yin et al., 2013; Zhang, 2013; Zhang and Zhou, 2008) that due to material inhomogenity, the neutral surface and physical mid-plane of FGM plate does not coincide with each other, which causes a strong coupling between stretching and bending deformations. With additional stretching–bending coupling term, the resulting constitutive and governing equations of FGM plate become more complex that in-turn makes the structural analysis of FGM plate more difficult. Meanwhile, the concept of correct neutral surface was adopted in several studies (Bellifa et al., 2016; Bouderba et al., 2013; Bouiadjra et al., 2013; Hamidi et al., 2015; Prakash et al., 2009; Yahia et al., 2015; Yin et al., 2013; Zhang, 2013; Zhang and Zhou, 2008) to vanish the coupling effect from the linear governing equations of FGM plate and to transform them into simpler forms as those for homogenous isotropic plates. As suggested in previous study (Prakash et al., 2009), the formulation based on the neutral surface or the physical mid-surface both produce same results and actual FGM plate behavior can be analyzed using either of the formulations. On the other hand, for geometrical nonlinear analysis of FGM plate, Arbate (2008) mentioned that the coupling effect cannot be eliminated using the concept of correct neutral surface. Therefore, in present thesis the kinematic equations based on physical mid-plane are utilized to simulate the geometric nonlinear response of FGM plate.

In the present study the displacement field is assumed to follow the first-order shear deformation theory (FSDT), commonly known as Mindlin plate theory. The FSDT is based on the assumptions that when plate deforms, the straight lines drawn perpendicular to the plate surface before deformation remain straight but not necessarily perpendicular to the surface after the deformation. These assumptions produce constant transverse shear strains along the thickness

and make the FSDT handle moderately thick plates more accurately than classical plate theory (CPT) wherein the transverse shear effects are neglected . In the FSDT, the displacement $u = [u, v, w]^{\mathrm{T}}$at (*x*, *y*, *z*) are expressed as functions of the mid-plane (*z = 0*) translations u_0, v_0, w_0 and independent normal rotations θ_x and θ_y in the *xz*- and *yz*-planes, respectively.

$$\begin{aligned} u(x,y,z) &= u_0(x,y) + z\theta_x(x,y) \\ v(x,y,z) &= v_0(x,y) + z\theta_y(x,y) \\ w(x,y,z) &= w_0(x,y) \end{aligned} \tag{3.12}$$

3.3.2 Strain-Displacement Relationship

Incorporating the von Karman's assumptions which imply that derivatives of u and v with respect to x, y and z are small and noting that w is independent of z allows to write the Green's strain components for moderately large deformations into following form (Reddy, 2004) :

$$\begin{aligned} \varepsilon_x &= \frac{\partial u_0}{\partial x} + z\left(\frac{\partial \theta_x}{\partial x}\right) + \frac{1}{2}\left(\frac{\partial w_0}{\partial x}\right)^2, \\ \varepsilon_y &= \frac{\partial v_0}{\partial y} + z\left(\frac{\partial \theta_y}{\partial y}\right) + \frac{1}{2}\left(\frac{\partial w_0}{\partial y}\right)^2, \\ \gamma_{xy} &= \frac{\partial u_0}{\partial y} + \frac{\partial v_0}{\partial x} + z\left(\frac{\partial \theta_x}{\partial y} + \frac{\partial \theta_y}{\partial x}\right) + \left(\frac{\partial w_0}{\partial x}\frac{\partial w_0}{\partial y}\right), \\ \gamma_{xz} &= \frac{\partial w_0}{\partial x} + \theta_x, \\ \gamma_{yz} &= \frac{\partial w_0}{\partial y} + \theta_y. \end{aligned} \tag{3.13}$$

Rewriting the Eq. (3.13) into matrix form as

$$\{\epsilon\} = \begin{Bmatrix} \epsilon_x \\ \epsilon_y \\ \gamma_{xy} \\ \gamma_{xz} \\ \gamma_{yz} \end{Bmatrix} = \{\epsilon\}^l + \{\epsilon\}^{nl}, \tag{3.14}$$

$$\{\epsilon\}^l = \begin{Bmatrix} \epsilon_p^0 \\ 0 \end{Bmatrix} + \begin{Bmatrix} z\epsilon_b^0 \\ \epsilon_s^0 \end{Bmatrix}, \{\epsilon\}^{nl} = \begin{Bmatrix} \epsilon_p^{NL} \\ 0 \end{Bmatrix}, \tag{3.15}$$

wherein, the linear in-plane strain ϵ_p^0, the bending strain ϵ_b^0, shear strain ϵ_s^0, and the nonlinear in-plane strain terms ϵ_p^{NL} are written as follows:

$$\{\epsilon_p^0\} = \begin{Bmatrix} \frac{\partial u_0}{\partial x} \\ \frac{\partial v_0}{\partial y} \\ \frac{\partial u_0}{\partial y} + \frac{\partial v_0}{\partial x} \end{Bmatrix}, \{\epsilon_b^0\} = \begin{Bmatrix} \frac{\partial \theta_x}{\partial x} \\ \frac{\partial \theta_y}{\partial y} \\ \frac{\partial \theta_x}{\partial y} + \frac{\partial \theta_y}{\partial x} \end{Bmatrix} \tag{3.16}$$

$$\{\epsilon_s^0\} = \begin{Bmatrix} \frac{\partial w_0}{\partial x} + \theta_x \\ \frac{\partial w_0}{\partial y} + \theta_y \end{Bmatrix}, \text{ and } \{\epsilon_p^{NL}\} = \begin{Bmatrix} \frac{1}{2}\left(\frac{\partial w_0}{\partial x}\right)^2 \\ \frac{1}{2}\left(\frac{\partial w_0}{\partial y}\right)^2 \\ \left(\frac{\partial w_0}{\partial x}\frac{\partial w_0}{\partial y}\right) \end{Bmatrix}. \tag{3.17}$$

3.3.3 Constitutive Relations

3.3.3.1 Elastic constitutive relations

Based on the generalized Hooke's law, the elastic stress-strain relations are given by:

$$\begin{Bmatrix} \sigma_x \\ \sigma_y \\ \tau_{xy} \\ \tau_{yz} \\ \tau_{xz} \end{Bmatrix} = \begin{bmatrix} Q_{11} & Q_{12} & 0 & 0 & 0 \\ Q_{12} & Q_{22} & 0 & 0 & 0 \\ 0 & 0 & Q_{44} & 0 & 0 \\ 0 & 0 & 0 & k_1^2 Q_{55} & 0 \\ 0 & 0 & 0 & 0 & k_2^2 Q_{66} \end{bmatrix} \begin{Bmatrix} \epsilon_x \\ \epsilon_y \\ \gamma_{xy} \\ \gamma_{xz} \\ \gamma_{yz} \end{Bmatrix} \tag{3.18}$$

Or $$\{\sigma\} = [D]\{\varepsilon\}, \tag{3.19}$$

Here, k_1 and k_2 are the shear correction factors, and Q_{ij} are the stiffness matrix components for the plane stress case and are functions of material properties, as mentioned below

$$Q_{11} = \frac{E(T,z)}{1-\nu^2}, \quad Q_{12} = Q_{13} = Q_{23} = \nu Q_{11}, \; Q_{22} = Q_{33} = Q_{11},$$

$$Q_{44} = Q_{55} = Q_{66} = \frac{E(T,z)}{(1+\nu)}, \tag{3.20}$$

where, $E(T, z)$ is Young's modulus that varies across the thickness of FGM plate at any temperature T calculated using Eqs. (3.3) or (3.9), and ν is the Poisson's ratio that is assumed to be constant through the thickness of FGM plate.

3.3.3.2 Thermo-elasto-plastic constitutive relations

To carry out elastic-plastic analysis, the material is assumed to obey the von-Mises yielding criterion, and the corresponding yield surface is assumed to undergo uniform expansion in the stress space with increasing plastic deformations. The yield function can be expressed as:

$$f = \sqrt{3J_2} - \sigma_y, \tag{3.21}$$

where,

$$J_2 = \frac{1}{6}\left[(\sigma_x - \sigma_y)^2 + (\sigma_y - \sigma_z)^2 + (\sigma_x - \sigma_z)^2 + 6(\tau_{xy}^2 + \tau_{yz}^2 + \tau_{xz}^2)\right]. \tag{3.22}$$

Due to the effect of strain hardening the initial yield surface varies at each stage of plastic deformation, and hence the equation of yield surface for a solid undergoing thermo-elasto-plastic deformation can be written as:

$$f = f(\sigma, \kappa, T), \tag{3.23}$$

where, κ and T denote the strain hardening parameter and temperature, respectively.

Differentiating the f using chain rule of partial differentiation, we can write:

$$df = \left(\frac{\partial f}{\partial \sigma}\right)^T d\sigma + \frac{\partial f}{\partial \kappa} d\kappa + \frac{\partial f}{\partial T} dT. \tag{3.24}$$

It is known that the hardening parameter (κ) is a function of plastic strain (ε_p), hence the equation of yield surface can be rewritten as

$$df = \left(\frac{\partial f}{\partial \sigma}\right)^T d\sigma + \frac{\partial f}{\partial \kappa}\left(\frac{\partial \kappa}{\partial \varepsilon_p}\right) d\varepsilon_p + \frac{\partial f}{\partial T} dT. \tag{3.25}$$

The variation in plastic strain energy should be zero, to satisfy the equilibrium of solid under small incremental plastic deformations, hence

$$df = \left(\frac{\partial f}{\partial \sigma}\right)^T d\sigma + \frac{\partial f}{\partial \kappa}\left(\frac{\partial \kappa}{\partial \varepsilon_p}\right) d\varepsilon_p + \frac{\partial f}{\partial T} dT = 0. \tag{3.26}$$

Now the total incremental strain combines the incremental parts of elastic strain ($\Delta\varepsilon_e$), thermal strain ($\Delta\varepsilon_T$), strain due to temperature-dependent material properties ($\Delta\varepsilon_{TD}$), and plastic strain ($\Delta\varepsilon_p$), i.e.,

$$\Delta\varepsilon = \Delta\varepsilon_e + \Delta\varepsilon_T + \Delta\varepsilon_{TD} + \Delta\varepsilon_p. \tag{3.27}$$

By virtue of Hooke's law, the total incremental stress ($\Delta\sigma$) can be written as

$$\Delta\sigma = [D]\{\Delta\varepsilon - (\Delta\varepsilon_T + \Delta\varepsilon_{TD} + \Delta\varepsilon_p)\}. \tag{3.28}$$

Putting the value of total incremental stress ($d\sigma$) into Eq. (3.26), we get

$$\begin{aligned} df = \left(\frac{\partial f}{\partial \sigma}\right)^T [D]\{\Delta\varepsilon - (\Delta\varepsilon_T + \Delta\varepsilon_{TD} + \Delta\varepsilon_p)\} \\ + \frac{\partial f}{\partial \kappa}\left(\frac{\partial \kappa}{\partial \varepsilon_p}\right)\Delta\varepsilon_p + \frac{\partial f}{\partial T}\Delta T = 0. \end{aligned} \tag{3.29}$$

The plastic potential function is assumed to be identical to the yield function in the so-called associative flow rule given by

$$\Delta\varepsilon p = d\lambda \frac{\partial f}{\partial \sigma}. \tag{3.30}$$

The components of thermal strain ($\Delta\varepsilon_T$) and strain due to temperature-dependent material properties ($\Delta\varepsilon_{TD}$) are given as

$$\Delta\varepsilon_T = \alpha\,\Delta T, \text{ and } \Delta\varepsilon_{TD} = \frac{\partial[D]^{-1}}{\partial T}\sigma\,\Delta T. \tag{3.31}$$

Let,

$$\left(\frac{\partial f}{\partial \sigma}\right)^T [D]\left(\frac{\partial f}{\partial \sigma}\right) - \frac{\partial f}{\partial k}\left(\frac{\partial k}{\partial \varepsilon_p}\right)^T \left(\frac{\partial f}{\partial \sigma}\right) = \eta^i. \tag{3.32}$$

Substituting Eqs. (3.31)-(3.32) into the Eq. (3.30), and rearranging the terms to obtain the value of flow variable $d\lambda$.

$$d\lambda = \left[\frac{\left(\frac{\partial f}{\partial \sigma}\right)^T [D]\left\{\Delta\varepsilon - (\alpha\,\Delta T + \frac{\partial[D]^{-1}}{\partial T}\sigma\,\Delta T)\right\} + \frac{\partial f}{\partial T}\Delta T}{\eta^i}\right] \tag{3.33}$$

The expression for $d\sigma$ is obtained by substituting from Eqs. (3.30)-(3.33) into Eq. (3.28) as:

$$\begin{aligned}\Delta\sigma = [D]&\left[(\Delta\varepsilon) - (\alpha\,dT + \frac{\partial[D]^{-1}}{\partial T}\sigma\,dT)\right] \\ &- [D]\frac{\partial f}{\partial \sigma}\left[\frac{\left(\frac{\partial f}{\partial \sigma}\right)^T [D]\left\{\Delta\varepsilon - (\alpha\,dT + \frac{\partial[D]^{-1}}{\partial T}\sigma\,dT)\right\} + \frac{\partial f}{\partial T}dT}{\eta^i}\right]\end{aligned} \tag{3.34}$$

Rearranging the Eq. (3.34) to obtain:

$$\begin{aligned}\Delta\sigma = &\left[[D] - \frac{1}{\eta^i}[D]\frac{\partial f}{\partial \sigma}\left(\frac{\partial f}{\partial \sigma}\right)^T [D]\right]\left[(\Delta\varepsilon) - \left(\alpha\,\Delta T + \frac{\partial[D]^{-1}}{\partial T}\sigma\,\Delta T\right)\right] \\ &- \frac{1}{\eta^i}[D]\frac{\partial f}{\partial \sigma}\frac{\partial f}{\partial T}\Delta T\end{aligned} \tag{3.35}$$

The term $\left[[D] - \frac{1}{\eta^i}[D]\frac{\partial f}{\partial \sigma}\left(\frac{\partial f}{\partial \sigma}\right)^T [D]\right]$ in Eq. (3.35) represents the elasto-plastic constitutive matrix $\left[D_{ep}\right]^i$, which finally, gives the thermo-elasto-plastic constitutive relationship as

$$\Delta\sigma = \left[D_{ep}\right]^i\{\Delta\varepsilon'\} \tag{3.36}$$

$$\Delta\varepsilon' = (\Delta\varepsilon) - (\Delta\varepsilon^t) \tag{3.37}$$

$$\Delta\varepsilon^t = \alpha\,\Delta T + \frac{\partial[D]^{-1}}{\partial T}\sigma\,\Delta T + \frac{1}{\eta^i}[D]\left[D_{ep}\right]^{-1}\frac{\partial f}{\partial \sigma}\frac{\partial f}{\partial T}\Delta T \tag{3.38}$$

3.3.4 FEM Formulation

The incremental displacement vector (Δu^e) within an element is interpolated in an expression of the form:

$$\Delta u^e = N\Delta a, \tag{3.39}$$

where, Δa is the incremental nodal displacement vector and N is the matrix of interpolation functions of a Lagrangian element. The incremental strain vector ($\Delta\varepsilon$) is given in the form of incremental nodal displacement vector (Δa) and strain-displacement matrix (B), as

$$\Delta\varepsilon = B\Delta a, \tag{3.40}$$

The principle of virtual work is given as

$$0 = \delta W^e \equiv (\delta U^e + \delta V^e) \tag{3.41}$$

where U^e is the strain energy stored and V^e is the work done by applied forces in an element.

Considering the aforementioned case of thermo-elasto-plastic isotropic hardening case, the virtual strain energy (δU^e) may be written as

$$\delta U^e = \int_V \delta(\Delta\varepsilon'^T)\Delta\sigma\, dV, \tag{3.42}$$

By using Eqs.(3.36)-(3.37) and Eq.(3.40), to rewrite Eq. (3.42) in the following form:

$$\delta U^e = \delta(\Delta a^T)\int_V B^T\left[D_{ep}\right]^i B\,\Delta a\, dV - \delta(\Delta a^T)\int_V B^T\left[D_{ep}\right]^i \Delta\varepsilon^t\, dV, \tag{3.43}$$

In the absence of body forces, the external virtual work (δV^e) can be splitted into two terms related to work done due to incremental tractions at plate surfaces (i.e., $z = \pm h/2$) and plate edges, i.e.,

$$\delta V^e = \delta(\Delta a^T)\int_A N^T\,\widetilde{\Delta P}\, dA + \delta(\Delta a^T)\int_s N^T\,\widetilde{\Delta P_e}\, ds, \tag{3.44}$$

where, $$\widetilde{\Delta P} = \left[\Delta P_x \quad \Delta P_y \quad \Delta P_z \quad \overline{\Delta M}_x \quad \overline{\Delta M}_y\right]^T, \tag{3.45}$$

and, the generalized edge forces are given as

$$\begin{aligned}\widetilde{\Delta P_e} &= \left[\overline{\Delta P}_x^e \quad \overline{\Delta P}_y^e \quad \Delta\bar{P}_z^e \quad \overline{\Delta M}_x^e \quad \overline{\Delta M}_y^e\right]^T \\ &= \int_{-h/2}^{h/2}\left[\left(\Delta P_x^e \quad \Delta P_y^e \quad \Delta P_z^e \quad \Delta M_x^e \quad \Delta M_y^e\right)dz\right]^T.\end{aligned} \tag{3.46}$$

Substituting Eqs. (3.43)-(3.44) into Eq. (3.41) to obtain the equilibrium equation for an arbitrary value of virtual displacement $\delta(\Delta a^T)$ in the following form:

$$\left(\int_V B^T\left[D_{ep}\right]^i B\, dV\right)\Delta a - \int_V B^T\left[D_{ep}\right]^i \Delta\varepsilon^t\, dV - \int_A N^T\, \widetilde{\Delta P}\, dA - \int_s N^T\, \widetilde{\Delta P_e}\, ds = 0. \tag{3.47}$$

Rewriting Eq. (3.47) after putting the value of $\Delta\varepsilon^t$ from Eq. (3.39) in the following manner:

$$\left(\int_V B^T\left[D_{ep}\right]^i B\, dV\right)\Delta a - \int_V B^T\left[D_{ep}\right]^i \left\{\alpha\, \Delta T + \frac{\partial[D]^{-1}}{\partial T}\sigma\, \Delta T + \frac{1}{\eta^i}[D]\left[D_{ep}\right]^{-1}\frac{\partial f}{\partial\sigma}\frac{\partial f}{\partial T}\Delta T\right\} dV - \int_A N^T\, \widetilde{\Delta P}\, dA - \int_s N^T\, \widetilde{\Delta P_e}\, ds = 0. \tag{3.48}$$

Finally, the set of nonlinear governing equations is obtained in the following marix form:

$$[K]\Delta a = \Delta R, \tag{3.49}$$

where, $[K]$ is the structural stiffness matrix given by:

$$[K] = \int_V B^T\left[D_{ep}\right]^i B\, dV, \tag{3.50}$$

ΔR in Eq. (3.49) is incremental external load vector due to combined mechanical loading(ΔR_M) and thermal loading(ΔR_T), i.e.,

$$\Delta R = \Delta R_M + \Delta R_T, \text{ having} \tag{3.51}$$

$$\Delta R_M = \int_A N^T\, \widetilde{\Delta P}\, dA + \int_s N^T\, \widetilde{\Delta P_e}\, ds, \text{ and} \tag{3.52}$$

$$\Delta R_T = \int_V B^T\left[D_{ep}\right]^i \left(\alpha\, \Delta T + \frac{\partial[D]^{-1}}{\partial T}\sigma\, \Delta T + \frac{1}{\eta^i}[D]\left\{[D_{ep}]^i\right\}^{-1}\frac{\partial f}{\partial\sigma}\frac{\partial f}{\partial T}\Delta T\right) dV \tag{3.53}$$

3.3.5 Incremental Solution Procedure

In the present study, the solution for nonlinear algebraic equations posted in Eq. (3.49) is obtained using Newton-Raphson iterative solution technique. Newton-Raphson solution technique is based on Taylor's series expansion, and it is convenient to rewrite the Eq. (3.49) as:

$$\psi\{\delta\} = [K(\delta)]\{\delta\} - \Delta R, \tag{3.54}$$

where, ψ is the residual force and $[K(\delta)]$ is structural stiffness matrix, which is a function of unknown deflection δ. If for an initial estimate of the displacement vector $\{\delta\}_i$ (i.e., for i^{th} iteration) we obtain residual forces $\psi\{\delta\}_i \neq 0$, then an

improved solution $\{\delta\}_{i+1}$ is obtained by equating the linearized Taylor's series expansion of $\psi\{\delta\}_{i+1}$ in the neighborhood of $\{\delta\}_i$ to zero, as below:

$$\psi\{\delta\}_{i+1} \cong \psi\{\delta\}_i + K_T\,\Delta\{\delta\}_i = 0, \tag{3.55}$$

where, $\Delta\{\delta\}_i$ is the incremental displacement vector, and K_T is the tangent stiffness matrix evaluated at $\{\delta\}_i$ and is given by:

$$K_T = \left[\frac{\partial\psi\{\delta\}_i}{\partial[\delta]}\right]. \tag{3.56}$$

The improved solution is then obtained as:

$$\{\delta\}_{i+1} = \{\delta\}_i + \Delta\{\delta\}_i. \tag{3.57}$$

To improve the numerical stability and convergence of the solution, the load is applied in small increments. The iterative solution is continued until the following convergence criterion is satisfied.

$$\delta_{i+1} - \delta_i \leq \beta, \tag{3.58}$$

where, β is a sufficiently small number, i.e., 0.005%

Since the elastic-plastic constitutive equations depend upon the present level of stresses and the deformation history; hence, for predicting the elastic-plastic buckling and postbuckling behavior of FGM plate, incremental iterative procedure as given in Table 3.3 is followed. As detailed in Table 3.3, the return mapping algorithm, based on the works of Wilkins (1963) and Simo and Taylor (1986), is applied to keep the position of final state of stress on the updated yield surface.

3.4 Definition of Buckling Load and Ultimate Load Capacity

It has been found that similar to unsymmetric composite plates, the simply-supported FGM plates posses non-bifurcation type of buckling and there is, instead, a continuous transition from a pre- to post-buckled state without a clear critical point on the equilibrium path. This can be attributed to the presence of higher degree of stretching-bending coupling effects which causes transverse deflection even in the absence of pronounced bending load. Due to the smooth load-deflection curves the buckling load cannot be identified as usual but an approach consistent with the criterion used to determine the buckling load of

imperfect shells by Yamaki (1960) is used in the present work. This approach requires the calculation of the second derivative (curvature) of the respective load-transverse deflection (equilibrium) path using a finite difference scheme and a change in the sign of the curvature at any given analysis increment is noted. The change in sign corresponds to the buckling point on postbuckling equilibrium path of the plate and the corresponding value of the load at this point is considered as the buckling load.

Moreover, an FEM based strategy that is followed to predict the ultimate load capacity of elastic-perfectly plastic and bilinear elastic-plastic isotropic homogeneous plates [Narayanan and Chow (1984), Shanmugam *et al.* (1999), El-sawy *et al.* (2004), Paik (2005), Ghavami and Khedmati (2006), Estefen *et al.* (2016)] is extended to predict ultimate load capacity of elastic-plastic FGM plate.

In the present study, FGM plate is subjected to axial compressive load (mechanical and/or thermal load) in an incremental manner (to ensure that the analysis closely follows the actual load-response curve of FGM plate) which causes recoverable elastic stresses and strains within elastic range; however, at relatively large value of load (i.e., beyond yield load) the yielding in FGM plate is followed by recoverable elastic strains as well as irrecoverable plastic strains in the plate. As the load further increases, the proportion of plastic strain reaches to an extent where the plate becomes unstable because of complete loss of stiffness of the plate resulting in the collapse of the FGM plate to cause failure of the plate, and the corresponding load is termed as ultimate load capacity.

3.5 Computer Implementation

The elastic buckling, postbuckling and failure analysis of FGM plate under mechanical loading conditions was carried out by developing a special-purpose FORTRAN computer program based on the finite-element formulation, whereas a general purpose finite element package ANSYS [by encrypting a macro in APDL (i.e., ANSYS Parametric Design Language)] using was utilized to perform thermal and thermomechanical buckling and postbuckling analysis of elastic FGM plates with temperature-dependent material properties. In addition, the elastic-plastic buckling, postbuckling and failure analysis of FGM plate with temperature-dependent material properties was also carried out using ANSYS.

3.6 Summary

In this chapter, nonlinear mathematical formulation for elastic-plastic buckling and postbuckling analysis of FGM plate with temperature-dependent material properties is presented. The layerwise modeling approach of FGM plate is presented, wherein the graded thermoelastic material properties of FGM plate are assumed to be governed either by the modified rule of mixtures (also called TTO model) or by the Mori-Tanaka homogenization scheme, whereas the elastic-plastic material characteristics (i.e., yielding strength and tangent modulus) are varied as per the TTO model. The governing equations for elastic-plastic FGM plate are developed using variational principle. Subsequently, the nonlinear finite element formulation based on the first-order shear deformation theory and the von Karman's nonlinear kinematics is presented. The incremental solution algorithm based on Newton-Raphson method is discussed to solve resulting nonlinear governing equations. Lastly, the ultimate load capacity of FGM plate is defined, and the computer implementation of the formulation presented to carry out the analysis is talked about.

Table 3.3: Solution procedure for thermo-elastic-plastic analysis of FGM plate.

1. The material properties *E* and α, and the yield strength $\sigma_{Yield}(z,T)$ and tangent modulus *H* at each layer of FGM plate are evaluated using Eqs. (3.7), (3.9) and (3.10)-(3.11) respectively, for current temperature T_i at ith time step and utilized to compute the temperature-dependent constitutive matrix $[D(T)]_i$ at present time step.
2. Initially the displacements (a_0), strains (ε_0) and stresses (σ_0) are known from previous load steps or are zero.
3. Determine the elasto-plastic constitutive matrix from previously known variables.
4. Apply the boundary conditions and obtain the incremental displacements (Δa) by solving the Eq.(3.49).
5. The Eq. (3.40) can be utilized to obtain the incremental strains ($\Delta\varepsilon$) with the aid of calculated incremental displacements (Δa). The incremental stresses ($\Delta\sigma$) are calculated by Eq.(3.46).
6. When computing the solution at time t_n, we first compute the trial elastic state by assuming that the material response is purely elastic (no plastic evolution) when applying $\Delta\varepsilon$ and total stresses and strains are updated as

   $$\sigma_n^{trial} = \sigma_0 + \Delta\sigma$$
   $$\varepsilon_n^{trial} = \varepsilon_0 + \Delta\varepsilon$$
7. The updated stresses and strains are substituted in Eq.(3.21) to perform plasticity check and following cases are identified
   a. If $f(\sigma_{n+1}^{trial}) < 0$ there is elastic deformation and go-to step 8
   b. If $f(\sigma_{n+1}^{trial}) > 0$ there is plastic deformation and stress correction procedure is to be applied to correct the state of stresses, value of $\Delta\epsilon_p$ is calculated by applying Eq.(3.30) and state variables are updated as follows

   $$\varepsilon_n = \varepsilon_0^p + \Delta\varepsilon_p$$
   $$\sigma_n = D:\left(\Delta\varepsilon + \varepsilon_0 - \varepsilon_0^p\right) = \sigma_0 + D:\left(\Delta\varepsilon - \Delta\varepsilon_p\right)$$
8. The nodal coordinates are updated by adding corresponding values of nodal displacements.
9. Go-to step 1 for next load increment.

CHAPTER 4

STABILITY AND FAILURE ANALYSIS OF ELASTIC FGM PLATES UNDER IN-PLANE MECHANICAL COMPRESSION

4.1 Introduction

The aim of this chapter is to present non-linear stability and failure analysis of imperforated and perforated FGM elastic plates under in-plane uniaxial and biaxial compression caused by mechanical loads. The failure of the FGM plate is predicted by applying 3-D von-Mises criterion. The FGM plate is assumed to be made of two constituents: TiB (i.e., ceramic phase) and Ti (i.e., metallic phase), with the following material properties (Jin et al., 2003): E_C = 375 GPa, E_m = 107 GPa, $\nu = 0.24$ (for ceramic and metal both) and σ_{ym} = 400 MPa. The subscripts *c* and *m*, respectively, correspond to the ceramic and the metallic constituents. It is to mention here that material is graded as per TTO model as specified in Chapter 3, i.e., using the volume fraction of the constituents at a particular value of thickness coordinate [calculated using Eq. (3.2)], Young's modulus and the yield strength of FGM plate at that thickness coordinate are calculated using Eqs. (3.3) and (3.10), respectively, taking the value of q as 4.5 GPa.

Before carrying out the study, convergence study is conducted to fix the number of elements and layers. To verify the analysis procedure, the results obtained from the present formulation, for imperforated and perforated plates, are compared with the available results in the literature. Various parametric studies are conducted to investigate the effects of material gradation, geometrical parameters, boundary conditions and loading conditions on nonlinear buckling and postbuckling behavior, and failure response of imperforated and perforated FGM plates.

The current study is carried out for the perforated and imperforated FGM plate with flexural boundary conditions (BCs) clamped on all edges (i.e., CCCC), except for the case where the effects of BCs are studied; wherein, in addition to CCCC (i.e., clamped at all edges), following flexural BCs are also considered for perforated and imperforated FGM plate:

SCSC: simply-supported at $y = 0$ and b edges and clamped at other two edges; SSSS: simply-supported at all edges.

Moreover, in the case of imperforated plate, following two more BCs are also considered while studying the effects of BCs:

SSSC: simply-supported at $x = a$ and $y = 0$ and b edges and clamped at $x = 0$ edge, and SCCC: simply-supported at $y = 0$ edge and clamped at other three edges (i.e., $y = b$, $x = 0$ and $x = a$) .

It is to be noted that in all the above mentioned BCs, the in-plane boundary conditions on edges $x = 0$, $x = b$, $y = 0$ and $y = b$ related to in-plane displacements in x- and y-directions (i.e., u and v, respectively) are taken to be same (as depicted in Fig. 4.2.1 for imperforated FGM plate and in Fig.4.3.1 for perforated FGM plate).

In-plane, uniformly distributed compressive load is applied as follows: on edge $x = a$ for uniaxial compression case and on edges $x = a$ and $y = b$ for biaxial compression case. Results for buckling and failure loads and the transverse deflection are presented in the following non-dimensionalized forms:

In-plane buckling and failure loads: $\frac{N_{x\,(or\,y)}\,b^2}{E_c h^3}$,

Maximum transverse deflection: $\frac{w_{max}}{h}$,

where, E_c is Young's modulus of ceramic, h represents the thickness of FGM plate, b is the width of plate, $N_{x\,(or\,y)}$ is the in-plane compressive load in x-direction (or y-direction) per unit edge length, applied at $x = a$ (or $y = b$), and w_{max} is the maximum transverse deflection.

4.2 Mechanical Stability and Failure Analysis of Imperforated Elastic FGM Plate

4.2.1 Convergence Study

To fix the number of elements in the finite element mesh of FGM plate and the number of layers, a convergence study was conducted for a clamped FGM plate using meshes of 9, 16, and 25 elements for 5, 10, 20 and 30 layers. The convergence of buckling and failure (i.e., yielding) loads was checked for FGM square plate with $b/h = 100$ and $n = 1$, under uniaxial compression. Results of convergence study are shown in Table 4.2.1. It can be observed from Table 4.2.1 that results for buckling and failure loads for FGM plate are converged reasonably for the mesh of 16 elements

(i.e., 4 × 4) when modeled with 20 layers. Schematic of finite element mesh along with element and node-numbering schemes for a typical FGM plate is shown in Fig.4.2.1.

Table 4.2.1: Convergence study for buckling load $\left(\lambda = \frac{N_x b^2}{E_c h^3}\right)$ and failure load $\left(\lambda^* = \frac{N_{fail} b^2}{E_c h^3}\right)$ for CCCC Ti/TiB FGM square plate under uniaxial compression, for b/h = 100 and n = 1.

No. of elements (along x × along y)	No. of layers							
	5		10		20		30	
	λ	λ^*	λ	λ^*	λ	λ^*	λ	λ^*
3 × 3	2.5424	2.7479	2.5328	2.7048	2.5185	2.6810	2.5185	2.6714
4 × 4	4.5113	4.6833	4.4540	4.5591	4.4157	4.5017	4.3966	4.4826
5 × 5	4.4731	4.6881	4.4109	4.5543	4.3727	4.4826	4.3584	4.4635

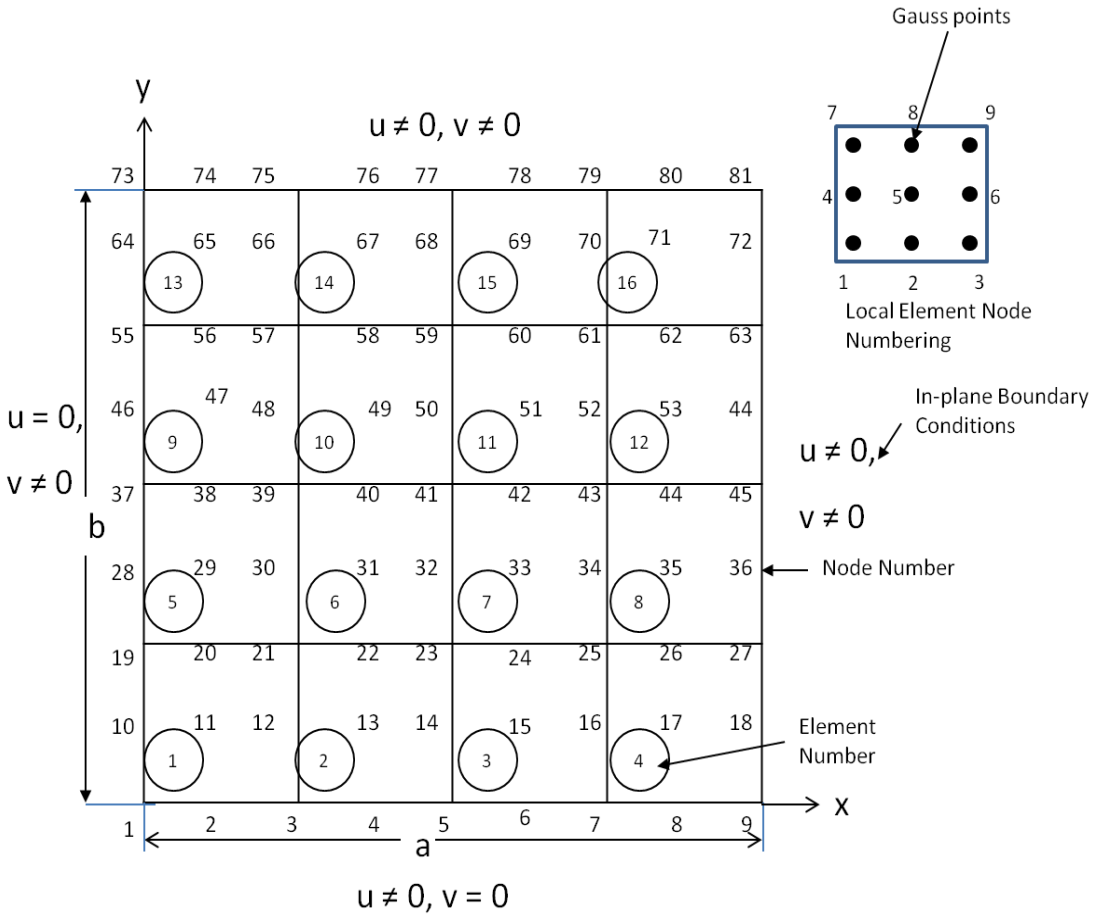

Fig. 4.2.1: Meshing of a typical FGM plate along with in-plane boundary conditions.

4.2.2 Verification of Results

The accuracy of the developed program is checked by comparing the results obtained from the present formulation with those available in the literature (Yamaki, 1961; J. Yang and Shen, 2003). Buckling load and postbuckling response of a thin clamped square plate (with b/h = 236) made of a homogeneous and isotropic material (E = 9.89 msi and ν = 0.326) under uniaxial compression are compared with that reported by Yamaki (1961). It can be seen in Fig. 4.2.2 that results agree well with that of Yamaki (1961). In addition, the results (i.e., buckling and postbuckling responses) are also validated with analytical results presented by Yang and Shen (2003a) for a CCCC square plate (with b/h = 100) made of homogeneous and isotropic materials [i.e., Silicon Nitride (Si_3N_4) having E = 322.2715 GPa & ν = 0.24 and Stainless Steel (referred as SUS304) having E = 207.7877 GPa & ν = 0.31776] as well as made of Si_3N_4/ SUS304 FGM (with n = 3) under uniaxial compression. Again, good agreement is achieved between the results of the current study and that of Yang and Shen (2003a), as depicted in Fig. 4.2.3.

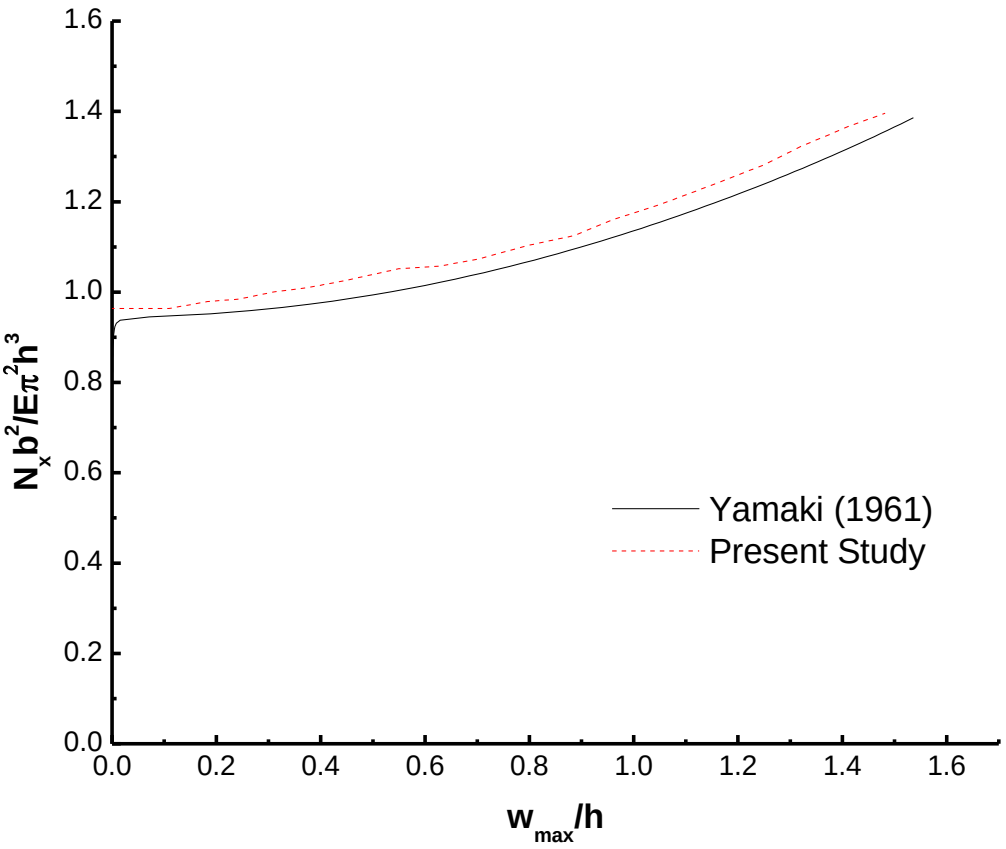

Fig. 4.2.2: Comparison of postbuckling load-deflection curves for an isotropic CCCC square plate under uniaxial compression obtained in the present study with Yamaki (1961).

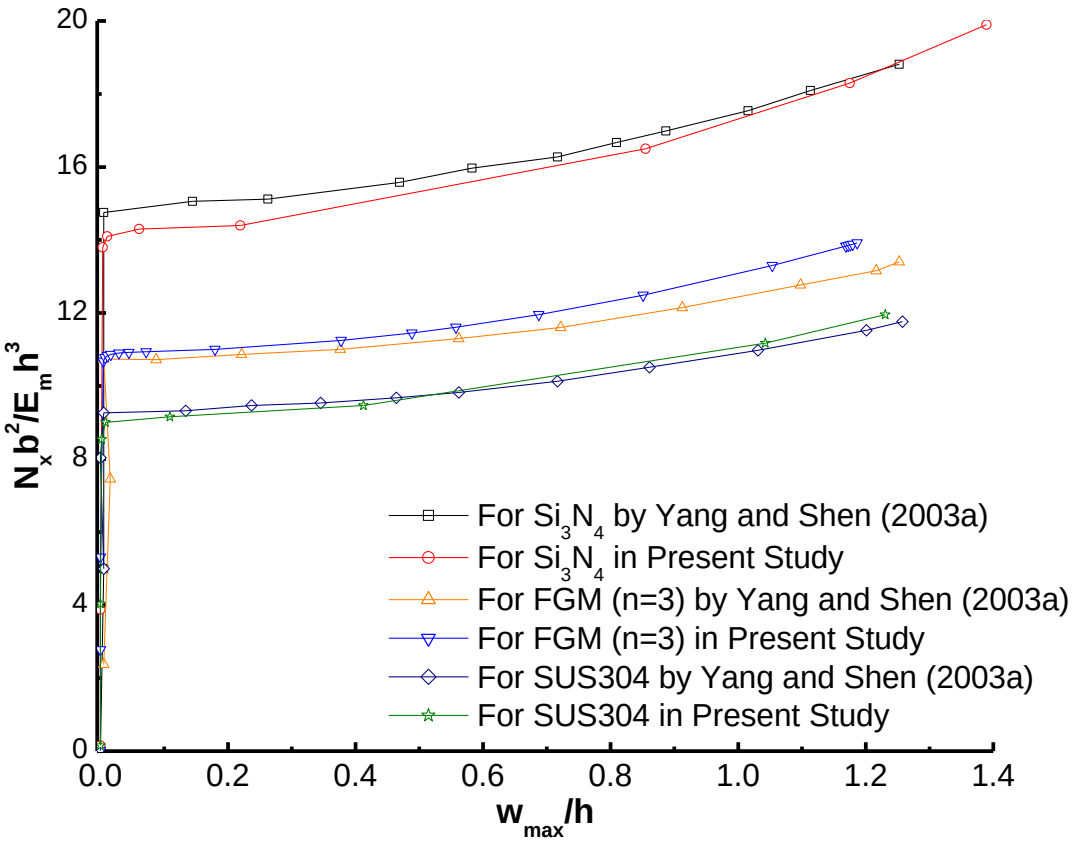

Fig. 4.2.3: Comparison of postbuckling load-deflection curves for Si_3N_4, SUS304 and FGM clamped square plate under uniaxial compression obtained in the present study with Yang and Shen (2003a).

4.2.3 Numerical Results and Discussion

Numerical studies are conducted to examine the effects of various parameters, viz. material inhomogeneity (i.e., power exponent *n*), boundary conditions, aspect ratio (i.e., *a*/*b*), slenderness ratio (i.e., *b*/*h*), and loading conditions (uniaxial and biaxial in-plane compression) on the buckling and postbuckling behavior, and the failure response of imperforated FGM plate.

The effects of material gradation (i.e., exponent *n*) on buckling load, postbuckling response, and failure of Ti/TiB CCCC FGM plate under uniaxial compression load are plotted in Fig. 4.2.4, and the corresponding values of non-dimensionalized buckling load, failure load and maximum transverse deflection at failure point are tabulated in Table 4.2.2. Moreover, the critical buckling mode shapes for Ti/TiB CCCC FGM plate with different values of power law index is depicted in Fig. 4.2.5. It can be observed from Fig. 4.2.4 and Table 4.2.2 that the buckling and failure loads of FGM plate is increased considerably as compared than that of a pure metal plate (i.e., corresponding to $n = 0$).

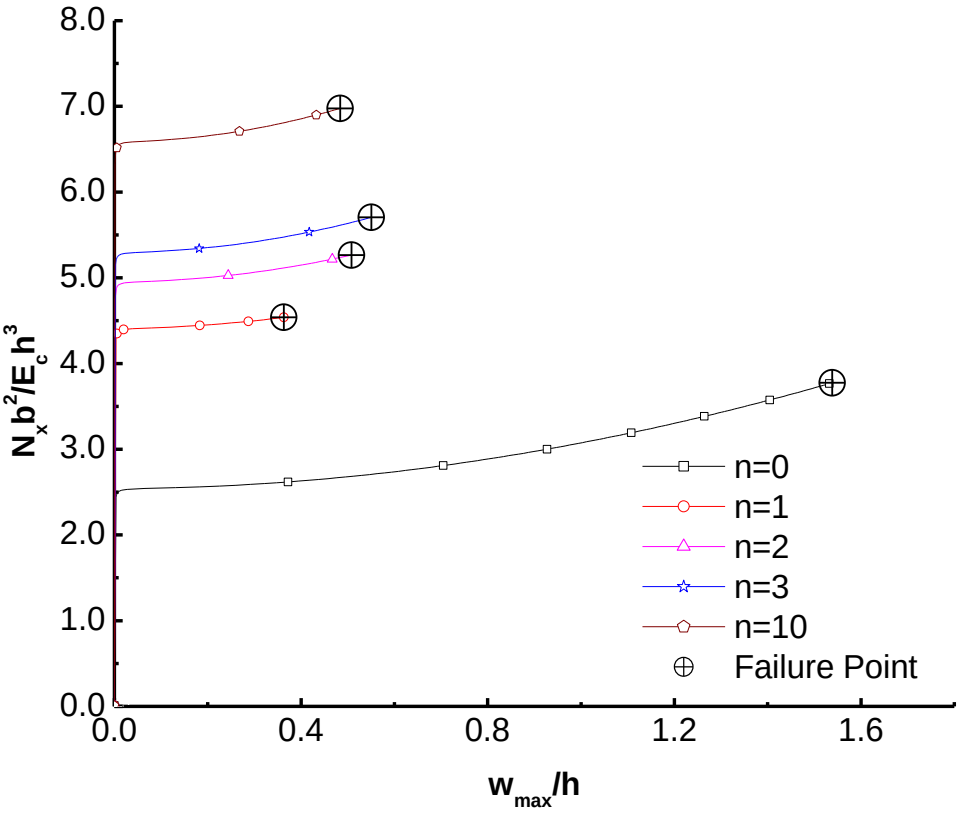

Fig. 4.2.4: Effect of material gradation on the postbuckling behavior of FGM plate under uniaxial compression.

Table 4.2.2: Buckling load and failure characteristics of the square CCCC Ti/TiB FGM plate under uniaxial compression.

n	Non-dimensionalized buckling load	Non-dimensionalized failure load	Non-dimensionalized maximum deflection at failure
0	2.55	3.77	1.53
1	4.42	4.53	0.36
2	4.96	5.26	0.50
3	5.31	5.70	0.55
10	6.61	6.97	0.48

It is important to mention that by increasing the value of *n*, proportion of TiB (which has higher buckling strength) content is increased that resulted in the increase of buckling load of FGM. It is further to be noted from Fig. 4.2.4 that FGM plate has slightly improved reserved postbuckling strength as well as stiffness (given by the slope of the load-deflection curve) after buckling, but before failure.

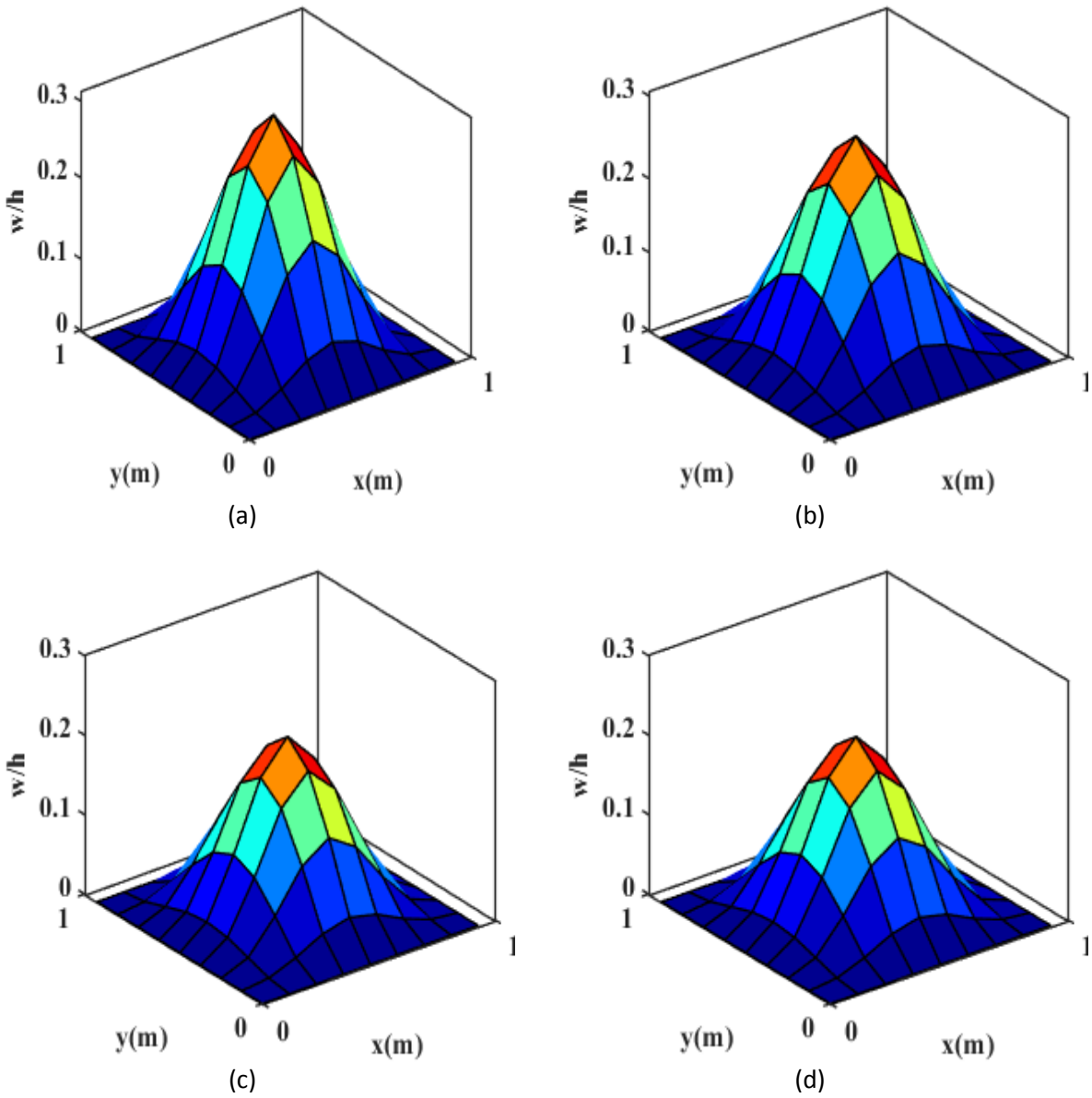

Fig. 4.2.5: Mode shapes corresponding to critical buckling load for a square CCCC Ti/TiB FGM plate with (a) n = 0, (b) n = 1, (c) n = 3, and (d) n = 10, under uniaxial compression.

The effect of flexural boundary conditions on postbuckling paths of FGM plate (for n = 1), subjected to uniaxial compression, is shown in Fig. 4.2.6. The load-deflection curves for five types of boundary conditions, abbreviated as CCCC, SCCC, SCSC, SSSC, SSSS (as specified in Section 4.1), are compared. It can be observed from Fig. 4.2.6 that CCCC plate depicts the highest buckling and postbuckling strengths whereas for SSSS plate the values are lowest. The maximum transverse deflection at the time of failure is minimum for CCCC FGM plate condition, whereas it is maximum for SSSS and SSSC boundary conditions.

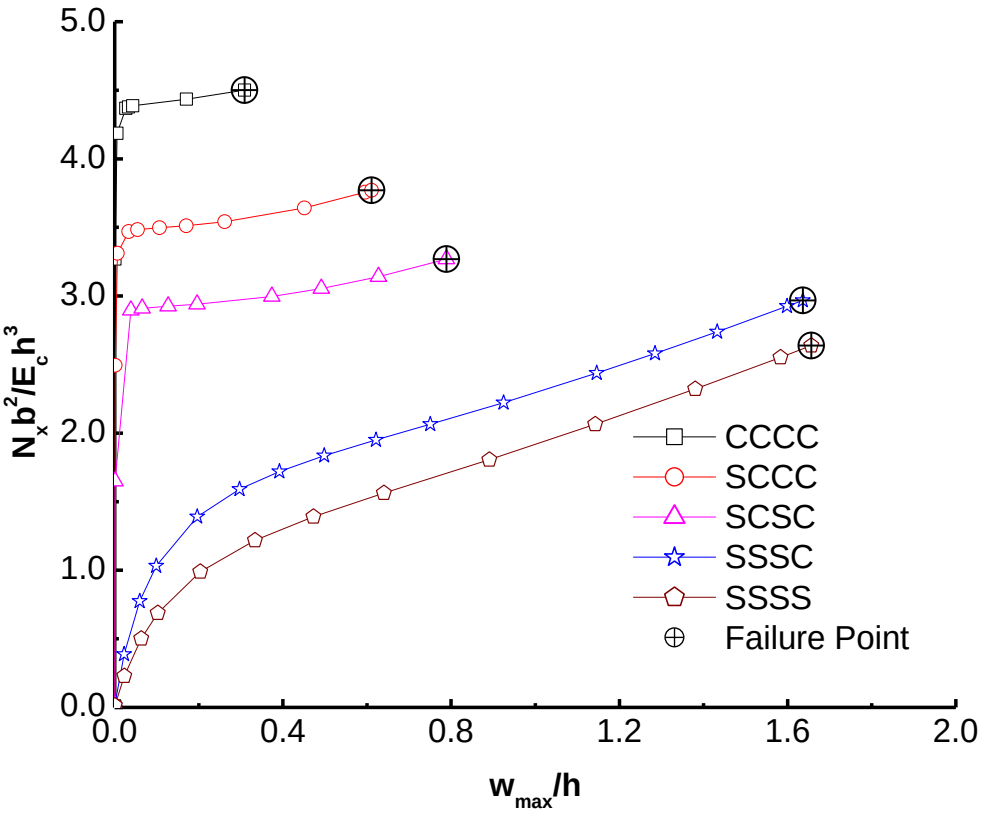

Fig. 4.2.6: Effects of flexural boundary conditions on postbuckling path and failure of FGM plate.

These findings can be attributed to the fact that increase in the rigidity of supports on edges of FGM plate results in the increase of buckling and postbuckling strengths and decrease in the transverse deflection. Moreover, it can also be noticed from Fig. 4.2.6 that the bifurcation buckling phenomenon remains absent in FGM plate with SSSS and SSSC boundary conditions, due to a higher degree of bending-extensional coupling, which causes transverse deflection even in the absence of any bending load. This finding is in good concurrence with the findings of various previous studies. For instance, in the studies on composite plates, Leissa (1986) and Qatu & Leissa (1993) concluded that although the clamped edge constraints supply the necessary bending moment to overcome the stretching-bending coupling effect and to keep the plate flat under in-plane compressive loading; but the simply-supported plate requires the external bending moment to remain flat and to possess bifurcational type of instability. Further, extending the work of Leissa (1986), Aydogdu (2008) applied the same method for FGM plates and found that like unsymmetrical composite plate, the FGM plate does not undergo the bifurcation-type of buckling unless the edges are clamped. Further, it can also be noted from Fig. 4.2.6 that the FGM plate with SSSC

and SSSS boundary conditions possesses postbuckling reserve strength and stiffness beyond buckling.

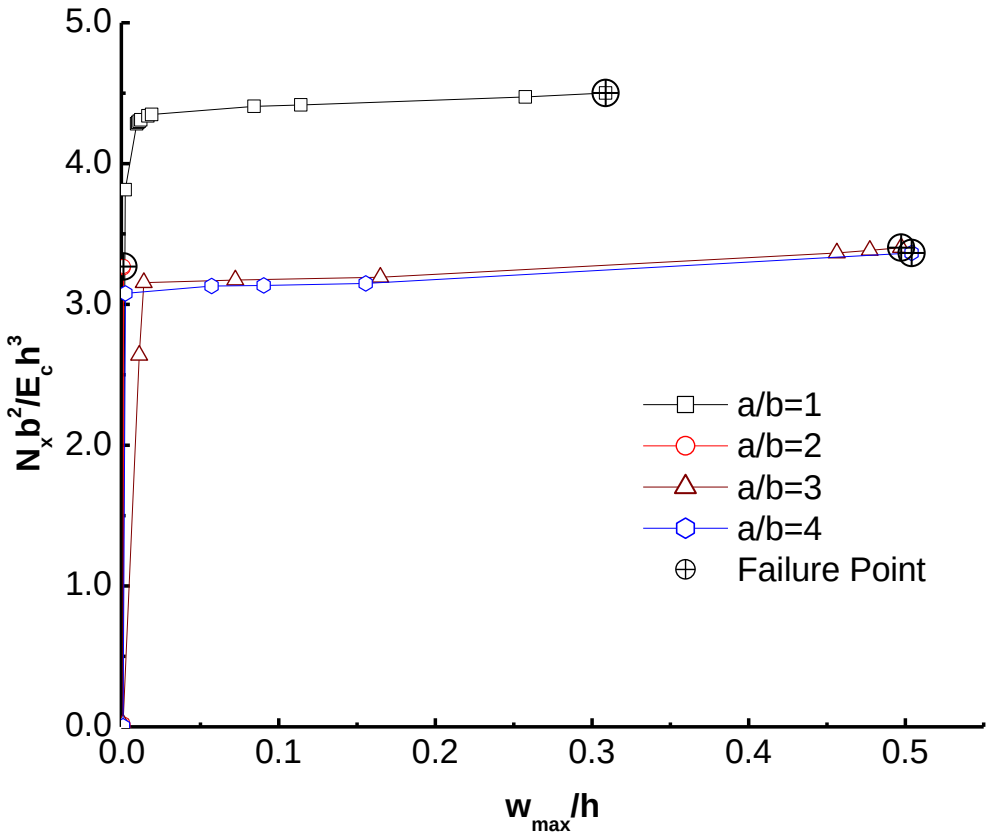

Fig. 4.2.7: Effect of aspect ratio on the postbuckling behavior of CCCC FGM (for n = 1) plate under uniaxial compression.

Table 4.2.3: Effect of slenderness ratio (i.e., b/h) on buckling and failure loads of CCCC Ti/TiB FGM plate under uniaxial compression.

b/h	Buckling load		Failure load	
	Dimensional (kN)	Non-Dimensional	Dimensional (kN)	Non-Dimensional
100	462.95	4.42481	474.94	4.53949
80	898.00	4.39451	732.00	3.58216
50	3650.00	4.36081	1166.00	1.39307
40	7090.00	4.33701	1455.00	0.89003
20	54250.0	4.14814	2899.90	0.22174

The effects of plate aspect ratio (i.e., a/b) and slenderness ratio (i.e., b/h) on buckling and postbuckling behavior of CCCC FGM (for n = 1) plate under uniaxial compression are shown in Fig. 4.2.7 and Table 4.2.3, respectively. It can be seen from Fig. 4.2.7 that buckling load and postbuckling strength (for a particular value of transverse deflection) are found to be maximum for square FGM plate (i.e., for a/b =1). Further, the buckling and postbuckling responses, and failure load of FGM plate for a/b = 3 & 4 are almost same. These findings are in good concurrence with the

similar findings reported by Wu *et al.* (2007), wherein it is attributed to the fact that FGM plate with a/b = 3 or higher would behave like a beam. It is also important to note from Fig. 4.2.7 that the FGM plate with a/b = 2, the failure occurs before the buckling and hence, there is no postbuckling strength possessed by the plate.

The effects of slenderness ratio (i.e., b/h) on buckling and failure loads (in dimensional and non-dimensional forms) of CCCC FGM (for n = 1) plate under uniaxial compression are given in Table 4.2.3. The results depict that there is no significant effect of slenderness ratio on the value of non-dimensional buckling load, but in dimensional form, the buckling load shows increasing trend with the decrease in slenderness ratio. Moreover, it is worth to mention that for slenderness ratios 20, 40, 50 and 80, failure of the FGM plate occurs before the buckling begins. The above discussion explains that thin FGM plate is expected to buckle before the stresses reach to a critical level as defined by the criterion, whereas thick FGM plate would resist buckling and fail because of large stresses developed inside the FGM.

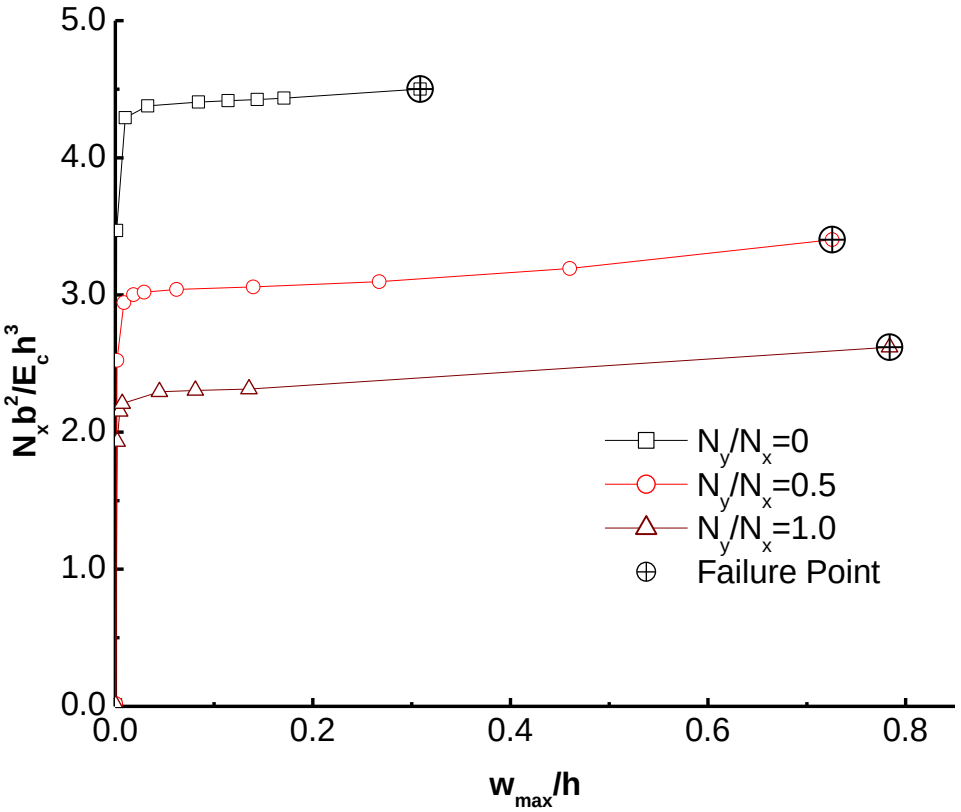

Fig. 4.2.8: Postbuckling behavior of CCCC Ti/TiB FGM (for n = 1) plate under combined in-plane compressive load.

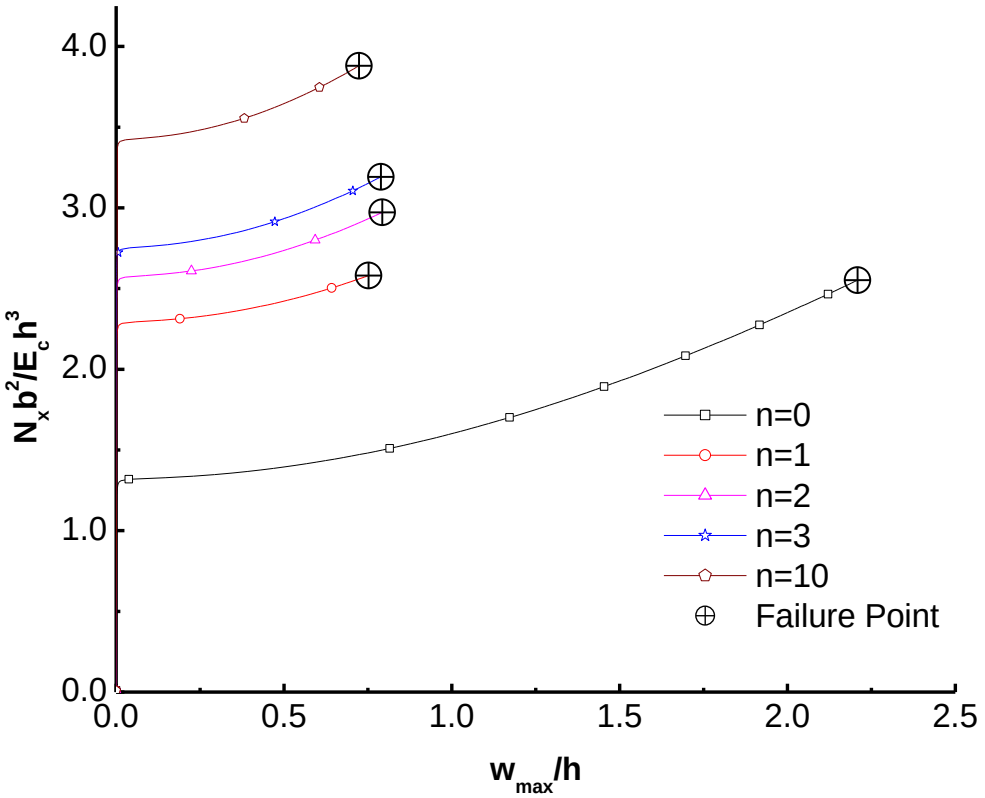

Fig. 4.2.9: Effect of power exponent *n* on postbuckling behavior of CCCC Ti/TiB FGM plate under biaxial compression (with $N_x = N_y$).

Table 4.2.4: Failure characteristics of the square CCCC Ti/TiB FGM plate under biaxial compression (with $N_x = N_y$).

Exponent *n*	Non-dimensionalized buckling load	Non-dimensionalized failure load	Non-dimensionalized maximum deflection at failure
0	1.3284	2.55167	2.20892
1	2.3032	2.58034	0.75231
2	2.58034	2.97217	0.7929
3	2.76192	3.19198	0.78851
10	3.44046	3.88007	0.72331

The postbuckling paths for a CCCC square FGM (for n = 1) plate of slenderness ratio 100 under combined in-plane compressive loads with different load ratios (i.e., N_y/N_x) are plotted in Fig. 4.2.8. The results show that maximum buckling load, postbuckling strength (for a particular value of strength) and failure load are obtained for plate under uniaxial compression (i.e., for $N_y/N_x = 0$). The postbuckling load-deflection curves become significantly lower as the N_y is increased, but it causes the increase in maximum transverse deflection corresponding to the failure point.

The effects of material gradation (i.e., exponent *n*) on buckling load, postbuckling response, and failure of Ti/TiB CCCC FGM plate under biaxial compression load, with $N_y = N_x$, are plotted in Fig. 4.2.9, and the corresponding non-dimensionalized values of the buckling load, failure load and maximum transverse deflection at failure point are tabulated in Table 4.2.4. It can be observed from Fig. 4.2.9 and Table 4.2.4 that the buckling and postbuckling strengths and failure load of FGM under biaxial compression are improved as compared to pure metal (i.e., for $n = 0$) and it show increasing trends with an increase in the value of *n*. It can also be observed that the values of buckling and failure loads of FGM plate under biaxial compression are decreased significantly in comparison to the corresponding values (Refer Fig. 4.2.9 and Table 4.2.4) under uniaxial compression load.

4.2.4 Conclusions

A study on non-linear finite element analysis of Ti/TiB FGM plate under in-plane compression is conducted. The elastic failure of the FGM plate is predicted by applying 3-D von-Mises criterion. After validating the results of the present formulation with the available results in the literature, the effects of material gradation (i.e., material inhomogeneity), geometrical parameters (i.e., aspect ratio and slenderness ratio), boundary conditions and loading conditions on non-linear buckling and postbuckling behavior, and failure of FGM plate are investigated. Based on the present work, following important conclusions are drawn.

- The buckling and postbuckling strengths and failure load of CCCC Ti/TiB FGM plate are increased considerably as compared to that of the pure metal plate under uniaxial as well as biaxial compression, and it shows increasing trends with an increase in the value of power law exponent *n*.
- Under uniaxial compression, increase in the rigidity of support on the edges of FGM plate results in the increase of buckling and postbuckling strengths and failure load, and reduces the transverse deflection; whereas SSSC and SSSS boundary conditions provide significant postbuckling reserve strength and stiffness to the FGM plate beyond buckling.
- Thin clamped FGM plate is expected to buckle before the stresses reach to a critical level as defined by the von-Mises criterion, whereas thick FGM plate

would resist buckling and fail, as per the criterion, because of large stresses developed in the FGM.

- Under biaxial loading, the postbuckling load-deflection curves become significantly lower (meaning thereby decrease in buckling and postbuckling strengths) as the N_y is increased, but it causes the increase in maximum transverse deflection corresponding to the failure point.

4.3 Mechanical Stability and Failure Analysis of Perforated Elastic FGM Plate

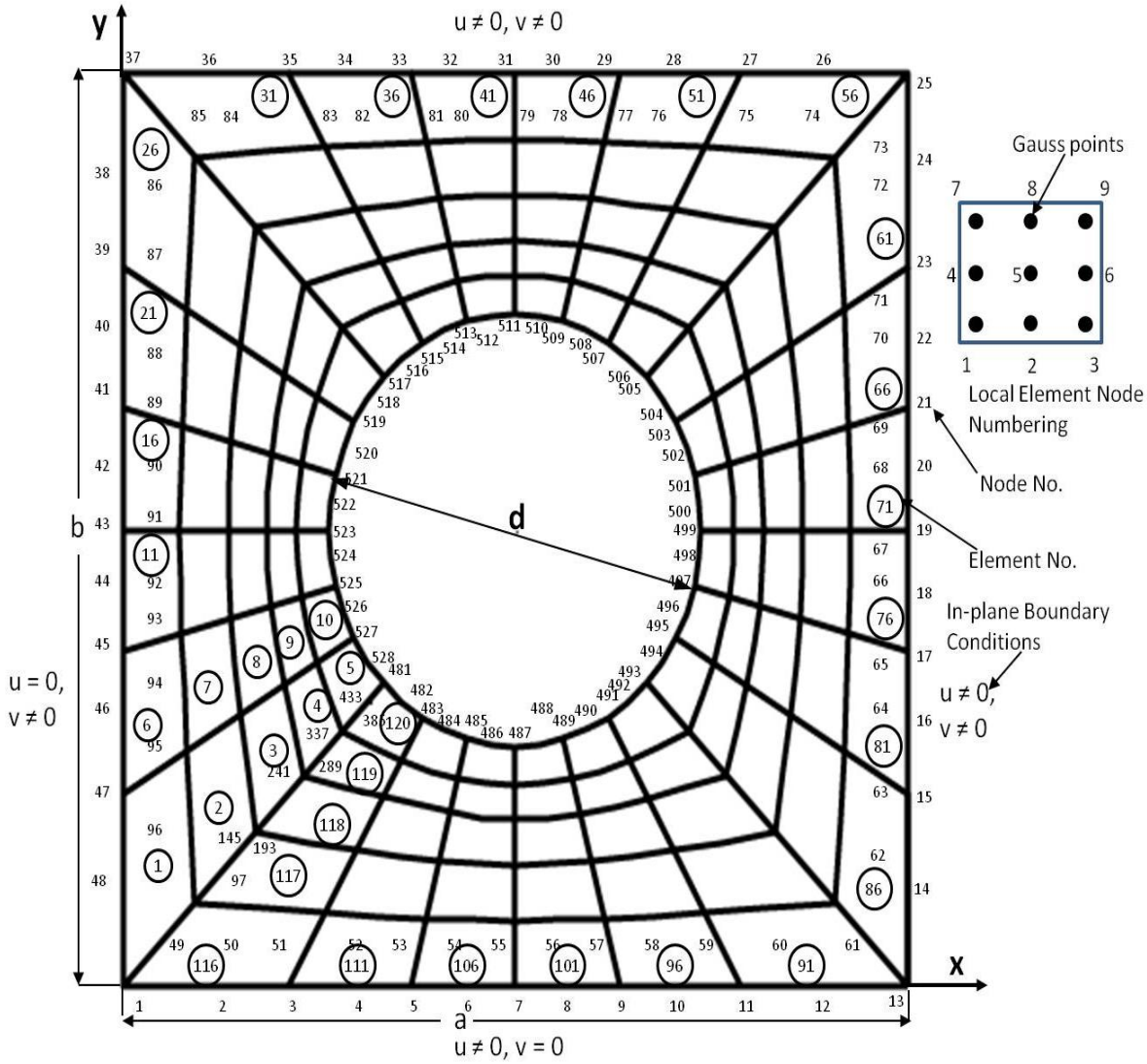

Fig. 4.3.1: Meshing of a typical perforated FGM plate along with in-plane boundary conditions.

4.3.1 Convergence Study

To fix the number of elements in the finite element mesh and the number of layers to model the FGM plate, a convergence study was conducted for a clamped (i.e., CCCC), square perforated Ti/TiB FGM (for n = 1) plate with centrally located circular hole of size $d/b = 0.1$ using 48, 72, 96, 120 and 144 elements having 10, 20, 30 and 40 layers. The convergence of buckling and elastic failure loads was checked under uniaxial compressive load, and the results are given in Table 4.3.1. It can be

observed from Table 4.3.1 that a reasonably good convergence of buckling loads and failure loads is obtained for the mesh of 120 elements having 30 layers. Schematic of finite element mesh along with element- and node-numbering schemes for a typical perforated FGM plate is shown in Fig. 4.3.1.

Table 4.3.1: Results of convergence study for buckling load $\left(\lambda = \frac{N_x b^2}{E_c h^3}\right)$ and failure load $\left(\lambda^* = \frac{N_{fail} b^2}{E_c h^3}\right)$.

Nos. of elements	No. of layers							
	10		20		30		40	
	λ	λ^*	λ	λ^*	λ	λ^*	λ	λ^*
48	4.5495	5.6965	4.5113	5.6583	4.5113	5.6200	4.5016	5.5698
72	4.4540	5.8876	4.2054	5.5818	4.0525	5.5053	4.1201	5.3409
96	4.2054	5.7347	4.1672	5.4671	4.1672	5.4671	4.1290	5.3409
120	4.1672	5.6583	4.1290	5.3906	4.1290	5.2759	4.1290	5.2646
144	4.1672	5.5818	4.1290	5.3142	4.1290	5.2377	4.1290	5.2646

4.3.2 Verification of Results

The accuracy of the developed program for perforated plate is checked by comparing the results obtained using the present formulation with the results available in the existing literature. A thin square plate (*b/h=100*) containing a central circular hole (of various sizes) under in-plane (uniaxial and biaxial) compressive loading conditions is considered to make the comparison of results with those published by Sabir and Chow (1986). The plate is considered to be made of isotropic and homogenous material with Young's modulus, E = 207 GPa, and Poisson's ratio, ν = 0.3 that are same as used by Sabir and Chow (1986). Buckling load (normalized as: $\frac{12\langle 1-\nu^2\rangle}{\pi^2}\frac{N_{cr}b^2}{Eh^3}$) are compared for simply-supported and clamped boundary conditions. The results of the comparison are shown in Table 4.3.2. It can be observed that the results obtained from the present work are in reasonably satisfactory agreement with the results as reported by Sabir and Chow (1986).

Table 4.3.2: Verification of Results.

Boundary condition	Loading condition	*d*/*b* ratio	Normalized buckling load $\left(\frac{12(1-\nu^2)}{\pi^2}\frac{N_{cr}b^2}{Eh^3}\right)$	
			Present study	Sabir and Chow (1986)
SSSS	Uniaxial	0.1	3.81	3.80
		0.3	3.19	3.20
		0.5	2.91	2.90
	Biaxial	0.1	1.91	1.88
		0.3	1.77	1.75
		0.5	1.66	1.65
CCCC	Uniaxial	0.1	9.40	9.45
		0.3	8.93	9.04
		0.5	10.90	9.40
	Biaxial	0.1	5.07	4.88
		0.3	5.27	5.10
		0.5	7.86	7.60

4.3.3 Numerical Results and Discussion

Various numerical studies are conducted here to examine the effects of various parameters, viz. material inhomogeneity (i.e., power exponent *n*), slenderness ratio (i.e., *b*/*h*), boundary conditions (i.e., SSSS, SCSC and CCCC), hole-size (i.e., *d*/*b* ratio) and loading conditions (uniaxial and biaxial in-plane compression) on the buckling and postbuckling behavior, and the failure response of perforated FGM plate. A Ti/TiB FGM square plate (of side 279 mm) with a central circular hole is considered.

To investigate the effect of material inhomogeneity (i.e., power exponent *n*), a CCCC FGM plate with a circular hole is considered under uniaxial compression. The width-to-thickness ratio (i.e., slenderness ratio, *b*/*h*) was taken to be 200. The ratio of the diameter of the circular hole to the width of the plate (i.e., *d*/*b*) is taken as 0.1. The corresponding results are given in Table 4.3.3 and plotted in Fig. 4.3.2.

The Fig. 4.3.2 and Table 4.3.3 depict higher value of buckling and failure loads corresponding to FGM plate (i.e., for $n > 0$) as compared to that of the pure metal plate (i.e., for $n = 0$).

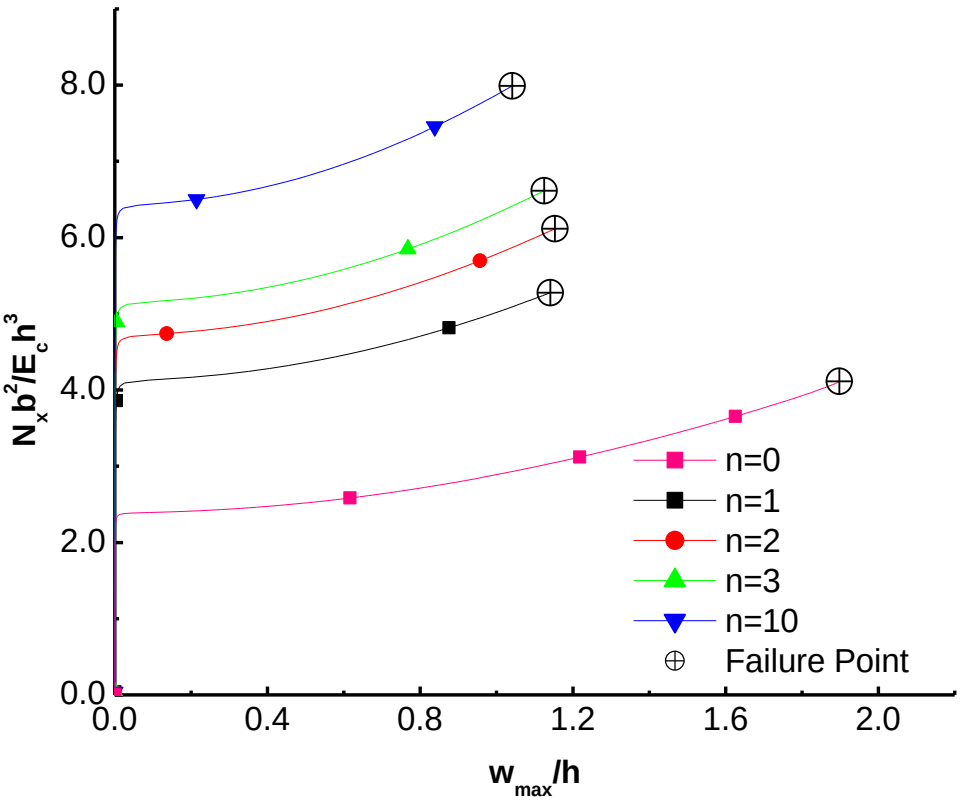

Fig. 4.3.2: Effects of power law exponent (i.e., *n*) on the postbuckling response of square perforated Ti/TiB FGM plate under uniaxial compression.

Table 4.3.3: Buckling load and failure characteristics of the square perforated CCCC Ti/TiB FGM plate under uniaxial compression.

n	Non-dimensionalized buckling load	Non-dimensionalized failure load	Non-dimensionalized maximum deflection at failure
0	2.39	4.11	1.89
1	4.13	5.27	1.14
2	4.74	6.11	1.15
3	5.16	6.61	1.12
10	6.46	7.99	1.04

At this point, it is necessary to mention that the proportions of constituent materials through the thickness of FGM plate are controlled by the value of power law exponent *n* in Eq. (3.2). A higher value of *n* means a high proportion of TiB which possesses higher buckling and failure strengths as compared to that of metal constituent and hence, the buckling and failure strength of the resulting FGM plate is increased. It is further to note from Fig. 4.3.2 that FGM plate also possesses reserved postbuckling strength, whereas the FGM have almost same postbuckling stiffness (given by the slope of the load-deflection curve at a particular value of transverse deflection) as that of the metal constituent. Moreover, it is also to report that for FGM

(n > 0) the failure is found to take place at the hole edge, whereas it happens at the outer edge of the plate for n = 0 (i.e., in the case of pure metal).

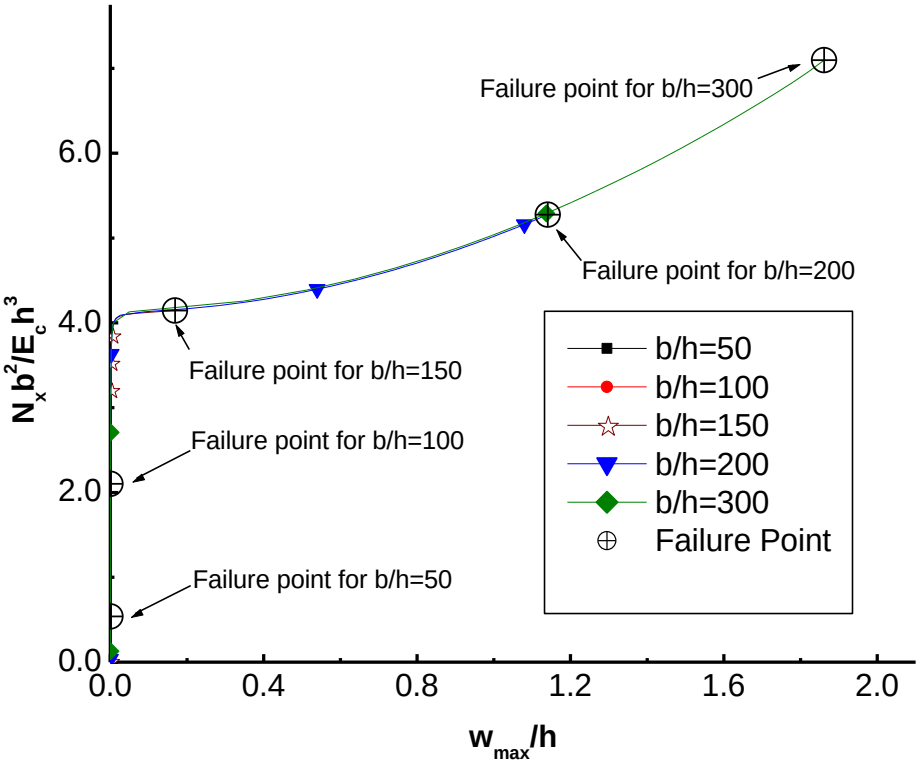

Fig. 4.3.3: Effects of slenderness ratio on postbuckling and failure behavior of perforated FGM plate under uniaxial compression.

Table 4.3.4: Effects of slenderness ratio (*b*/*h*) on buckling load and failure load of the square CCCC TiB/Ti FGM plate (n = 1) under uniaxial compression with a circular hole.

b/*h*	Buckling load		Failure load	
	Dimensional (kN)	Non-Dimensional	Dimensional (kN)	Non-Dimensional
50*	854.57	1.02	449.97	0.53
100*	359.99	3.44	219.99	2.10
150	127.49	4.11	128.49	4.14
200	54.00	4.13	68.99	5.27
300	16.50	4.25	33.99	8.77

* In the cases of *b*/*h* =50 & 100 failure would take place before buckling.

Results of effect of slenderness ratio (i.e., *b*/*h*) on buckling and postbuckling behavior and the failure of clamped FGM (for n = 1) plate with a circular hole (of *d/b=0.1*) under uniaxial compression are shown in Table 4.3.4 and Fig. 4.3.3. The various values of slenderness ratio taken are 50, 100, 150, 200 and 300. It is necessary to mention here that while carrying out the study on the effects of slenderness ratio, the number of layers was increased proportionally based on the convergence study

conducted in Section 4.3.1 to get the converged results. For example, for b/h = 100, the numbers of layers were taken as 60, as against 30 for b/h = 200 calculated in the convergence study carried out in Section 4.3.1. As observed from Fig. 4.3.3 and Table 4.3.4 that although the effect of b/h is not evident in the non-dimensional load-deflection plots (because of the presence of b/h term in non-dimensional form), but the effects of b/h ratio is very significant on dimensional values of buckling and failure loads, as observed in Table 4.3.4. It can also be observed from Fig. 4.3.3 and Table 4.3.4 that for FGM plate with slenderness ratios equal to 50 and 100, failure occurs before the buckling starts, and for all other cases (i.e., b/h = 150, 200 and 300), the FGM fails in the postbuckling region after buckling. The current findings explain that thin FGM plate is expected to buckle before the stresses reach to a critical level as defined by the criterion, whereas thick FGM plate would fail before buckling because of large stresses developed inside the FGM.

Furthermore, Table 4.3.4 shows that the dimensional value of buckling and failure loads are decreased considerably with the decrease in the thickness of FGM plate (i.e., with the increase in b/h). It is to mention here that the observed location of failure in FGM plate for all slenderness ratios remains same at hole edge, except for b/h = 300, wherein the failure occurs at the outer edge of FGM plate.

The effect of circular hole-size (i.e., d/b = 0.1, 0.2, 0.3, 0.4 and 0.5) on the response of clamped FGM (for n = 1) plate (with b/h = 200) under uniaxial compression load is also investigated, and the corresponding results are given in Table 4.3.5 and shown Fig. 4.3.4. It can be observed from Fig. 4.3.4 and Table 4.3.5 that the buckling load decreases slightly with an increase in d/b ratio up to 0.3, but subsequently, the buckling load start increasing with the increase in d/b ratio. As against the conventional wisdom, this peculiar phenomenon of increase in buckling load of clamped FGM plate with a large hole as compared to small hole-size can be explained as follows. When the hole-size becomes greater than d/b = 0.3, it affects the load carrying pattern of the plate with most of the compressive load carried by the narrow side strips of material along the clamped boundaries of the plate. In such cases, the rigid clamped conditions at the boundary edges provide the required rigidity to the load carrying material of the plate which in turn results in the increase in the buckling load of FGM plate with hole sizes larger than 0.3. It is worth mentioning here that similar anomalous findings of increase in buckling load with an increase in hole-size have been reported by many other investigators/researchers for the case of

composite plates but for the right combination of boundary conditions and the plate's aspect ratio (Hu and Lin, 1995; Nemeth, 1996; Prajapat et al., 2015). It can also be observed from Fig. 4.3.4 and Table 4.3.5 that the increase in the hole-size also results in the monotonic decrease in the failure load and associated maximum transverse deflection as well as the postbuckling stiffness (given by the slope of the load-deflection curve at a particular value of deflection) of FGM plate.

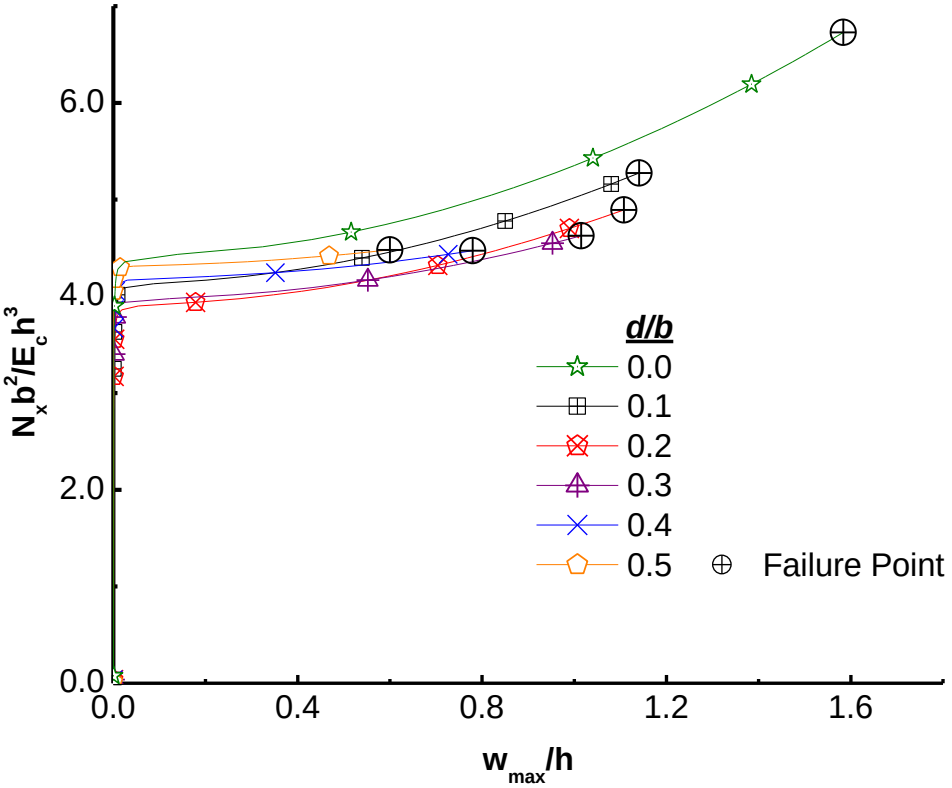

Fig. 4.3.4: Effects of hole-size on buckling and postbuckling responses and failure load of square Ti/TiB FGM (n = 1) plate with a circular hole under uniaxial compression.

Table 4.3.5: Effects of hole-size on buckling and failure characteristics of square Ti/TiB FGM (n = 1) plate with a circular hole under uniaxial compression.

d/b	Non-dimensionalized buckling load	Non-dimensionalized failure load	Non-dimensionalized maximum deflection at failure
0.0	4.43	6.72	1.58
0.1	4.12	5.27	1.14
0.2	3.93	4.89	1.10
0.3	3.97	4.62	1.01
0.4	4.20	4.47	0.77
0.5	4.32	4.48	0.60

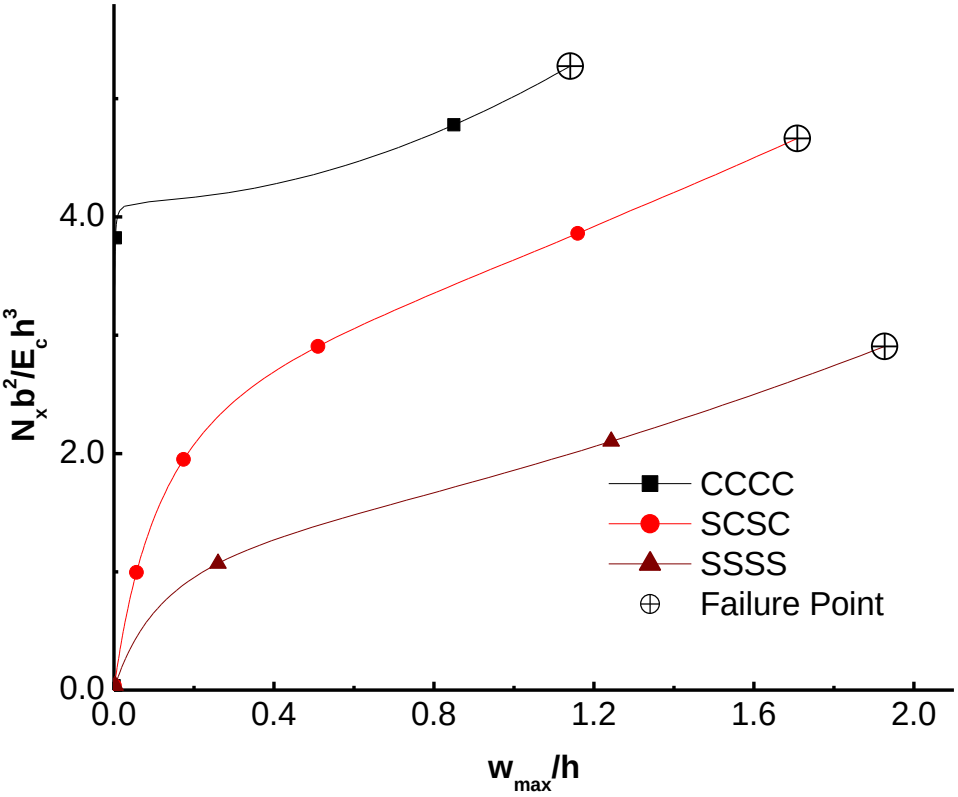

Fig. 4.3.5: Load-deflection response and failure of perforated FGM plate with different boundary conditions.

Fig. 4.3.5 contains the plots corresponding to the effects of boundary conditions (i.e., SSSS, SCSC and CCCC) on the buckling and postbuckling behavior, and the failure response of FGM (for n = 1) plate (b/h = 200) with a circular hole of size d/b = 0.1 under uniaxial compression. It can be observed from Fig. 4.3.5 that CCCC plate depicts the highest buckling and postbuckling strength (for a particular value of deflection) and failure load whereas for SSSS plate the values are the lowest. The maximum transverse deflection at the time of failure is minimum for CCCC FGM plate condition, whereas it is maximum for SSSS boundary condition. These findings can also be attributed to the fact that increase in the rigidity of supports on the edges of FGM plate results in the increase of buckling and postbuckling strengths and failure load, and the decrease in transverse deflection.

The effects of loading conditions (i.e., in-plane uniaxial and biaxial compression) on the buckling and postbuckling responses, and failure of clamped FGM (for n = 1) plate (of b/h = 200) with a circular hole of size d/b = 0.1 are investigated, and the corresponding results are plotted in Fig. 4.3.6. The results show that maximum buckling load is obtained for plate under uniaxial compression (i.e., for $N_y/N_x = 0$) as

compared to biaxial loading. The postbuckling load-deflection curve becomes significantly lower as the N_y is increased, but it causes the increase in maximum transverse deflection corresponding to the failure point.

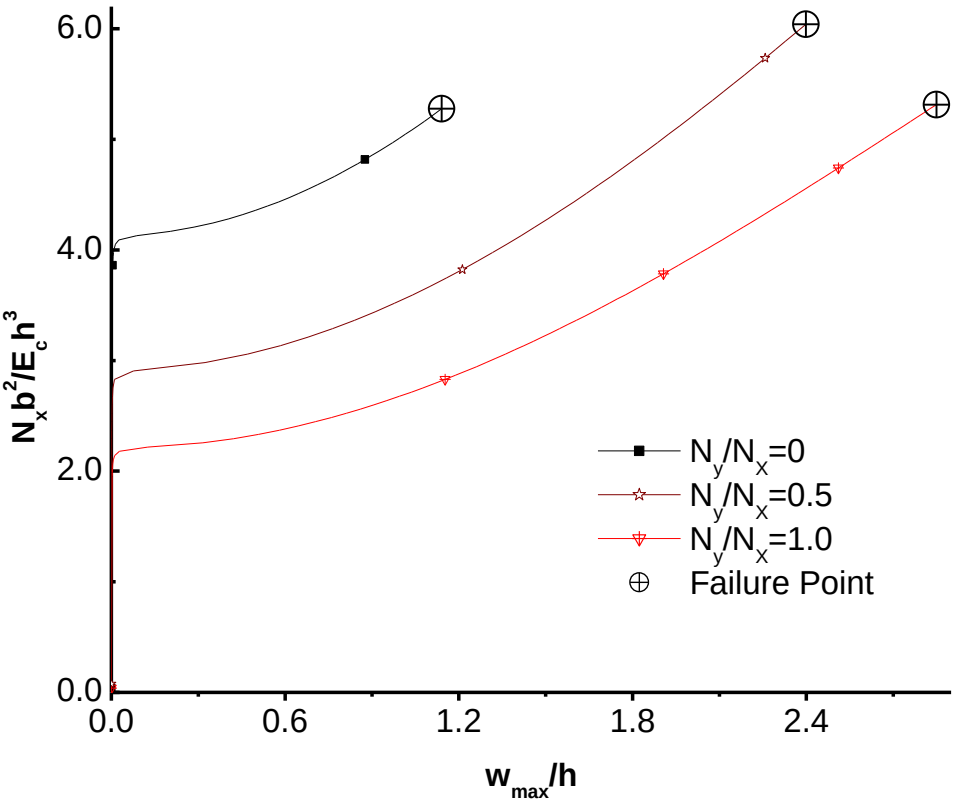

Fig. 4.3.6: Load-deflection response of perforated CCCC Ti/TiB FGM (for n = 1) plate under in-plane uniaxial and biaxial compression.

4.3.4 Conclusions

Based on the present formulation and the various numerical studies conducted on perforated Ti/TiB FGM square plate to examine the effects of various parameters, viz. material inhomogeneity (i.e., power exponent n), slenderness ratio (i.e., b/h), boundary conditions (i.e., SSSS, SCSC and CCCC), hole-size (i.e., d/b ratio) and loading conditions (uniaxial and biaxial in-plane compression) on the buckling and postbuckling behavior, and the failure response of FGM plate, following important conclusions are drawn.

- The FGM plate with a central hole under uniaxial compression exhibits a monotonic increase in buckling and postbuckling strength with the increase in the value of power law exponent n. FGM plate with a hole is also found to possess reserved postbuckling

strength, whereas the postbuckling stiffness is found to be same as that of the metal constituent.

- The thin FGM plate with a hole buckles before the stresses reach to a critical level, whereas the thick FGM plate with a hole would fail before buckling because of large stresses developed inside the FGM.
- In the case of FGM plate with large hole-size, the rigid clamped conditions at the boundary edges of the FGM plate are found to provide the required rigidity to increase its buckling load as compared to small hole-size.
- Increase in the hole-size results in a monotonic decrease in the failure load and associated maximum transverse deflection as well as the postbuckling stiffness of FGM plate.
- The effects of applying a compressive load in the *y*-direction, in addition to axial compressive load in the *x*-direction, are to decrease the buckling load and lowering of postbuckling load-deflection curves, but it results in the increase in maximum transverse deflection corresponding to the failure point.

CHAPTER 5

STABILITY ANALYSIS OF ELASTIC FGM PLATE WITH TEMPERATURE-DEPENDENT MATERIAL PROPERTIES UNDER THERMAL LOAD

5.1 Introduction

In this chapter, the nonlinear thermoelastic stability analysis of imperforated and perforated Ni/Al_2O_3 FGM plates with temperature-dependent material properties is carried out. The FGM plate is assumed to be made of two constituents: Al_2O_3 (i.e., ceramic phase) and Ni (i.e., metallic phase). The effect of temperature-dependent material properties of FGM on non-linear thermal postbuckling response of FGM plate is examined by taking the material property P_j (i.e., Young's modulus and thermal expansion coefficient) as a non-linear function of temperature, as defined in Eq. (3.1) of Chapter 3. The thermoelastic material properties of FGM plate are calculated using Mori-Tanaka homogenization scheme as discussed in Section 3.2 of Chapter 3. Convergence studies are conducted to fix the number of elements and layers in FEM models for both imperforated and perforated FGM plates. The accuracy of present FEM model has been verified by comparing the thermal buckling and postbuckling response obtained using present formulation with the available results in the literature. Numerical studies are conducted to examine the effect of temperature-dependent material properties on thermal buckling and postbuckling responses of imperforated and perforated FGM plates. In addition, the effects of different material and geometrical parameters, viz. material inhomogeneity, slenderness ratio, and aspect ratio, on the nonlinear thermal stability of both imperforated and perforated FGM plates, with various flexure boundary conditions, are also examined through parametric studies. Moreover, the effects of cutout shape and size on thermal buckling and postbuckling response of perforated FGM plate are also investigated. It is to mention that unless otherwise stated, the FGM plate is graded linearly by assuming power law index equal to unity (i.e., $n = 1$), and likewise, the slenderness ratio of FGM plate is kept 100 for all cases except the case wherein the effect of slenderness ratio is studied. Similarly, TD material properties are

considered for all cases except for the case wherin the effects of TD and TID material properties on thermal buckling and postbuckling responses are examined.

The current study is carried out for a FGM plate with all edges simply-supported having freely movable edges, namely BC1, with prescribed displacements and rotations at various edges as follows. The associated in-plane boundary conditions on different edges for BC1 case are shown in Fig. 5.2.1 for imperforated FGM plate, and in Fig. 5.3.1 for perforated FGM plate.

BC1 (simply-supported with freely movable edges):

$u = 0, v \neq 0, w = 0, \theta_x \neq 0, \theta_y = 0$ at $x = 0$ & a,

$u \neq 0, v = 0, w = 0, \theta_x = 0, \theta_y \neq 0$ at $y = 0$ & b.

While studying the effects of BCs on thermal buckling and postbuckling behavior of imperforated and perforated FGM plates, in addition to BC1, other two boundary conditions, namely BC2 and BC3 are also considered. BC2 refers to all edges simply-supported with immovable edges, and BC3 refers to all edges clamped. Displacements and rotations at various edges of the plates corresponding to BC2 and BC3 boundary conditions are given below.

BC2 (simply-supported with immovable edges):

$u = 0, v = 0, w = 0, \theta_x \neq 0, \theta_y = 0$ at $x = 0$ & a,

$u = 0, v = 0, w = 0, \theta_x = 0, \theta_y \neq 0$ at $y = 0$ & b.

BC3 (clamped on all edges):

$u = 0, v = 0, w = 0, \theta_x = 0, \theta_y = 0$ at $x = 0$ & a,

$u = 0, v = 0, w = 0, \theta_x = 0, \theta_y = 0$ at $y = 0$ & b ,

where, u, v and w are the displacement components in *x*, *y* and z directions respectively; θ_x and θ_y represent the mid-plane rotation of the normal about the *y* and *x* axes, respectively.

Results for thermal (buckling and postbuckling) load and the transverse deflection are presented in the following non-dimensionalized forms:

Thermal load, $\lambda = \alpha_c \Delta T \times 10^3$,

Maximum transverse deflection, = $\frac{w_{max}}{h}$,

where, α_c is thermal expansion coefficient of ceramic, h represents thickness of the FGM plate, ΔT is uniform temperature rise, and w_{max} is the maximum transverse deflection. ΔT denoted the temperature rise with respect to ambient temperature, i.e., $\Delta T = T_{final} - T_{ambient}$. Hence absolute value of temperature considered to calculate TD

properties is given by $T_{final} = \Delta T + T_{ambient}$. The value of ambient temperature taken in thesis is 27^0C (i.e., 300 K). This practice is followed throughout in the thesis.

5.2 Thermal Stability Analysis of Imperforated Elastic FGM Plate

5.2.1 Convergence-cum-Validation Study

To verify the present FEM based formulation, the thermal buckling load of an Al/Al_2O_3 FGM plate under uniform temperature rise is compared with that reported by Zhao *et al.* (2009). The material and geometrical parameters are kept same as taken by Zhao *et al.* (2009), and comparison of thermal buckling loads of FGM plate for SSSS (designated as BC2 in present thesis) and CCCC (designated as BC3 in prsented thesis) are given in Table 5.2.1. While carrying out the verification study, a convergence study is also conducted to fix the number of elements, and the number of layers across the thickness of FGM plate. FGM plate is assumed to be composed of 10, 20 and 40 layers across the thickness. The corresponding results are also shown in the Table 5.2.1. As noted from Table 5.2.1, a reasonable convergence of thermal buckling load is observed for 20 number of layers while considering 10 × 10 elements. Moreover, a satisfactory agreement between thesis and Zhao et al. (2009) results for clamped FGM plate and for simply supported & clamped homogenous (i.e., n = 0) plates can be observed from Table 5.2.1. However present results are different from that obtained by Zhao et al. (2009) for simply-supported (SSSS) FGM plate, this discrepancy between results may be attributed to the fact that Zhao et al. (2009) performed linear bifurcation analysis to calculate thermal buckling load of FGM plates contrary to present work wherein nonlinear analysis is adopted.

As mentioned in previous studies (Prakash et al., 2009), the clamped FGM plates and simply-supported & clamped homogenous (i.e., n = 0) plates, posses bifurcation buckling and can be studied using linear analysis. However, due to the presence of nontrivial stretching-bending coupling matrix bifurcation buckling remain absent in simply-supported FGM plates, and hence linear analysis may not predict the actual buckling load. and the results also agree well with that obtained by Zhao *et al.* (2009). Moreover, the thermal buckling and postbuckling response under uniform temperature rise obtained from the present non-linear FEM formulation is validated for a simply-supported square plate (of *b/h =10*) made of a homogeneous and isotropic material with that reported by Shen (2007) (refer Fig. 5.2.2).

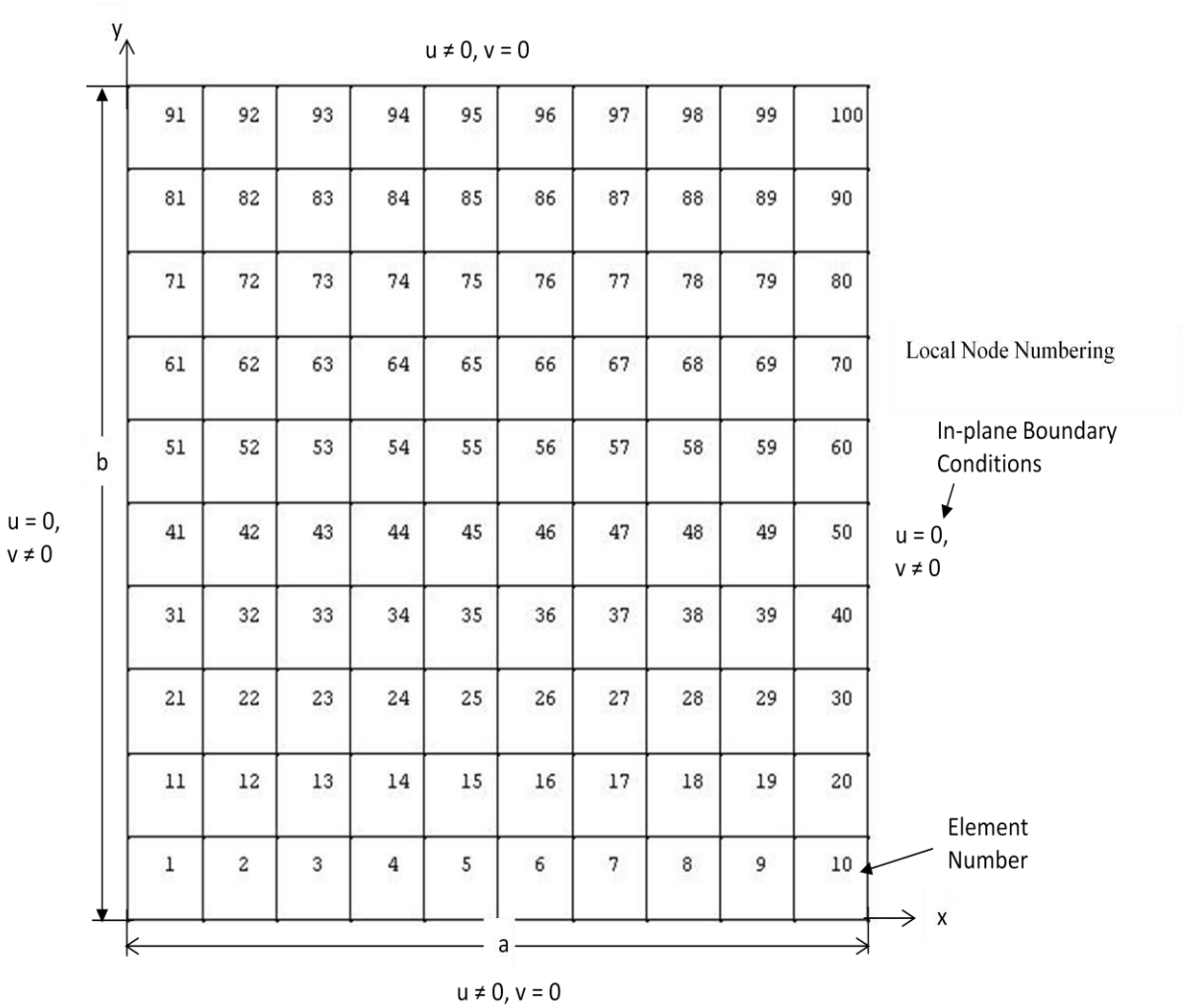

Fig. 5.2.1: Meshing of a typical FGM plate along with simply-supported FM edges.

Table 5.2.1: Convergence-cum-verification study for thermal buckling temperature of Al/Al_2O_3 FGM plate under constant and uniform temperature rise with that reported by Zhao *et al.* (2009).

n	BC[$]	Present study									Zhao *et al.* (2009)
		10 layers			20 layers			40 layers			
		9×9	10×10	11×11	9×9	10×10	11×11	9×9	10×10	11×11	
0	SSSS	17.254	17.181	17.151	17.201	17.158	17.135	17.385	17.241	17.103	17.361
	CCCC	44.374	44.301	44.274	45.628	44.912	44.260	45.432	44.432	44.246	44.171
1	SSSS	9.352	9.272	9.257	9.145	9.140	9.135	9.176	9.152	9.137	7.944
	CCCC	20.917	20.871	20.824	21.123	21.016	20.925	21.025	21.004	20.899	20.771
2	SSSS	9.563	9.472	9.437	9.226	9.196	9.182	9.205	9.172	9.1493	6.925
	CCCC	19.233	19.216	19.207	18.991	18.940	18.901	18.841	18785	18.777	18.489
5	SSSS	10.068	10.063	10.061	9.581	9.567	9.564	9.538	9.541	9.541	7.423
	CCCC	20.524	20.494	20.463	19.961	19.864	19.837	19.588	19.559	19.545	19.150

[$] BCs, meaning boundary conditions, taken for verification are same as used by Zhao *et al.*(2009).

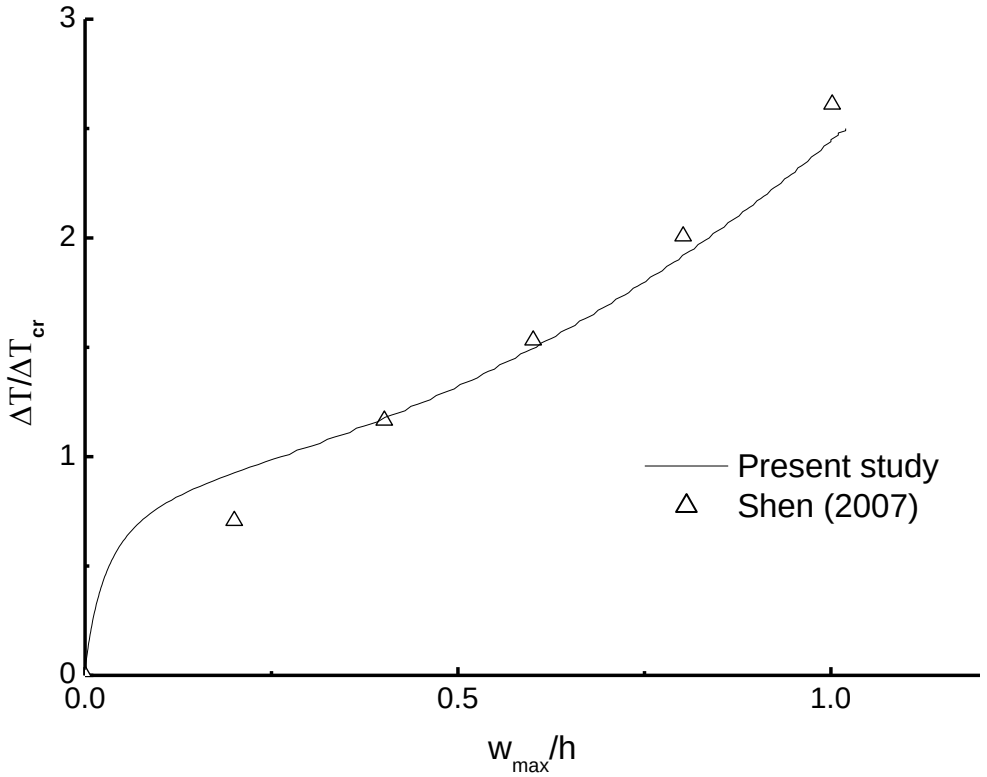

Fig 5.2.2: Comparison of postbuckling load-deflection curves for an isotropic simply-supported moderately thick (*b/h*=10) square isotropic plate under constant and uniform temperature rise obtained in the present study with Shen (2007).

5.2.2 Numerical Results and Discussion

Various numerical studies are conducted to examine the effects of various parameters, viz. temperature-dependent material properties, material inhomogeneity (i.e., power exponent *n*), boundary conditions, aspect (i.e., *a/b*) and slenderness ratios (i.e., *b/h*) on the thermal buckling and postbuckling behavior of imperforated FGM plate. The Ni/Al_2O_3 FGM square plate of side 1 m under constant and uniform temperature rise of 550^0C is studied.

The influence of temperature-dependent material properties on the thermal postbuckling response of simply-supported (i.e., BC1) FGM plate is studied by taking properties to be temperature-dependent (TD) as well as temperature-independent (TID). The corresponding plots of thermal postbuckling paths are shown in Fig. 5.2.3. As noticed from Fig. 5.2.3, the effect of considering temperature dependence of material properties is apparent, especially at higher applied thermal loading, on the thermal postbuckling path of FGM plate. The FGM plate with temperature-dependent material properties exhibits more transverse deflection than that for the temperature-independent case, for a particular value of the thermal load.

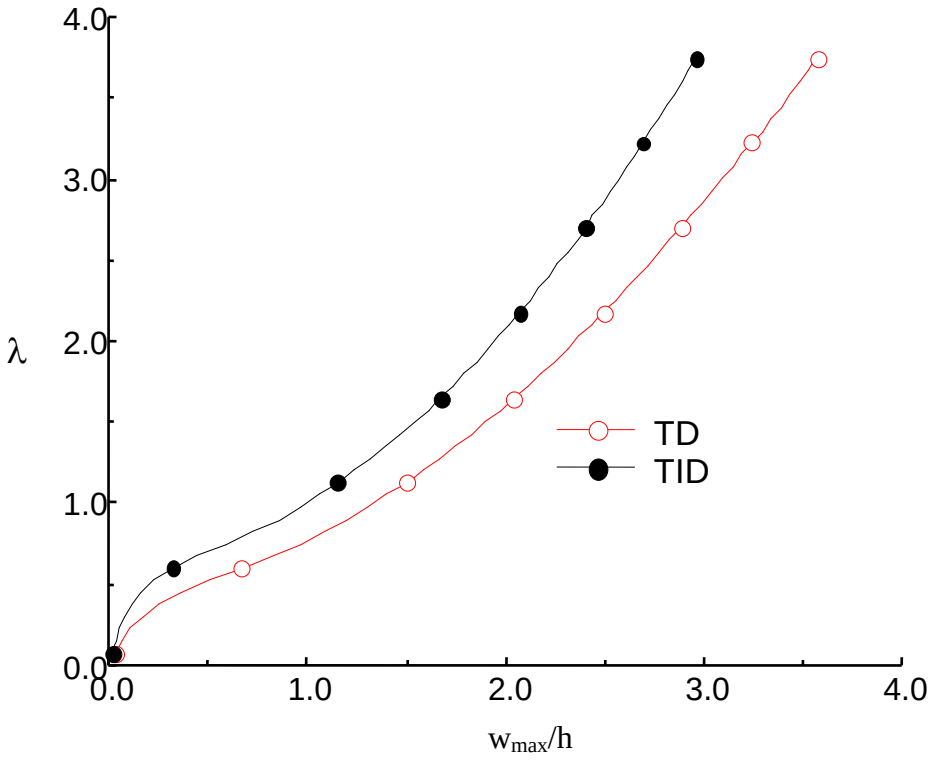

Fig. 5.2.3: Effect of temperature-dependent material properties on the thermal postbuckling path of simply-supported (i.e., BC1) FGM plate.

This finding may be described through the inverse temperature dependence of Young's modulus on temperature (reduction in Young's modulus with the rise in temperature), and direct proportionality of thermal expansion coefficient with temperature (as shown in Fig. 3.2). Fig. 5.2.3 also depicts that the FGM plate with temperature-independent material properties underestimates the maximum transverse deflection at a particular value of the thermal load. Said differently, the thermal postbuckling strength (at a particular value of transverse deflection) is overestimated in the case of FGM plate with temperature-independent material properties. This observation establishes the fact that for realistic and accurate analysis of the thermal postbuckling behavior of FGM plate, it is important to consider temperature-dependent material properties of FGM.

The effect of material property variation [obtained by varying volume fraction using Eq. (3.2) for different values of exponent n (i.e., 0, 1, 2, 3, 10)] on thermal buckling load and postbuckling response of simply-supported (i.e., BC1) FGM plate is studied, and the related thermal postbuckling paths are plotted in Fig. 5.2.4, and the corresponding values of buckling load and postbuckling strength (at $w^* = 2$) are shown in Table 5.2.2.

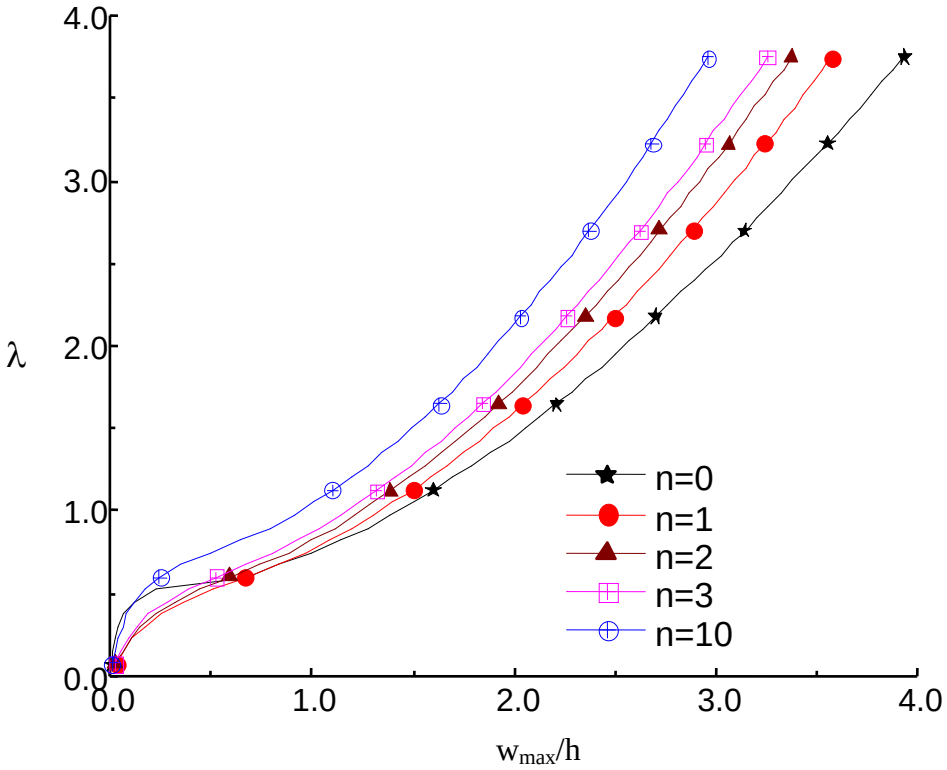

Fig. 5.2.4: Effect of material inhomogeneity on the thermal postbuckling behavior of FGM plate with temperature-dependent material properties under constant and uniform temperature rise.

Table 5.2.2: Effect of material inhomogeneity on thermal buckling load and postbuckling strength of a simply-supported square Ni/Al_2O_3 FGM plate.

n	Buckling load λ_{cr}	Postbuckling strength, λ (at $w^* = 2$)
0	0.57	1.46
1	0.52	1.61
2	0.55	1.75
3	0.59	1.84
10	0.76	2.14

Fig. 5.2.4 depicts that the postbuckling strength of FGM plate under constant and uniform temperature rise (i.e., at a particular value of w^*) is increased considerably as compared to that of the pure metal plate (i.e., corresponding to n = 0). It is worth mentioning here that by increasing the value of n, proportion of Al_2O_3 which possess more thermal resistance is increased resulting in the increase in postbuckling strength of FGM plate. Moreover, it can also be noticed from Fig. 5.2.4 that the bifurcation buckling phenomenon is found to be absent in FGM plate due to a higher degree of thermal bending-extensional coupling, which causes transverse deflection even in the

absence of any bending load. This finding is in good concurrence with the finding of Liew *et al.* (2004) for FGM plate.

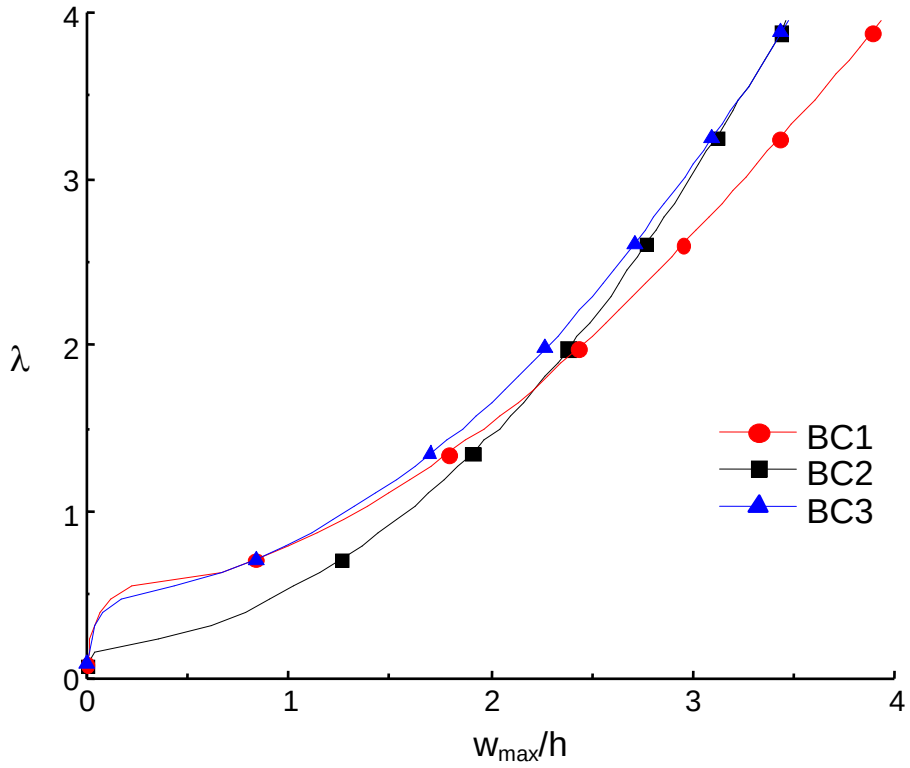

Fig. 5.2.5: Effect of boundary condition on the thermal postbuckling behavior of FGM plate.

The effects of boundary conditions (BC1, BC2, and BC3- described in Section 5.1) on the postbuckling response of Ni/Al_2O_3 FGM plate under constant and uniform temperature rise is examined, and corresponding results are plotted in Fig. 5.2.5. By comparing the thermal postbuckling paths for three types of boundary conditions, shown in Fig. 5.2.5, it can be observed that initially, the FGM plate with BC1 and BC3 boundary conditions depicted higher thermal postbuckling strength (i.e., for a particular value of transverse deflection), whereas FGM plate having simply-supported immovable edges (i.e., BC2) possess lowest thermal postbuckling strength. Further, it is important to mention here that the movable edges (except four corners of the plate) of FGM plate in the case of BC1 boundary condition, delay the occurrence of buckling through free expansion, and hence the buckling strength of FGM plate is more than that of FGM plate with BC2 boundary condition having immovable edges.

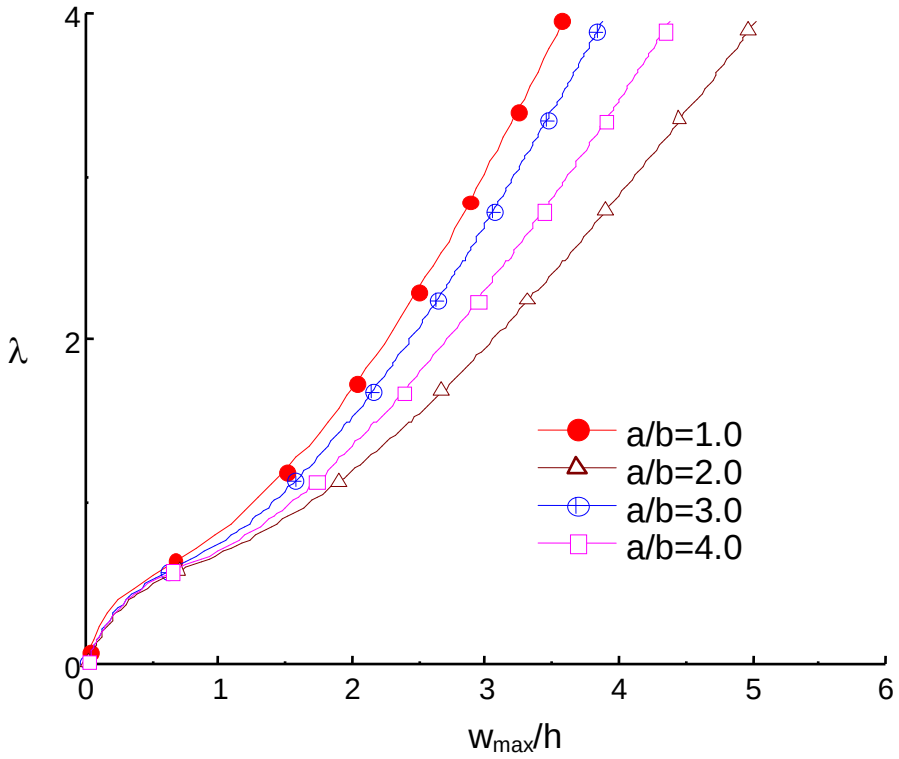

Fig. 5.2.6: Effect of aspect ratio (*a/b*) on the thermal postbuckling behavior of simply-supported FGM plate.

The effects of aspect ratio (length-to-width ratio, i.e., *a/b*) and slenderness ratio (width-to-thickness ratio, i.e., *b/h*) on the thermal postbuckling behavior of simply-supported (i.e., BC1) FGM plate are also studied under constant and uniform temperature rise. To study the effect of aspect ratio, the slenderness ratio is fixed at 100, and for a fixed width (b = 1 m), different aspect ratios (i.e., 1, 2, 3 and 4) are obtained by varying the length of the plate; whereas the effect of different slenderness ratios (i.e., 50,100 and 150) is obtained by varying the thickness of the square FGM plate of size $a = b$ = 1 m. The thermal postbuckling paths for various aspect ratios of FGM plate and the deformed shapes corresponding to maximum thermal load are shown in Figs. 5.2.6 and 5.2.7, respectively; whereas, the effect of slenderness ratio on the thermal postbuckling paths of FGM plate is shown in Fig. 5.2.8.

Fig. 5.2.6 depicts a considerable effect of aspect ratio on thermal buckling and postbuckling response of FGM plate. For a particular value of w, the square FGM plate (i.e., a/b = 1) is found to possess highest thermal postbuckling strength, and FGM plate with a/b = 2 depicted highest transverse deflection. It can also be noted from Fig. 5.2.6 that the thermal postbuckling resistance is decreased considerably with an increase in aspect ratio from 1 to 2, which may be attributed to the increasing

thermal effect with the increase in the length of sides that are constrained to move in *y*-direction. However distinguish thermal postbuckling response of FGM plate with *a/b*=3 and *a/b*=4 is obtained, showing higher postbuckling strength than that for *a/b*=2. To understand this peculiar phenomenon, the deformed shapes, corresponding to maximum thermal load, of FGM plate with these different aspect ratios were plotted (refer Fig. 5.2.7) and analyzed. Figs. 5.2.7 (i)-(iv) show that for *a/b*=1 and 2, postbuckling is preceded by the global buckling mode with one peak, whereas for *a/b*=3 and 4, the postbuckling follows the local buckling of the plate wherein the final deformed shape divide into number of half waves. Also evident from the previous study (Nemeth, 1996) that plate with local buckling possess higher buckling load than the plate buckled in global mode, that causes FGM plate to show an increase in strength in the postbuckling region for higher values of aspect ratios (i.e., *a/b*=3 and 4) even after an initial decrease when the aspect ratio is changed from *a/b*=1 to *a/b*=2.

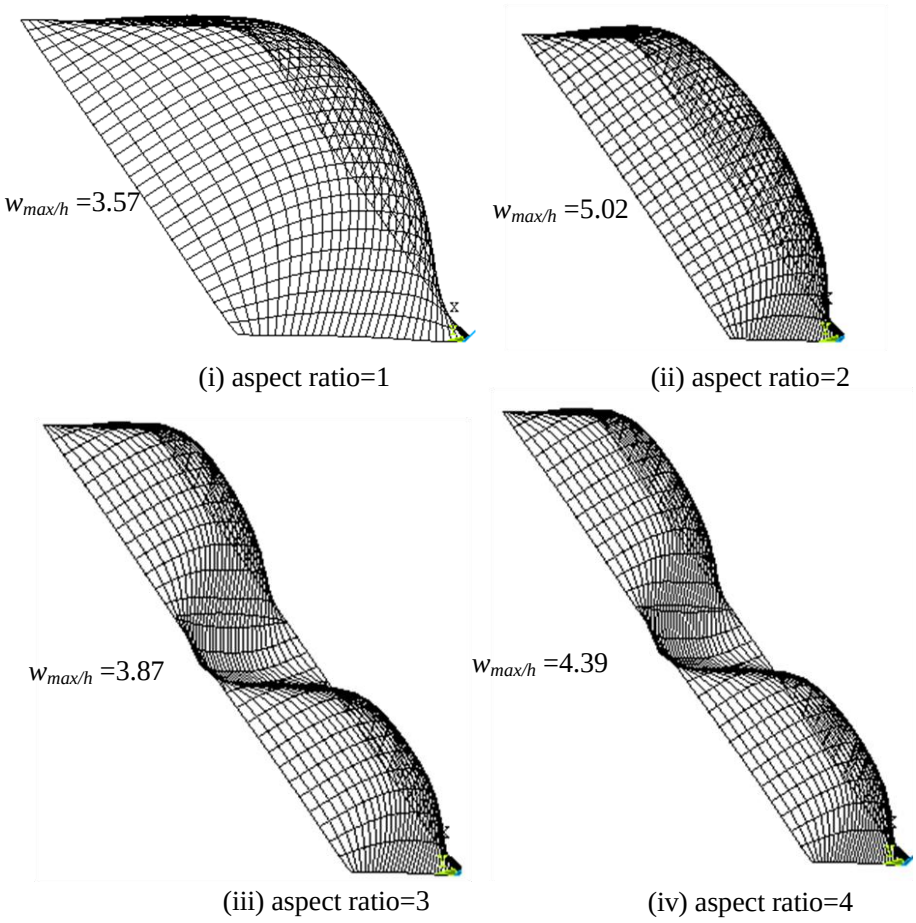

Fig. 5.2.7: Effect of aspect ratios (*a/b*) on deformed shapes of simply-supported FGM plate under constant and uniform temperature rise.

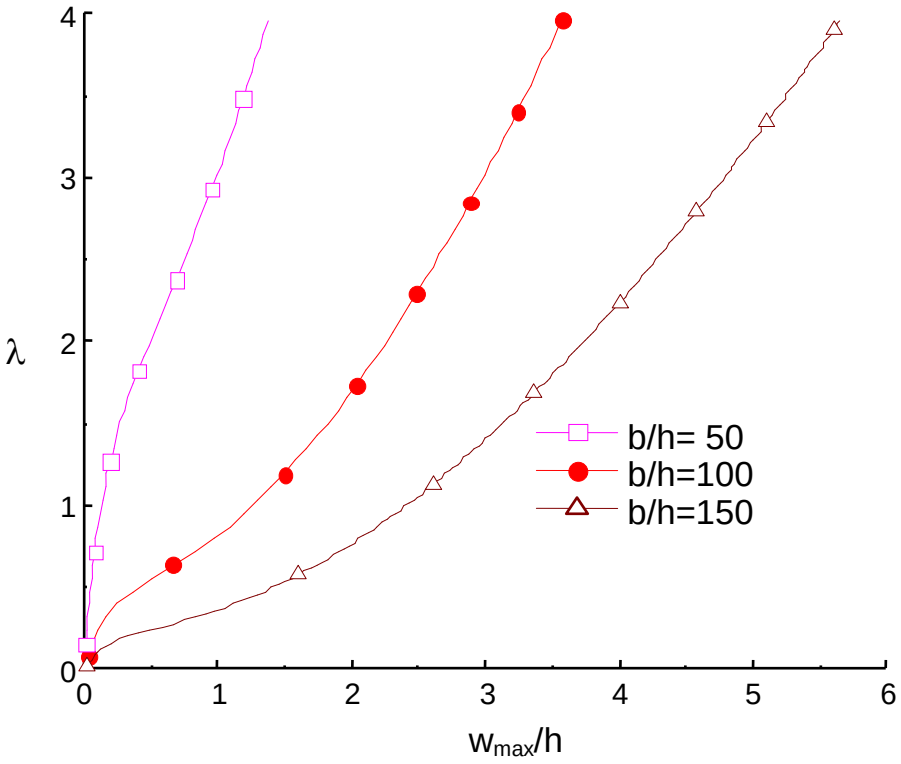

Fig. 5.2.8: Effect of slenderness ratio (*b/h*) on the thermal postbuckling behavior of simply-supported FGM plate.

The effect of slenderness ratio on the thermal postbuckling behavior of simply-supported (BC1) FGM plate is shown in Fig. 5.2.8. It can be observed from Fig. 5.2.8 that the thermal postbuckling strength (corresponding to a particular value of w^*) of FGM plate decreases monotonically with an increase in the slenderness ratio, and thin FGM plate exhibit higher transverse deflection for a particular value of thermal load.

5.2.3 Conclusions

A study on non-linear finite element analysis of imperforated plate made of Ni/Al_2O_3 FGM is conducted under constant and uniform temperature rise. After validating the results of present formulation with the available results in literature, the effects of temperature-dependent material properties, material gradation (i.e., material in-homogeneity), boundary conditions, and geometrical parameters (i.e., aspect ratio and slenderness ratio) on thermal buckling and postbuckling behavior of FGM plate are investigated. Out of this study, following important conclusions are drawn.

- The thermal postbuckling strength (at a particular value of deflection) of FGM plates is overestimated in the case of temperature-independent material properties when compared with the case of temperature-dependent material properties, hence for realistic and accurate analysis of the thermal postbuckling behavior of FGM plate the temperature-dependent material properties should be considered.
- Unlike isotropic plates (which exhibit bifurcation buckling) the FGM plate does not possess bifurcation type of buckling, which is attributed to the presence of thermal bending-extensional coupling which causes transverse deflection even in the absence of bending load.
- Ascribed by the freely expandable movable edges, the postbuckling strength of simply-supported FGM plate with movable edges is found to be more than that of simply-supported FGM plate having immovable edges of the plate.
- For lower values of aspect ratio (i.e., a/b=1 and 2), postbuckling is preceded by the global buckling mode with one peak, whereas for a/b=3 and 4, the postbuckling follows the local buckling, with two peaks, that causes FGM plate to show an increase in postbuckling strength for higher values of aspect ratios (i.e., a/b=3 and 4) after an initial decrease when the aspect ratio is changed from a/b=1 to 2.
- The thermal postbuckling strength of FGM plate is found to decrease monotonically with an increase in slenderness ratio, and thin FGM plate is found to exhibit excessive out-of-plane deflection for a given load.

5.3 Thermal Stability Analysis of Perforated Elastic FGM Plate

5.3.1 Details of Perforation

A FGM plate of dimension ($a \times b \times h$) is perforated by making a central cutout of various shapes (i.e., circular, square, diamond, and elliptical) to observe the effect of cutout shape on thermal buckling and postbuckling response of the FGM plate. Three cutout areas (i.e., sizes) designated as A_1, A_2, and A_3, as mentioned in Table 5.3.1, have been considered. The area A_1 is equal to the area of the square cut-out having cutout ratio (i.e., c/b, where c refers to the side of the square cutout and b to the width of the square plate) equal to 0.14, while the areas A_2 and A_3 are equal to the area of square cutout of cutout ratios 0.28 and 0.42, respectively. The areas (i.e., A_1, A_2, and A_3) of other cutout shapes are same and are taken equal to the areas of the corresponding square cutout.

Table 5.3.1: Specific details of cutout shapes and their dimensions.

Cutout shape	Cutout ratio[a]	Cutout size		
		A_1	A_2	A_3
Square	c/b	0.140	0.280	0.420
Circular	d/b	0.158	0.316	0.474
Diamond	c/b	0.140	0.280	0.420
Elliptical	e/b	0.224	0.447	0.670

[a] For various notations see Figs. 5.3.1 and 5.3.2.

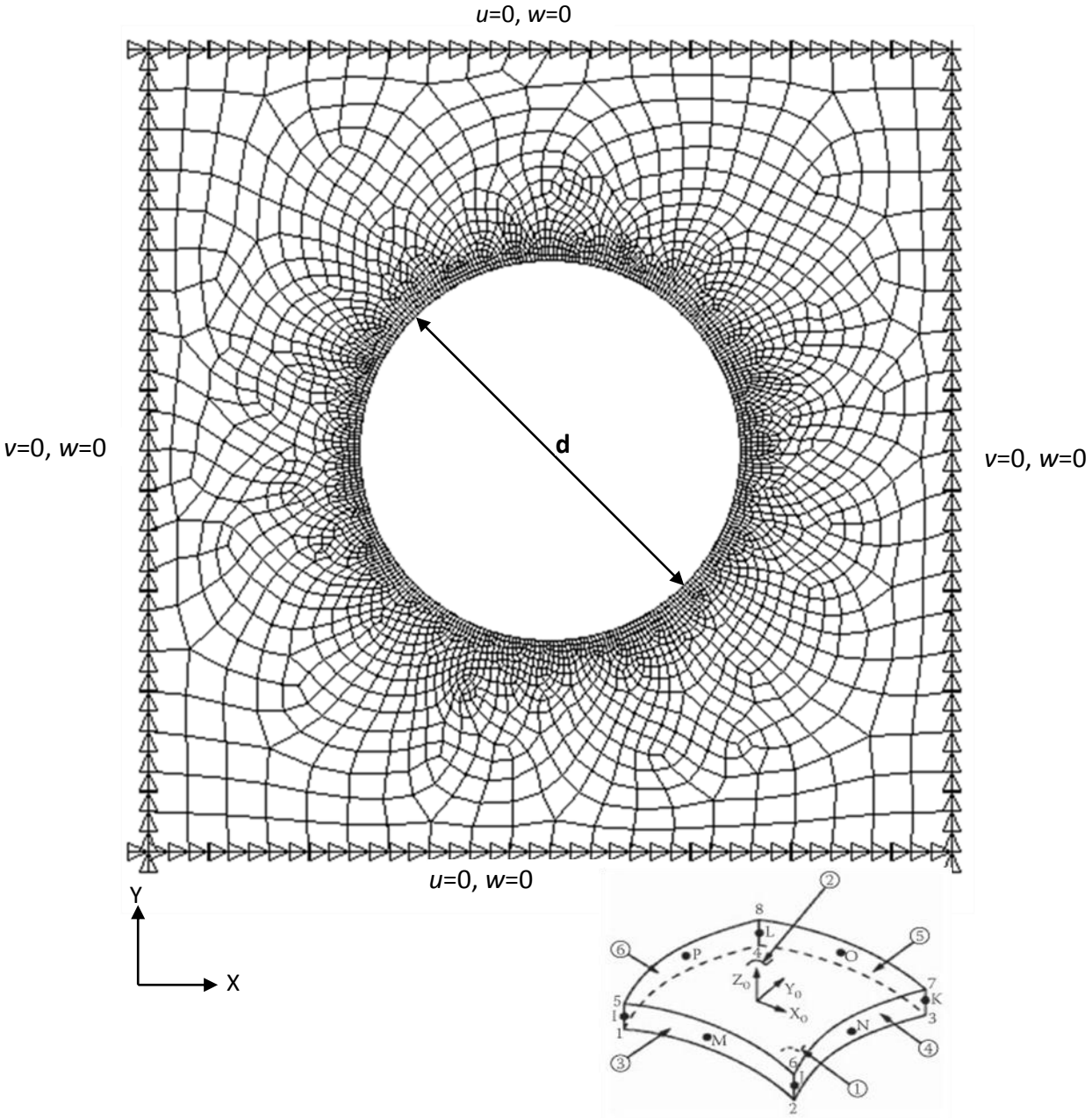

Fig. 5.3.1: Finite element mesh of a typical FGM plate with a circular cutout along with BC1 boundary condition.

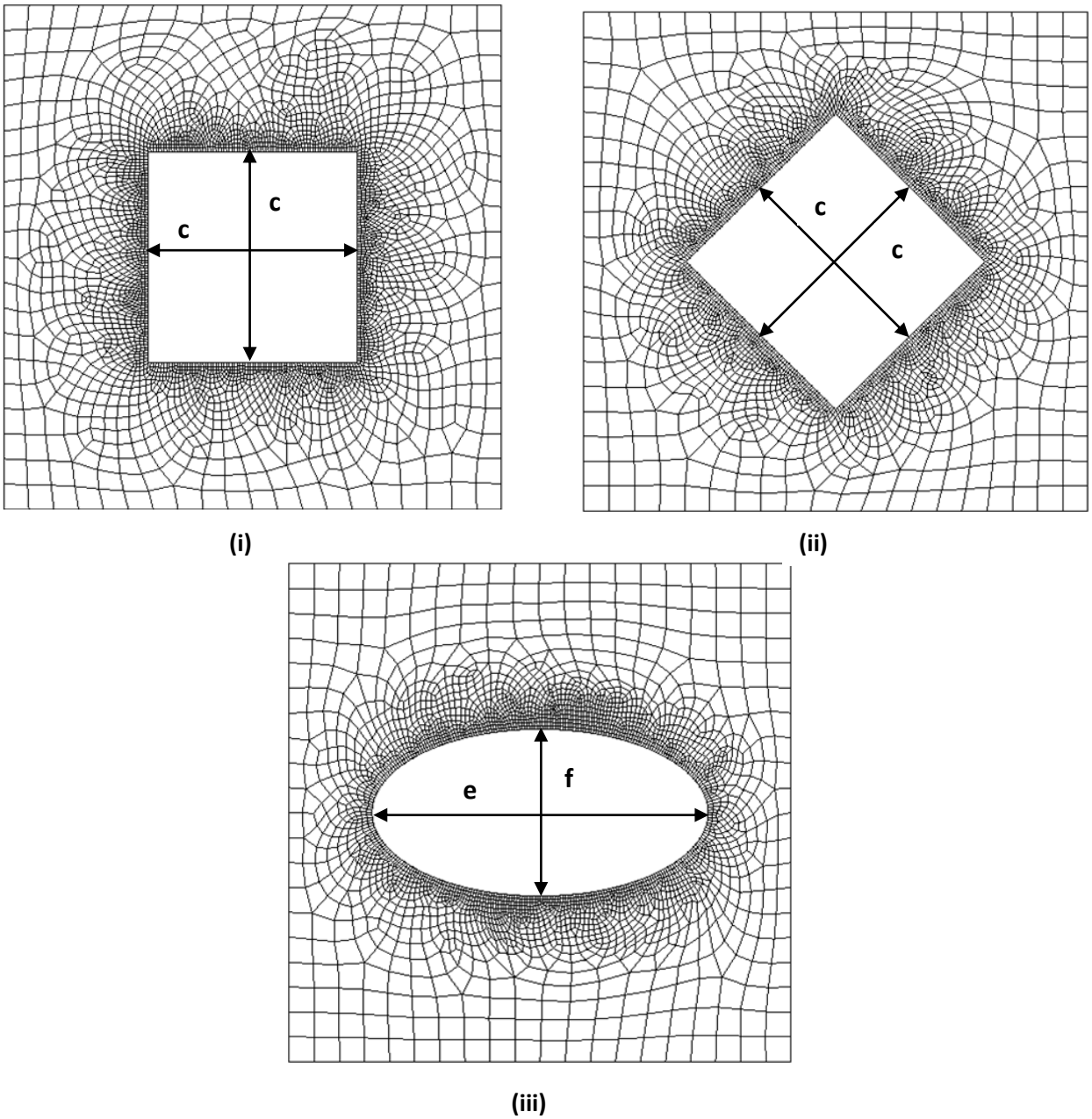

Fig. 5.3.2: Meshing of square FGM plate of side *b* with (i) square, (ii) diamond, and (iii) elliptical cutouts.

5.3.2 Convergence Study

To fix the number of elements in the finite element analysis, a convergence study was conducted for a simply-supported perforated FGM plate, with freely movable edges (i.e., BC1), containing a centrally located circular cutout of size A_3 (*d*/*b*=0.47). The plate was meshed with SHELL281 element of size varying (decreasing) from the outer edge of the plate to the periphery of the circular hole, as shown in Fig. 5.3.1.

The convergence study for non-dimensionalized thermal buckling load was conducted by meshing the plate using the mesh-size control feature of ANSYS by taking:
(i) the default element size over the outer edges of the plate as b/η, and
(ii) the element size along the hole perimeter as $b/4\eta$.
Where, b represents edge size of the square plate. The values of η are taken as 10, 20, 30 & 40 to obtain 195, 718, 3042 and 6279 number of elements, respectively. Moreover, to approximate continuous variation of properties of FGM plate, the plate is assumed to compose of 20 perfectly-bonded layers. The results of convergence are tabulated in Table 5.3.2. A reasonable convergence of normalized thermal buckling temperature can be observed from Table 5.3.2 for the mesh of 3042 elements (i.e., for η = 30). For the sake of uniformity, the similar meshing procedure with the same mesh control parameter (i.e., η = 30) was followed to mesh the plate with other cutout shapes. Schematics of meshed FGM plate with cutouts of other (than circular) shapes are shown in Fig. 5.3.2.

Table 5.3.2: Results of convergence study for normalized thermal buckling temperature ($\lambda = \alpha_c \Delta T \times 10^3$).

Nos. of elements for (Circular cutout/Square cutout)	Buckling load, λ	
	Circular cutout	Square cutout
195/208	1.1607	1.0923
718/797	1.1264	1.0581
3042/3049	1.0923	1.0581
6279/6309	1.0923	1.0581

5.3.3 Numerical Results and Discussion

Numerical studies are conducted to examine the effects of various parameters, viz. cutout shape, material inhomogeneity (i.e., power exponent n), slenderness ratio (i.e., b/h), cutout size (i.e., A_1, A_2, and A_3) and boundary conditions on the thermal buckling and postbuckling behavior of perforated FGM plate. Ni/Al_2O_3 FGM square plate of side 1 m with a central cutout is analyzed under constant and uniform temperature rise of 500^0C. It is to be noted that TD material properties are

The effect of cutout shape on the thermal postbuckling behavior of FGM plate having temperature-dependent (TD) and temperature-independent (TID) material properties is studied, and thermal postbuckling paths of simply-supported (i.e., BC1)

FGM plate with a central cutout of size A_3 and of various shapes are shown in Fig. 5.3.3.

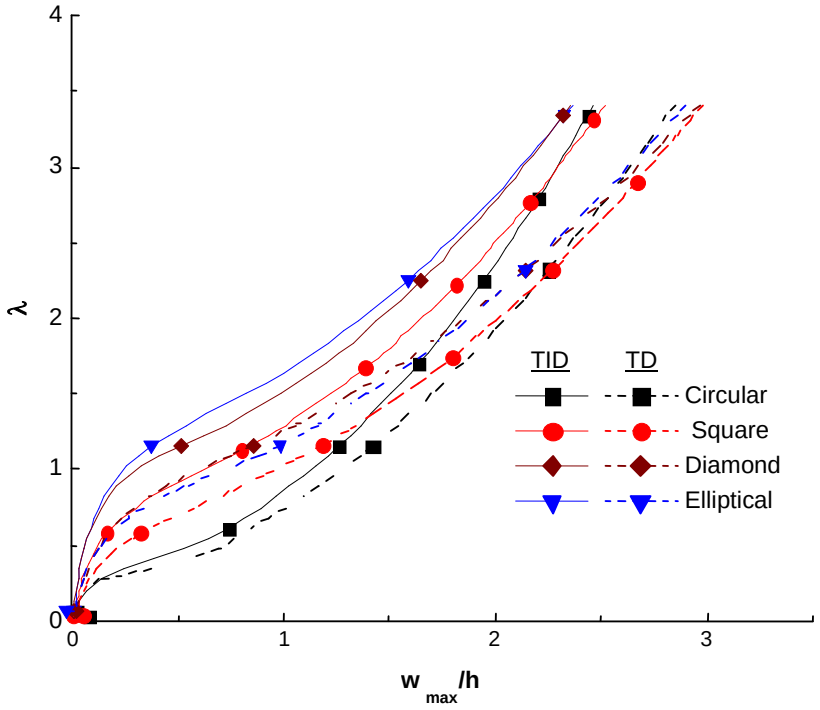

Fig. 5.3.3: Effect of the temperature-dependent material properties on the thermal postbuckling response of simply-supported (i.e., BC1) FGM plate with cutout of various shapes.

It can be observed in Fig. 5.3.3 that the postbuckling path of perforated FGM plate is greatly affected by the temperature dependence of material properties for all cutout shapes and this effect becomes considerable with an increase in applied thermal loading. Irrespective of cutout shape, the thermal postbuckling strength (at a particular value of deflection) of FGM plates is overestimated in the case of temperature-independent material properties when compared the case of temperature-dependent material properties. This observation establishes the fact that for realistic and accurate analysis of thermal postbuckling behavior of FGM plate it is important to consider temperature-dependent material properties. Fig. 5.3.3 also reveals that for a particular value of transverse deflection (i.e., w_{max}/h), the FGM plate with a elliptical cutout possesses highest thermal postbuckling strength whereas the FGM plate with a square cutout has a minimum strength, for both temperature-independent as well as temperature-dependent material properties. The similar findings can also be observed from Table 5.3.3 in which the maximum difference in the non-dimensional thermal buckling load of perforated (square cutout) FGM plate (for n = 1) with temperature-

dependent material properties and with temperature-independent material properties is almost 40%.

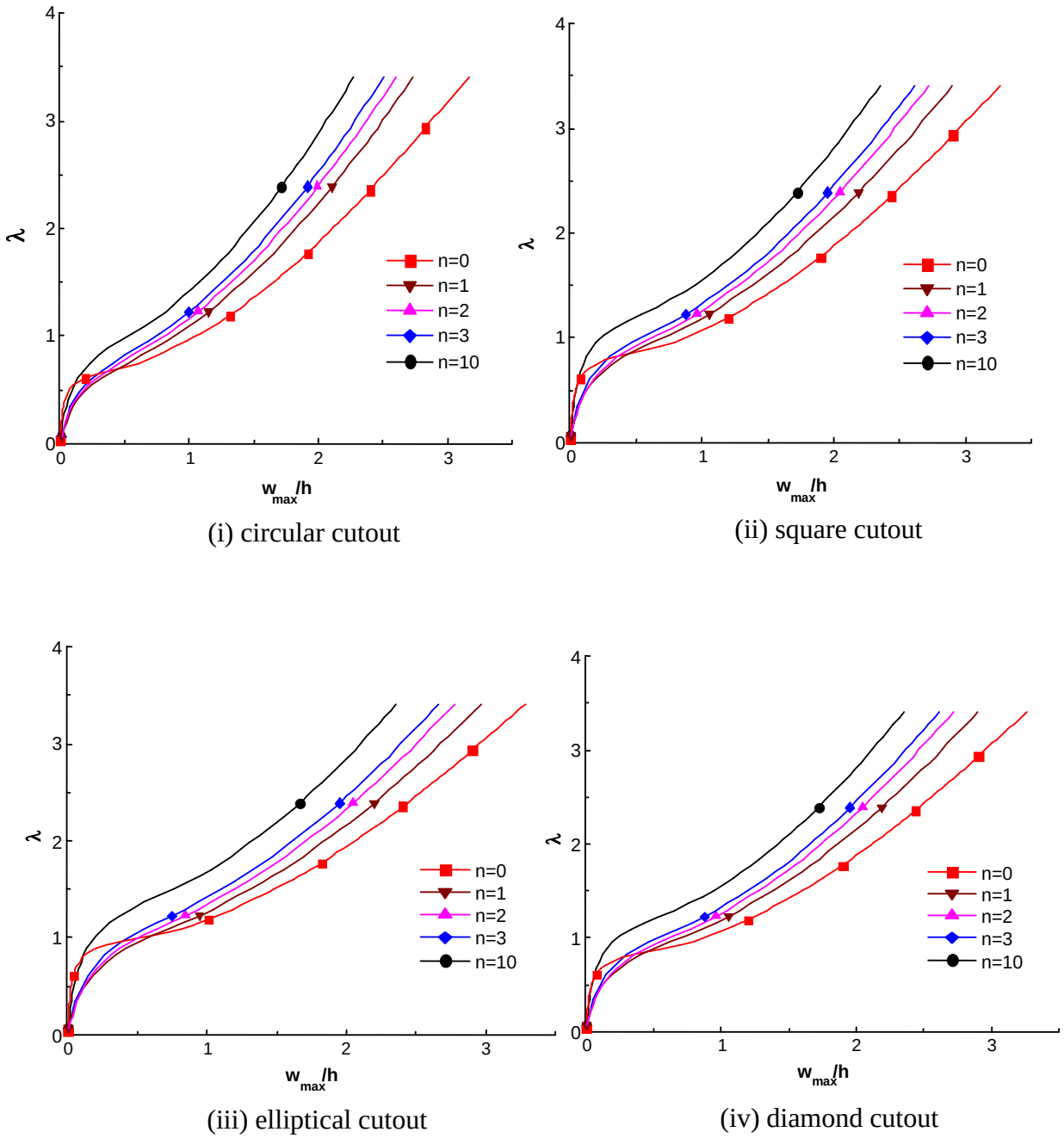

(i) circular cutout (ii) square cutout

(iii) elliptical cutout (iv) diamond cutout

Fig. 5.3.4: Effect of material inhomogenity on the thermal postbuckling behavior of simply-supported FGM plate with TD material properties and A_3 size perforation of (i) circular cutout (ii) square cutout (iii) elliptical cutout, and (iv) diamond cutout.

The effect of material property variation through the thickness [obtained by varying volume fraction using Eq. (3.2) for different values of exponent *n* (i.e., 0, 1, 2, 3, 10)] on thermal buckling and postbuckling response of simply-supported (i.e., BC1) FGM plate having cutout of various shapes of size A_3 is studied, and the related

results are plotted in Fig. 5.3.4. It can be observed from Fig. 5.3.4 that for all cutout shapes, the thermal postbuckling strength at a particular value of w_{max}/h of perforated FGM plate is increased considerably as compared to that of the pure metal plate (i.e., corresponding to $n = 0$). It can also be noted from Figs. 5.3.4 that the bifurcation buckling phenomenon is found to remain absent in FGM plate due to a higher degree of thermal bending-extensional coupling, which causes transverse deflection even in the absence of pronounced bending load. This finding is in good concurrence with the similar finding for FGM plate reported by Liew *et al.* (2004).

Table 5.3.3: Effect of material inhomogeneity on thermal buckling load for simply-supported square Ni/Al_2O_3 FGM plate with various shape cutouts of size A_3.

n	Cutout shape	Buckling load (TID)	Buckling load (TD)
0	Circular	1.1215	0.9705
	Square	1.1875	0.8972
	Elliptical	1.5171	1.1911
	Diamond	1.4196	1.0600
1	Circular	1.1605	1.0923
	Square	1.5133	1.0581
	Elliptical	1.6473	1.2660
	Diamond	1.2946	1.1822
2	Circular	1.5019	1.1685
	Square	1.6110	1.0936
	Elliptical	1.7410	1.3409
	Diamond	1.3750	1.2592
3	Circular	1.5312	1.2293
	Square	1.6428	1.1501
	Elliptical	1.7667	1.4172
	Diamond	1.3383	1.3259
10	Circular	1.6348	1.4172
	Square	1.7946	1.3296
	Elliptical	1.9598	1.6814
	Diamond	1.5178	1.3531

It can also be observed from Table 5.3.3 that the thermal buckling load of perforated FGM plate is greatly dependent on the shape of the cutout and for all values of power law index (*n*), the FGM plate with elliptical cutout depicted maximum thermal buckling load. It is observed that for the same value of *n*, the FGM plate with square cutout possesses minimum buckling load, that is nearly 20-25% lower than that of the plate carrying elliptical cutout.

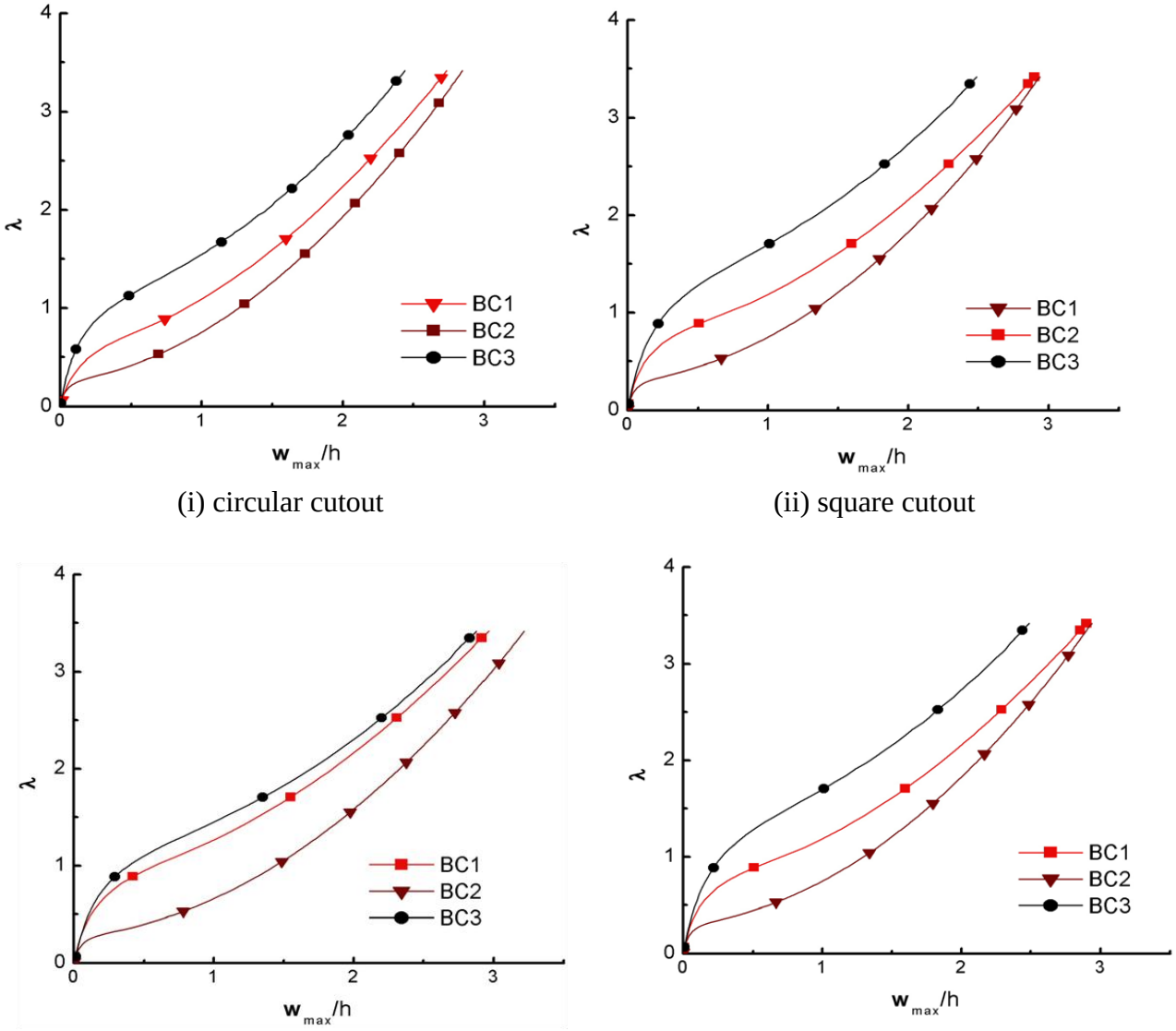

(i) circular cutout (ii) square cutout

(iii) elliptical cutout (iv) diamond cutout

Fig. 5.3.5: Effect of boundary conditions on the thermal postbuckling behavior of FGM plate with cutout of various shapes (i) circular cutout (ii) square cutout (iii) elliptical cutout (iv) diamond cutout.

The effect of boundary conditions (BC1, BC2, and BC3, as described in Section 5.1) on the postbuckling response of Ni/Al_2O_3 FGM plate having a different-shaped central cutout of size A_3 is investigated under uniform temperature rise. The

corresponding results are plotted in Fig. 5.3.5. By comparing the thermal load-deflection curves shown in Fig. 5.3.5 for three types of boundary conditions, it can be observed that for all values of transverse deflection clamped (i.e., BC3) FGM plate depicted the highest strength, whereas FGM plate having simply-supported with immovable edges (i.e., BC2) possess the lowest strength, irrespective of cutout shape. Further, it is to mention that the movable edges (except four corners) of FGM plate in BC1 conditions delay the occurrence of buckling and subsequent postbuckling stage through free expansion, and hence the postbuckling strength of FGM plate is more than that of FGM plate with BC2 boundary condition having immovable edges.

Table 5.3.4: Effect of boundary conditions on thermal postbuckling load (corresponding to $\frac{w_{max}}{h} = 2$) for square Ni/Al_2O_3 FGM plate with various shape cutouts of size A_3.

Cutout shape	Boundary condition	Postbuckling load corresponding to $\frac{w_{max}}{h} = 2$
Circular	BC1	2.1559
	BC2	1.8495
	BC3	2.6237
Square	BC1	1.9560
	BC2	1.5714
	BC3	2.5714
Elliptical	BC1	2.1666
	BC2	1.5833
	BC3	2.3111
Diamond	BC1	2.2089
	BC2	1.8407
	BC3	2.7582

The values of thermal postbuckling loads of Ni/Al_2O_3 FGM plate having different-shaped central cutout of size A_3 corresponding to a particular value of transverse deflection(i.e., $w_{max}/h = 2$) are tabulated in Table 5.3.4. As observed from Table 5.3.4, the restraints on in-plane movements of plate edges have considerable influence on postbuckling strengths of FGM plate and maximum postbuckling

strength is obtained for BC3 boundary condition. It can also be observed that for all cutout shapes, the FGM plate with BC2 boundary conditions depicted minimum postbuckling strength, which is approximately 20-30 % lower than that obtained for BC1 boundary condition.

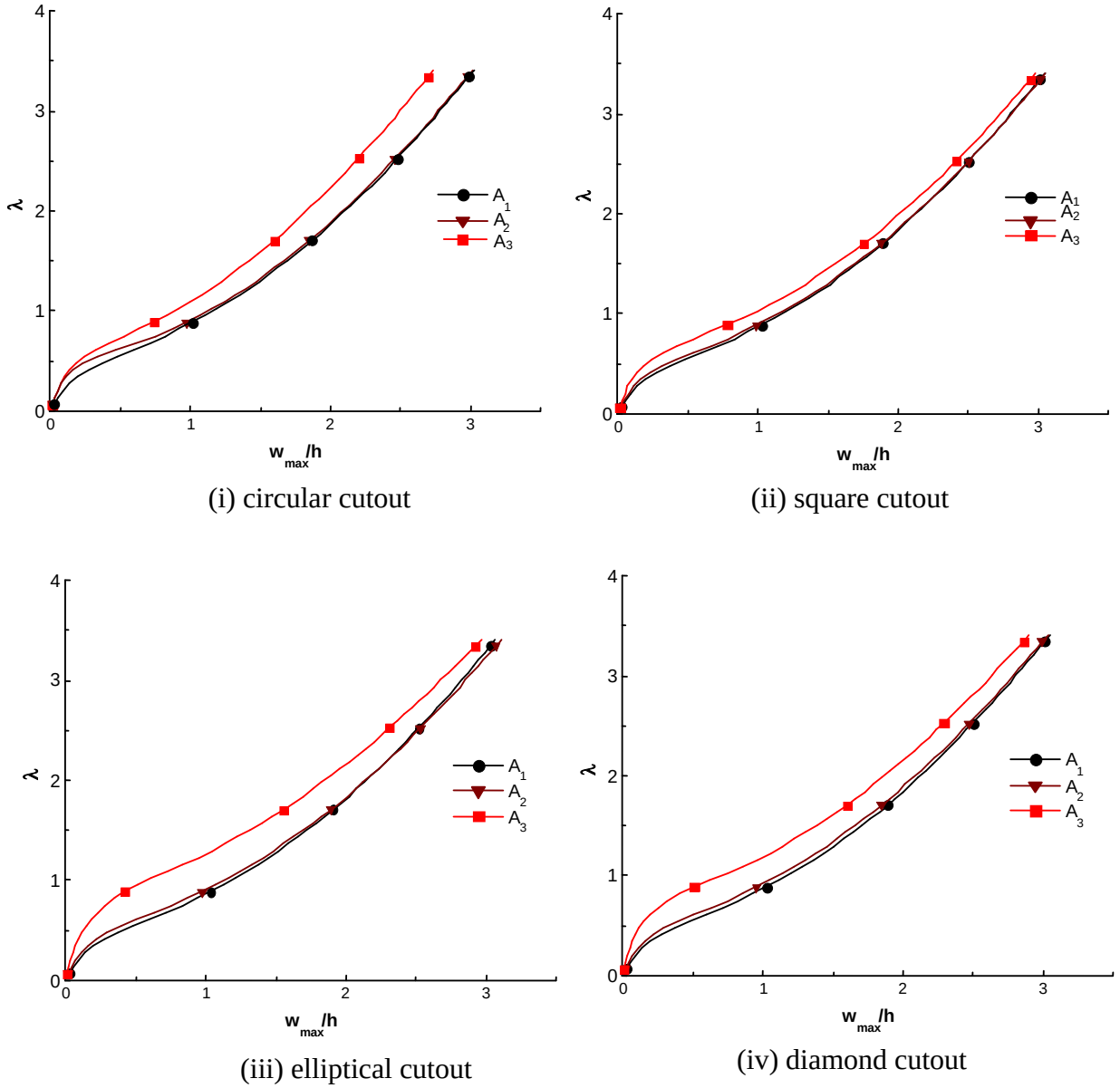

(i) circular cutout (ii) square cutout

(iii) elliptical cutout (iv) diamond cutout

Fig. 5.3.6: Effect of cutout size on the postbuckling behavior of FGM plate with a central cutout under thermal load: (i) circular cutout (ii) square cutout (iii) elliptical cutout (iv) diamond cutout.

The thermal postbuckling behavior of FGM plate with a central cutout of various shapes and sizes is studied for simply-supported with movable edges (i.e., BC1) boundary condition. The corresponding thermal postbuckling paths are depicted in Fig. 5.3.6. It can be observed from Fig. 5.3.6 that for all cutout shapes, although the

load-deflection plots of postbuckling response of FGM plate with a cutout is almost same for cutout sizes A_1 and A_2, but when the cutout size is increased to A_3, the thermal postbuckling strength (i.e., for a particular value of $\frac{w_{max}}{h}$) of FGM plate is increased significantly. As against the conventional wisdom, this peculiar phenomenon of increase in postbuckling strength of FGM plate with large cutout size as compared to small cutout can be attributed to the fact that with an increase in cutout area the domain of tensile stresses (caused by free expansion of cutout edges because of thermal load) near cutout edges also increases, which provide more resistance against buckling and subsequent postbuckling phenomenon. This unusal finding is in concurrence with earlier study conducted by Abolghasemi *et al.* (2014) on FGM plate with a hole under thermal load to conclude that buckling load increases as the size of the hole increases, provided a right combination of boundary condition and the plate's aspect ratio are chosen. The corresponding numerical values of nondimensional thermal postbuckling load corresponding to $\frac{w_{max}}{h} = 2$ are tabulated in Table 5.3.5. The FGM plate with large size cutout (i.e., A_3) possesses 10-15 % higher postbuckling load than the plate with smaller cutouts (i.e., A_1 and A_2).

Table 5.3.5: Effect of cutout size on thermal buckling load for simply-supported square Ni/Al_2O_3 FGM plate with various cutout shapes.

Cutout shape	Cutout size	Postbuckling load corresponding to $\frac{w_{max}}{h} = 2$
Circular	A_3	2.2660
	A_2	1.8935
	A_1	1.8937
Square	A_3	2.0001
	A_2	1.8530
	A_1	1.8527
Elliptical	A_3	2.1790
	A_2	1.8425
	A_1	1.8420
Diamond	A_3	2.1809
	A_2	1.8562
	A_1	1.8511

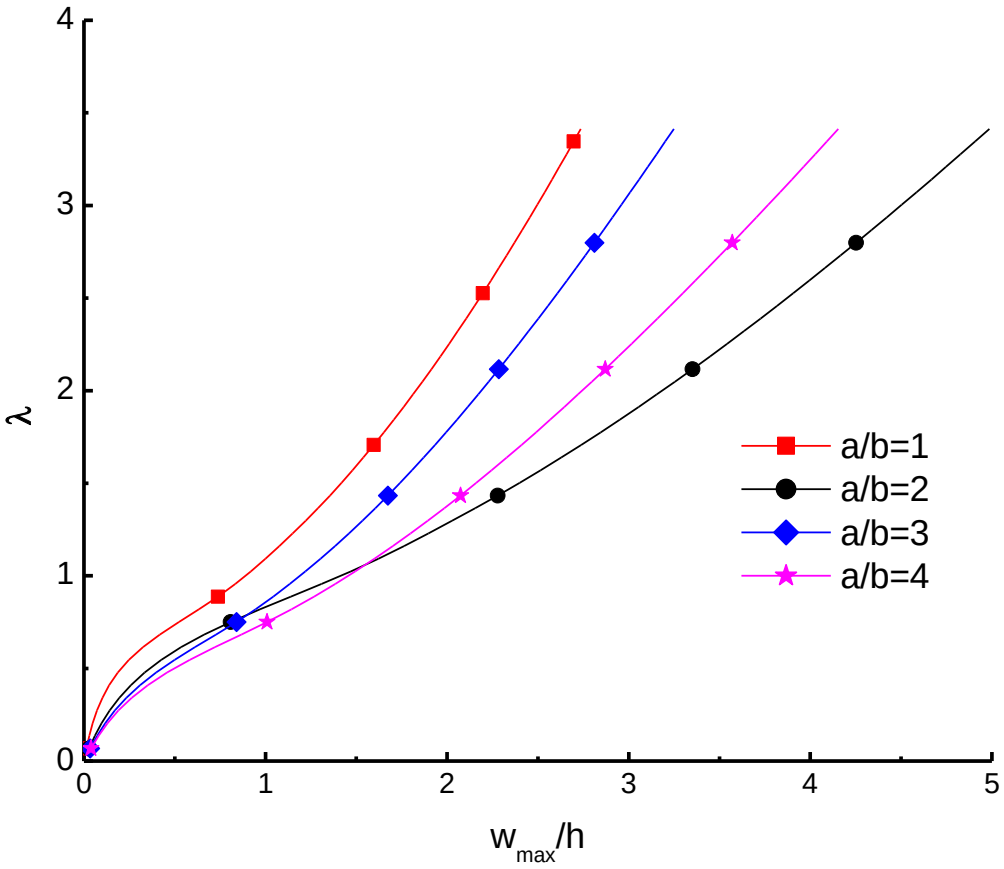

Fig. 5.3.7: Effect of aspect ratio (*a/b*) on the thermal postbuckling behavior of simply-supported FGM plate with a central circular cutout.

In addition, the effects of aspect ratio (length-to-width ratio, i.e., *a/b*) and slenderness ratio (width-to-thickness ratio, i.e., *b/h*) on thermal buckling and postbuckling behavior of simply-supported (i.e., BC1) FGM plate with a central circular cutout of size A_3 are studied under constant and uniform temperature rise. To study the effect of aspect ratio, the slenderness ratio is fixed at 100, and for a fixed width (b = 1 m), the different aspect ratios (i.e., 1, 2, 3 and 4) are obtained by varying the length of the plate; whereas, the different slenderness ratios (i.e., 60, 80 and 100) are obtained by varying the thickness of the square FGM plate of size $a = b$ = 1 m. The thermal postbuckling paths for various aspect ratios and the deformed shapes corresponding to maximum thermal load (i.e., 500^{o}C) are shown in Figs. 5.3.7 and 5.3.8, respectively; whereas, the effect of slenderness ratio on the thermal postbuckling paths is shown in Fig. 5.3.9. It can be observed from Fig. 5.3.7 that the thermal postbuckling response of FGM plate with a central circular cutout is significantly affected by the aspect ratio of the plate. For a particular value of $w_{max}/$

h, square FGM plate (i.e., unit aspect ratio) is found to possess highest thermal postbuckling strength, and FGM plate with *a/b* = 2 possesses highest transverse deflection corresponding to maximum thermal load which is approximately 200% of that depicted by square FGM plate. It can also be noticed from Fig. 5.3.7 that the thermal postbuckling resistance is decreased considerably with an increase in aspect ratio from 1 to 2, which may be attributed to the increasing thermal effect with the increase in the length of sides that are constrained to move in *y*-direction. However, distinguish thermal postbuckling response of FGM plate with *a/b* = 3 and *a/b* = 4 is obtained, showing higher postbuckling strength than that for *a/b* = 2. To understand this peculiar phenomenon, the deformed shapes, corresponding to maximum thermal load, of FGM plate with these different aspect ratios were plotted (refer Fig. 5.3.8) and analyzed. As seen from Figs. 5.3.8 that for *a/b*=1 and 2, postbuckling is preceded by the global buckling mode with one peak around the cutout edge, whereas for *a/b*=3 and 4, the postbuckling follows the local buckling of the plate wherein the cutout straddles the buckle pattern to divide the final deformed shape into number of half waves. As it is evident from the previous study (Nemeth, 1996) that plate with local buckling possess higher buckling load than the plate buckled in global mode, that causes FGM plate to show an increase in strength in the postbuckling region for higher values of aspect ratios (i.e., *a/b* = 3 and 4) even after an initial decrease when the aspect ratio is changed from *a/b*=1 to *a/b*=2.

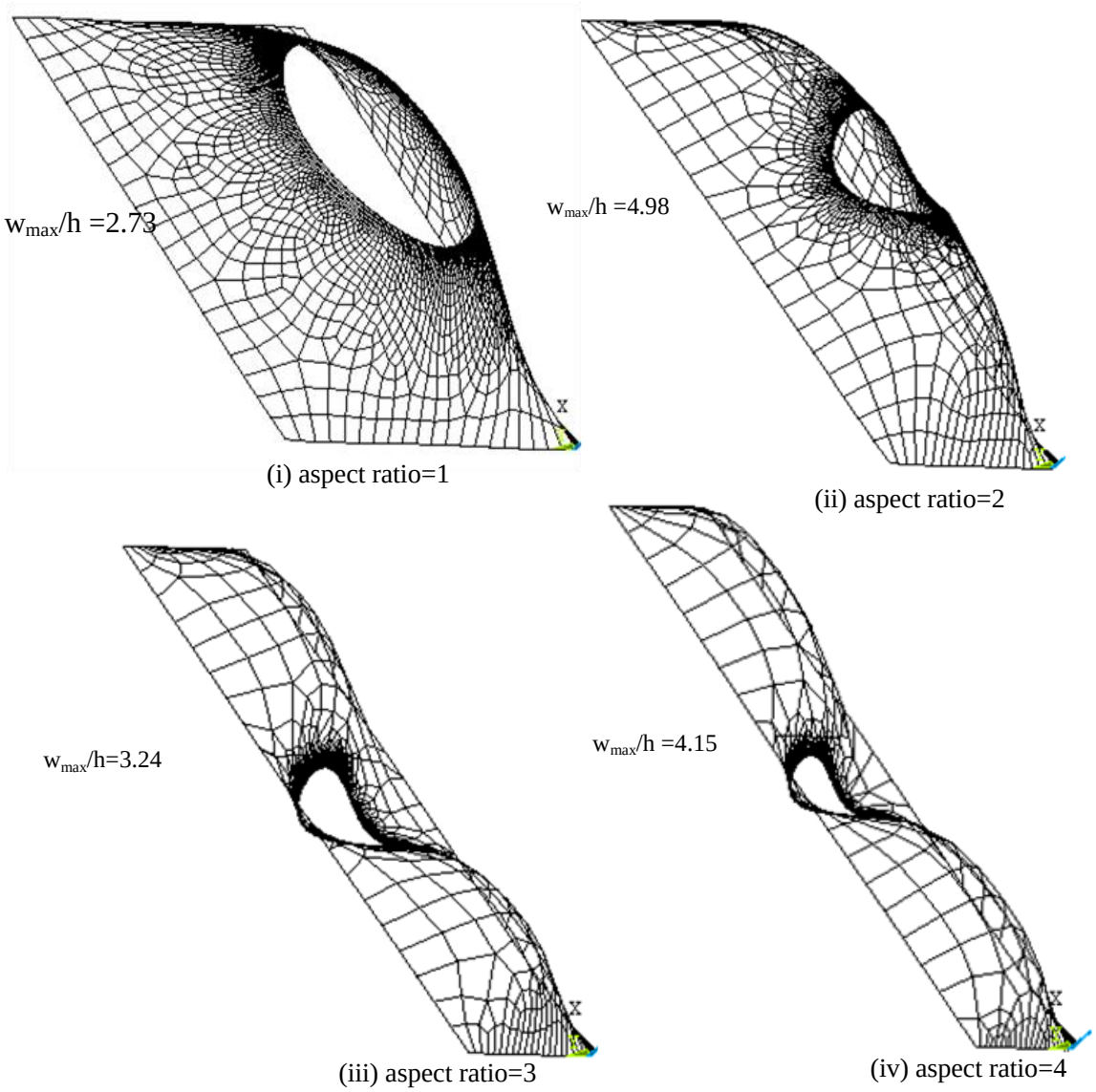

`Fig. 5.3.8: Effect of aspect ratios (*a/b*) on deformed shapes of simply-supported FGM plate with central circular cutout under constant and uniform temperature rise.

The effect of slenderness ratio on the thermal postbuckling behavior of simply-supported (BC1) FGM plate with a central circular cutout of size A_3 is shown in Fig. 5.3.9. It can be observed from Fig. 5.3.9 that the thermal postbuckling strength (corresponding to a particular value of w_{max}/h) of FGM plate decreases monotonically with an increase in the slenderness ratio, and thin FGM plate exhibit excessive out-of-plane deflection for a particular load.

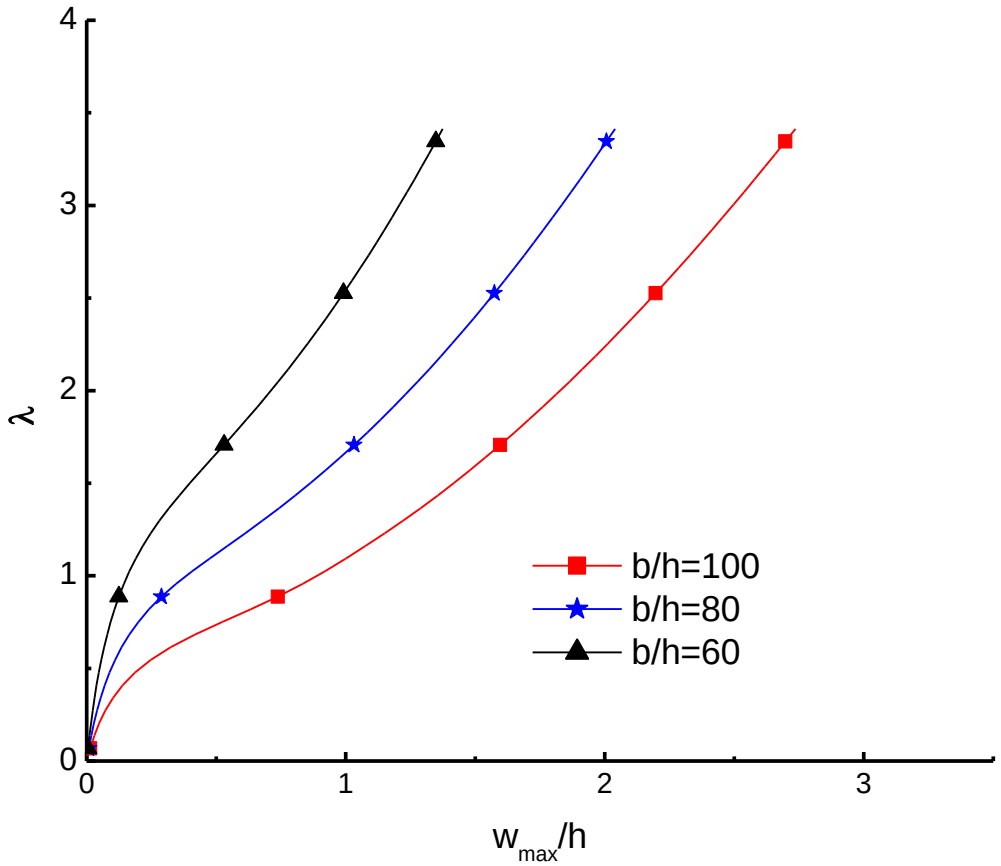

Fig. 5.3.9: Effect of slenderness ratio (*b/h*) on the thermal postbuckling behavior of simply-supported FGM plate with a central circular cutout.

.

5.3.4 Conclusions

A study on nonlinear finite element analysis of perforated elastic Ni/Al_2O_3 FGM plate is conducted under uniform temperature rise. After validating the results of present formulation with the available results in literature, the effects of temperature-dependent material properties, material gradation (i.e., material inhomogeneity), cutout shape and size, boundary conditions and geometrical parameters (i.e., aspect ratio and slenderness ratio) on thermal postbuckling behavior of perforated FGM plate are investigated. Based on the study, following important findings are observed.

- The thermal buckling load of perforated FGM plate is greatly dependent on the shape of the cutout, and for the same cutout area, the FGM plate with elliptical cutout depicted maximum thermal buckling load, whereas the FGM plate with square cutout possesses minimum buckling load.
- The thermal postbuckling strength (at a particular value of deflection) of perforated FGM plate is overestimated in the case of temperature-independent material

properties when compared with the case of temperature-dependent material properties and hence, for realistic and accurate analysis of thermal postbuckling behavior of FGM plate, the temperature-dependent material properties should be considered.

- Unlike isotropic plates (which exhibit bifurcation buckling) the perforated FGM plate does not possess bifurcation type of buckling, which is attributed to the presence of thermal bending-extensional coupling which causes transverse deflection even in the absence of pronounced bending load.
- Ascribed by the freely expandable movable edges, the postbuckling strength of simply-supported perforated FGM plate with movable edges is found to be more than that of FGM plate having immovable edges.
- Perforated FGM plate with a larger central cutout area possess more resistance against buckling and subsequent, postbuckling phenomenon due to the increase in the domain of tensile stresses (caused by free expansion of cutout edges because of thermal load) near cutout edges as compared to the corresponding FGM plate with smaller size cutout.
- Like imperforated FGM plate, the perforated FGM plate also shows an increase in strength in the postbuckling region for higher values of aspect ratios (i.e., a/b = 3 and 4), after an initial decrease when the aspect ratio is changed from a/b = 1 to 2.

CHAPTER 6

STABILITY ANALYSIS OF ELASTIC FGM PLATE WITH TEMPERATURE-DEPENDENT MATERIAL PROPERTIES UNDER THERMOMECHANICAL LOADING

6.1 Introduction

The aim of this chapter is to present thermomechanical buckling and postbuckling analysis of imperforated and perforated FGM elastic plates with temperature-dependent thermoelastic material properties. As in Chapter 5, the FGM plate is assumed to be made of Al_2O_3 (i.e., ceramic phase) and Ni (i.e., metallic phase) with temperature-dependent material constants same as given in Table 3.1 of the Chapter 3. The material properties P_j (i.e., Young's modulus and thermal expansion coefficient) are taken as a non-linear function of temperature, as defined in Eq. (3.1), and are calculated using Mori-Tanaka homogenization scheme, as discussed in Section 3.2. After conducting the convergence study to fix the number of elements and layers in the models of imperforated and perforated FGM plate, various numerical studies are conducted to examine the effects of temperature-dependent material properties, material inhomogeneity, and loading conditions on the thermomechanical buckling and postbuckling response of imperforated and perforated FGM plates with BC1 boundary conditions (i.e., all edges simply-supported with movable edges), as mentioned in Section 5.1 of Chapter 5. Moreover, the effects of cutout shape and size on the response of perforated FGM plate under thermomechanical loading conditions are also investigated.

For a particular temperature rise, the in-plane, uniformly distributed compressive load is applied on edges $x = 0$ & a for uniaxial compression, and on edges $x = 0$ & a, $y = 0$ & b for biaxial compression. Results for buckling/postbuckling load and the transverse deflection are presented in the following non-dimensionalized forms:

In-plane buckling load: $\frac{N_x\ b^2}{E_c h^3}$ (represented as λ);

Maximum transverse deflection: $\frac{w_{max}}{h}$;

where, E_c is Young's modulus of ceramic, h represents the thickness of FGM plate, b is the width of plate, N_x is the in-plane compressive load in *x*- direction (or *y*-direction) per unit edge length, and $w_{\max}$ is the maximum transverse deflection.

6.2 Thermomechanical Stability Analysis of Imperforated Elastic FGM Plate

6.2.1 Convergence Study

To fix the number of elements in the finite element mesh of imperforated FGM plate and the number of layers, a convergence study was conducted for a simply-supported FGM plate (with n =1) under thermomechanical load (i.e., uniaxial compression combined with constant and uniform temperature rise of 150^{o}C). The results of convergence study are tabulated in Table 6.2.1. A reasonable convergence of thermomechanical buckling load can be observed from Table 6.2.1 for the mesh of 225 (15×15) elements when modeled with 20 layers.

Table 6.2.1: Results of convergence study for thermomechanical buckling load $\left(\lambda = \frac{N_x\ b^2}{E_c h^3}\right)$ of simply-supported FGM plate, under uniaxial compression and constant and uniform temperature rise, $\Delta T = 150^0 C$.

Nos. of elements	$\lambda = \frac{N_x\ b^2}{E_c h^3}$		
	10 layers	20 layers	30 layers
10×10	4.2979	4.3338	4.3481
15×15	4.3338	4.1905	4.1905
20×20	4.3481	4.1690	4.1762

6.2.2 Numerical Results and Discussions

Numerical studies are conducted to examine the effects of various parameters, viz. temperature-dependent material properties, material inhomogeneity (i.e., power exponent *n*), and loading condition on the thermomechanical buckling and postbuckling behavior of imperforated Ni/Al_2O_3 FGM square plate of side 1 m.

The effect of temperature-dependent material properties on thermomechanical buckling and postbuckling response is investigated by considering both temperature-

dependent (TD) as well as temperature-independent (TID) material properties for FGM plate having different material inhomogenity. The plate is subjected to in-plane, uniaxial compression load and constant and uniform temperature rise of $\Delta T = 150^0 C$. The postbuckling paths are drawn in Fig. 6.2.1, and corresponding buckling and postbuckling loads (i.e., at $\frac{w_{max}}{h} = 1$) are tabulated in Table 6.2.2.

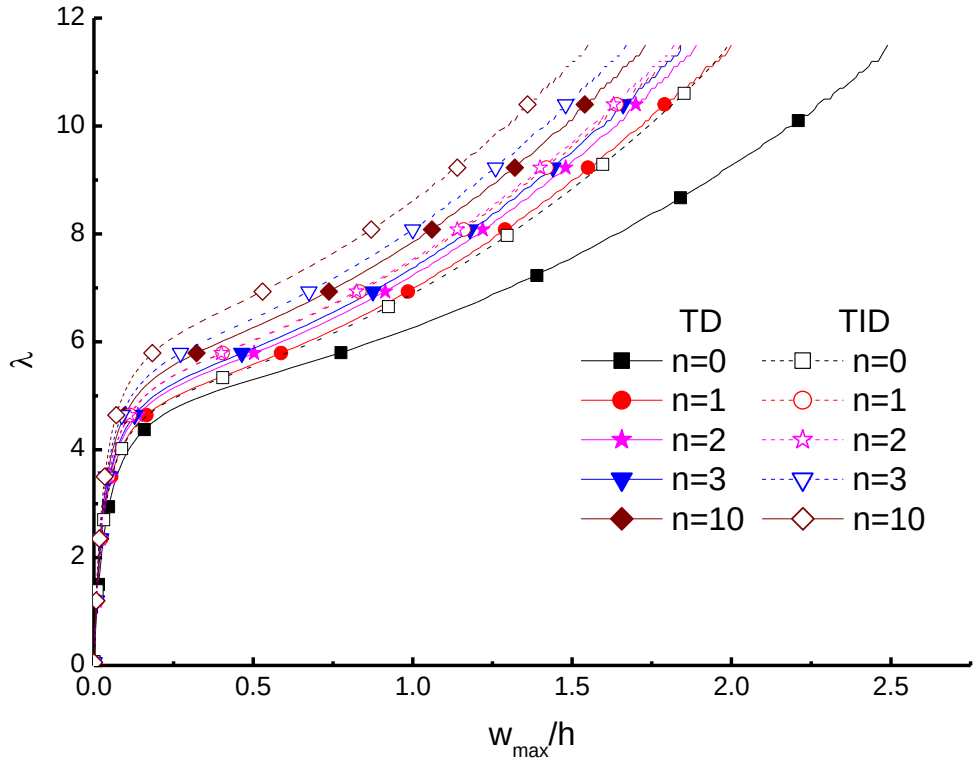

Fig. 6.2.1: Effect of the temperature-dependent material properties on the thermomechanical postbuckling response of FGM plate.

Table 6.2.2: Effect of materail inhomogenity on thermomechanical buckling and postbuckling load of imperforated FGM plate with temperature-dependent and temperature-independent material properties.

n	TD		TID	
	Buckling load λ_{cr}	Postbuckling load corresponding to $\frac{w_{max}}{h} = 1$	Buckling load λ_{cr}	Postbuckling load corresponding to $\frac{w_{max}}{h} = 1$
0	3.94	6.30	4.21	6.91
1	4.24	6.99	4.53	7.51
2	4.36	7.28	4.58	7.56
3	4.41	7.39	4.81	8.08
10	4.70	7.85	5.16	8.65

It can be observed in Fig. 6.2.1 and Table 6.2.2 that the thermomechanical buckling and postbuckling response of FGM plate is greatly affected by the temperature dependence of material properties for all values of power law indices (*n*). The FGM plate with temperature-dependent materials exhibits more transverse deflection as compared to temperature-independent case, for a particular value of load. Again, this can be described by the inverse temperature dependence of Young's modulus on temperature (reduction in Young's modulus due to high temperature) and the direct proportionality of thermal expansion coefficient with temperature (see Fig. 3.2). Irrespective of value of *n*, the postbuckling strength (at a particular value of deflection) of FGM plates is overestimated in the case of temperature-independent material properties when compared with the case of temperature-dependent material properties. This observation establishes the fact that for realistic and accurate analysis of postbuckling behavior of FGM plate under thermomechanical loading, it is important to consider temperature-dependent material properties.

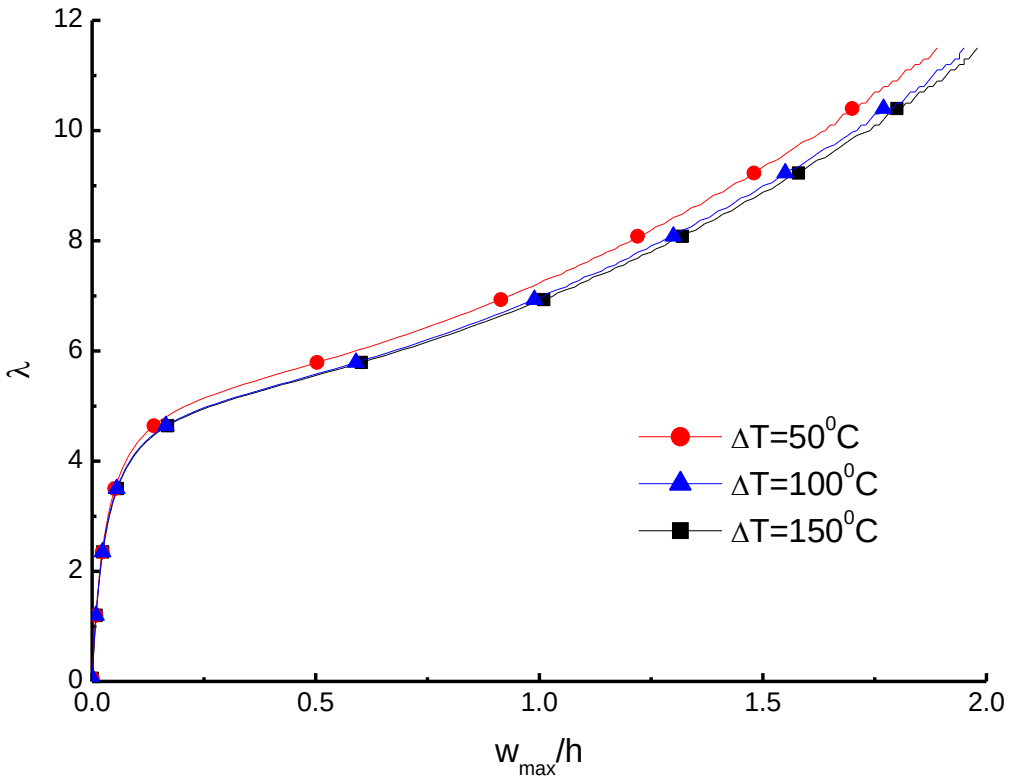

Fig. 6.2.2: Effect of applied thermal loading on the thermomechanical postbuckling response of FGM plate.

The thermomechanical buckling and postbuckling response for FGM plate is calculated under uniaxial mechanical compression loading and constant and uniform temperature rises of $\Delta T = 50,\ 100$ and $150℃$. It can be seen from Fig. 6.2.2 that for a particular value of mechanical load, FGM plate exhibits an increase in the value of transverse deflection with the increase in temperature. This response is caused by the higher thermal load as well as by the reduced stiffness of FGM plate at high temperature because of the inverse dependence of Young's modulus on temperature and the direct proportionality of thermal expansion coefficient with temperature.

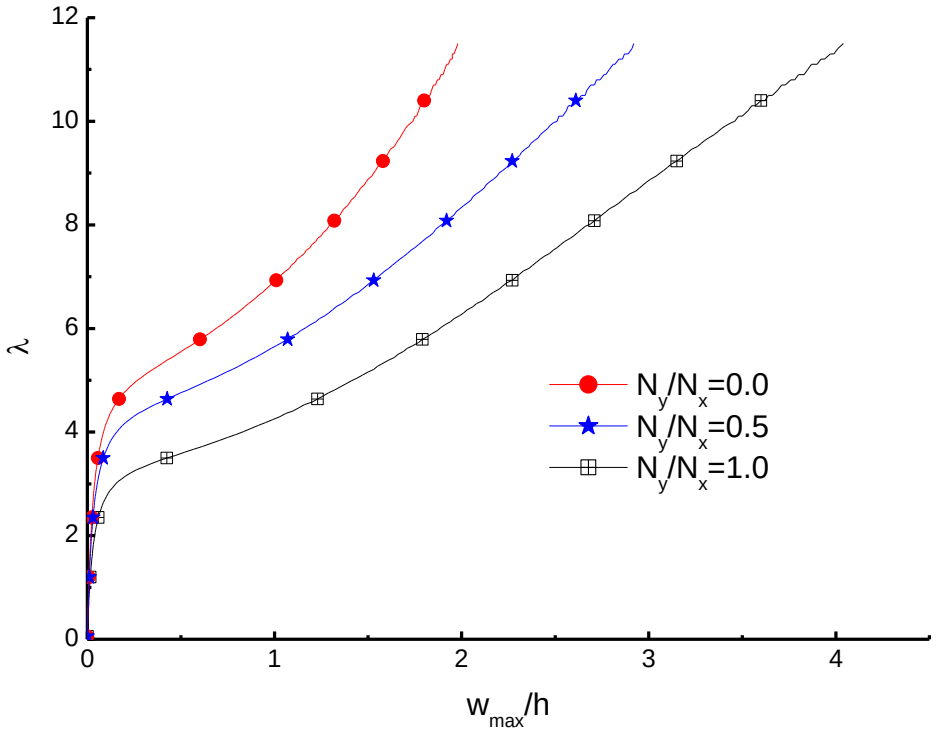

Fig. 6.2.3: Effect of applied biaxial loading on the thermomechanical postbuckling response of FGM plate.

The buckling and postbuckling response of FGM plate under constant and uniform temperature rise of $\Delta T = 150℃$, for different load ratios (i.e., N_y/N_x) are plotted in Fig. 6.2.3. The results show that the maximum values of buckling load and postbuckling strength (for a particular value of deflection) are obtained for plate under uniaxial compression (i.e., for $N_y/N_x = 0$), and the postbuckling curves become significantly lower with the increase in N_y/N_x ratio.

6.2.4 Conclusions

A study on non-linear stability analysis of Ni/Al_2O_3 FGM plate is conducted under thermomechanical loading condition. The effects of temperature-dependent material properties, material gradation (i.e., material inhomogeneity), and thermal and mechanical loading conditions on thermomechanical postbuckling behavior of FGM plate are investigated. Following important findings are obtained out of this study.

- Irrespective of material gradation profile, the postbuckling strength of FGM plate is overestimated in the case of temperature-independent material properties; therefore, for realistic and accurate analysis of thermomechanical postbuckling behavior of FGM plate, the temperature-dependent material properties should be considered.
- Buckling and postbuckling response of FGM plate is found to be significantly affected by its material gradation profile, and the FGM plate with higher ceramic proportion depicted higher buckling load and postbuckling strength.
- Effect of rise in temperature difference (i.e., ΔT) is to develop more transverse deflection of FGM plate.
- Under biaxial loading, the thermomechanical postbuckling load-deflection curves of FGM plate become significantly lower (meaning thereby decrease in buckling and postbuckling strengths) as the N_y is increased, and it causes the increase in maximum transverse deflection.

6.3 Thermomechanical Stability Analysis of Perforated Elastic FGM Plate

6.3.1 Details of Perforation

In the present study, perforated FGM plate with a central cutout of various shapes (i.e., circular, square, diamond, and elliptical) and sizes [i.e., (A_1, A_2, and A_3) as mentioned in Section 5.3.1 of Chapter 5] is considered to observe the effect of shape and size of perforation on thermomechanical buckling and postbuckling response of the FGM plate.

6.3.2 Convergence Study

To fix the number of elements and layers in the finite element model for conducting thermomechanical stability analysis of perforated elastic FGM plate, a convergence study was conducted for FGM plate with a centrally located square cutout of size A_3 (c/b = 0.420) under uniaxial compression, and constant and uniform temperature rise of 150^{o}C. The plate was meshed using the mesh size control feature of ANSYS, as discussed in Section 5.3.2 of Chapter 5. The results of convergence study for non-dimensionalized buckling load are tabulated in Table 6.3.1. A reasonable convergence of thermomechanical buckling load can be observed from Table 6.3.1 for the mesh of 3049 elements (i.e., for the mesh control parameter, η = 30, as mentioned in Section 5.3.2) when modeled with 20 layers. For the sake of uniformity, the same meshing procedure with the same mesh control parameter (i.e., η = 30) was followed to mesh the plate with other cutout shapes.

Table 6.3.1: Results of convergence study for thermomechanical buckling load $\left(\lambda = \frac{N_x\ b^2}{E_c h^3}\right)$ of FGM plate with a central square cutout of size A_3, under uniaxial compression and constant and uniform temperature rise of 150^{o}C.

Nos. of elements	No. of layers		
	10	20	30
797	2.8653	3.2243	3.2451
3049	2.8512	3.1518	3.1518
6309	2.8510	3.1510	3.1510

6.3.3 Numerical Results and Discussion

Various numerical studies are conducted to examine the effects of temperature-dependent material properties, cutout shape, material inhomogeneity, cutout size, thermal loading condition, and aspect ratio on the thermomechanical buckling and postbuckling behavior of perforated FGM plate.

The effect of cutout shape on thermomechanical buckling and postbuckling behavior of FGM plate having temperature-dependent (TD) and temperature-independent (TID) material properties is studied by considering a elastic FGM plate with a central cutout of size A_3 under uniaxial mechanical load, and constant and uniform temperature rise of $\Delta T = 150^0 C$. Corresponding plots of thermomechanical buckling and postbuckling response of perforated FGM plate are drawn in Fig. 6.3.1. It can be observed from Fig. 6.3.1 that the thermomechanical postbuckling response of perforated FGM plate is greatly affected by the temperature dependence of material properties for all cutout shapes. Similar to preceding chapters the perforated FGM plate with temperature-dependent material properties exhibits more transverse deflection as compared to temperature-independent case, for a particular value of load. Irrespective of cutout shape, the thermomechanical postbuckling strength (at a particular value of transverse deflection) of FGM plates is higher for the case of temperature-independent material properties when compared with the case of temperature-dependent material properties. Hence, it is necessary to consider temperature-dependent material properties of FGM plate to predict the thermomechanical buckling and postbuckling strength of perforated FGM plate accurately. Fig. 6.3.1 also reveals that initially, for a particular value of transverse deflection (i.e., w_{max}/h), the FGM plate with diamond cutout possesses highest postbuckling strength, whereas the FGM plate with elliptical cutout has a minimum postbuckling strength, for both the temperature-independent and temperature-dependent material properties.

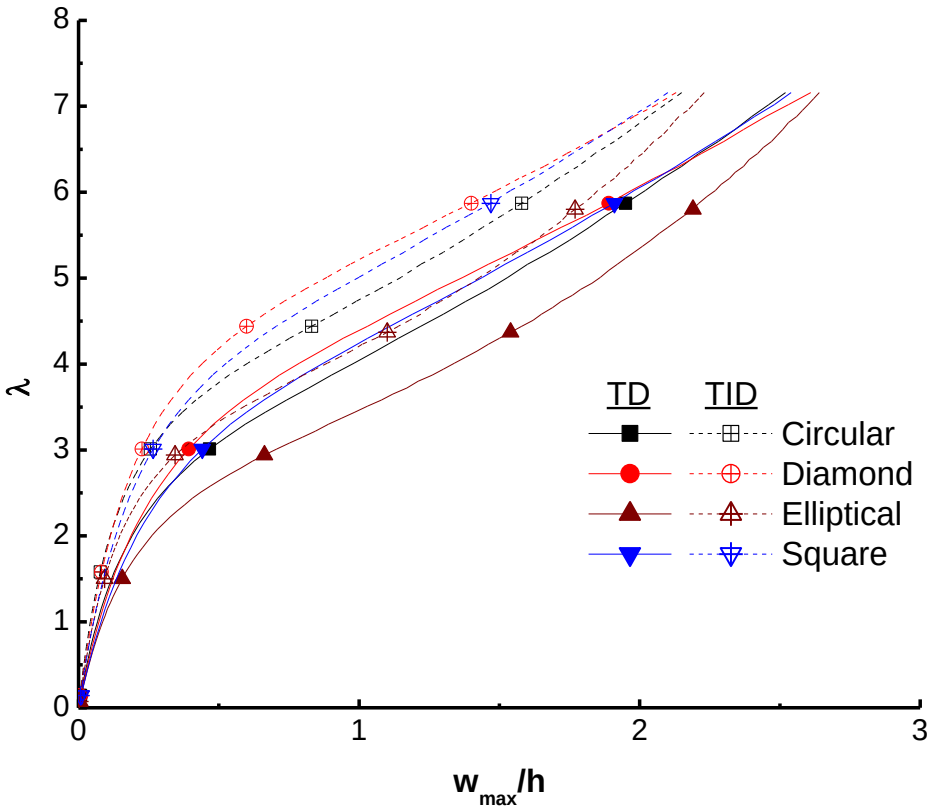

Fig. 6.3.1: Effect of the temperature-dependent material properties on the thermomechanical postbuckling response of FGM plate with a cutout of various shapes under combined uniaxial compressive load and constant and uniform temperature rise.

The effect of material property gradation on thermomechanical buckling and postbuckling response of FGM plate having cutout of various shapes and of size A_3 is studied, and the corresponding results are plotted in Fig. 6.3.2. The Fig. 6.3.2 shows that the thermomechanical buckling and postbuckling response of perforated FGM plate is significantly affected by the value of *n*, and irrespective of the cutout shape, the postbuckling strength (at a particular value of transverse deflection) of perforated FGM plate is enhanced considerably by increasing the value of *n.* It is to mention here that by increasing the value of *n*, the proportion of ceramic phase (i.e., which possess higher stiffness and better thermal properties) in FGM plate is also increased; hence, the FGM plate became stiffer with increased value of *n*, and for all cutout shapes, the FGM plate with $n = 10$ depicted minimum transverse deflections for a particular value of load.

In Fig. 6.3.2, the $n = 0$ corresponds to homogenous isotropic material Ni which possess bifurcation buckling phenomenon; whereas, for all nonzero values of *n* which corresponds to FGMs, the bifurcation buckling phenomenon remain absent due to a

higher degree of bending-extensional coupling. As revealed in previous studies (Abrate, 2006; Aydogdu, 2008; Prakash et al., 2009) that in FGM plate (i.e., for all nonzero values on n), the non-symmetric distribution of material properties causes additional bending moment with the initiation of in-plane compression along with constant and uniform temperature rise. This additional bending moment induces transverse deflection in FGM plate at the onset of compressive loading and leads to overall different buckling and postbuckling response of FGM plate as compared to homogenous plate with $n = 0$.

The buckling and postbuckling behavior of perforated FGM plate with a central cutout of various shapes and sizes under thermomechanical loading is studied to observe the effect of cutout size on the thermomechanical buckling and postbuckling behavior of perforated FGM plate, and corresponding results are shown in Fig. 6.3.3. It can be observed from Fig. 6.3.3 that for all cutout shapes, the value of buckling and postbuckling loads of FGM plate decrease considerably with an increase in the cutout size, and the plate with smallest perforation size (i.e., A_1) depicted highest thermomechanical buckling and postbuckling resistance. It is also evident from Fig. 6.3.3 that irrespective of size of cutout, the FGM plate with diamond shape cutout possesses maximum thermomechanical postbuckling strength (i.e., at a particular value of transverse deflection) .

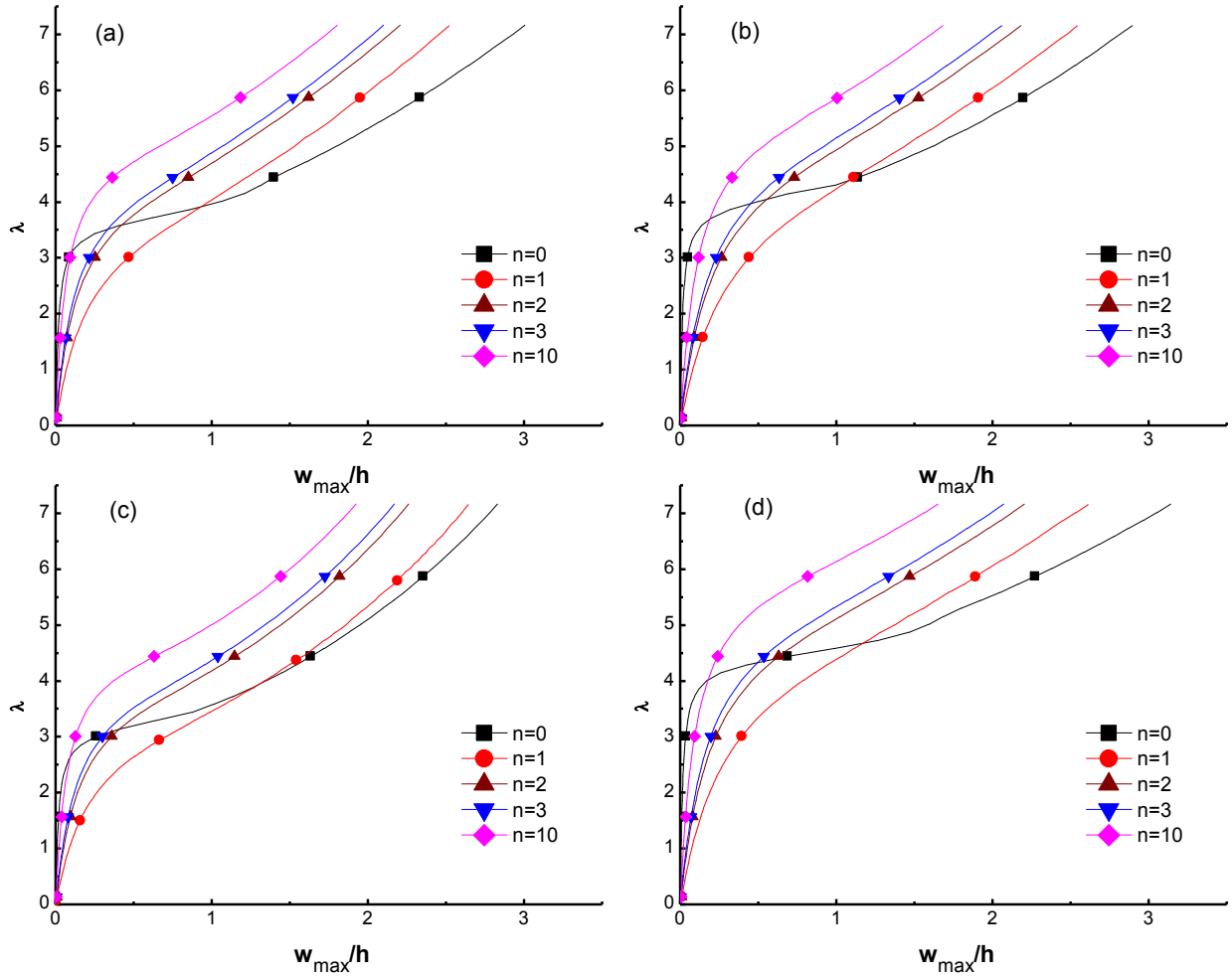

Fig. 6.3.2: Effect of material inhomogenity on the thermomechanical postbuckling behavior of FGM plate with a central cutout of size A_3 and of: (a) circular (b) square (c) elliptical, and (d) diamond shape.

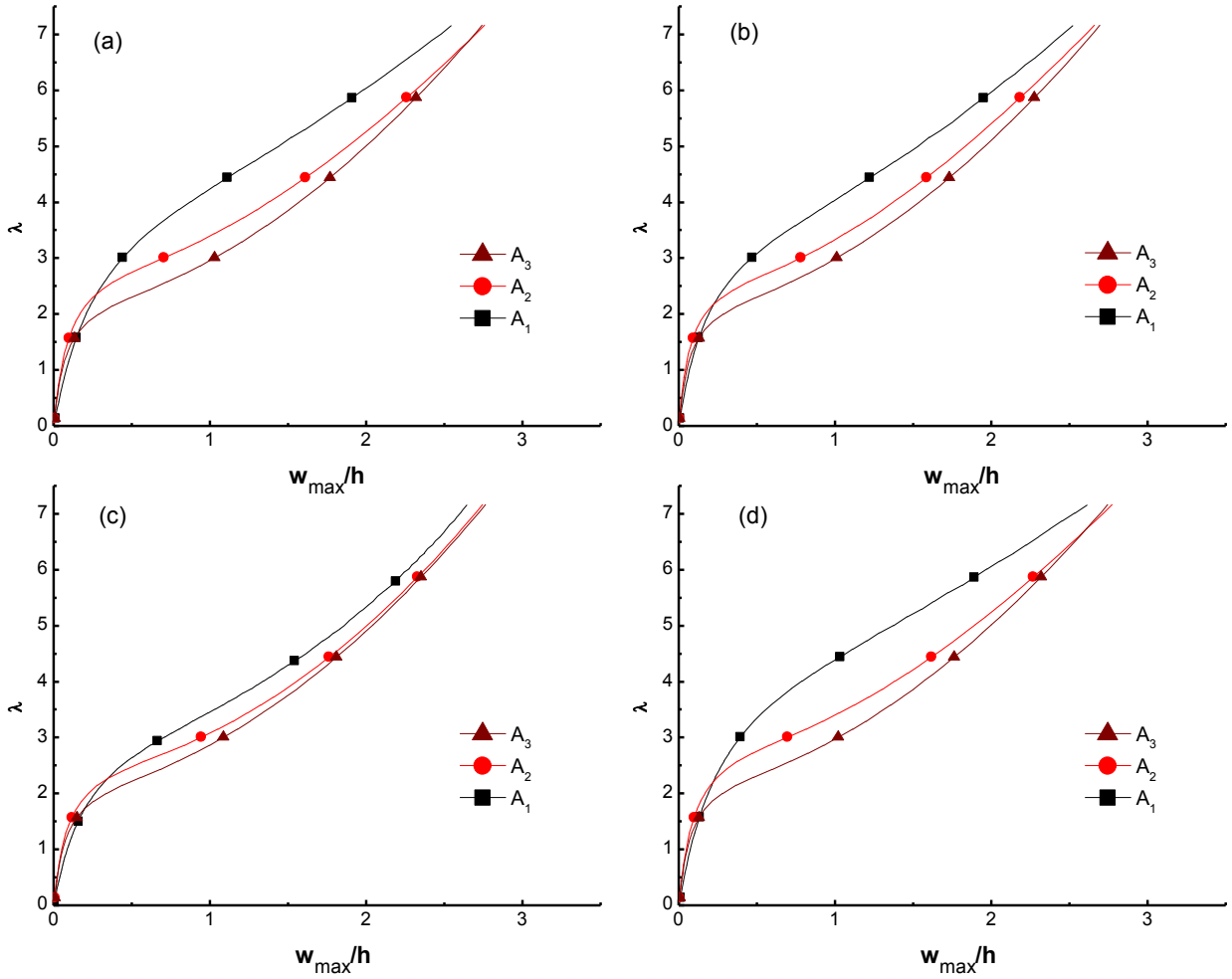

Fig. 6.3.3: Effect of cutout size on the thermomechanical postbuckling behavior of FGM plate with a central cutout of: (a) circular (b) square (c) elliptical, and (d) diamond shape.

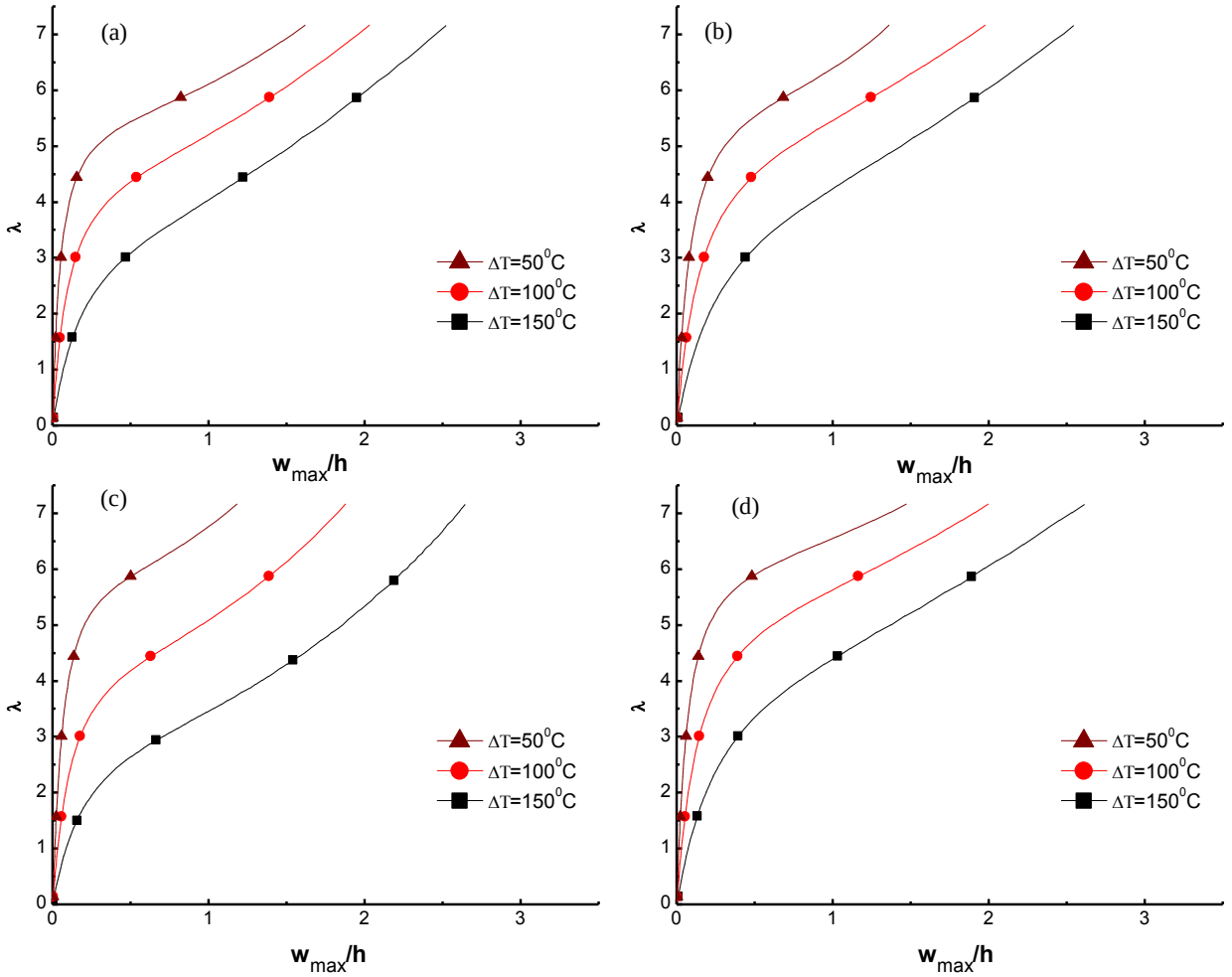

Fig. 6.3.4: Effect of applied thermal load on the thermomechanical postbuckling behavior of FGM plate with a central cutout of size A_3 and of (a) circular (b) square (c) elliptical, and (d) diamond shape.

Effect of applied thermal loading on thermomechanical buckling and postbuckling responses of perforated FGM plates with various cutout shapes is studied with the results plotted in Fig.6.3.4. It can be seen from Fig. 6.3.4 that for all cutout shapes, the postbuckling paths of perforated FGM plate are strongly dependent on temperature rise (i.e.,ΔT), and for a particular value of mechanical load, FGM plate exhibit an increase in the value of transverse deflection with the increase in temperature. This response is caused by the high thermal load as well as by the reduced stiffness of FGM plate at high temperature because of the inverse dependence of Young's modulus on temperature (reduction in Young's modulus with increase in temperature) and the direct proportionality of thermal expansion coefficient with temperature.

In addition, the effect of aspect ratio (length-to-width ratio, i.e., *a/b*) on thermomechanical buckling and postbuckling behavior of simply-supported FGM plate with a central cutout of size A_3 is studied under constant and uniform temperature rise of $\Delta T = 150℃$. To study the effect of aspect ratio, the slenderness ratio is fixed at 100, and for a fixed width (b = 1 m), the different aspect ratios (i.e., 1, 2, 3 and 4) are obtained by varying the length of the plate. The thermomechanical buckling and postbuckling paths for different aspect ratios of FGM plate having central cutout of various shapes are shown in Figs. 6.3.5.

It can be observed from Fig. 6.3.5 that the postbuckling response of square (i.e., $a = b$) FGM plate with a central cutout differs significantly with that of rectangular (i.e., $a \neq b$) FGM plate. For a particular value of w_{max}/h, square FGM plate (i.e., unit aspect ratio) is found to possess highest thermomechanical postbuckling strength. It can also be noticed from Fig. 6.3.5 that the thermal postbuckling resistance is decreased considerably with an increase in aspect ratio from 1 to 4, which may be attributed to the increasing thermal effect with the increase in the length of sides that are constrained to move in *y*-direction.

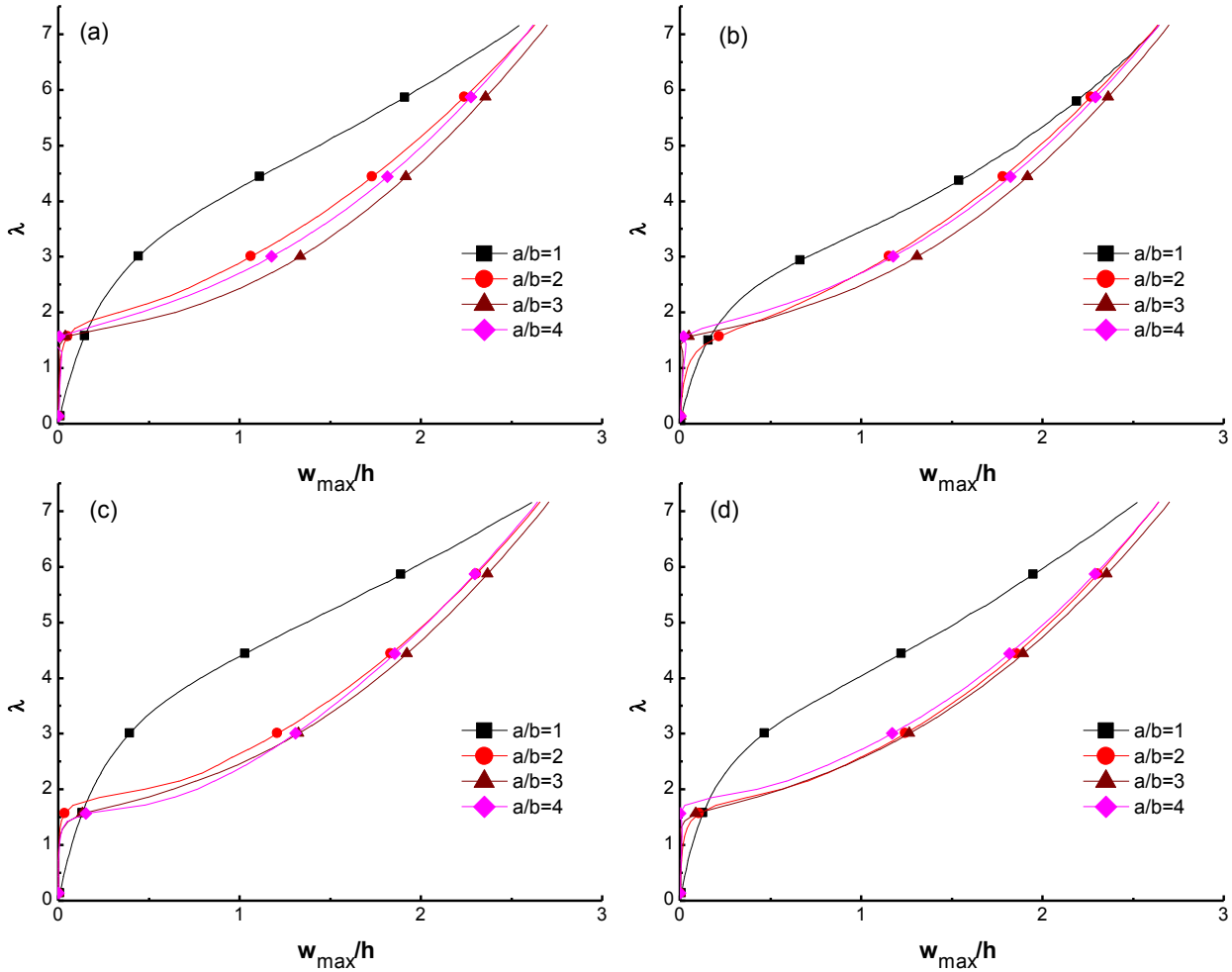

Fig. 6.3.5: Effect of aspect ratio (*a/b*) on the thermomechanical postbuckling behavior of FGM plate with a central cutout of size A_3 and of: (a) circular (b) square (c) elliptical, and (d) diamond shape.

6.3.4 Conclusions

A study on non-linear finite element analysis of Ni/Al_2O_3 FGM plate carrying a central cutout of various shapes is conducted under thermomechanical loading conditions. The effects of temperature-dependent material properties, material gradation (i.e., material inhomogeneity), cutout shape and size, and aspect ratio on thermomechanical buckling and postbuckling behavior of FGM plate are investigated, and based on the results following important conclusions are drawn.

- Buckling and postbuckling responses of perforated FGM plate under thermomechanical loading is considerably affected by the shape of perforation, and the FGM plate with diamond shape cutout depicted maximum resistance towards thermomechanical buckling and postbuckling phenomenon, whereas the FGM plate with elliptical shape cutout posses minimum buckling and postbuckling strength.
- FGM plate with a larger central cutout size possesses lesser resistance against thermomechanical buckling and postbuckling phenomenon as compared to the corresponding FGM plate with smaller size cutout.
- Thermomechanical postbuckling resistance of perforated FGM plate is overestimated in the case of temperature-independent material properties, when compared with the case of temperature-dependent material properties; hence, for realistic and accurate analysis of thermomechanical postbuckling behavior of FGM plate, the temperature-dependent material properties should be considered.
- Buckling and postbuckling response of square FGM plate differs significantly from that of rectangular plates, and the buckling and postbuckling strength of FGM plate under thermomechanical loading conditions decreases considerably with an increase in aspect ratio of the plate.

CHAPTER 7

STABILITY AND FAILURE ANALYSIS OF ELASTIC-PLASTIC FGM PLATE UNDER IN-PLANE MECHANICAL COMPRESSION

7.1. Introduction

The aim of present chapter is to present the nonlinear stability and failure analysis of imperforated and perforated elastic-plastic FGM plates under in-plane mechanical compression. Geometrical and material nonlinearities are integrated into the analysis to obtain the ultimate load capacity of the FGM plate, as discussed in Chapter 3. The FGM plate is assumed to be made of two constituents: TiB (i.e., ceramic phase) and Ti (i.e., metallic phase), with the following material properties (Jin et al., 2003): E_C = 375 GPa, E_m = 107 GPa, $\nu = 0.24$ (for ceramic and metal both), σ_{ym} = 400 MPa and H_m=14 GPa. The subscripts *c* and *m*, respectively, correspond to the ceramic and the metallic constituents. It is to mention here that material is graded as per TTO model as specified in Chapter 3, i.e., using the volume fraction of the constituents at a particular value of thickness coordinate [calculated using Eq. (3.2)], Young's modulus, yield strength and elastic-plastic tangent modulus of FGM plate at that thickness coordinate are calculated using Eqs. (3.3), (3.10) and (3.11), respectively, taking the value of the load transfer parameter q as 4.5 GPa. The elastic-plastic behavior of FGM plate is assumed to follow J_2-plasticity and isotropic hardening in which the ceramic phase was considered to be elastic whereas the metal is taken to be elastic-plastic material in accordance with the TTO model. Before carrying out the study, convergence studies are conducted to fix the number layers to model FGM plate and number of elements for FEM analysis of imperforated and perforated FGM plates. To verify the analysis procedure, the ultimate load capacities obtained from the present formulation, for elastic-plastic imperforated and perforated plates, are compared with the available results in the literatures. Various parametric studies are conducted to investigate the effects of material inhomogenity, loading conditions, aspect, and slenderness ratios on nonlinear buckling and postbuckling behavior, and failure response of imperforated and perforated elastic-plastic FGM plates. Moreover, the effects of cutout shape and

size on the elastic-plastic buckling, postbuckling and failure response of perforated FGM plate are also investigated. The current study is carried out for FGM plates with BC1 boundary conditions (i.e., all edges simply-supported with movable edges), as mentioned in Section 5.1 of Chapter 5. The in-plane, uniformly distributed compressive load is applied on edges $x = 0$ & a for uniaxial compression, and on edges $x = 0$ & a, $y = 0$ & b for biaxial compression.

Results for mechanical buckling and failure loads, and the transverse deflection are presented in the following non-dimensionalized forms:

In-plane buckling and failure load: $\frac{N_x\ b^2}{E_c h^3}$ (represented as λ);

Maximum transverse deflection: $\frac{w_{max}}{h}$;

Maximum axial deflection: $\frac{u_{max}}{h}$

where, E_c is Young's modulus of ceramic, h represents the thickness of FGM plate, b is the width of plate, N_x is the in-plane compressive load per unit edge length, w_{max} is the maximum transverse deflection, and u_{max} is maximum axial deflection.

7.2 Mechanical Stability and Failure Analysis of Imperforated Elastic-Plastic FGM Plate

7.2.1 Convergence Study

To fix the number of layers to model FGM and number of elements in the finite element mesh, used for conducting mechanical stability and failure analysis of imperforated elastic-plastic FGM plate, a convergence study was conducted for FGM plate using meshes of 81, 100, and 121 elements having 10, 20 and 30 layers. The convergence of buckling and failure loads was checked for simply-supported FGM ($n = 1$) square plate with $b/h = 50$ under uniaxial compression. The results of convergence study are shown in Table 7.2.1. It can be seen from Table 7.2.1 that results for buckling and failure loads for FGM plate are converged reasonably for the mesh of 100 elements (i.e., 10 × 10) when modeled with 20 layers.

Table 7.2.1: Convergence study for buckling load $\left(\lambda = \frac{N_x b^2}{E_c h^3}\right)$ and failure load $\left(\lambda_{fail} = \frac{N_{fail} b^2}{E_c h^3}\right)$ for FGM plate under uniaxial compression.

No. of elements (along x× along y)	No. of layers					
	10		20		30	
	λ	λ_{fail}	λ	λ_{fail}	λ	λ_{fail}
$\mathbf{9 \times 9}$	1.4953	7.0093	1.4486	6.6355	1.4019	6.4579
$\mathbf{10 \times 10}$	1.4660	6.9159	1.4019	6.5421	1.3730	6.4019
$\mathbf{11 \times 11}$	1.4673	6.8692	1.3730	6.5140	1.3451	6.3551

Table 7.2.2: Comparison between the normalized ultimate load carrying capacity(σ_u/σ_y) computed in the present study and that of Shanmugam *et al.* (1999).

b/h	σ_u/σ_y	
	Shanmugam *et al.* (1999)	Present Study
60	0.72	0.68
50	0.81	0.84
40	0.90	0.94
30	0.95	0.99
20	1.01	1.01

7.2.2 Verification of Results

The validity of present procedure for elastic-plastic analysis is verified by comparing the normalized ultimate load carrying capacity (defined as the ratio of ultimate load carrying capacity of plate to yield strength of the material, i.e., σ_u/σ_y) of a simply-supported plate obtained in the present study with that reported by Shanmugam *et al.* (1999). The material (i.e., A572 Grade 50 steel with Young's modulus, E = 207 GPa, Poisson's ratio, ν = 0.3 and Yield strength, σ_y= 343 MPa) of the plate is considered to be isotropic, homogeneous, elastic and perfectly plastic, as assumed in the Ref. (Shanmugam *et al.*, 1999). Table 7.2.2 shows a good concurrence between the results of present study with the results reported by Shanmugam *et al.* (1999).

7.2.3 Numerical Results and Discussion

Various numerical studies are conducted to examine the effects of material inhomogeneity (i.e., power exponent n), loading conditions (uniaxial and biaxial in-plane compression), aspect ratio (i.e., a/b), and slenderness ratio (i.e., b/h) on the elastic-plastic buckling and postbuckling behavior, and the ultimate load carrying capacity (i.e., denoted here as failure load) of FGM plate.

The effect of material gradation (i.e., power law exponent *n*) on elastic-plastic buckling load, postbuckling response and failure of Ti/TiB FGM plate under uniaxial mechanical compression are shown in Fig. 7.2.1, and the corresponding values of buckling load, yielding load and failure load are tabulated in Table 7.2.3. It can be observed from Fig. 7.2.1 and Table 7.2.3 that although the failure load of FGM plate is increased considerably with the increase in the value of *n*, however the FGM plate with higher value of *n* possesses smaller transverse deflection at the time of failure. Here it is worth to mention that by increasing the value of *n*, the proportion of TiB (which comprise high stiffness and brittleness) is increased, that results in the increase of failure load at lesser deflection of FGM plate. Moreover, Fig. 7.2.1 also shows that the bifurcation buckling phenomenon remains absent in the case of FGM plate (i.e., non-zero values of *n*) due to a higher degree of bending-extensional coupling, which causes transverse deflection even in the absence of any bending load. Moreover, the plate with *n* = *0*, which corresponds to the metal plate, depicted higher value of buckling load than the corresponding FGM plates (i.e., with *n* = 1, 2, 3 and 10) due to bifurcation buckling response.

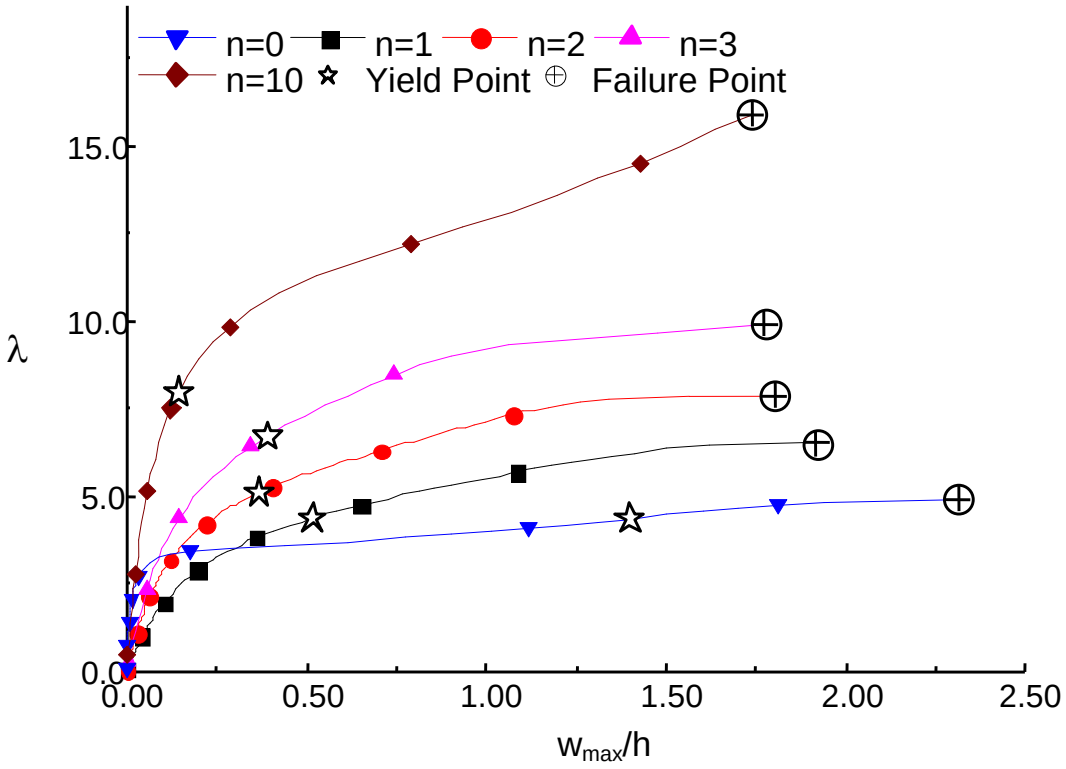

Fig. 7.2.1: Effect of material gradation profile (*n*) on elastic-plastic buckling, postbuckling and failure behavior of Ti/TiB FGM plate under uniaxial compression.

Table 7.2.3: Effect of material gradation profile (n) on elastic-plastic buckling load, yielding load and failure load of Ti/TiB FGM plate under uniaxial compression.

n	Buckling load (λ)	Yielding load (λ_y)	Failure load (λ_{fail})
0	3.11	4.41	4.93
1	1.40	4.43	6.54
2	1.95	5.06	7.86
3	2.27	6.69	9.86
10	5.02	7.95	15.81

The effect of loading conditions (i.e., in-plane uniaxial and biaxial compression) on the elastic-plastic buckling, postbuckling and failure response of square FGM (with n = 1) plate of slenderness ratio 50 (i.e., b/h = 50) is examined, and the corresponding plots of load versus transverse deflection are presented in Fig. 7.2.2. It may be observed that there is a monotonic decrement in the ultimate load capacity and the corresponding transverse deflection with an increase in the value of load ratios (i.e., *Ny/Nx*). Moreover, the yielding load is also found to decrease considerably at higher value of load ratio.

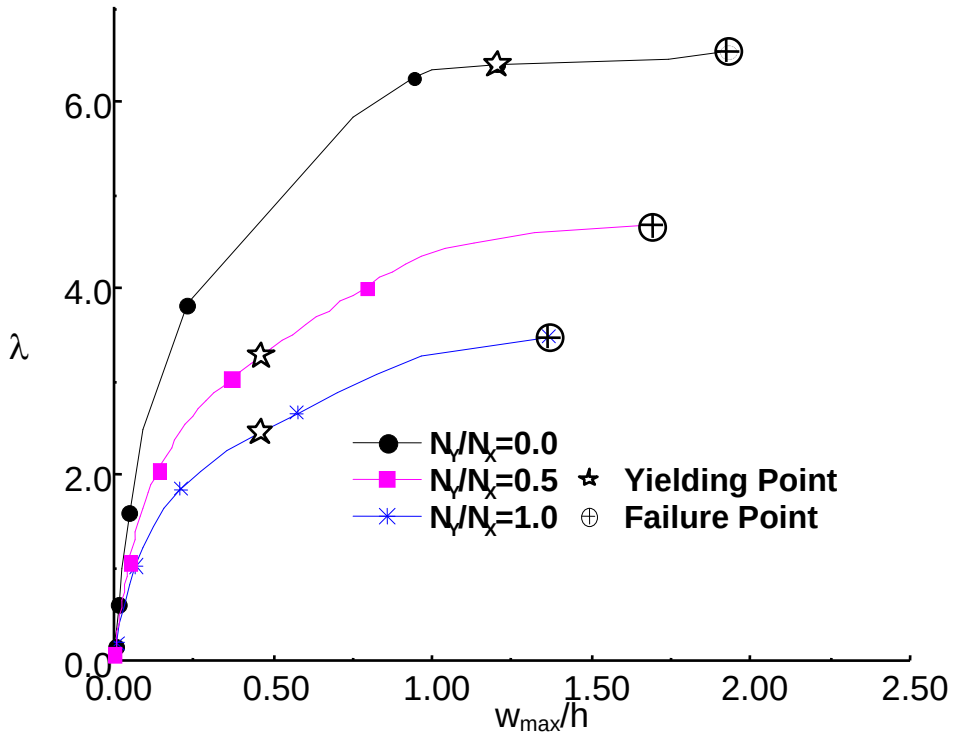

Fig. 7.2.2: Effect of loading condition on elastic-plastic buckling, postbuckling and failure behavior of Ti/TiB FGM plate.

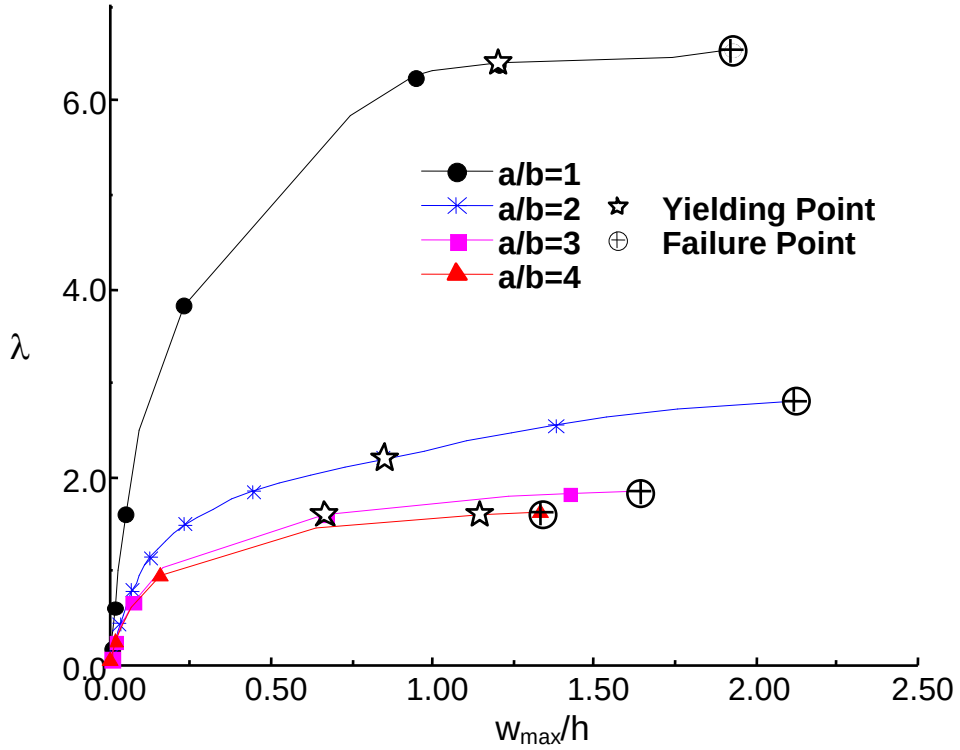

Fig. 7.2.3: Effect of aspect ratio (*a*/*b*) on elastic-plastic buckling, postbuckling and failure behavior of FGM plate.

In addition, the effect of plate aspect ratio (i.e., *a*/*b*) on elastic-plastic buckling postbuckling and failure response of FGM (for n = 1) plate under uniaxial compression is also studied, and the postbuckling paths for various values of aspect ratios (i.e., *a*/*b* =1, 2, 3 and 4) are depicted in Fig.7.2.3. It can be seen from Fig.7.2.3 that the buckling, postbuckling strength and ultimate load capacity of square FGM plate (i.e., for *a*/*b* =1) are found to be maximum. The yielding and failure load of FGM plate with *a*/*b* =1 are almost 300% higher than the corresponding plate with *a*/*b* = 2. However, the difference between yielding and failure loads decreases with the increase in the value of aspect ratio, and the differences in buckling load and postbuckling response of FGM plate for *a*/*b* = 3 & 4 are comparatively small. These findings seem to be reasonable because the plate with larger aspect ratio (*a*/*b* > 3) behave like a beam.

Table 7.2.4: Effects of slenderness ratio (*b/h*) on absolute values of buckling, yielding and failure loads of square simply-supported TiB/Ti FGM plate under uniaxial compression.

b/h	Buckling load (kN)	Yielding load (kN)	Failure load (kN)
30	24000	26350	50150
50	4200	13056	19620
100	656	3230	5270
200	82	884	1564
300	24	476	799

Various values of slenderness ratio taken are 30, 50, 100, 200 and 300 to discuss the effect of slenderness ratio on the buckling, yielding and failure loads of elastic-plastic simply-supported FGM plate. A monotonic decrement in the absolute values of buckling, yielding and failure loads with increase in the slenderness ratio of FGM plate can be noticed from Table 7.2.4.

7.2.4 Conclusions

A study on non-linear finite element analysis of imperforated elastic-plastic Ti/TiB FGM plate under in-plane mechanical compression is conducted. After validating the results of the present formulation with the available results in the literature, the effects of material inhomogenity, loading conditions, aspect, and slenderness ratios on elastic-plastic buckling, postbuckling and ultimate load capacity of FGM plate are investigated under the framework of J_2 plasticity theory associated with the isotropic hardening flow rule. Followings are the important findings out of the present work:

- Buckling and postbuckling response, and ultimate load capacity of elastic-plastic FGM plate are found to be significantly affected by its material gradation profile, and FGM plate with higher ceramic proportion depicted higher ultimate load capacity with lesser transverse deflections at failure point.
- Effect of biaxial compression loading, in comparison to uniaxial compression, is to reduce the buckling load, postbuckling strength (for a particular value of deflection), and yielding and failure loads.

- Elastic-plastic buckling and postbuckling response of square FGM plate differs considerably from that of rectangular FGM plate, and buckling load, yielding load and ultimate load capacity of FGM plate is found to decrease with the increase in aspect ratio.
- Monotonic decrements in the buckling, yielding and failure loads are observed with the increase in slenderness ratio of the plate.

7.3 Mechanical Stability and Failure Analysis of Elastic-Plastic Perforated FGM plate

7.3.1 Details of Perforation

In the present study, perforated FGM plate with a central circular/square cutout of size = 0.1 (i.e., d/b = 0.1, here, d is diameter/side of circular/square cutout, and b is width of FGM plate) is considered (i.e., as shown in Figs. 7.3.1 and 7.3.2). In addition, the effect of size of cutout is also studied by considering the perforated FGM plate with a central circular/square cutout of different cutout ratios (i.e., d/b = 0.10, 0.15, 0.20, 0.25 and 0.30).

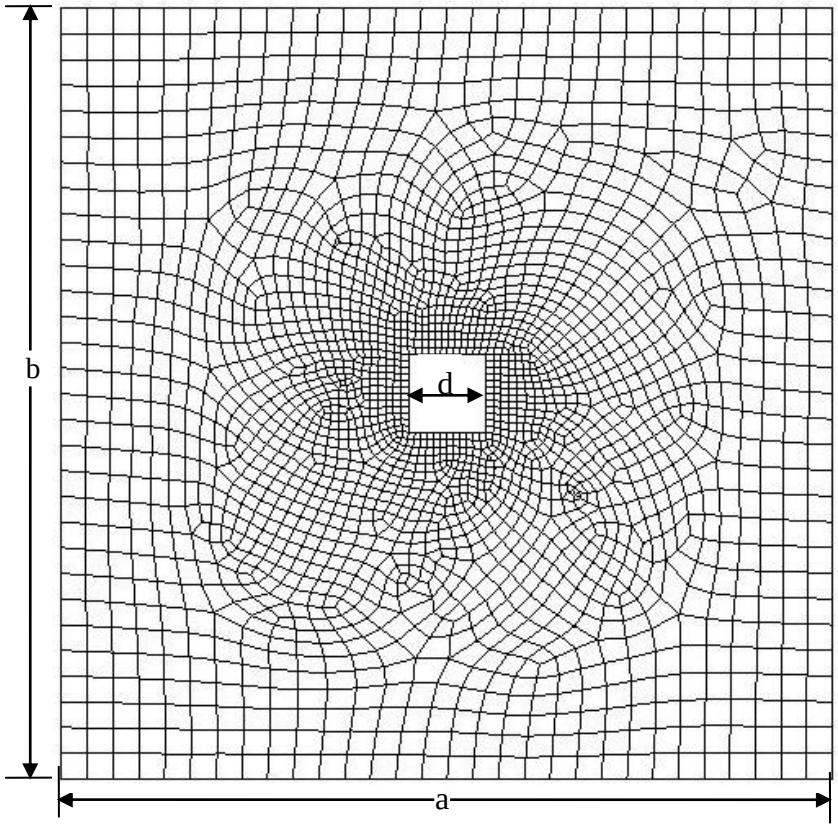

Fig. 7.3.1: Finite element mesh of a typical FGM plate with a central square cutout.

7.3.2 Convergence Study

To fix the number of layers to model FGM plate and the number of elements in the finite element mesh of FGM plate, a convergence study was conducted for a square FGM plate containing a centrally located square cutout of size d/b = 0.1 under uniaxial compression. The plate was meshed using the mesh size control feature of

ANSYS, as discussed in Section 5.3.2 of Chapter 5. The values of mesh control parameter η are taken as 10, 20 and 30 to obtained 1081, 2109 and 3819 number of elements, respectively. The FGM plate was modelled using 10, 20 and 30 layers. A reasonable convergence of buckling and failure loads can be observed from Table 7.3.1 for the FGM plate modeled with 20 layers and meshed with 2109 elements (i.e., for η = 20). For the sake of uniformity, the same meshing procedure with same mesh control parameter (i.e., η = 20) was followed to mesh the plate with cutout of other shape (i.e., circular) and sizes.

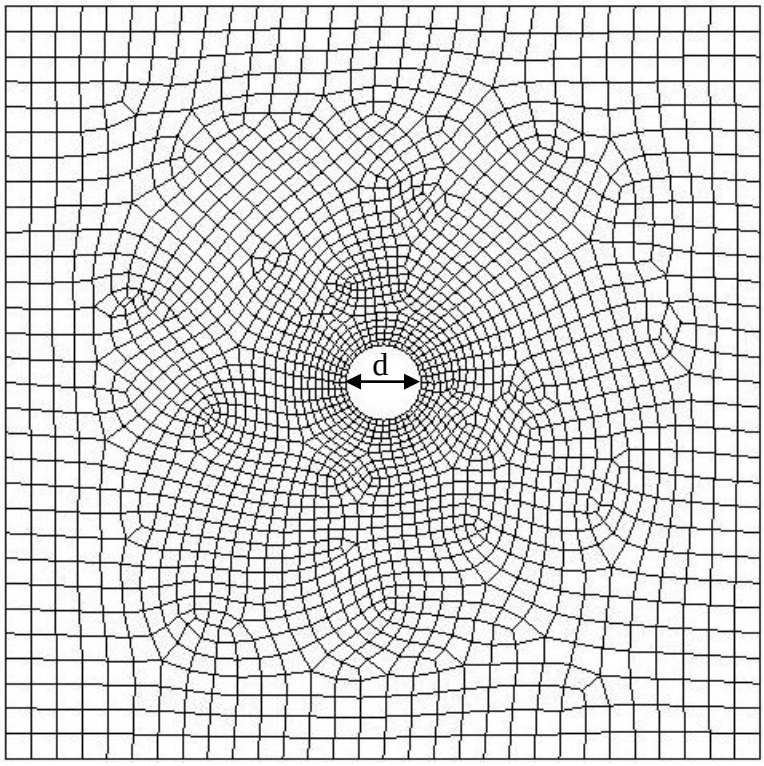

Fig. 7.3.2: Finite element mesh of a typical FGM plate with a circular cutout.

Table 7.3.1: Results of convergence study for non-dimensional buckling $\left(\lambda = \frac{N_x\ b^2}{E_c h^3}\right)$ and failure $\left(\lambda_{fail} = \frac{N_{fail} b^2}{E_c h^3}\right)$ loads of simply-supported FGM plate with a central square cutout.

No. of elements	No. of layers					
	10		20		30	
	λ	λ_{fail}	λ	λ_{fail}	λ	λ_{fail}
1081	1.6687	3.7333	1.6535	3.7333	1.6481	3.6000
2109	1.6672	3.7333	1.6521	3.6000	1.6467	3.5733
3819	1.6614	3.7333	1.6463	3.5733	1.6414	3.5200

Table 7.3.2: Comparison of normalized ultimate load capacity (σ_u/σ_y) obtained in the present work with reported by Shanmugam et *al*. (1999).

b/h	Hole shape	*d/b*=0.1		*d/b*=0.2		*d/b*=0.3	
		Present Study	Shanmugam et *al*. (1999)	Present Study	Shanmugam et *al*. (1999)	Present Study	Shanmugam et *al*. (1999)
30	Square	0.92	0.91	0.80	0.76	0.72	0.67
	Circular	0.91	0.91	0.81	0.81	0.72	0.71
40	Square	0.89	0.90	0.77	0.71	0.69	0.64
	Circular	0.90	0.85	0.81	0.79	0.69	0.67
50	Square	0.75	0.75	0.67	0.65	0.62	0.60
	Circular	0.75	0.76	0.69	0.72	0.62	0.64

7.3.3 Verification of Results

The accuracy of the present elastic-plastic analysis for perforated plate is checked by comparing the normalized ultimate load capacity with that reported by Shanmugam *et al*.(1999), for a homogenous isotropic plate carrying a concentric circular/square cutout. The normalized ultimate load carrying capacities (defined as the ratio of ultimate load carrying capacity of plate to yield strength of the material, i.e., σ_u/σ_y) for a simply-supported square plate of *b* width, *h* thickness, and containing a central cutout of *d* diameter/side (i.e., *d* denotes diameter for circular cutout, and it is side length for square cutout) are compared with the results published by Shanmugam *et al*.(1999). For validating the results, the material and geometric parameters are taken same as used in Ref. (Shanmugam *et al.,* 1999), and the comparison of ultimate load carrying capacities for different slenderness ratios and cutout shape/size is presented in Table 7.3.2 . It can be observed that the results from the present work are in good agreement with the reference work.

7.3.4 Numerical Results and Discussion

Numerical studies are conducted to examine the effects of various parameters, viz. material inhomogeneity (i.e., power exponent *n*), aspect ratio (i.e., *a/b*), loading

condition (i.e., in-plane uniaxial and biaxial compression), slenderness ratio (i.e., b/h), and cutout size/shape (i.e., d/b ratio, circular/square shape cutouts) on the nonlinear stability and ultimate load carrying capacity (denoted here as failure load) of elastic-plastic perforated FGM caused by mechanical in-plane compression.

The effect of cutout size (i.e., d/b = 0.10, 0.15, 0.20, 0.25 and 0.30) on the elastic-plastic buckling and failure responses of FGM (for n = 1) plate (with b/h = 100) under uniaxial compression load are also investigated, and the corresponding plots of load - axial deflection and load - transverse deflection are depicted in Figs. (7.3.3)-(7.3.6).

The ultimate failure points in Figs. (7.3.3)-(7.3.6) correspond to the maximum applied load at which the FGM plate loses its stiffness (i.e., given by the slope of load-axial deflection curve) completely and thereafter, the plate is not able to resist even a slight increment in the applied load. Although the ultimate load capacity of FGM plate not strongly affected with the size of cutout, however it may be observed from Figs. (7.3.3)-(7.3.6) that the plate with larger cutout size shows large deflection at the time of failure. Moreover, it is also noticed by corresponding plots [i.e., Figs. (7.3.3)-(7.3.6)] that FGM plate with circular cutout possesses higher yielding and failure load as compared to plate with square cutout of same cutout ratio.

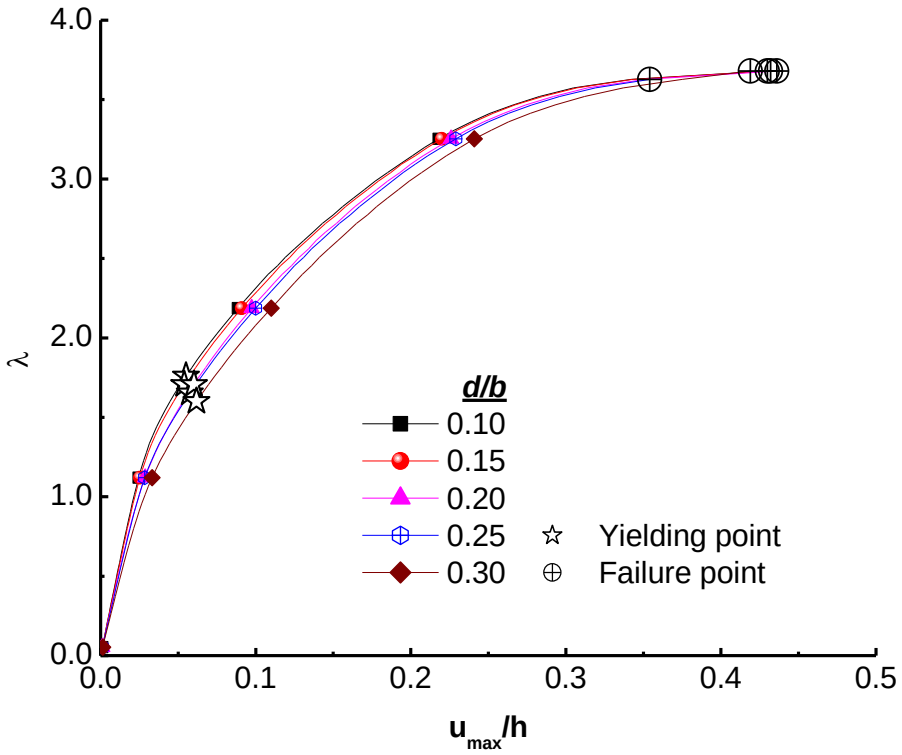

Fig. 7.3.3: Effect of cutout size on load-axial deflection curve of Ti/TiB FGM (n = 1) plate with a circular cutout under uniaxial compression.

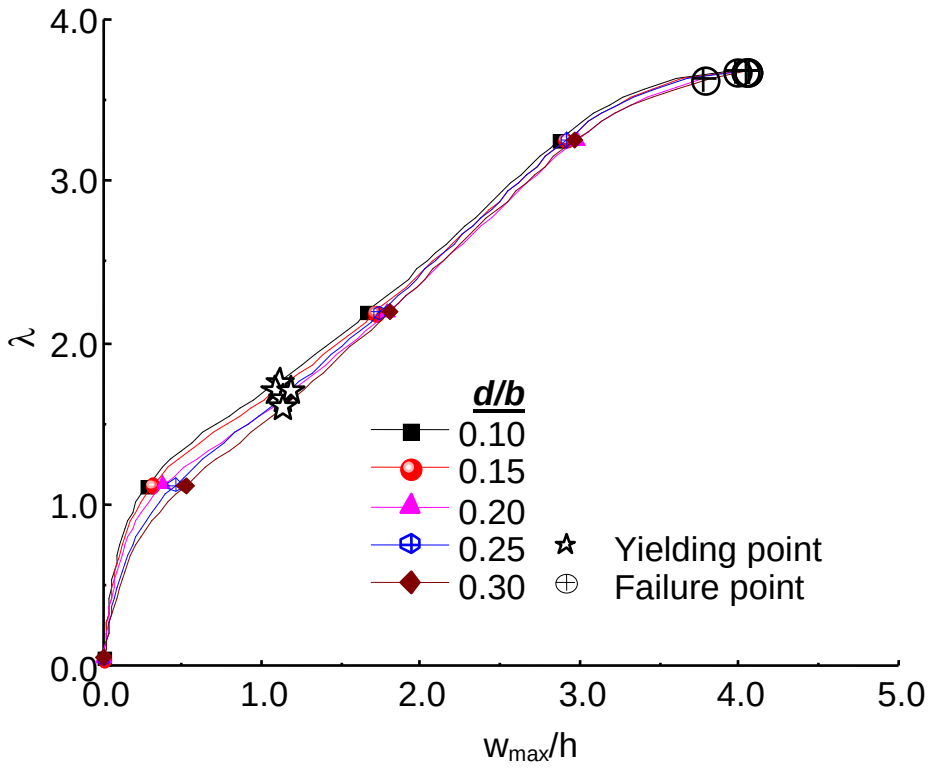

Fig. 7.3.4: Effect of cutout size on elastic-plastic buckling, postbuckling and failure behavior of Ti/TiB FGM (n = 1) plate with a circular cutout under uniaxial compression.

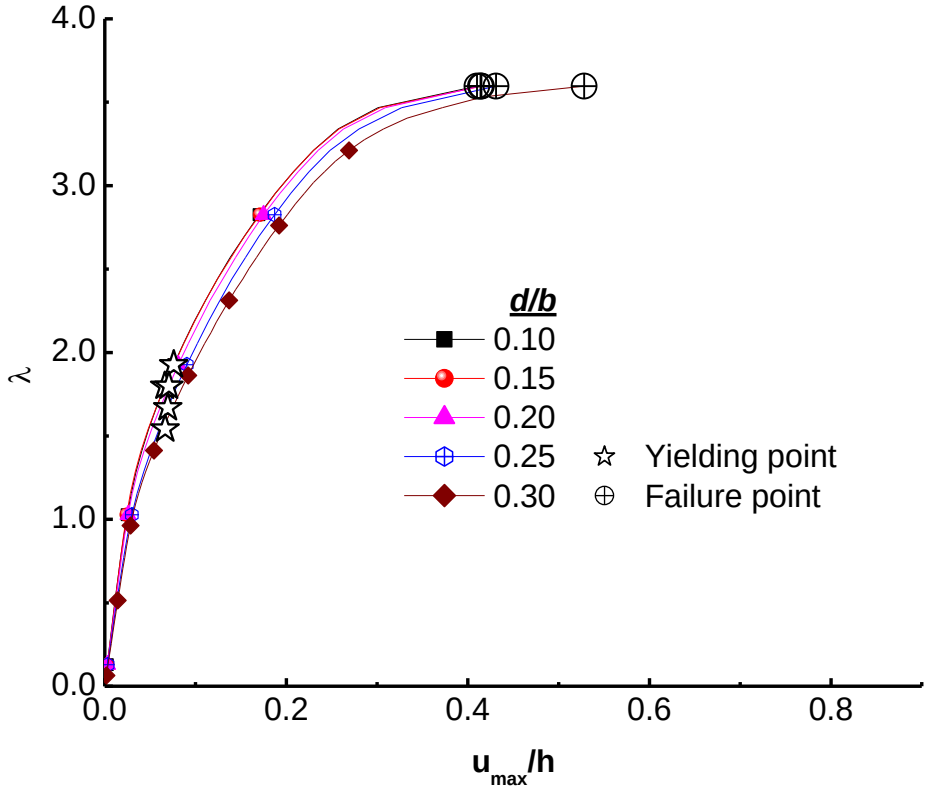

Fig. 7.3.5: Effect of cutout size on load-axial deflection curve of square Ti/TiB FGM (n = 1) plate with a square cutout under uniaxial compression.

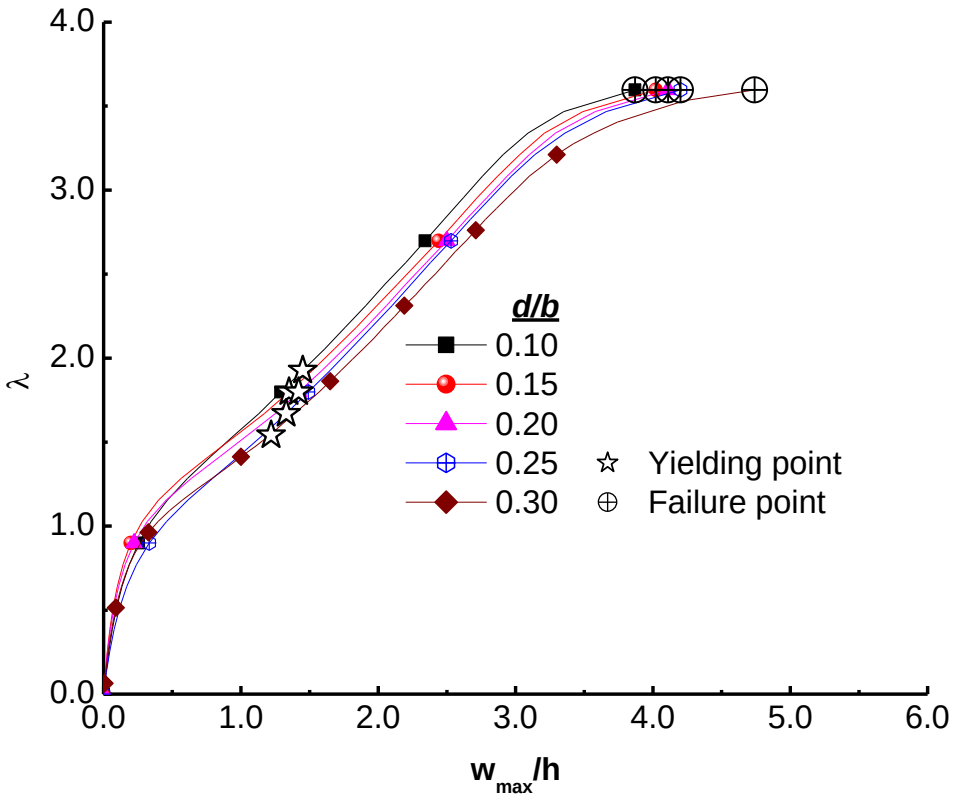

Fig. 7.3.6: Effect of cutout size on elastic-plastic buckling, postbuckling and failure behavior of Ti/TiB FGM plate with a square cutout under uniaxial compression.

FGM with different material inhomogeneity is obtained by varying volume fraction through the thickness using Eq. (3.2) for different values of exponent *n* (i.e., 0, 1, 2, 3, and 10). A FGM plate with a central cutout of circular/square shape is studied under uniaxial compression. The width-to-thickness ratio (i.e., slenderness ratio, *b/h*) was taken to be 100. The ratio of diameter/side of circular/square cutout to width of the plate (i.e., *d/b*) is taken as 0.1. The corresponding results tabulated in Table 7.3.3. depict higher values of buckling load and ultimate load carrying capacity corresponding to FGM plate (i.e., for n $>$ 0) as compared to that of pure metal plate (i.e., for *n* = 0). Higher value of *n* means high proportion of TiB which possess higher buckling and failure strengths as compared to those of metal constituent, and hence, the buckling and failure load of the resulting FGM plate is increased. It may also observed by Table 7.3.3 that the FGM plate with circular shape cutout buckles at higher load as compared to FGM plate carrying a square shape cutout of same cutout ratio (i.e., *d*/*b*).

Table 7.3.3: Effect of material inhomogenity (power law index *n*) on normalized buckling, yielding, and failure loads of square Ti/TiB FGM (*n* = 1) plate with cutout of size *d/b=0.1* under uniaxial compression.

n	Circular hole			Square hole		
	Buckling load	Yielding Load	Failure load	Buckling load	Yielding Load	Failure load
0	0.96	2.02	2.50	0.95	2.00	2.40
1	1.66	1.86	3.68	1.64	1.86	3.62
2	1.87	2.13	4.13	1.84	2.00	4.13
3	2.00	2.40	8.40	1.98	2.40	8.13
10	2.49	2.66	15.20	2.46	2.66	15.20

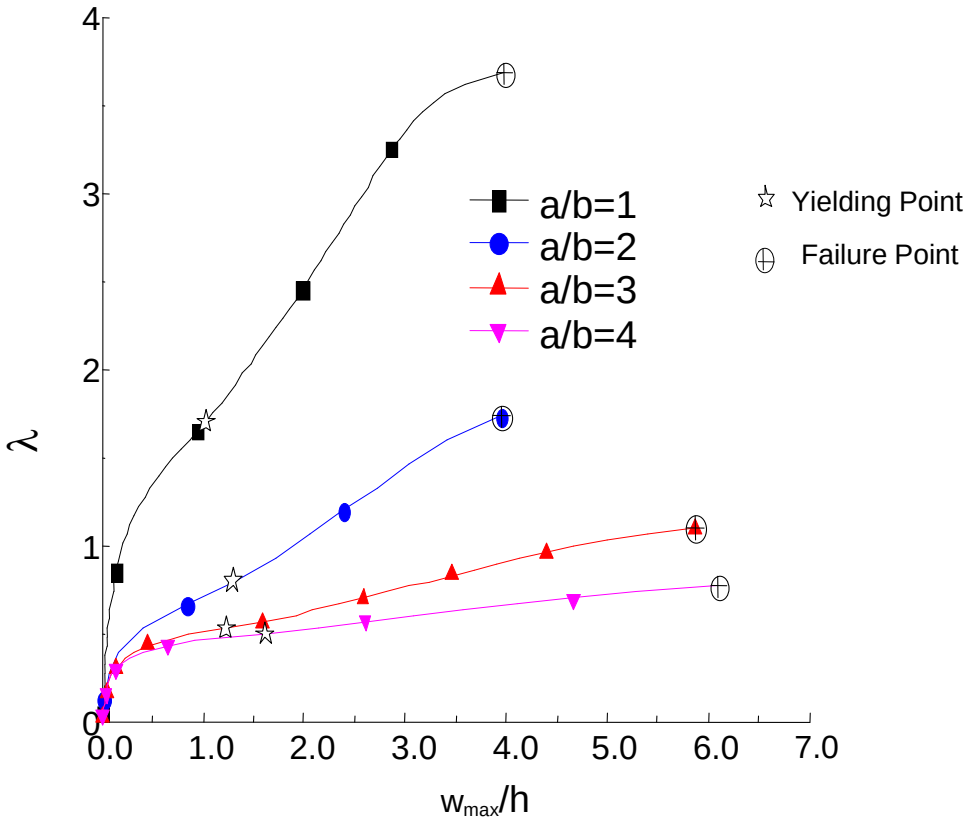

Fig. 7.3.7: Effect of aspect ratio (*a/b*) on elastic-plastic buckling, postbuckling and failure behavior of Ti/TiB FGM (*n* = 1) plate with a central circular cutout under uniaxial compression.

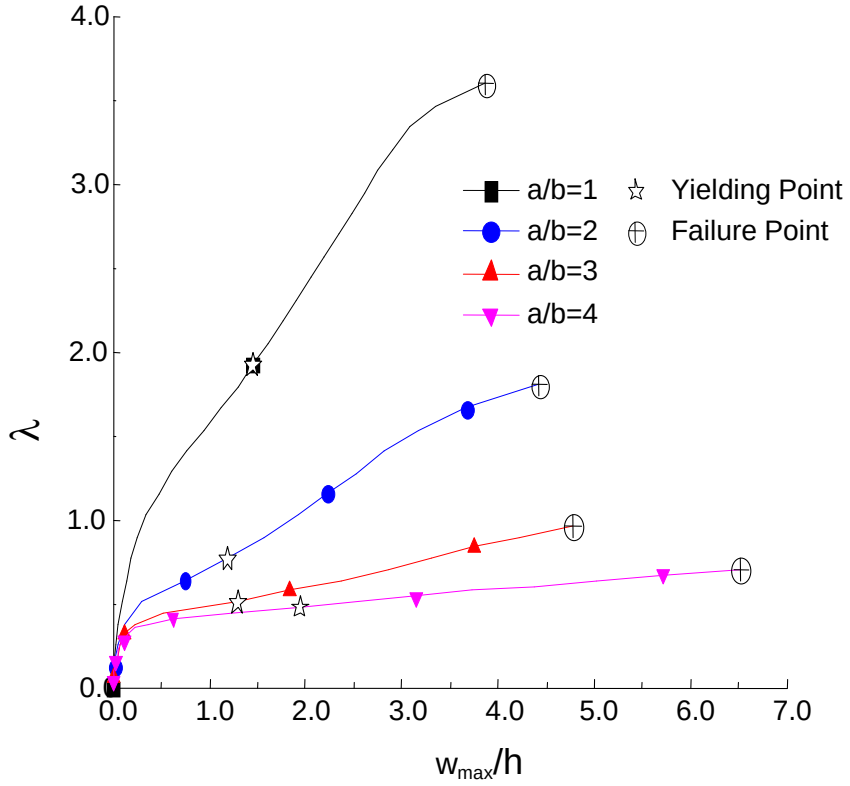

Fig. 7.3.8: Effect of aspect ratio on elastic-plastic buckling, postbuckling and failure behavior of Ti/TiB FGM (n = 1) plate with a central square cutout under uniaxial compression.

The effect of aspect ratio (i.e., a/b) on elastic-plastic buckling, postbuckling and failure behavior of perforated FGM plate with a central circular or square cutout of size d/b = 0.1 is examined, and the results are plotted in Figs. 7.3.7 and 7.3.8, respectively. It can be seen from Figs. 7.3.7 and 7.3.8 that buckling load, postbuckling strength (for a particular value of transverse deflection) and failure load of perforated FGM plate are maximum for square FGM plate (i.e., for a/b =1) for both cutout shapes, and a monotonic decrement in the failure load is observed with an increase in aspect ratio of perforated FGM plate. Furthermore, it is also revealed that irrespective of shape of cutout, the perforated FGM plate with higher value of aspect ratio fails due to excessive out-of-plane deflection.

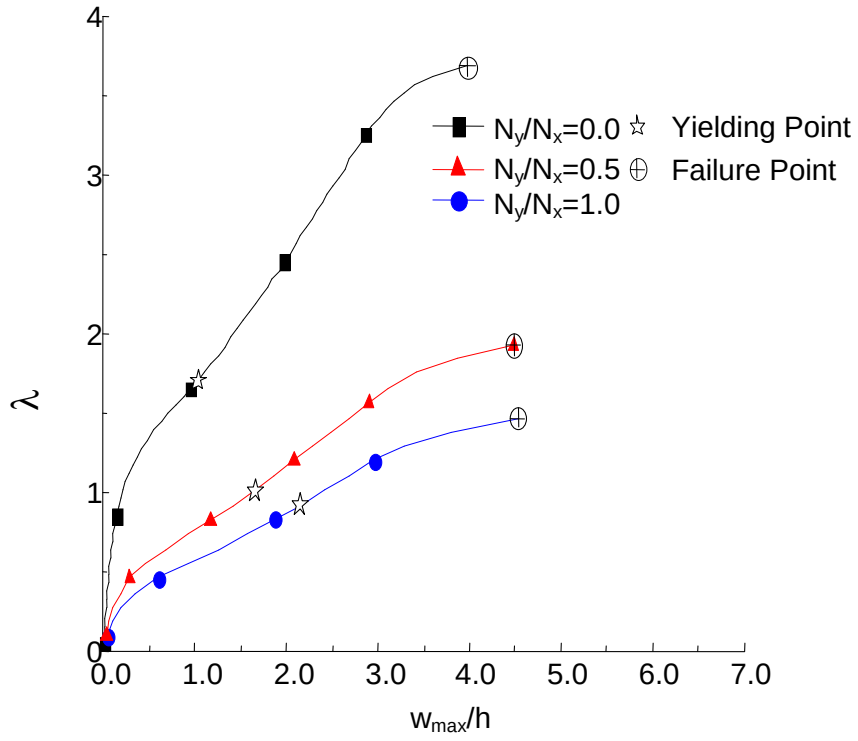

Fig.7.3.9: Effect of loading condition on elastic-plastic buckling, postbuckling and failure behavior of Ti/TiB FGM (n = 1) plate with a central circular cutout under uniaxial compression.

The effect of loading conditions (i.e., in-plane uniaxial and biaxial compression) on the elastic-plastic buckling and postbuckling responses, and failure of perforated FGM (for n = 1) plate (of b/h = 100) with a circular/ square cutout of size d/b = 0.1 are investigated, and the corresponding results are plotted in Figs. 7.3.9 and 7.3.10, respectively. The results show that irrespective of shape of cutout, maximum buckling and failure loads are obtained for perforated FGM plate under uniaxial compression (i.e., for $N_y/N_x = 0$) as compared to biaxial loading. The postbuckling load-deflection curve becomes significantly lower as the N_y is increased, and it causes the increase in maximum transverse deflection in FGM plate corresponding to the failure point.

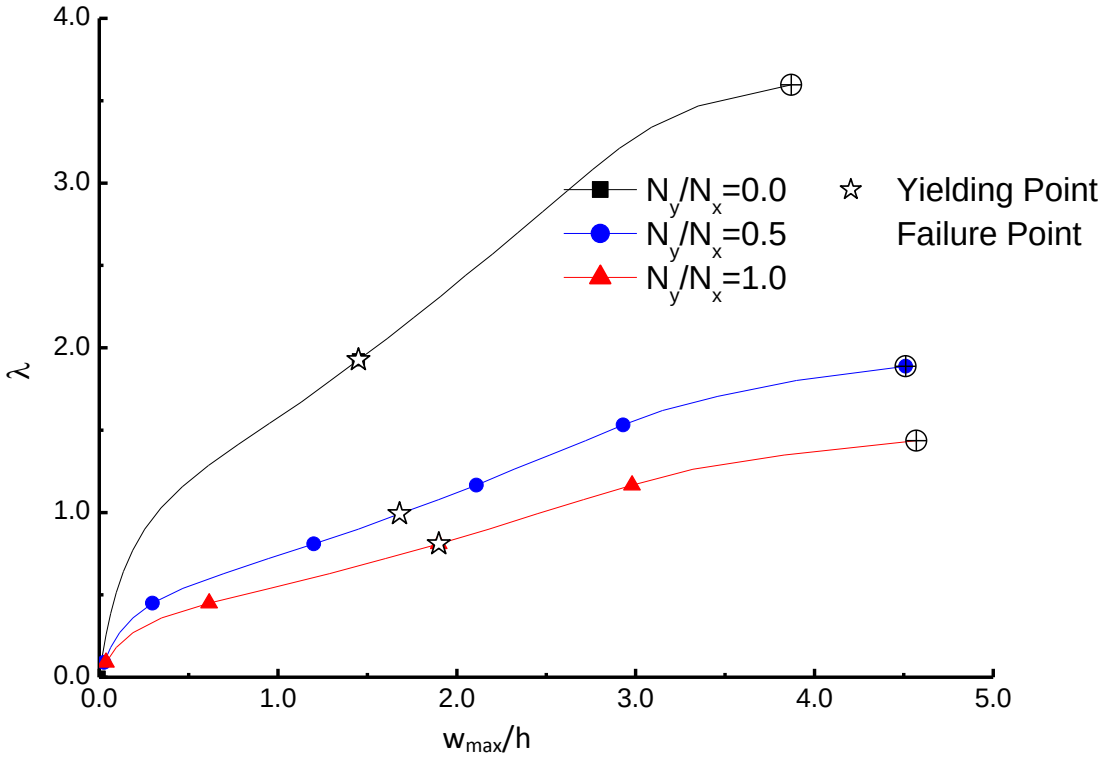

Fig. 7.3.10: Effect of loading condition on elastic-plastic buckling, postbuckling and failure behavior of Ti/TiB FGM (n = 1) plate with a central square cutout under uniaxial compression.

Table 7.3.4: Effect of slenderness ratio on absolute values of buckling and failure load of perforated Ti/TiB FGM (n=1) plate with a central cutout under uniaxial compression.

b/h	Circular cutout		Square cutout	
	Buckling load (MN)	Failure load (MN)	Buckling load (MN)	Failure load (MN)
30	22.49	14.52	22.49	14.31
50	4.93	5.48	4.89	5.42
100	0.62	1.38	0.62	1.36
200	0.07	0.37	0.07	0.36
300	0.02	0.16	0.02	0.15

The results on effect of slenderness ratio (i.e., b/h) on buckling load and the failure of simply-supported FGM (for n = 1) plate with a circular/square cutout (with d/b = 0.1) under uniaxial compression are shown in Table 7.3.4. The various values of slenderness ratio considered are: 30, 50, 100, 200 and 300, and the corresponding

values of dimensional buckling and failure loads are presented. As observed from Table 7.3.4 that the effect of slenderness ratio is very significant on dimensional values of buckling and failure loads. It can also be noticed from Table 7.3.4 that for FGM plate with slenderness ratio equal to 30, failure occurs before the buckling starts; for all other cases (i.e., b/h = 50, 100, 200 and 300) the FGM fails in postbuckling region after the occurance of buckling. The current findings explains that thin FGM plate is expected to buckle in elastic region, whereas the thick FGM plate (b/h = 30 in present case) would be likely to fail due to large plastic stresses well before the buckling.

7.3.5 Conclusions

Based on the various numerical studies conducted on perforated elastic-plastic Ti/TiB FGM square plate to examine the effects of various parameters, viz. material inhomogeneity (i.e., power exponent n), aspect ratio (i.e., a/b), loading condition, slenderness ratio (i.e., b/h), and cutout shape/size (i.e., d/b ratio) on the buckling and postbuckling behavior, and the failure response of perforated FGM plate, the following important conclusions are drawn.

- Buckling, postbuckling strength and maximum out-of-plane deflection at failure of perforated FGM plate are significantly affected by its material gradation profile, and the FGM plate with higher ceramic proportion depicted better buckling and postbuckling resistance.
- Buckling, postbuckling and failure loads of perforated FGM plate are found to be strongly dependent on the aspect ratio of plate, and these are found to decrease monotonically with the increase in the plate aspect ratio. The perforated FGM plate with higher aspect ratio exhibits excessive out-of-plane deflection at the time of failure.
- Irrespective of cutout shape, the effect of applying a compressive load in the y-direction, in addition to axial compressive load in the x-direction, is to decrease the postbuckling strength and failure load of elastic-plastic perforated FGM plate, and it results in the increase in maximum transverse deflection corresponding to the failure point.
- Ultimate load carrying capacity of perforated FGM plate is decreased considerably with an increase in slenderness ratio.

- FGM plate with a circular shape cutout posseses better load carrying capacity as compared to plate with a square cutout of same cutout ratio.
- The ultimate load carrying capacity of FGM plate remains unaffected with cutout size; however, the FGM plate with larger cutout size exhibits higher transverse deflections at the failure point.

CHAPTER 8

STABILITY ANALYSIS OF ELASTIC-PLASTIC FGM PLATE WITH TEMPERATURE-DEPENDENT MATERIAL PROPERTIES UNDER THERMAL LOAD

8.1 Introduction

The aim of present chapter is to investigate the nonlinear thermal buckling and postbuckling response of imperforated and perforated elastic-plastic FGM plates with temperature-dependent material properties. The FGM contains two constituents, namely Al_2O_3 (i.e., ceramic phase) and Ni (i.e., metallic phase), with their temperature-dependent coefficients given in Table 3.1 to evaluate thermoelastic properties. The temperature-dependent elastic-plastic strength coefficients to evaluate yield strength and tangent modulus of metallic phase are given in Table 3.2. The effects of temperature-dependent material properties and elastic-plastic strength parameters of FGM plate on non-linear thermal buckling and postbuckling response of imperforated and perforated plate made of elastic-plastic FGM are examined by taking the material property and elastic-plastic strength parameters P_j as a non-linear function of temperature, as defined in Eq. (3.1). The thermoelastic material properties of FGM plate are calculated using Mori-Tanaka homogenization scheme and TTO model is used to calculate the yield strength and tangent modulus of FGM plate, as discussed in Chapter 3. After conducting a convergence study to fix the number of elements in the finite element models of imperforated and perforated FGM plate, various numerical studies are conducted to examine the effects of temperature-dependent material properties, material in-homogeneity, slenderness and aspect ratios, on the nonlinear elastic-plastic stability behaviour of imperforated and perforated FGM plates under thermal load. The boundary condition on the edges of the plate is simply-supported with movable edges (i.e., BC1 boundary conditions), as mentioned in Section 5.1 of Chapter 5. Moreover, the effects of cutout shape and size on thermal buckling and postbuckling response of elastic-plastic perforated FGM plate are also investigated. It is to be noted that unless otherwise stated the FGM plate is graded linearly by assuming power law index equal to unity (i.e., $n = 1$).

Results for thermal (buckling, postbuckling and yielding) load and the transverse deflection are presented in the following non-dimensionalized forms:

Thermal load, $\lambda = \alpha_c \Delta T \times 10^3$,

Maximum transverse deflection, $w^* = \frac{w_{max}}{h}$,

where, α_c is thermal expansion coefficient of ceramic, h represents thickness of the FGM plate, ΔT is constant and uniform temperature rise, and w_{max} is the maximum transverse deflection.

8.2 Nonlinear Thermal Stability Analysis of Imperforated Elastic-Plastic FGM Plate

8.2.1 Convergence Study

Based on the convergence study conducted to fix the number of elements in the finite element analysis, the plate is meshed with 100 (10×10) elements. For this study, a simply-supported, imperforated FGM (for n = 1) plate having b/h = 50 is considered. Moreover, to approximate continuous variation of properties of FGM plate, the plate is assumed to compose of 20 perfectly-bonded layers. The corresponding results for convergence of non-dimensionalized thermal loads (i.e., λ and λ_y) corresponding to buckling and yielding, respectively, are shown in the Table 8.2.1.

Table 8.2.1: Result of convergence of thermal buckling load ($\lambda_b = \alpha_c \Delta T_b \times 10^3$) and yielding load ($\lambda_y = \alpha_c \Delta T_y \times 10^3$) for simply-supported FGM plate.

No. of elements (along x × along y)	$\boldsymbol{\lambda_b}$	$\boldsymbol{\lambda_y}$
$\mathbf{9 \times 9}$	1.037495	0.558558
$\mathbf{10 \times 10}$	0.896417	0.578236
$\mathbf{11 \times 11}$	0.888546	0.592616

8.2.2 Numerical Results and Discussion

The results for thermal buckling and postbuckling response of imperforated elastic-plastic FGM plate with temperature-dependent (TD) and temperature-independent (TID) material properties, and power law index n = 1 are compared in Fig. 8.2.1. As depicted in Fig. 8.2.1, the thermal buckling and postbuckling response of elastic-plastic FGM plate is greatly affected by temperature dependency of material

properties, and this effect increases considerably with an increase in applied thermal loading. Moreover, as expected, the FGM plate with temperature-dependent materials exhibits more transverse deflection than the plate with temperature-independent material properties, for a particular value of thermal load. It is also observed from the same figure that for both TD and TID cases, the yielding in FGM plate take place well before buckling, and hence, the whole thermal postbuckling response of FGM plate involves plastic effect.

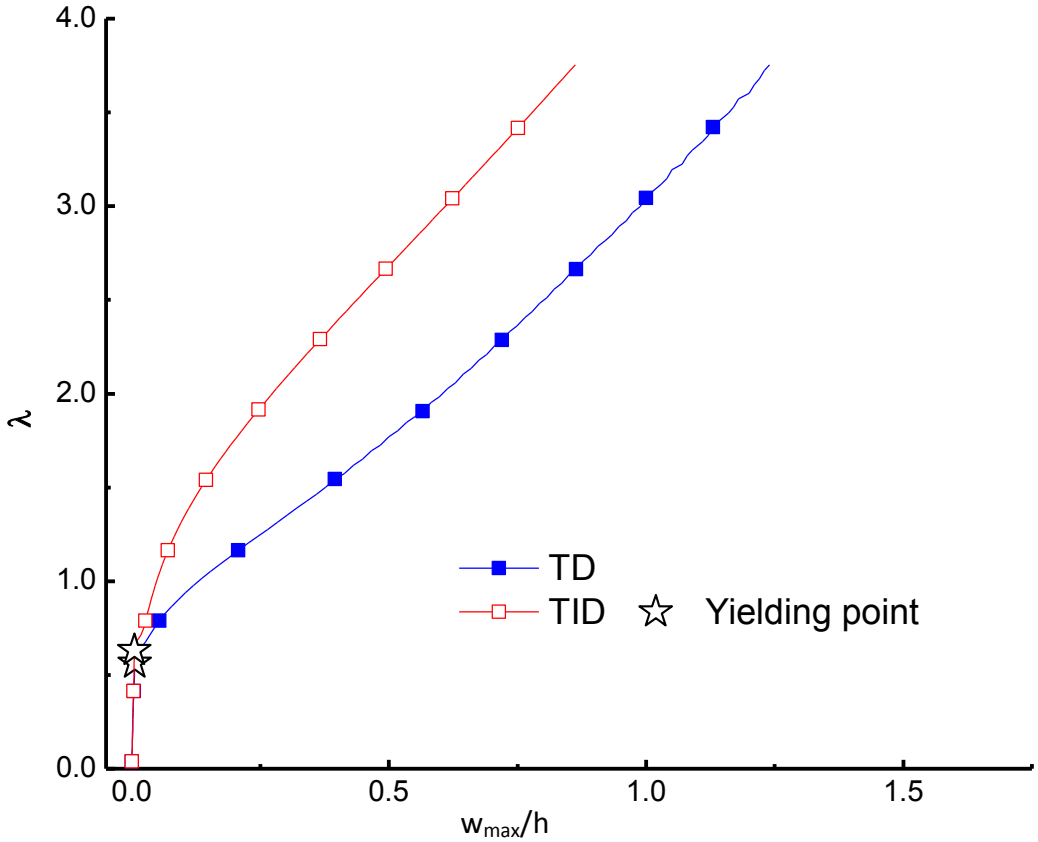

Fig. 8.2.1: Effect of temperature dependence of material properties on buckling and postbuckling behavior of FGM plate under thermal load.

The effect of material property variation [obtained by varying volume fraction using Eq. (3.2) for different values of exponent n (i.e., 0, 1, 2, 3, and 10)] on thermal buckling and postbuckling response of simply-supported FGM plate is studied, and the corresponding results are plotted in Fig. 8.2.2. It can be observed from Fig. 8.2.2 that the thermal buckling resistance and postbuckling strength (for a particular value of transverse deflection) of FGM plate is increased considerably as compared to those of pure metallic plate (i.e., corresponding to $n = 0$) . This may be attributed to the fact that by increasing the value of n, proportion of Al_2O_3 (having higher thermal

resistance) is increased, which causes improved thermal buckling resistance and postbuckling strength of FGM plate. It is further to be noted from Fig. 8.2.2 that FGM plate has improved reserved postbuckling thermal strength (given by the slope of the postbuckling curve) after buckling. Also for all FGM plates (i.e., nonzero value of n), the buckling take place in elastic-plastic region, however the metal plate (i.e., $n = 0$) buckles in the elastic region.

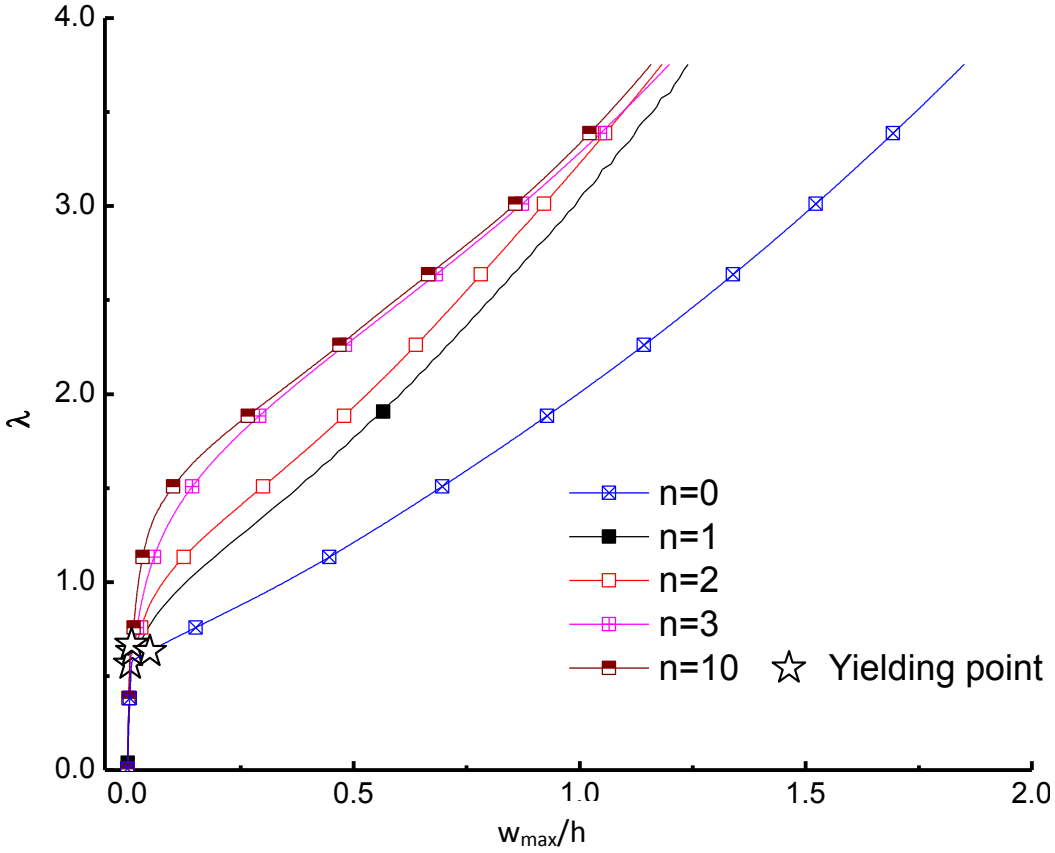

Fig. 8.2.2: Effect of material inhomogenity (i.e., n) on thermal buckling and postbuckling behavior of FGM plate.

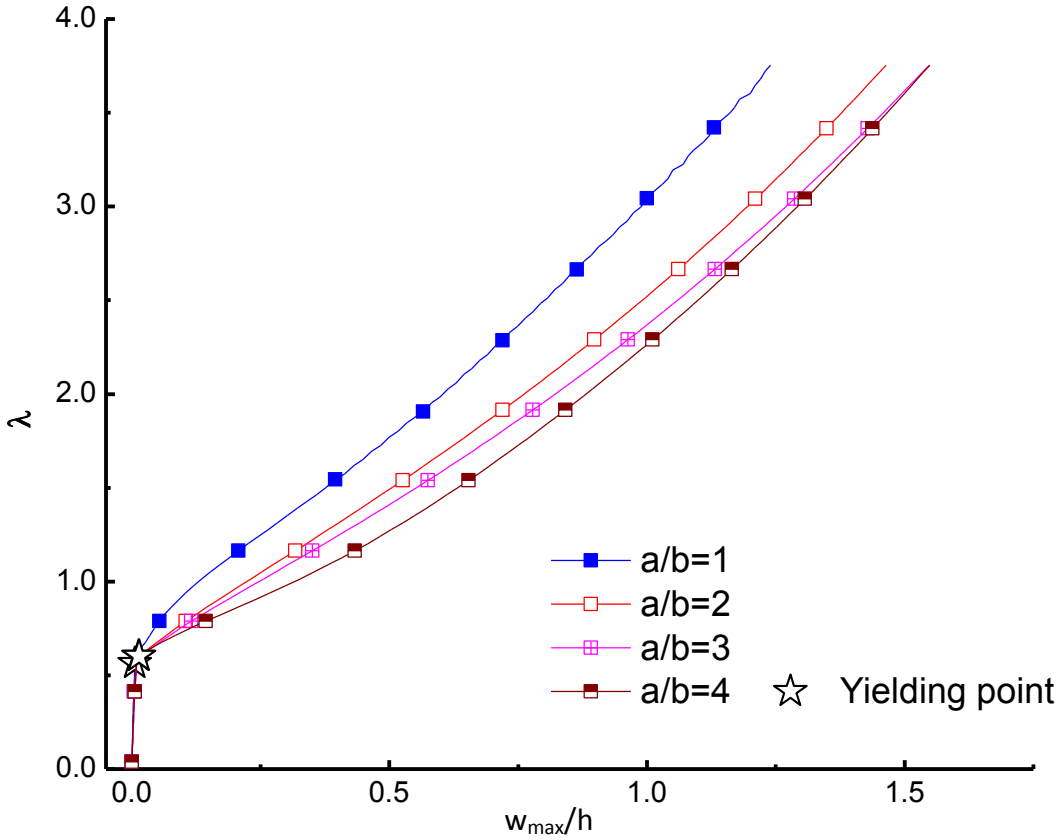

Fig. 8.2.3: Effect of aspect ratio on thermal buckling and postbuckling behavior of FGM plate.

The effect of plate's aspect ratio on thermal buckling and postbuckling response of elastic-plastic FGM plate is depicted in Fig. 8.2.3. It shows that the thermal buckling load and postbuckling strength (for a particular value of transverse deflection) are maximum for square FGM plate (i.e., for a/b = 1). Fig. 8.2.3 also depicts that for all values of aspect ratios, the yielding in FGM plate take place before buckling, and postbuckling in FGM plate occurs in elastic-plastic region. Further, the aspect ratio of FGM plate does not affect the yielding load of the plate considerably and FGM plate with all aspect ratios depicted almost same yielding load. Also, for larger values of aspect ratios (i.e., a/b = 3 and 4), the effect is less significant on the postbuckling response of plate, which may be attributed to the fact that for higher value of aspect ratios the FGM plate would behave like a beam.

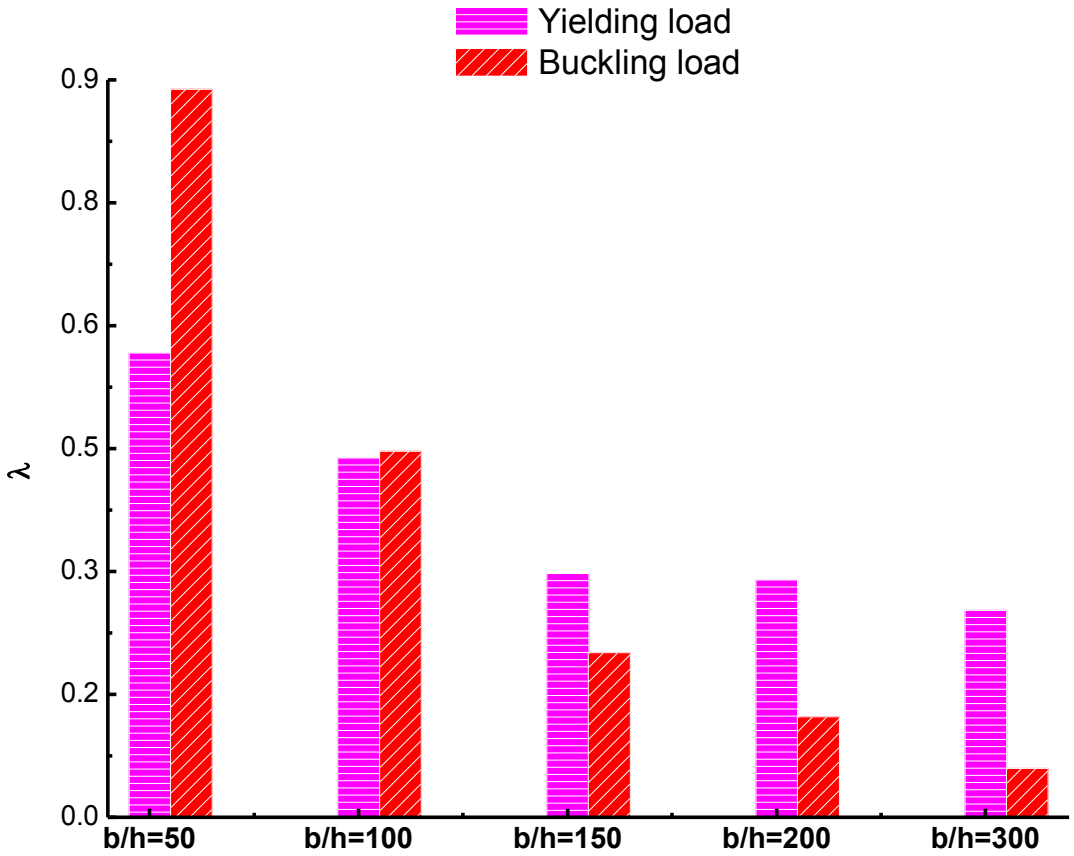

Fig. 8.2.4: Effect of slenderness ratio on thermal buckling and yielding loads of FGM plate.

The effect of thickness on thermal buckling and yielding loads of square simply-supported elastic-plastic imperforated FGM plate is examined by considering various values of slenderness ratios (i.e., b/h = 50, 100, 150, 200 and 300), and the corresponding values of thermal buckling and yielding loads of FGM plate are presented in Fig. 8.2.4. As evident from Fig. 8.2.4 that slenderness ratio greatly affects the buckling and yielding loads of elastic-plastic FGM plate under thermal loading, and for slenderness ratios = 50 and 100, the yielding load is lower than the buckling load. Hence, for these slenderness ratios, the plate buckles in elastic-plastic region, and consideration of plasticity is more important to correctly predict the buckling and postbuckling response of FGM plate. Fig. 8.2.4 also shows that for thin FGM plate (i.e., with slenderness ratio = 150, 200 and 300) the buckling and initial postbuckling regime would occur in elastic region.

8.2.3 Conclusions

A study on non-linear stability analysis of elastic-plastic imperforated FGM plate under in-plane compression caused by constant and uniform temperature rise is conducted. The effects of temperature-dependent material properties, material gradation (i.e., material inhomogeneity), and geometrical parameters (i.e., aspect and slenderness ratios) on thermal buckling and postbuckling behavior of elastic-plastic FGM plate are investigated. Following are the important findings obtained out of this study:

- Thermal buckling and postbuckling response of elastic-plastic FGM plate is greatly affected by temperature-dependent material properties.
- Buckling and postbuckling response of elastic-plastic FGM plate under thermal loading is found to be significantly affected by the material gradation profile, and FGM plate with higher ceramic proportion depicted better thermal buckling and postbuckling strength.
- Thermal buckling and yielding loads of elastic-plastic FGM plate are significantly affected by the slenderness ratio of the plate, and for moderately thick FGM plate (i.e., $b/h \leq 100$), buckling occurs in elastic-plastic region.

8.3 Nonlinear Thermal Stability Analysis of Perforated Elastic-Plastic FGM Plate

8.3.1 Details of Perforation

Perforated FGM plate of dimension ($a \times b \times h$) with a central cutout of various shapes (i.e., circular, square, diamond and elliptical) is considered to observe the effect of cutout shape on thermal buckling and postbuckling response of the elastic-plastic FGM plate. Three cutout sizes designated as A_1, A_2, and A_3, as mentioned in Table 5.1.1 of Chapter 5, have been considered.

8.3.2 Convergence study

Table 8.3.1 presents the results of convergence study, conducted for a simply-supported FGM plate with a centrally located cutout (i.e., circular and square cutouts) of size A_3. The plate was meshed using the mesh size control feature of ANSYS, as discussed in Section 5.3.2 of Chapter 5. A reasonable convergence of thermal buckling and yielding loads for FGM plate with both cutout shapes (i.e., circular and square) can be observed from Table 8.3.1 for the mesh of 3042/3049 elements (i.e., for mesh control parameter, η = 30). For the sake of uniformity, same meshing procedure with same mesh control parameter (i.e., η = 30) was followed to mesh the plate with other cutout shapes.

Table 8.3.1: Results of convergence study for thermal buckling $(\lambda_b = \alpha_c \Delta T \times 10^3)$ and yielding loads $\left(\lambda_y = \alpha_c \Delta T_y \times 10^3\right)$ for elastic-plastic perforated FGM plate.

Nos. of elements for Circular cutout/Square cutout	Square cutout		Circular cutout	
	λ_b	λ_y	λ_b	λ_y
195/208	0.68206	0.32739	0.70390	0.54564
718/797	0.70934	0.31802	0.69119	0.60001
3042/3049	0.70931	0.24584	0.68206	0.57293
6279/6309	0.70928	0.24554	0.68196	0.57241

8.3.3 Numerical Results and Discussion

Different numerical studies are conducted to examine the effects of various parameters, viz. cutout shape, material inhomogeneity (i.e., power exponent *n*), cutout size (i.e., A_1, A_2, and A_3), and aspect (*a/b*) and slenderness (i.e., *b/h*) ratios on the thermal buckling and postbuckling behavior of perforated elastic-plastic FGM plate.

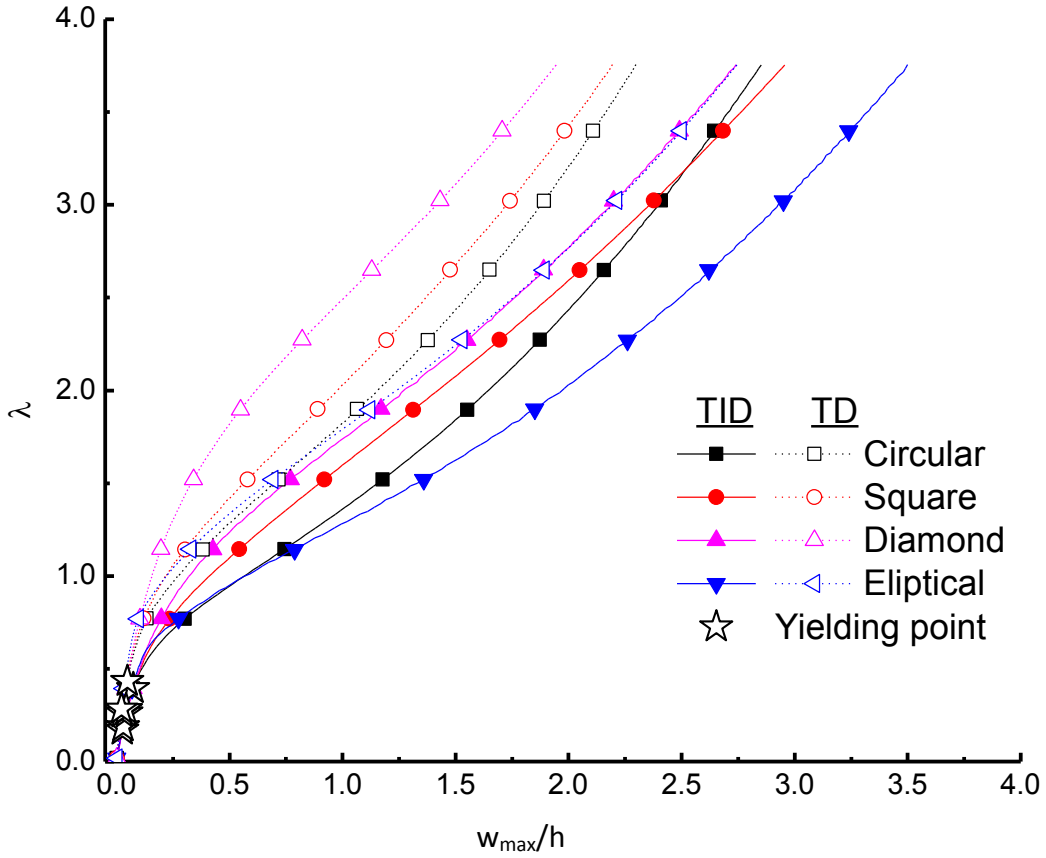

Fig. 8.3.1: Effect of the temperature-dependent material properties on the thermal buckling and postbuckling behavior of simply-supported elastic-plastic FGM plate with a cutout of various shapes.

The effect of cutout shape on nonlinear thermal postbuckling behavior of FGM (*n* = 1) plate having temperature-dependent (TD) as well as temperature-independent (TID) material properties is studied. Simply-supported FGM plate with a central cutout of size A_3 and of various shapes under constant and uniform temperature rise up to 550^{o}C is considered. Corresponding thermal buckling and postbuckling paths are shown in Fig. 8.3.1. It can be observed from Fig. 8.3.1 that the thermal buckling and postbuckling response of perforated elastic-plastic FGM plate is considerably affected by the temperature dependence of material properties for all cutout shapes, and this effect becomes significant with an increase in applied thermal loading. It can also be observed from Table 8.3.2 that the maximum difference in between non-

dimensional thermal buckling load of perforated FGM plate with temperature-dependent material properties and with temperature-independent material properties is almost 49% (i.e., for FGM (n = 1) plate with elliptical cutout). Fig. 8.3.1 also reveals that for a particular value of transverse deflection, the FGM plate with diamond cutout possesses highest thermal postbuckling strength, whereas the FGM plate with elliptical cutout has a minimum strength, for both the temperature-independent as well as temperature-dependent material properties.

Table 8.3.2: Effect of material inhomogenity on thermal buckling and yielding loads of elastic-plastic FGM plate with a cutout of various shape.

n	Cutout shape	(TD)		(TID)	
		λ_b^*	λ_y^{**}	λ_b	λ_y
0	Circular	1.0912	0.5456	1.4186	0.6547
	Square	1.2277	0.2455	1.6642	0.2728
	Elliptical	1.0640	0.3819	1.3914	0.4365
	Diamond	1.4196	0.2455	1.6642	0.3001
1	Circular	0.6820	0.5729	0.9821	0.6274
	Square	0.7093	0.2455	1.0367	0.2728
	Elliptical	0.7639	0.3819	1.1458	0.3819
	Diamond	0.7366	0.2455	1.0912	0.2455
2	Circular	0.7366	0.6002	1.0367	0.6820
	Square	0.7639	0.2455	1.0640	0.2728
	Elliptical	0.8184	0.3819	1.2004	0.3819
	Diamond	0.7639	0.2455	1.1458	0.2728
3	Circular	0.7911	0.6002	1.0367	0.6274
	Square	0.8184	0.3819	1.0912	0.3819
	Elliptical	0.9003	0.4092	1.4732	0.4365
	Diamond	0.8184	0.2728	1.2004	0.3001
10	Circular	0.9821	0.6002	1.1731	0.6274
	Square	1.1185	0.2455	1.3095	0.2728
	Elliptical	1.4732	0.4365	1.5005	0.4365
	Diamond	1.1458	0.2728	1.4186	0.3819

$^{*,**}\lambda_b$ and λ_y are normalized buckling and yielding loads respectively.

The effect of material property variation through the thickness [obtained by varying volume fraction using Eq. (3.2) for different values of exponent *n* (i.e., 0, 1, 2, 3, 10)] on thermal buckling and postbuckling response of simply-supported elastic-plastic FGM plate having a central cutout of various shapes and of size A_3 is studied, and the related results are plotted in Fig. 8.3.2 and tabulated in Table 8.3.2. It can be observed from Fig. 8.3.2 that for all cutout shapes, the thermal postbuckling strength of perforated FGM plate is higher than the pure metal plate (i.e., corresponding to $n = 0$). It is important to mention that increasing the value of *n* means proportion of Al_2O_3, having higher thermal resistance, is increased that in turn results in the increase in the postbuckling strength of FGM plate under thermal load. It can also be noted from Fig. 8.3.2 that the bifurcation buckling phenomenon remain absent in FGM plate. It is also observed from Table 8.3.2 that the thermal buckling load of perforated FGM plate is greatly dependent on the shape of cutout, and the FGM ($n > 0$) plate with an elliptical cutout depicted maximum thermal buckling load and with a circular cutout showed minimum buckling load, that is nearly 20-25% lower than that of plate carrying elliptical cutout.

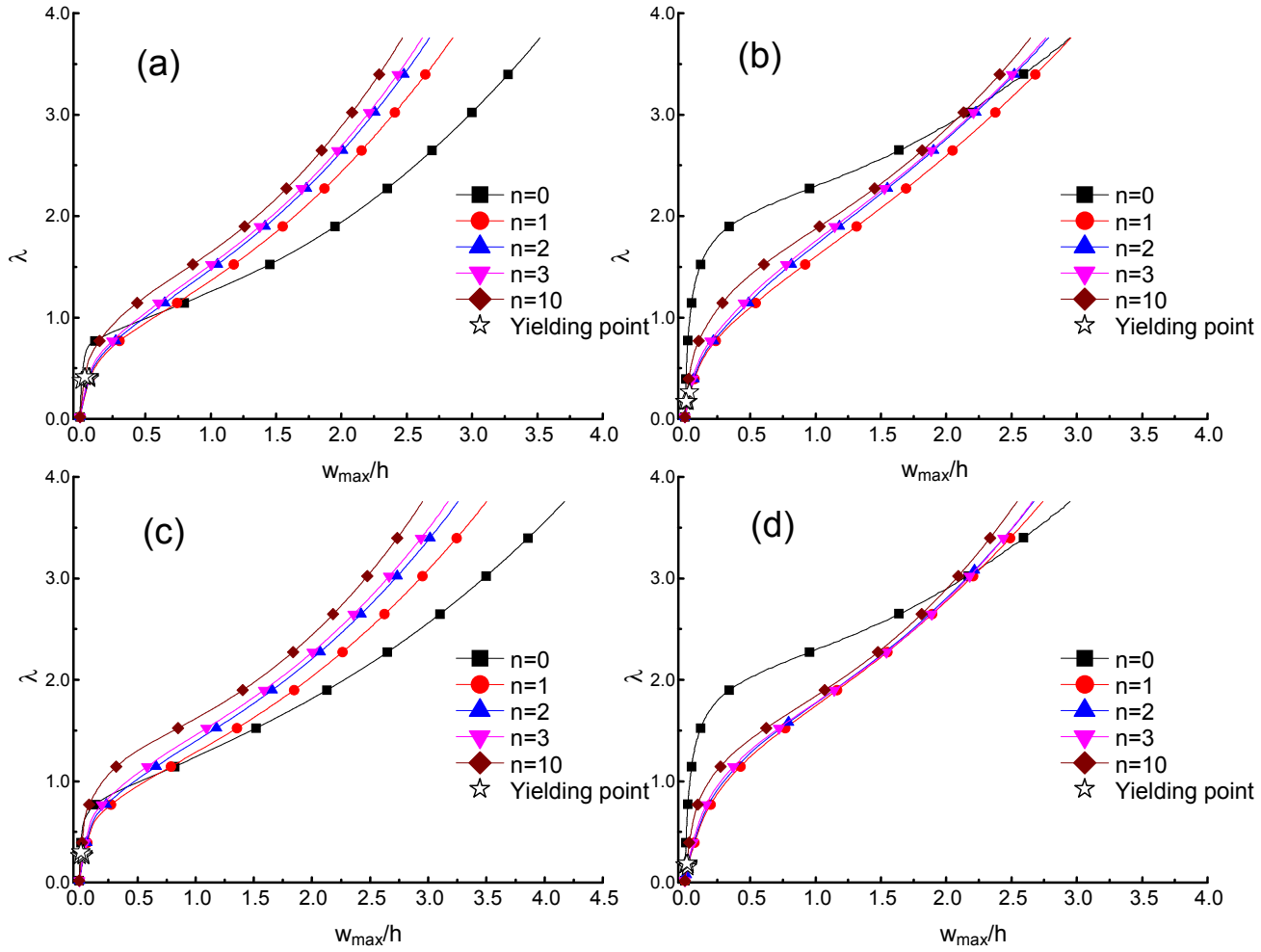

Fig. 8.3.2: Effect of material inhomogenity on the thermal buckling and postbuckling behavior of elastic-plastic perforated FGM plate with a central cutout of size A_3 and of: (a) circular (b) square (c) elliptical, and (d) diamond shape.

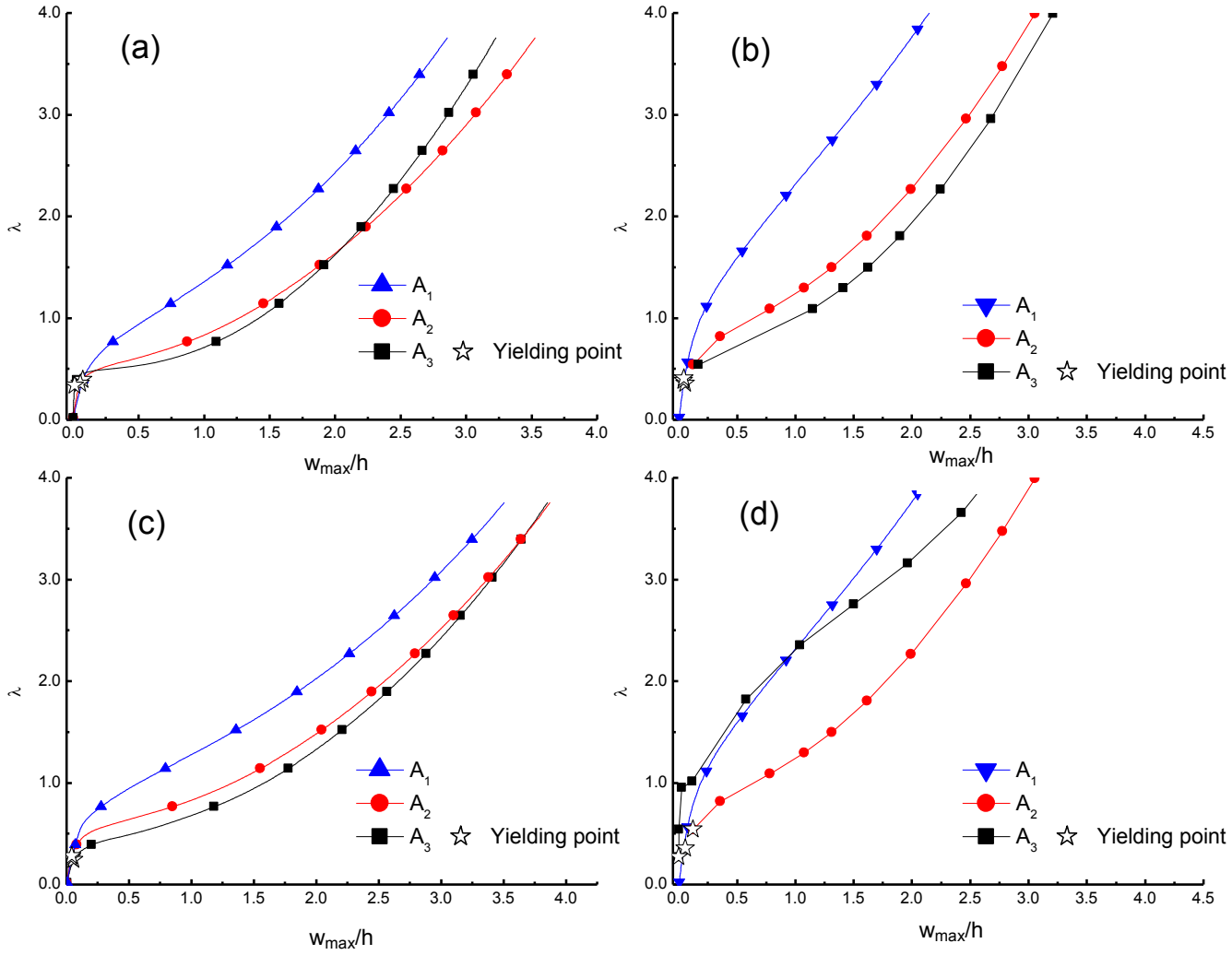

Fig. 8.3.3: Effect of cutout size on thermal buckling and postbuckling behavior of elastic-plastic perforatedFGM plate with a central cutout of: (a) circular (b) square (c) elliptical, and (d) diamond shape.

The thermal buckling and postbuckling behavior of elastic-plastic FGM plate with a central cutout of various shapes and sizes is studied for simply-supported boundary condition. The corresponding thermal buckling and postbuckling plots in Fig. 8.3.3 depict that the cutout size affects the thermal postbuckling paths of FGM plate considerably, and for all cutout shapes, the thermal postbuckling strength decreases with an increase in cutout size. Fig. 8.2.3 also shows that at a particular thermal load, the elastic-plastic FGM plate with large cutout size (A_2 and A_3 sizes) depicted higher value of transverse deflection than A_1 size of cutout.

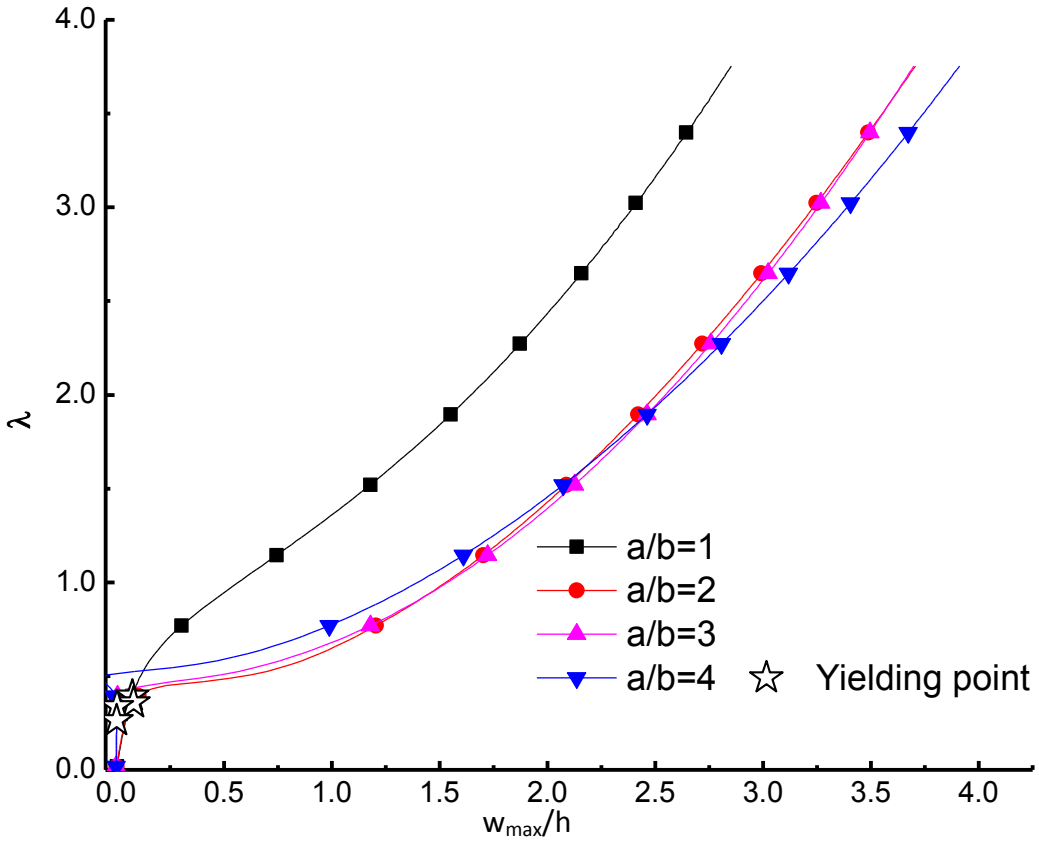

Fig. 8.3.4: Effect of aspect ratio (*a/b*) on the thermal postbuckling behavior of elastic-plastic perforated FGM plate with a central circular cutout.

The thermal buckling and postbuckling paths for various aspect ratios are shown in Fig. 8.3.4, and the effect of slenderness ratio is shown in Fig. 8.3.5. It can be observed from Fig. 8.3.4 that the thermal buckling and postbuckling response of FGM plate with a central circular cutout is significantly affected by the aspect ratio of the plate. For a particular value of transverse deflection, square FGM plate (i.e., $a/b = 1$) possesses highest thermal postbuckling strength, and FGM plate with $a/b = 4$ exhibits highest transverse deflection corresponding to maximum thermal load (i.e., $\Delta T =$

550^{o}C), nearly 150% of that depicted by square FGM plate. It can also be noticed from Fig. 8.3.4 that the thermal postbuckling resistance is decreased considerably with an increase in aspect ratio from 1 to 2, and thereafter, there is no substantial change with further increase in aspect ratio.

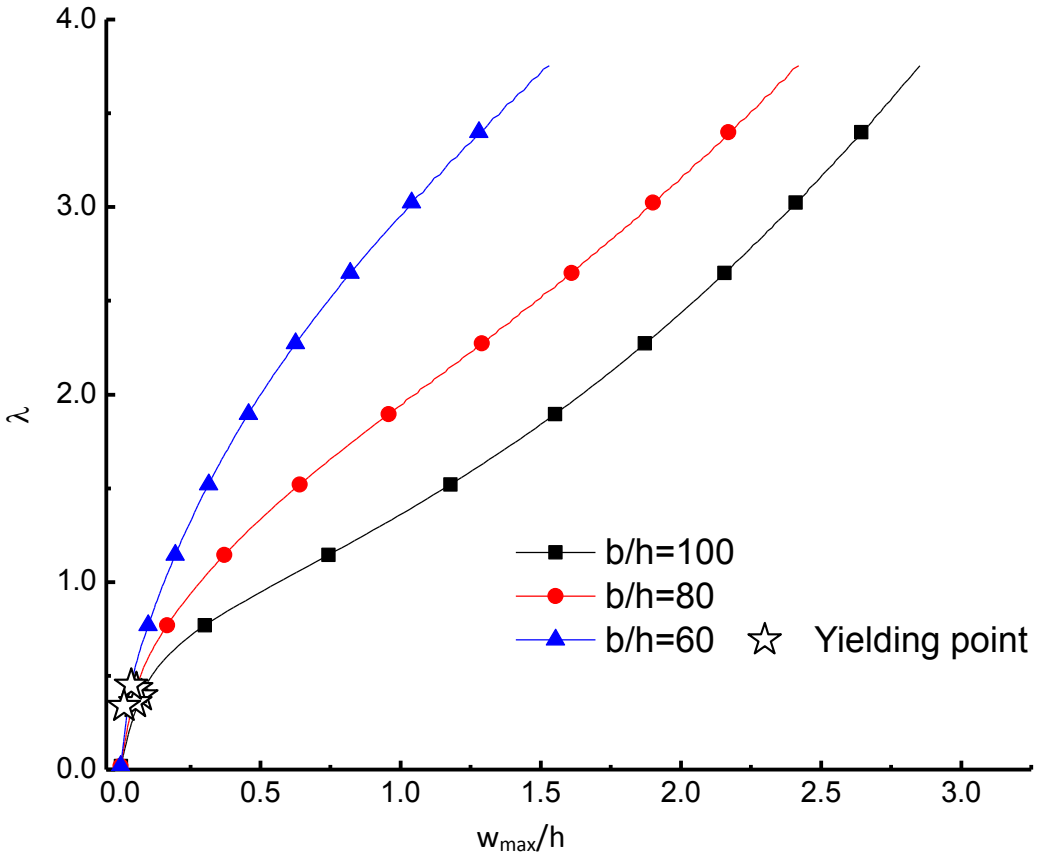

Fig. 8.3.5: Effect of slenderness ratio (*b*/*h*) on the thermal buckling and postbuckling behavior of simply-supported FGM plate with a central circular cutout.

The effect of slenderness ratio on thermal buckling and postbuckling behavior of simply-supported FGM plate with a central circular cutout of size A_3 is shown in Fig. 8.3.5. It can be observed from Fig. 8.3.5 that the thermal buckling load and postbuckling strength of FGM plate decrease monotonically with an increase in the slenderness ratio, and thin FGM plate exhibit higher out-of-plane deflection for a particular value of thermal load.

8.3.4 Conclusions

A study on non-linear stability analysis of elastic-plastic perforated FGM plate carrying a central cutout of various shapes is conducted under constant and uniform

temperature rise up to 550^{o}C. Numerical studies, to examine the effects of temperature-dependent material properties, material gradation (i.e., material inhomogeneity), cutout shape and size, and geometrical parameters (i.e., aspect and slenderness ratios) on thermal buckling and postbuckling behavior of elastic-plastic perforated FGM plate, are conducted, and the following important findings are obtained:

- Irrespective of the shape of cutout, the thermal postbuckling strength of perforated FGM plate is found to be decreased with an increase in the size of cutout.
- Square FGM plate with circular cutout possesses maximum thermal postbuckling strength, whereas rectangular FGM plate with circular cutout of same size depicted maximum value of transverse deflection.
- Effect of increase in aspect ratio on thermal postbuckling response of rectangular perforated FGM plates (i.e., for a/b = 2, 3 and 4) is less significant and almost same thermal postbuckling path is noticed for all values of aspect ratio greater than 1.0.
- Thermal buckling load and postbuckling strength of elastic-plastic perforated FGM plate is found to decrease monotonically with an increase in slenderness ratio, and thin FGM plate is found to exhibit higher out-of-plane deflection for a particular value of thermal load.

CHAPTER 9

STABILITY AND FAILURE ANALYSIS OF ELASTIC-PLASTIC FGM PLATE WITH TEMPERATURE-DEPENDENT MATERIAL PROPERTIES UNDER THERMOMECHANICAL LOADING

9.1 Introduction

Present chapter explores the stability and failure response of elastic-plastic imperforated and perforated Ni/Al_2O_3 FGM plates under thermomechanical load. The FGM contains two constituents, namely Al_2O_3 (i.e., ceramic phase) and Ni (i.e., metallic phase), with their temperature-dependent coefficients given in Table 3.1 to evaluate thermoelastic properties. The temperature-dependent elastic-plastic strength coefficients to evaluate yield strength and tangent modulus of metallic phase are given in Table 3.2. The thermoelastic material properties as well as elastic-plastic strength parameters of FGM plate are taken as non-linear function of temperature, as defined by Eq. (3.1). The thermoelastic material properties of FGM plate are calculated using Mori-Tanaka homogenization scheme, and TTO model is used to calculate the yield strength and tangent modulus of FGM plate, as discussed in Chapter 3. The elastic-plastic behavior of FGM plate is assumed to follow J_2-plasticity and isotropic hardening in which the ceramic phase was considered to be elastic whereas the metal is taken to be elastic-plastic material in accordance with the TTO model. Before carrying out the present study, a convergence study is conducted to fix the number of layers to model FGM plate and the number of elements in its FEM model, for both imperforated and perforated FGM plates. A detailed comprehensive parametric study is performed in order to examine the effects of material inhomogeneity, thermomechanical loading conditions, slenderness and aspect ratios on the elastic-plastic buckling and postbuckling behavior, and the failure response of imperforated and perforated FGM plates. In addition, the effects of cutout shape and size on thermomechanical buckling, postbuckling and failure behavior of perforated elastic-plastic FGM plate are also investigated.

The current study is carried out for FGM plate with BC1 boundary conditions (i.e., all edges simply-supported with movable edges), as mentioned in Section 5.1 of

Chapter 5, and at a given temperature rise, the in-plane, uniformly distributed compressive loads are applied on edges $x = 0$ & a for uniaxial compression, and on edges $x = 0$ & a, $y = 0$ & b for biaxial compression.

Results for buckling and failure loads, and the transverse deflection are presented in the following non-dimensionalized forms:

In-plane buckling and failure load: $\frac{N_{x\,(or\,y)}\,b^2}{E_c h^3}$ (represented as λ);

Maximum transverse deflection: $\frac{w_{max}}{h}$;

where, E_c is Young's modulus of ceramic, h represents the thickness of FGM plate, b is the width of plate, $N_{x\,(or\,y)}$ is the in-plane compressive load in x- direction (or y-direction) per unit edge length, and w_{max} is the maximum transverse deflection. Whereas, the effect of plasticity is represented in the following form:

Magnitude of maximum plastic strain: $\left(\frac{2}{3}\varepsilon_p : \varepsilon_p\right)^{1/2}$,

where, $\varepsilon_p : \varepsilon_p$ is the scalar product of the plastic strain tensors corresponding to failure point.

9.2 Thermomechanical Stability and Failure Analysis of Imperforated Elastic-Plastic FGM Plate

9.2.1 Convergence study

The effects of numbers of elements in the finite element mesh and layers in FGM plate on buckling and failure loads of FGM (n = 1) square plate with b/h = 100 under uniaxial compression and constant and uniform temperature rise of 100^{o}C are examined by performing a convergence study. The convergence study was conducted for a simply-supported FGM plate using meshes of 81, 100, and 121 elements having 10, 20 and 30 layers. Results of convergence study are shown in Table 9.2.1. It can be observed from Table 9.2.1 that a reasonably good convergence of buckling load and failure load is obtained for the mesh of 100 (10×10) elements having 20 layers.

Table 9.2.1: Convergence study for buckling load $\left(\lambda_b = \frac{N_x b^2}{E_c h^3}\right)$ and failure load $\left(\lambda_f = \frac{N_{fail} b^2}{E_c h^3}\right)$ for simply-supported FGM plate under uniaxial compression and constant and uniform temperature rise of $\Delta T = 100$, for *b/h* = 100 and *n* = 1.

No. of elements (along *x* × along *y*)	No. of layers					
	10		20		30	
	λ_b	λ_f	λ_b	λ_f	λ_b	λ_f
9 × 9	0.6030	3.9851	0.5660	3.7404	0.5528	3.4257
10 × 10	0.6074	3.9053	0.5528	3.4607	0.5417	3.3915
11 × 11	0.5924	3.9151	0.5472	3.4257	0.5374	3.3643

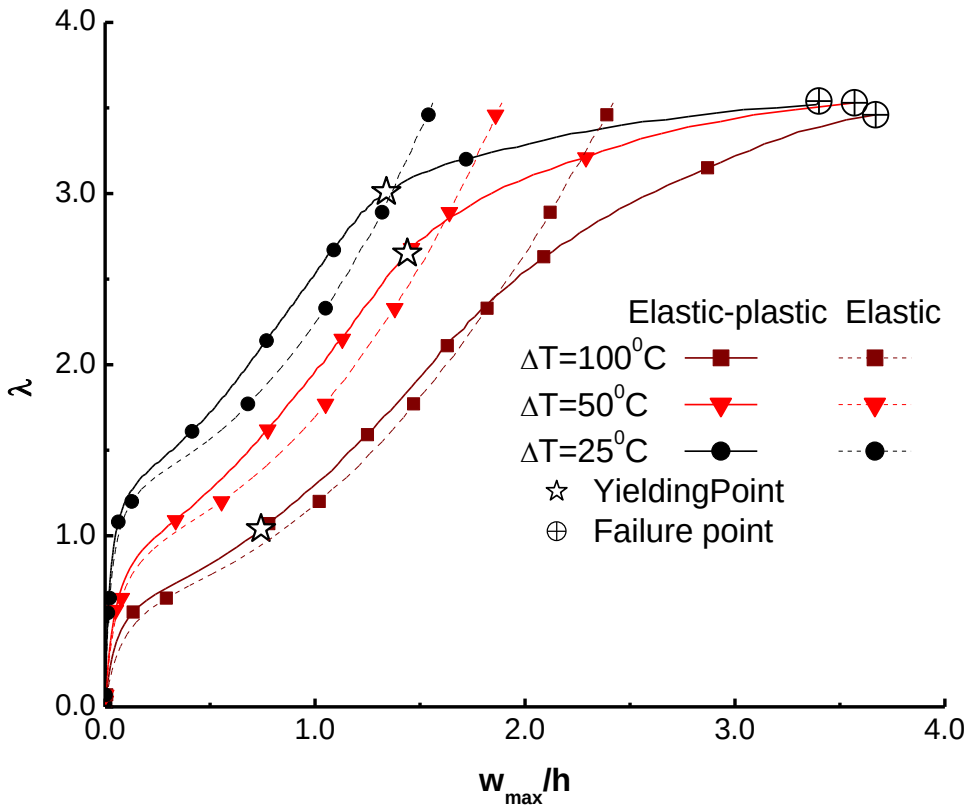

Fig. 9.2.1 : Comparison of elastic and elastic-plastic postbuckling paths for FGM plate under uniaxial compression and constant and uniform temperature rise.

9.2.2 Numerical Results and Discussion

Numerical studies are conducted to analyze the elastic-plastic buckling, postbuckling path and failure characteristics of simply-supported FGM plate under

combined thermomechanical loading condition. Effects of material inhomogeneity (i.e., power exponent n), aspect ratio (i.e., a/b), slenderness ratio (i.e., b/h), and loading conditions (i.e., uniaxial and biaxial loading) on the buckling load, postbuckling path, yielding load, maximum plastic strain and failure load of FGM plate are investigated.

The effect of plasticity on nonlinear thermomechanical buckling and postbuckling behavior of FGM square plate (of side 1 m) having temperature-dependent (TD) material properties is studied. The corresponding plots of elastic and elastic-plastic buckling and postbuckling paths are shown in Fig. 9.2.1. The yield and failure points are also marked in the Fig. 9.2.1 for the cases of elastic-plastic studies. It can be seen from Fig. 9.2.1 that the postbuckling paths for both elastic and elastic-plastic FGM plates are strongly dependent on temperature rise (i.e., ΔT), and for a particular value of mechanical load, both elastic and elastic-plastic FGM plate exhibit an increase in the value of transverse deflection with the increase in temperature. This response is caused by the high thermal load as well as by the reduced stiffness of FGM plate at high temperature because of the inverse dependence of Young's modulus on temperature (reduction in Young's modulus with increase in temperature) and the direct proportionality of thermal expansion coefficient with temperature. It can also be observed from Fig. 9.2.1 that postbuckling paths of FGM plate are greatly affected by the plasticity, as it is evident from the considerable difference in postbuckling paths of elastic and elastic-plastic FGM plates. Fig. 9.2.1 also depicts that irrespective of increase in applied thermal and mechanical loadings, the FGM plate with elastic material properties exhibits only stable equilibrium path, whereas the elastic-plastic FGM plate shows destabilizing response at the point of maximum postbuckling strength because the behavior of elastic-plastic FGM plate is dominated by plasticity after the point of intersection of postbuckling curves for elastic and elastic-plastic FGMs.

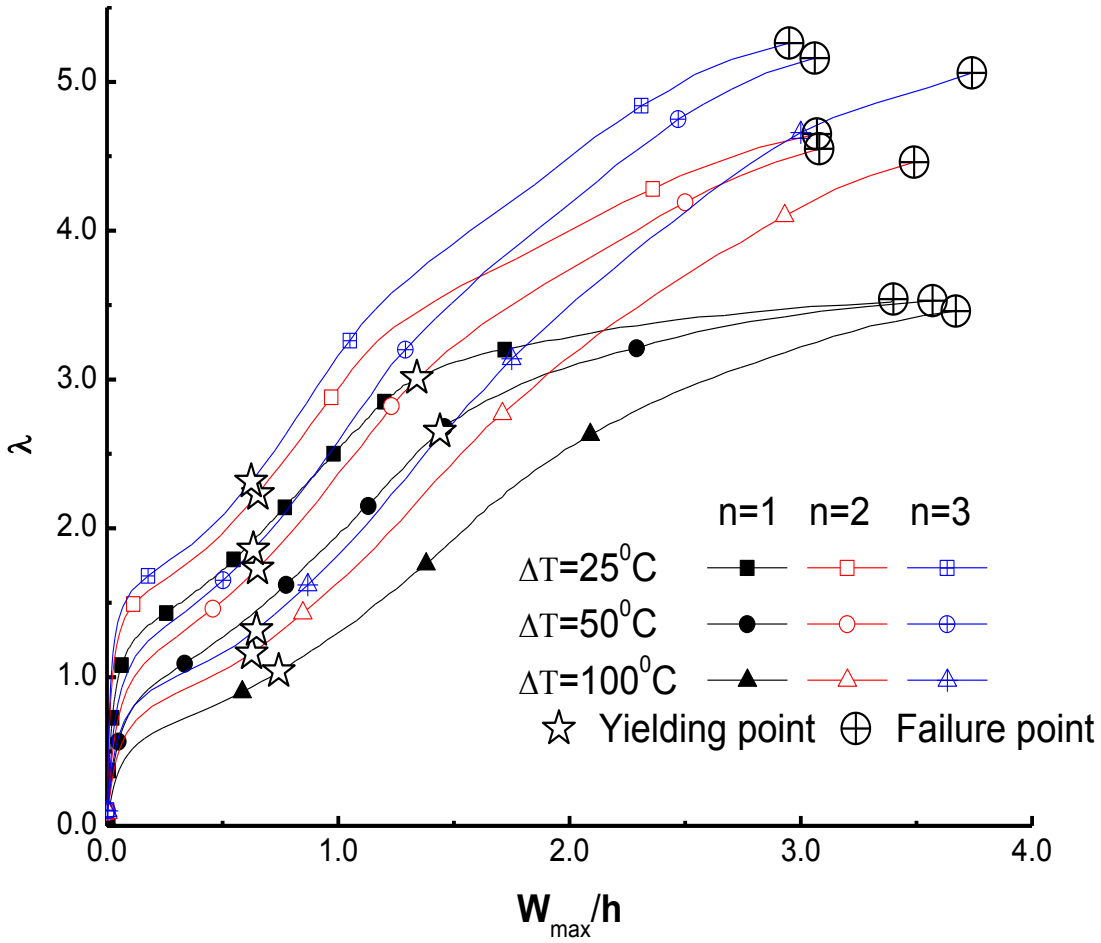

Fig. 9.2.2: Effect of material gradation on elastic-plastic buckling, postbuckling and failure behavior of Ni/Al_2O_3 FGM plate under uniaxial compression combined with constant and uniform temperature rise.

The effect of material property variation [through the thickness obtained by varying volume fraction using Eq. (3.2) of Chapter 3 for different values of exponent *n* (i.e., 1, 2, and 3)] on elastic-plastic buckling and postbuckling responses of simply-supported FGM square plate under uniaxial mechanical compression loading combined with constant and uniform temperature rise (i.e., $\Delta T = 25℃,\ 50℃$ and $100℃$) is studied. The corresponding postbuckling paths are plotted in Fig. 9.2.2. It is to mention here that the yielding point on a particular load-deflection curve corresponds to the minimum value of the load at which elastic to plastic transition of the metallic phase present anywhere in the FGM takes place, whereas the excessive plasticity preceding the failure load point on a particular load-deflection curve causes the complete loss of load carrying capacity of the FGM plate beyond this point, termed as failure point. It can be observed from Fig. 9.2.2 that for all values of power law exponent *n*, the FGM plate loses its postbuckling strength (at

a particular value of maximum transverse deflection) considerably due to increase in temperature rise (ΔT). Moreover, at large temperature rise the plastic flow in FGM plate spreads more rapidly, prompting ultimate failure at a relatively lower value of mechanical load. Fig. 9.2.3 also show that the ultimate load carrying capacity of FGM plate increases with the increase in value of power law index, for all values of temperature rise. This finding is attributed to the fact that at higher value of *n*, proportion of ceramic (i.e., Al_2O_3), possessing higher thermal resistance, is increased which in turn causes this increase in ultimate failure load of FGM.

Further, the effect of plastic flow in FGM plate is more prominent for $n = 1$ that corresponds to a higher metal proportion at a particular thickness coordinate than $n = 2$ & 3, and because of this effect the FGM plate with $n = 1$ would fail at a lower value of mechanical load for a given uniform temperature rise. Furthermore, the effect of equivalent plastic strain developed across the thickness of FGM plate at a particular value (equal to the failure load for FGM with $n = 1$) of thermomechanical loading is compared for different values of exponent *n* (i.e., 1, 2, and 3), and the corresponding plots are drawn in Fig. 9.2.3. It is necessary to mention here that the FGM plate comprises of pure ceramic at bottom (i.e., at $z/h = -0.5$), whereas top (i.e., at $z/h = +0.5$) is constituted with pure metallic phase. For a particular value of *n*, the plastic flow is observed to be more dominating in the upper region of the FGM plate (which corresponds to a high metal proportion) with peak value of equivalent plastic strain noted at the top of the FGM plate, whereas at the lower part of the FGM plate, plasticity is minimum with zero plastic strain at the bottom, and at particular thickness point, the plasticity effect is more pronounced in the case of FGM plate with $n = 1$. Further, it is also evident from Fig. 9.2.3 that irrespective of value of *n*, the effect of higher thermal environment is to provoke more plasticity effects in the FGM plate.

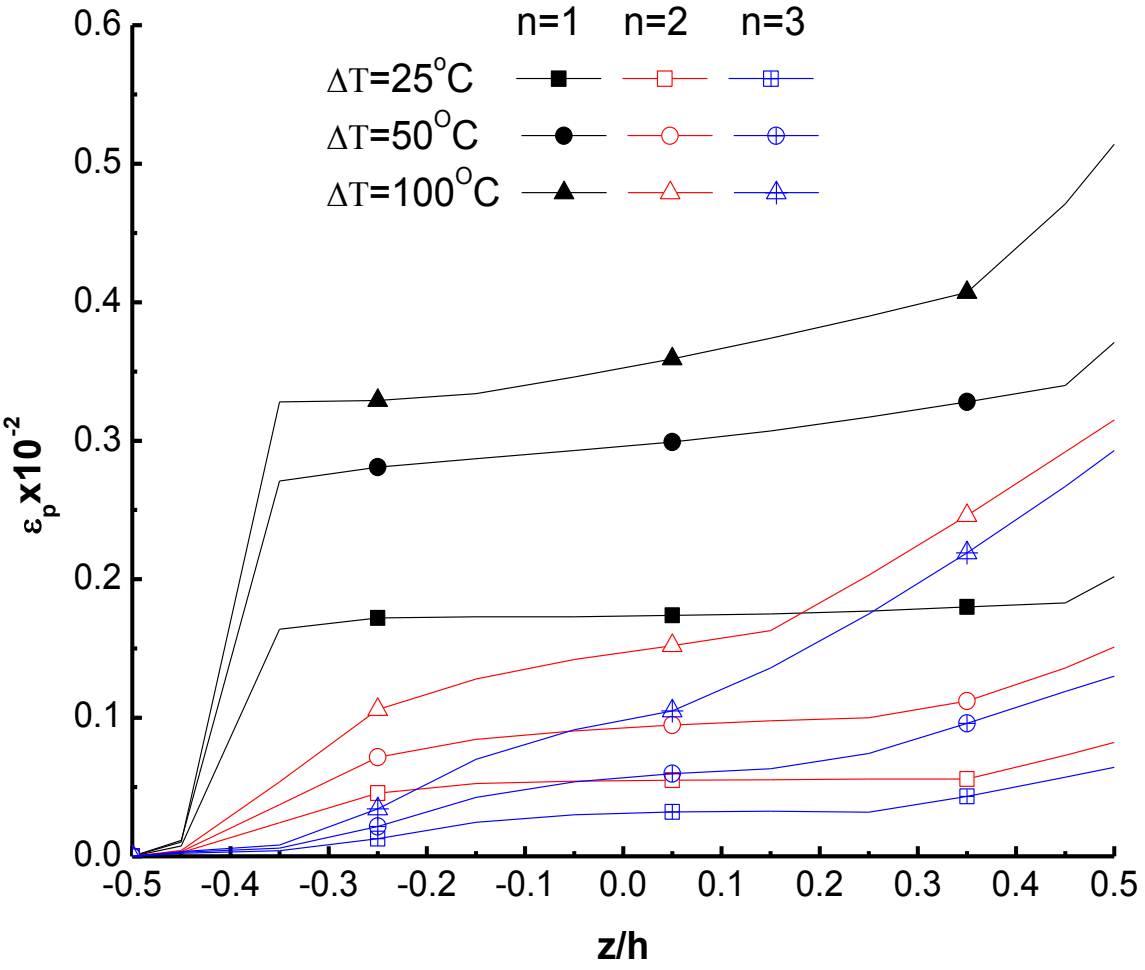

Fig. 9.2.3: The accumulated plastic strain as a function of thickness for FGM plate with different material gradation profile (i.e., *n*) under thermomechanical loading.

The effects of uniaxial and biaxial loading conditions combined with constant and uniform temperature rise (i.e., ΔT) on elastic-plastic buckling and postbuckling behavior and failure of FGM square plate under is examined, and the postbuckling paths for different load ratios (i.e., N_y/N_x) are plotted in Fig. 9.2.4. The corresponding values of buckling load, yielding stress, failure load and maximum plastic strain are given in Table 9.2.2. The results show that for all values of temperature rise, the maximum values of buckling load, postbuckling strength (for a particular value of deflection) and failure load are obtained for plate under uniaxial compression (i.e., for $N_y/N_x = 0$). The postbuckling load-deflection curves become significantly lower, and the plasticity commences at a lower value of yield load with the increase in N_y/N_x ratio.

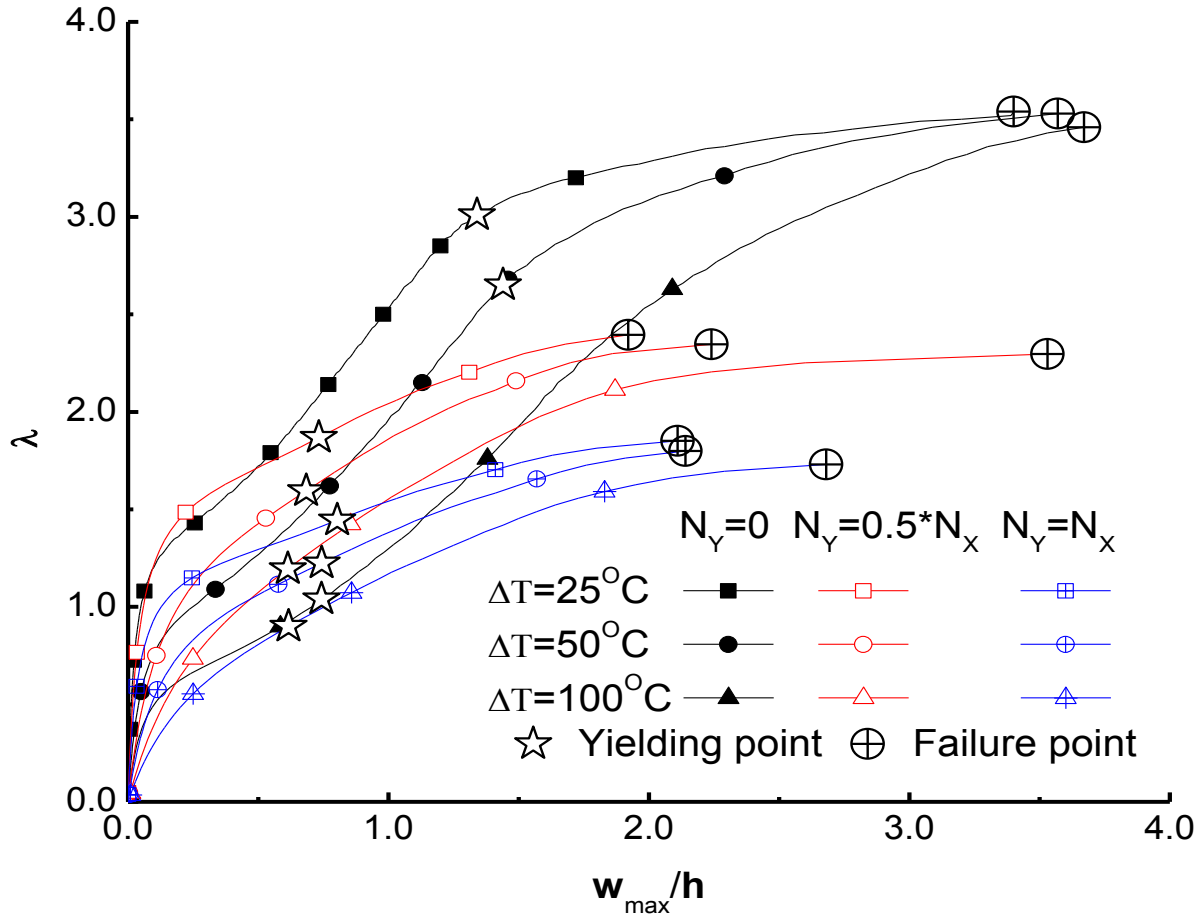

Fig. 9.2.4: Effect of loading on elastic-plastic buckling and postbuckling behavior of FGM (for n = 1) plate under thermomechanical loading.

Table 9.2.2 : Effect of loading (N_y/N_x) on buckling, yielding and failure characteristics of the simply-supported square FGM plate under thermomechanical loading.

N_y/N_x	ΔT	λ_b	λ_y	λ_f	Accumulated Max. plastic strain ($\varepsilon_p \times 10^{-2}$)
0	25	1.06	3.01	3.54	0. 20
	50	0.83	2.65	3.53	0. 37
	100	0.55	1.04	3.46	0. 51
0.5	25	1.05	1.87	2.37	0. 11
	50	0.80	1.58	2.33	0. 16
	100	0.49	1.19	2.27	0. 34
1	25	1.00	1.44	1.84	0.14
	50	0.64	1.21	1.78	0.15
	100	0.40	0.89	1.71	0.27

λ_b, λ_y and λ_f are buckling, yielding and failure loads respectively.

To study the effect of aspect ratio, the slenderness ratio is fixed at 100, and for a fixed width (b = 1 m), different aspect ratios (i.e., 1, 2, and 3) are obtained by varying the length of the plate, and while studying the effect of slenderness ratio, different values of slenderness ratios (i.e., 50, 100 and 200) are obtained by varying the thickness of a square (of side 1 m) FGM plate. The corresponding values of buckling load, yielding load, failure load and equivalent plastic strains for different aspect ratios and slenderness ratios are presented in Tables 9.2.3 and 9.2.4, respectively. It is necessary to mention here that while carrying out the study on the effects of aspect and slenderness ratios, the number of elements and number of layers in FGM plate were increased proportionately based on the convergence study conducted in Section 9.2.1 to get the converged results.

It can be seen from Table 9.2.3 that for all values of temperature rise (ΔT) buckling and postbuckling strengths are found to be decreased with the increase in aspect ratio, and the highest buckling and postbuckling strengths are obtained for a square FGM plate (i.e., for *a/b* =1).

Table 9.2.3: Effect of aspect ratio (*a*/*b*) on buckling, yielding and failure characteristics of the rectangular simply-supported FGM plate under thermomechanical loading.

a/*b*	ΔT	λ_b	λ_y	λ_f	Max. plastic strain ($\varepsilon_p \times 10^{-2}$)
1	25	1.06	3.01	3.54	0. 20
	50	0.83	2.65	3.53	0. 37
	100	0.55	1.04	3.46	0. 51
2	25	0.86	2.40	3.33	0.11
	50	0.52	1.63	3.26	0.19
	100	0.32	0.96	3.22	0.39
3	25	0.85	2.32	3.32	0.11
	50	0.50	1.64	3.29	0.23
	100	0.32	0.97	3.19	0.39

A monotonic decrement in the absolute values of buckling load, yielding load and failure load with increase in the slenderness ratio of FGM plate can be noticed from Table 9.2.4. Moreover irrespective of value of temperature rise, thick FGM plate exhibits a large value of plastic strain at the time of ultimate failure. It can also be noticed by Table 9.2.4 that for all values of slenderness ratios, the increase in

temperature rise (ΔT) causes reduction in buckling and postbuckling strengths of FGM plate caused by more plastic flow.

Table 9.2.4: Effect of slenderness ratio (*b/h*) on absolute values of buckling, yielding and failure loads of simply-supported rectangular FGM plate under thermomechanical loading.

b/h	ΔT	Buckling load (kN)	Yielding load (kN)	Failure load (kN)	Max. plastic strain ($\varepsilon_p \times 10^{-2}$)	$\frac{w_{max}}{h}$
50	25	2401.12	2568.64	5835.28	2.89	3.21
	50	2317.36	2515.64	5830.28	2.94	3.24
	100	2290.36	2291.0	5807.36	2.95	3.35
100	25	369.94	1050.49	1235.46	0. 20	3.54
	50	289.67	924.85	1231.97	0. 37	3.57
	100	191.95	362.96	1207.54	0. 51	3.67
200	25	47.6	171.7	335	0.07	3.71
	50	29.07	117.3	322	0.10	3.92
	100	19.38	71.06	305	0.32	4.21

9.2.3 Conclusions

A study on non-linear finite element analysis of elastic-plastic imperforated FGM plate under in-plane compression caused by mechanical loading and constant and uniform temperature rise is conducted. The effects of plasticity, material inhomogenity, aspect and slenderness ratios, and thermomechanical loading on elastic-plastic buckling, postbuckling and collapse behavior of FGM plate are analyzed under the framework of J_2 deformation theory associated with the isotropic hardening flow rule. Based on the present study, the following important conclusions are drawn.

- Postbuckling response of FGM plate is found to be greatly affected by the plasticity consideration. FGM plate with elastic material properties exhibits only stable equilibrium path, whereas the elastic-plastic FGM plate shows destabilizing response after the point of maximum postbuckling strength, also called ultimate failure point.
- Along the thickness of FGM plate, the effect of plastic flow is observed to be more dominating in the metal rich upper portion of FGM plate as compared to the ceramic rich lower region.

- Effect of rise in temperature difference (i.e., ΔT) is to develop more plastic strain, irrespective of the value of material gradation index n and the mechanical loading condition.
- Buckling load and postbuckling strength of elastic-plastic FGM plate are found to be significantly affected by its material gradation profile; FGM plate with higher ceramic proportion depicted higher buckling load and postbuckling strength.
- Effect of biaxial loading is to reduce the buckling load, postbuckling strength (for a particular value of deflection), and yielding and failure loads, for all values of temperature difference.
- Buckling, yielding and ultimate failure loads of FGM plate are found to decrease with the increase in aspect ratio as well as slenderness ratio of the plate. The failure of thick FGM plate is occurred due to large plastic flow, whereas thin FGM plate shows excessive out-of-plane deflection at the time of failure.

9.3 Thermomechanical Stability and Failure Analysis of Perforated Elastic-Plastic FGM Plate

9.3.1 Details of Perforation

Perforated FGM plate of dimension ($a \times b \times h$), with a central cutout of various shapes (i.e., circular, square, diamond, and elliptical) is considered to observe the effect of cutout shape on elastic-plastic buckling, postbuckling and failure response of the perforated FGM plate. Three cutout sizes designated as A_1, A_2, and A_3, as mentioned in Table 5.1.1, have been also considered.

9.3.2 Convergence Study

A convergence study was performed for a simply-supported FGM plate containing a centrally located circular cutout of size A_1 (d/b = 0.158). The convergence of buckling and failure loads was checked for FGM (n = 1) square plate with b/h = 100 under uniaxial compression and constant and uniform temperature rise of 100^{o}C. The FGM plate modeled with 10, 20 and 30 number of layers was meshed using the mesh size control feature of ANSYS, as discussed in Section 5.3.2 of Chapter 5, with 718, 3042 and 6279 number of elements. A reasonable convergence of buckling and failure loads for FGM plate with circular cutout can be observed from Table 9.3.1 for the mesh of 3042 elements (i.e., for mesh control parameter, η = 30) when modeled with 20 layers. For the sake of uniformity, the same meshing procedure with and same mesh control parameter (i.e., η = 30) was followed to mesh the FGM plate with other cutout shapes while keeping the number of layers 20.

Table 9.3.1: Convergence study for buckling $\left(\lambda_b = \frac{N_x b^2}{E_c h^3}\right)$ and failure loads $\left(\lambda_f = \frac{N_{fail} b^2}{E_c h^3}\right)$ for FGM plate with a central circular cutout under thermomechanical loading.

No. of elements	No. of layers					
	10		20		30	
	λ_b	λ_f	λ_b	λ_f	λ_b	λ_f
718	2.8019	3.753939	2.6109	3.5234	2.5518	3.2270
3042	2.7817	3.678853	2.5518	3.2607	2.4989	3.1948
6279	2.7329	3.688075	2.5242	3.2270	2.4790	3.1692

9.3.3 Numerical Results and Discussion

Various numerical studies are conducted to analyze the elastic-plastic buckling, postbuckling and failure characteristics of a simply-supported FGM plate having a centrally located cutout of various shapes (i.e., circular, square, diamond, and elliptical) under thermomechanical loading condition. Effects of material inhomogeneity (i.e., power exponent n), cutout size (i.e., A_1 A_2, and A_3) and cutout shape (i.e., circular, square, diamond, and elliptical) on the buckling load, postbuckling path, yielding load, maximum plastic strain and failure strength of perforated FGM plate are investigated.

The effects of cutout shape and size on elastic-plastic thermomechanical buckling and postbuckling behavior of a simply-supported square plate with a central cutout and made of FGM with temperature-dependent (TD) material properties are shown in Figs. 9.3.1-9.3.3. The study is conducted for uniaxial mechanical compression combined with different values of uniform and constant temperature rise (i.e., $\Delta T = 50℃,\ 100℃$ and $150℃$). In addition, the corresponding values of normalized buckling and failure loads, and maximum transverse deflections are tabulated in Table 9.3.2. It can be seen from Figs. 9.3.1-9.3.3 that for all cutout shapes, the postbuckling paths for elastic-plastic FGM plate are strongly dependent on temperature rise (i.e.,ΔT), and for a particular value of mechanical load, the perforated FGM plate exhibit an increase in the value of transverse deflection with an increase in the temperature. This response is attributed to the high thermal load at higher temperature as well as to the reduced stiffness of FGM plate with rise in temperature, because of the inverse dependence of Young's modulus on temperature (reduction in Young's modulus with increase in temperature) and the direct proportionality of thermal expansion coefficient with temperature.

It can also be observed from Figs. 9.3.1-9.3.3 that irrespective of cutout shape, postbuckling paths of FGM plate are greatly affected by the plasticity, as yielding in FGM plate take place at much lower load than ultimate failure load, and the ultimate failure of FGM plate occurs due to excessive plasticity.

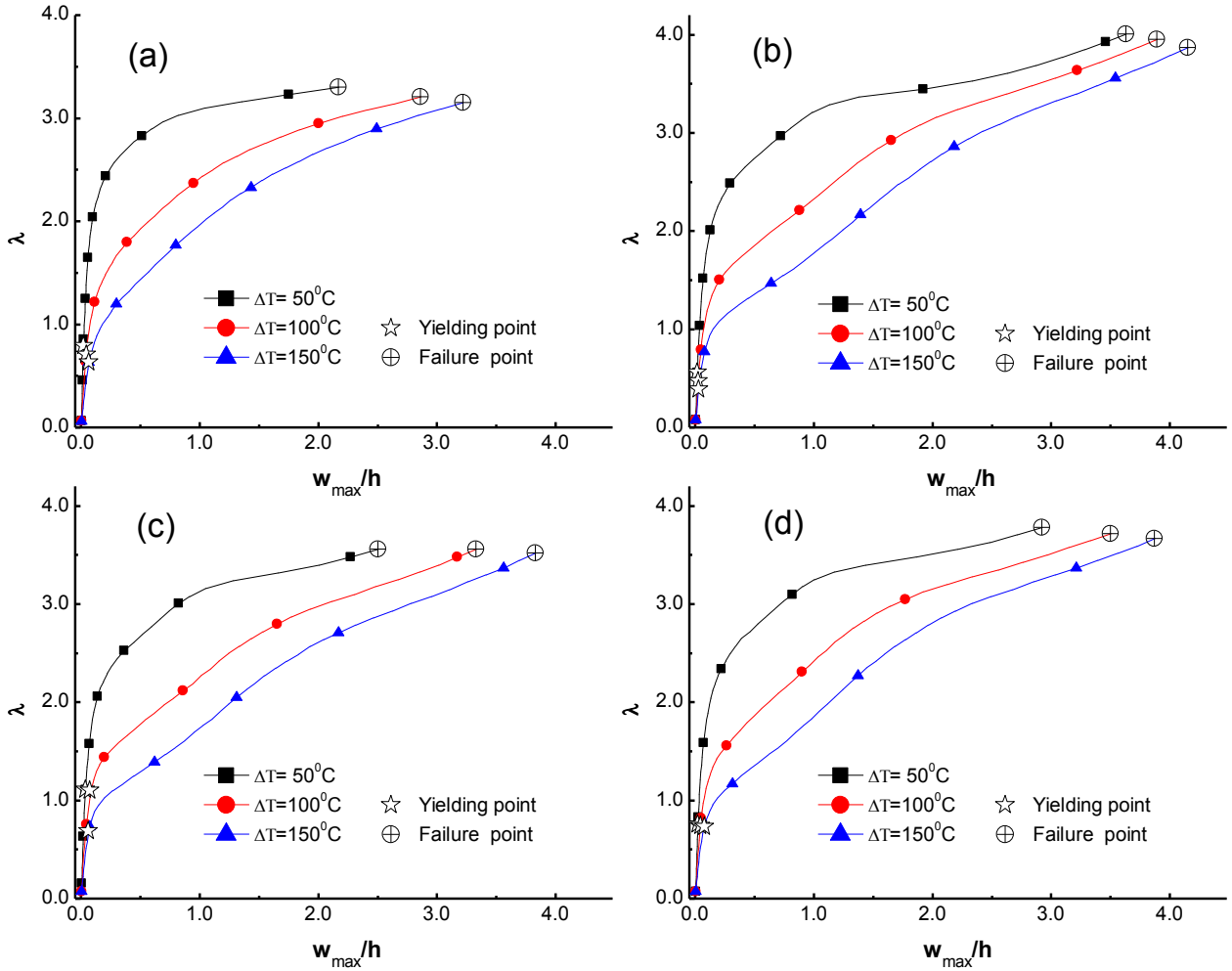

Fig. 9.3.1: Elastic-plastic buckling and postbuckling behavior of FGM (for n = 1) plate with A_1 size cutout of (a) circular (b) square (c) elliptical (d) diamond shape, under thermomechanical loading.

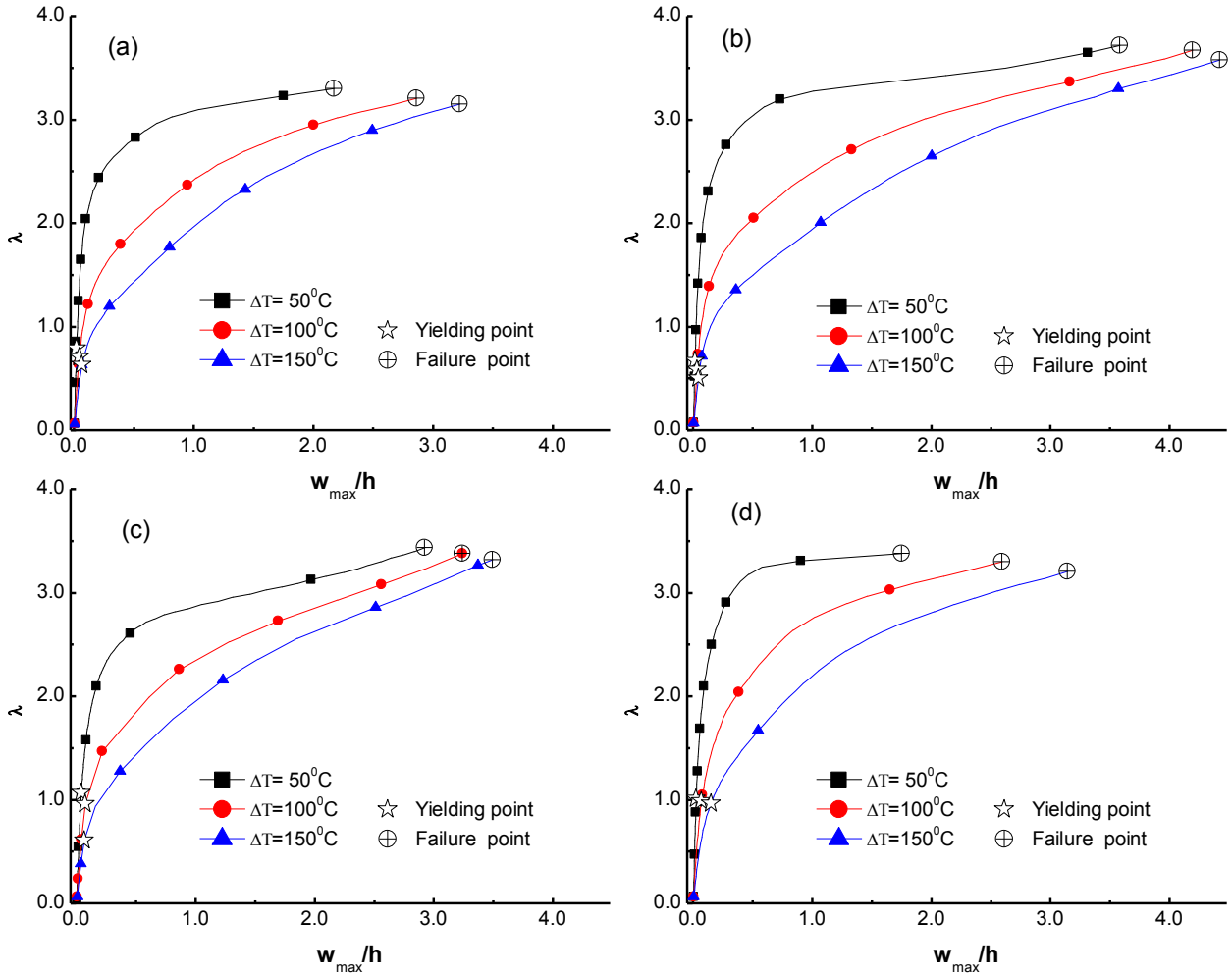

Fig. 9.3.2: Elastic-plastic buckling and postbuckling behavior of FGM (for n = 1) plate with A_2 size cutout of (a) circular (b) square (c) elliptical (d) diamond shape, under thermomechanical loading.

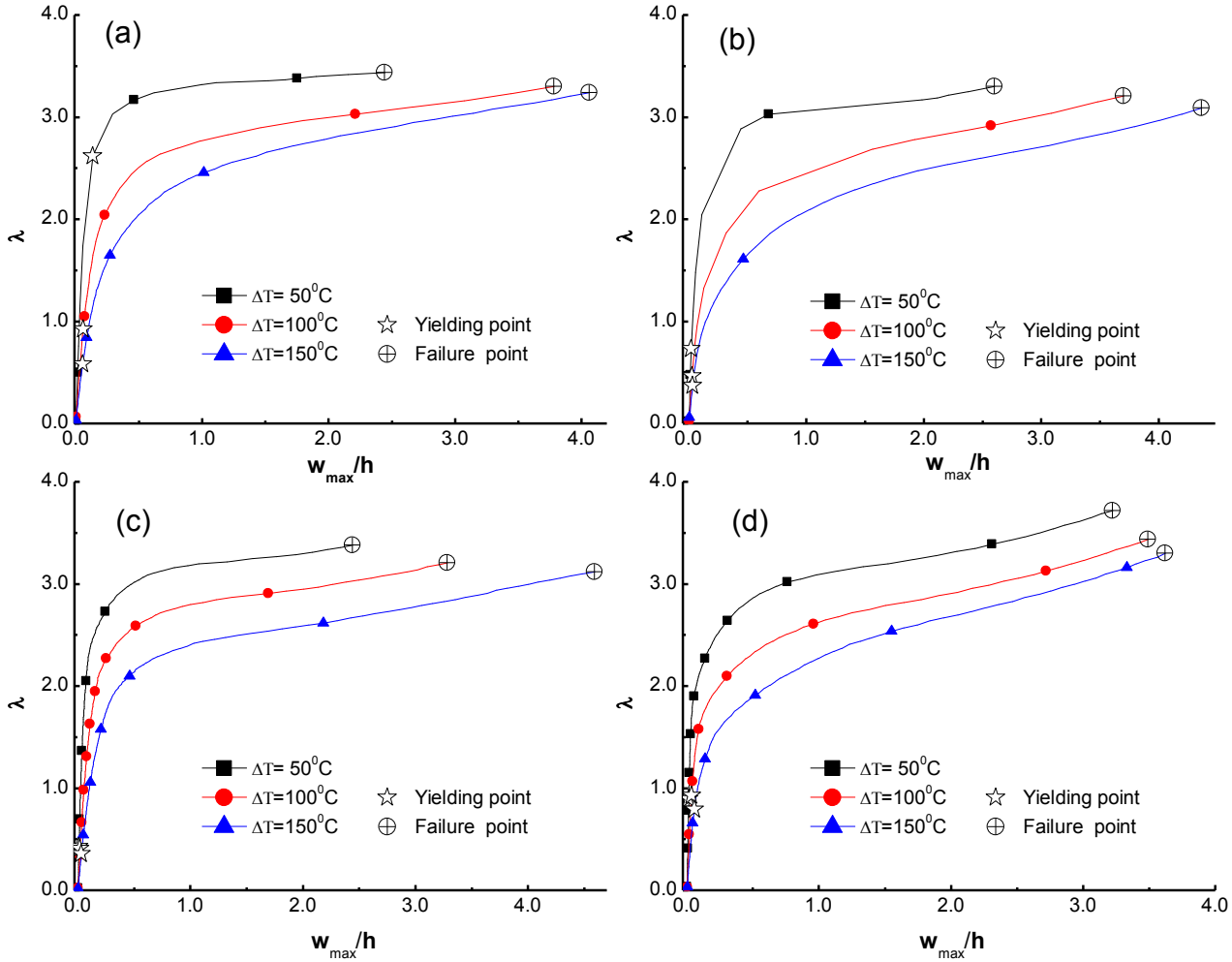

Fig. 9.3.3: Elastic-plastic buckling and postbuckling behavior of FGM (for n = 1) plate with A_3 size cutout of (a) circular (b) square (c) elliptical (d) diamond shape, under thermomechanical loading.

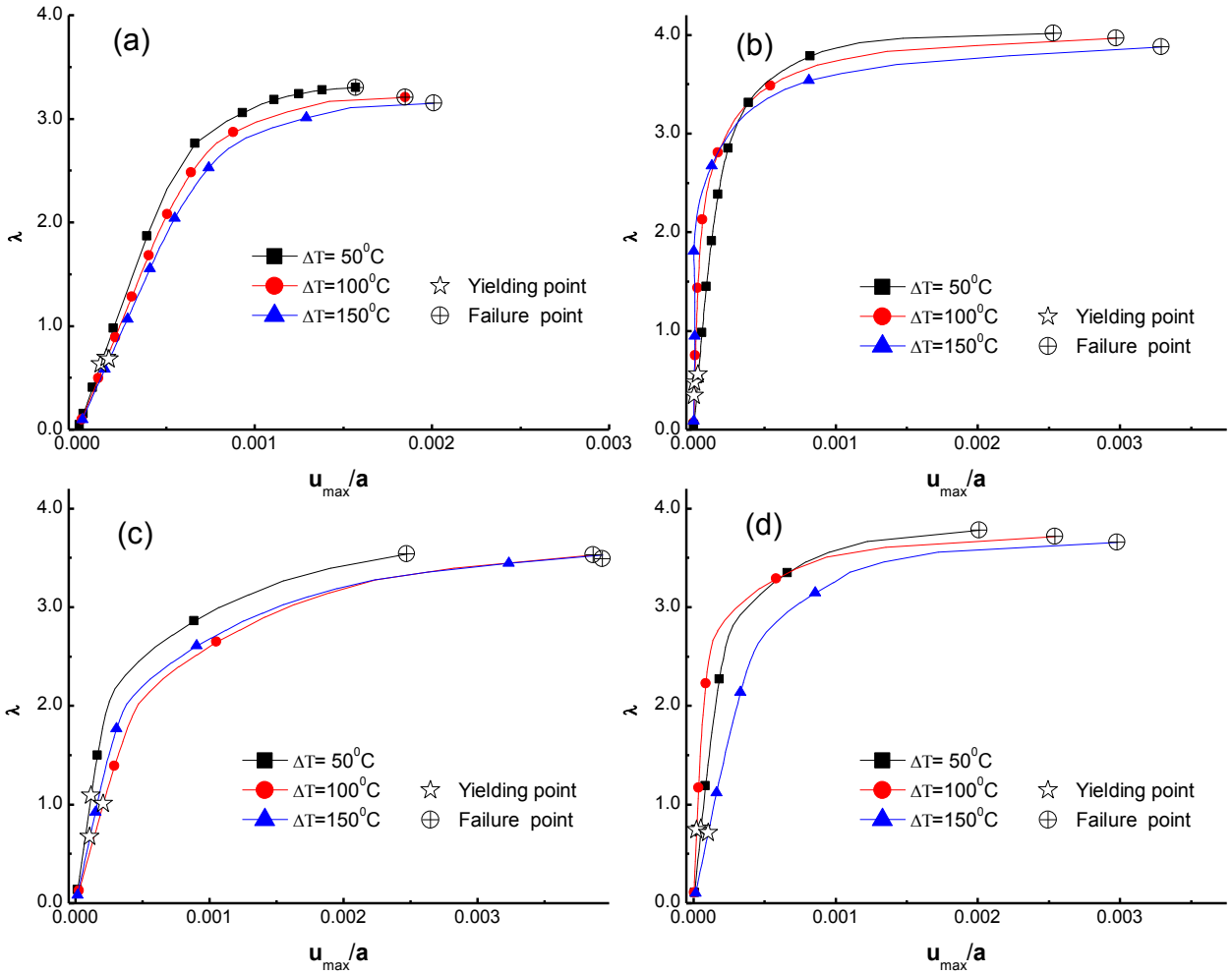

Fig. 9.3.4: Elastic-plastic load-axial deflection curve of FGM (for n = 1) plate with A_1 size cutout of (a) circular (b) square (c) elliptical (d) diamond shape under thermomechanical loading.

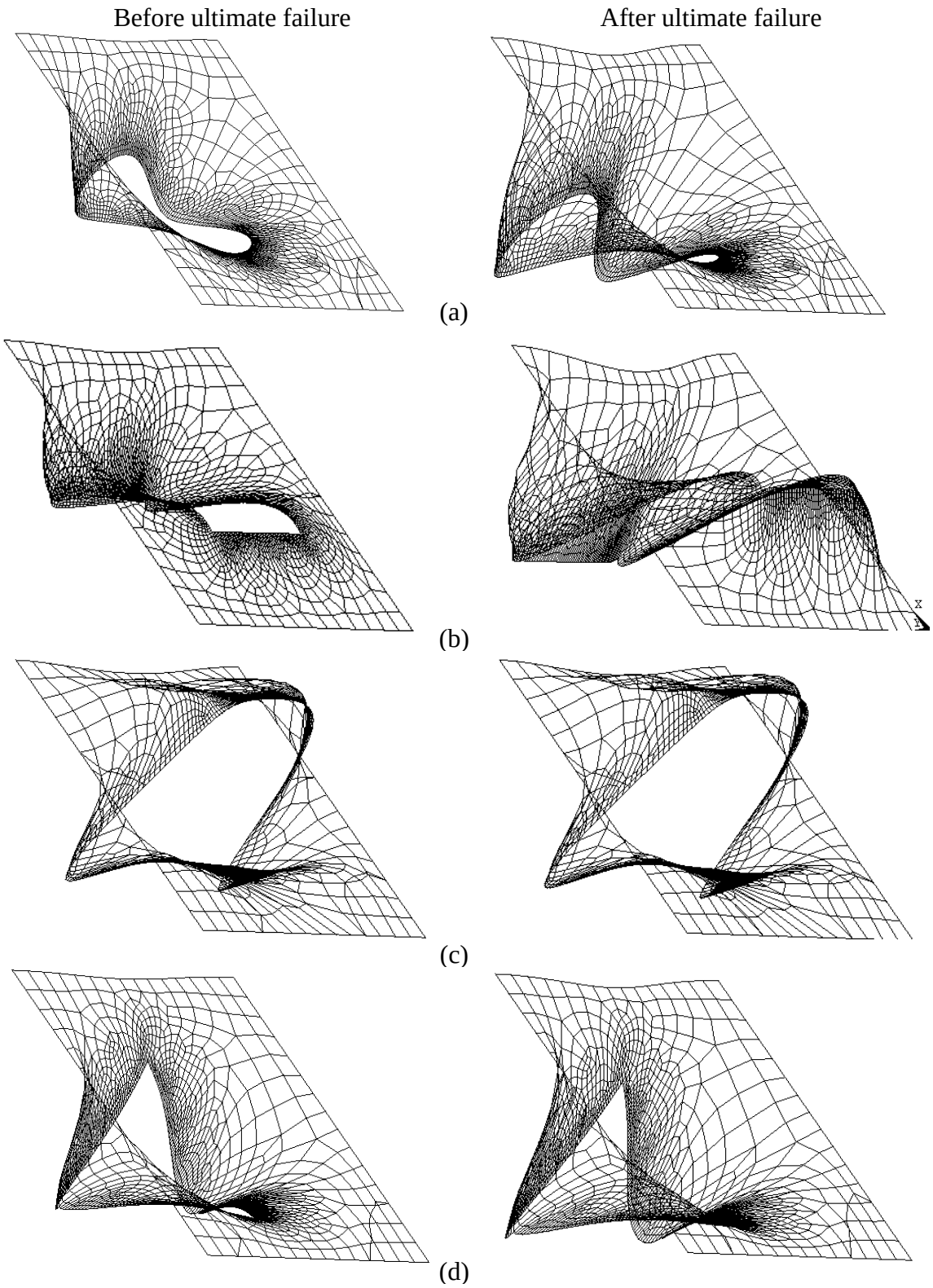

Fig. 9.3.5: Deformed shapes just before and after ultimate failure of FGM (for n = 1) plate with A_1 size cutout of (a) circular (b) square (c) elliptical (d) diamond shape, under thermomechanical loading ($\Delta T = 50$).

The load-axial deflection paths are also traced to understand the effect of plasticity on stiffness and hence, on the overall ultimate load capacity of the FGM plate. To demonstrate the ultimate failure, the load-axial deflection paths and the deformed shapes, just before and after ultimate failure, for FGM plate with A_1 size cutout of various shapes are depicted in Figs. 9.3.4 and 9.3.5, respectively. The ultimate failure points in Fig. 9.3.4 correspond to the maximum applied load at which the FGM plate loses its stiffness (i.e., given by the slope of load-axial deflection curve) completely and thereafter, the plate is not able to resist even a slight increment in the applied load. In addition, it can also be observed from Figs. 9.3.1-9.3.3 that for all cutout shapes, the ultimate failure load of FGM plate decreases with the increase in cutout size.

Table 9.3.2 shows that for A_1 and A_2 sizes of cutout, the FGM plate with square cutout possesses maximum value of failure load; however, for larger cutout size (i.e., A_3) the FGM plate with diamond cutout depicts highest failure load.

The effect of material property variation [through the thickness obtained by varying volume fraction using Eq. (3.1) for different values of exponent *n* (i.e., 1, 2, and 3)] on elastic-plastic buckling and postbuckling response of simply-supported FGM square plate having cutout of various shapes of size A_3 under uniaxial mechanical compression combined with different values of constant and uniform temperature rise (i.e., $\Delta T = 50℃,\ 100℃ \text{ and } 150℃$) is studied. The postbuckling paths are plotted in Fig. 9.3.6, and the corresponding normalized values of buckling and failure loads, and maximum deflection are given in Table 9.3.3. It can be observed from Fig. 9.3.6 that for all values of power law exponent *n*, FGM plate with a cutout loses its postbuckling strength (at a particular value of maximum transverse deflection) considerably due to increase in uniform temperature rise (ΔT). Fig. 9.3.6 also show that irrespective of cutout shape in an FGM plate, its ultimate load carrying capacity increases with the increase in value of power law index for all values of temperature rise. This finding is attributed to the fact that at higher value of *n*, proportion of ceramic (i.e., Al_2O_3), possessing higher thermal resistance, is increased which in turn causes this increase in ultimate failure load of FGM.

Table 9.3.2: Effect of cutout shape on buckling and failure response of simply-supported square FGM plate with a central cutout under thermomechanical loading.

Cutout Size / Cutout Shape		A_1			A_2			A_3		
	ΔT	$\lambda_b{}^*$	$\lambda_f{}^*$	$\frac{w_{max}*}{h}$	λ_b	λ_f	$\frac{w_{max}}{h}$	λ_b	λ_f	$\frac{w_{max}}{h}$
Circular	50	3.23	3.41	2.18	2.84	3.37	2.21	2.80	3.30	2.50
	100	2.55	3.26	2.88	1.94	3.30	2.91	1.90	3.21	3.84
	150	2.06	3.20	3.23	1.44	3.25	3.28	1.42	3.15	4.12
Square	50	2.75	4.02	3.64	3.02	3.71	3.57	2.95	3.30	2.67
	100	1.86	3.97	3.90	2.03	3.67	4.18	2.14	3.20	3.78
	150	1.36	3.88	4.17	1.49	3.59	4.41	1.66	3.09	4.44
Elliptical	50	2.66	3.54	2.53	2.68	3.49	3.00	3.01	3.29	2.50
	100	1.77	3.53	3.37	1.86	3.45	3.23	2.56	3.16	3.33
	150	1.29	3.49	3.89	1.44	3.38	3.58	2.14	3.07	4.67
Diamond	50	2.76	3.78	2.97	3.18	3.39	1.78	2.84	3.65	3.29
	100	1.85	3.72	3.55	2.20	3.31	2.63	2.29	3.38	2.57
	150	1.35	3.66	3.93	1.60	3.23	3.18	1.88	3.23	3.70

* λ_b and λ_f are normalized buckling and failure loads respectively, whereas w_{max}/h is normalized maximum transverse deflection corresponding to failure point.

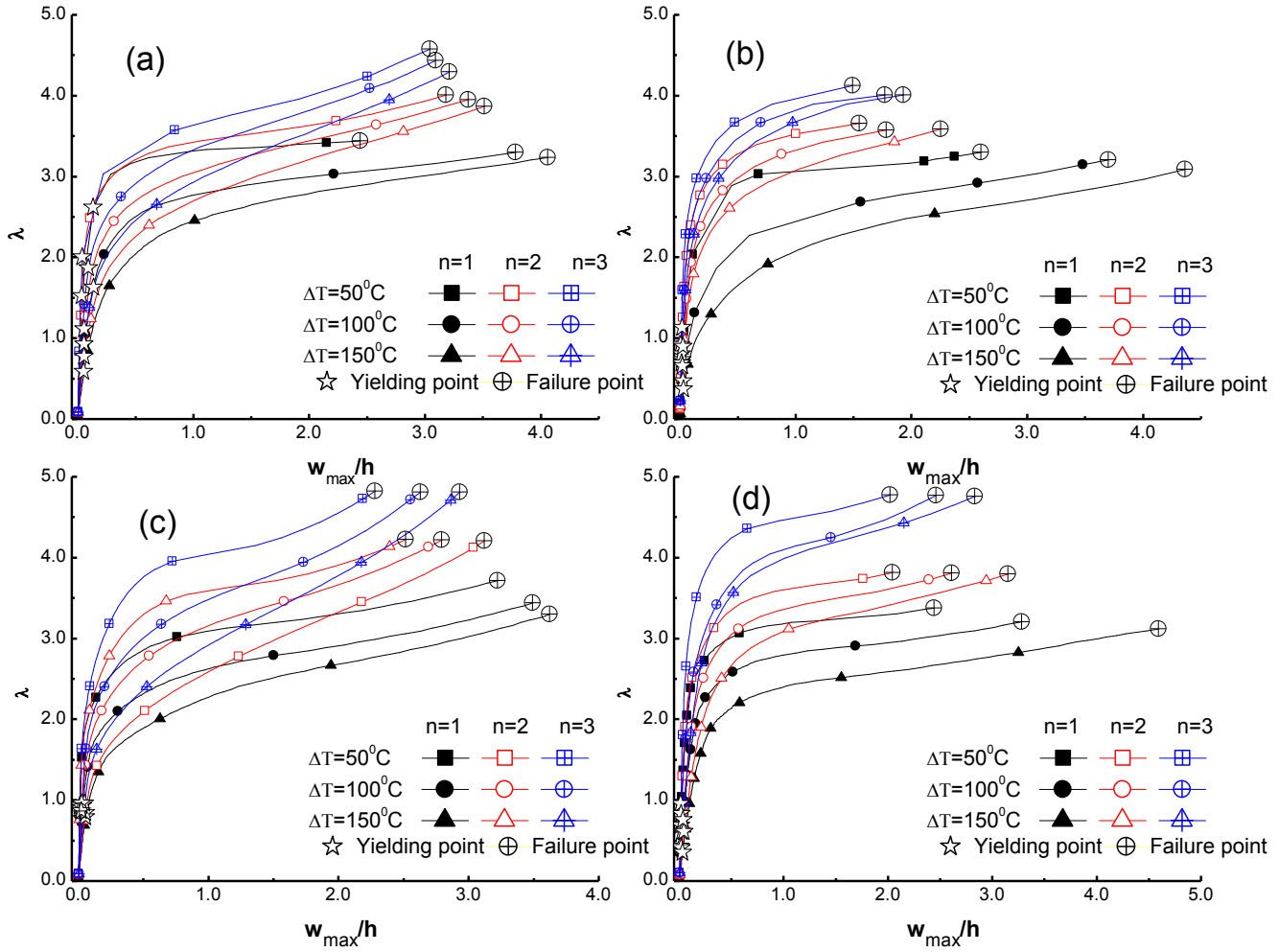

Fig. 9.3.6: Effect of material gradation on elastic-plastic buckling, postbuckling and failure behavior of FGM plate with A_3 size cutout of (a) circular (b) square (c) elliptical (d) diamond shape under uniaxial compressive load combined with constant and uniform temperature rise.

The equivalent plastic strains developed under thermomechanical loading across the thickness of an FGM plate with a central cutout (size A_3) of various shapes are shown in Fig. 9.3.7, for different values of exponent *n* (i.e., 1, 2, and 3). It is to mention that in Fig. 9.3.7, plastic strains for all values of *n* are plotted, at a particular value of temperature rise, corresponding to the ultimate failure load of FGM plate with $n = 1$. For a particular value of *n*, the plastic flow is observed to be more dominating in the metal-rich upper region of the FGM plate with peak value of equivalent plastic strain at the top of the FGM plate, whereas at the lower ceramic-rich part of the FGM plate, plasticity is minimum with zero plastic strain at the bottom. Further, at a particular thickness, the plasticity effect in FGM plate with a cutout is more prominent for $n = 1$ that corresponds to a higher proportion of metal at a particular thickness coordinate than $n = 2$ & 3, and because of this effect the FGM plate with $n = 1$ would fail at a lower value of mechanical load for a given temperature rise (see Fig. 9.3.6 and Table 9.3.3).

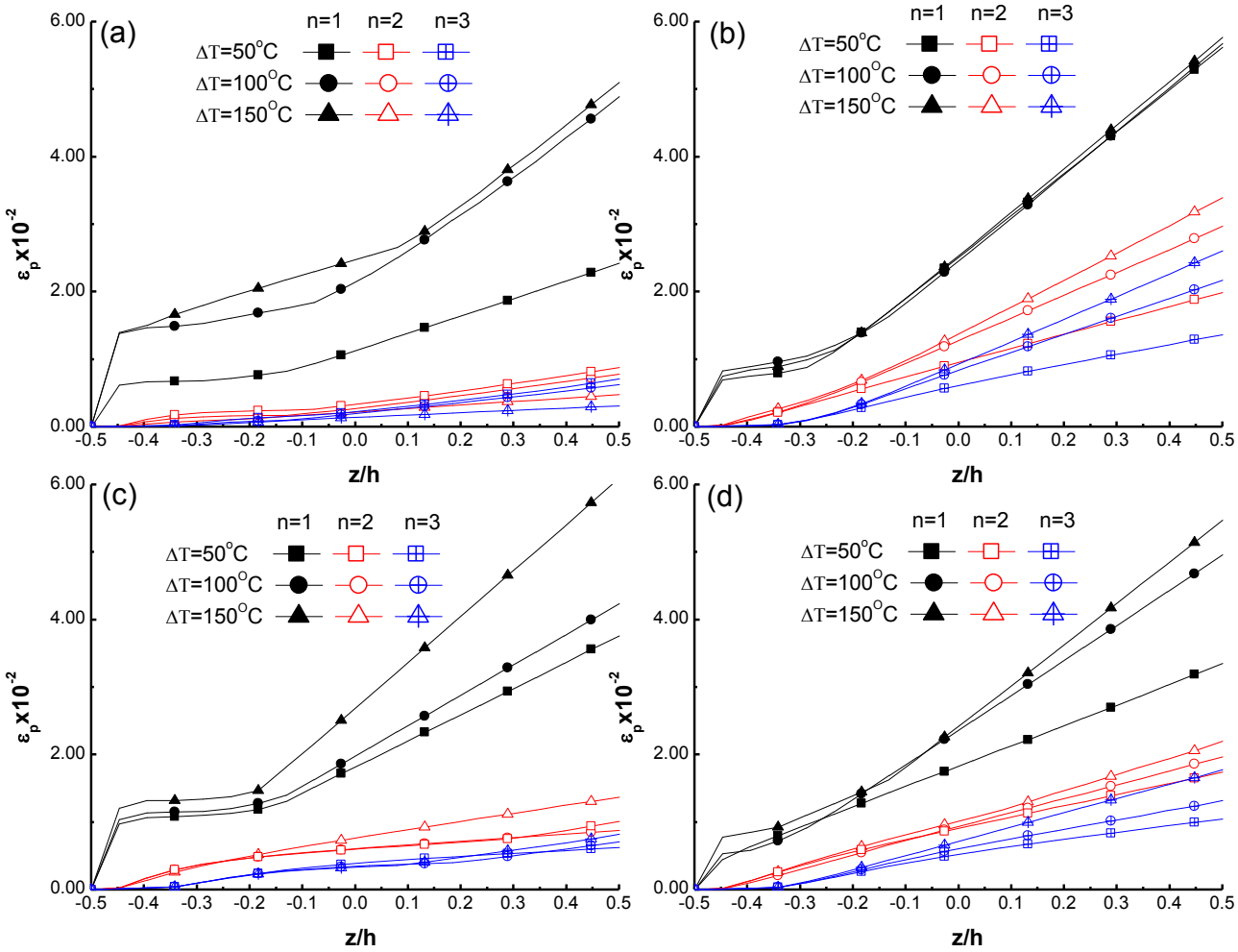

Fig. 9.3.7: Plastic strain as a function of thickness for FGM plate with A_3 size cutout of (a) circular (b) square (c) elliptical (d) diamond shape, under thermomechanical load for different material gradation profile (i.e., *n*).

Table 9.3.3: Effect of material inhomogenity on buckling, yielding and failure characteristics of simply-supported square Ni/Al_2O_3 FGM plate with various shapes cutout of size A_3, under thermomechanical load.

Cutout Shape	ΔT	n = 1			n = 2			n = 3		
		$\lambda_b{}^*$	$\lambda_f{}^*$	$\frac{w_{max}{}^*}{h}$	λ_b	λ_f	$\frac{w_{max}}{h}$	λ_b	λ_f	$\frac{w_{max}}{h}$
Circular	50	3.23	3.41	2.50	3.30	3.67	1.60	3.30	4.62	3.05
	100	2.55	3.26	3.84	3.00	3.59	1.82	2.93	4.48	3.10
	150	2.06	3.20	4.12	2.74	3.61	2.31	2.45	4.33	3.21
Square	50	2.95	3.30	2.67	3.30	4.23	2.54	3.71	4.15	1.52
	100	2.14	3.20	3.78	2.71	4.21	2.83	3.50	4.02	1.81
	150	1.66	3.09	4.44	2.08	4.21	3.14	3.24	4.01	1.99
Elliptical	50	3.01	3.29	2.50	3.31	3.81	2.30	3.76	4.82	2.30
	100	2.56	3.16	3.33	3.01	3.79	2.66	3.03	4.81	2.66
	150	2.14	3.07	4.67	2.64	3.78	2.97	2.40	4.81	2.97
Diamond	50	2.84	3.65	3.29	3.30	3.67	1.60	4.21	4.77	2.06
	100	2.29	3.38	2.57	3.00	3.59	1.82	3.65	4.76	2.52
	150	1.88	3.23	3.70	2.74	3.61	2.31	3.50	4.75	2.91

* λ_b and λ_f are normalized buckling and failure loads respectively, whereas w_{max}/h is normalized maximum transverse deflection corresponding to failure point.

9.3.4 Conclusions

A study on nonlinear finite element analysis of elastic-plastic perforated Ni/Al_2O_3 FGM plate carrying a central cutout of various shapes is carried out under in-plane, uniaxial compression load combined with constant and uniform temperature rise. The effects of cutout shape and size, material inhomogenity and thermomechanical loading conditions on elastic-plastic buckling, postbuckling and failure responses of FGM plate are investigated under the framework of J_2 plasticity theory associated with the isotropic hardening flow rule. Following are the important observations based on the present study:

- Postbuckling response of FGM plate carrying a central cutout is found to be greatly affected by the plasticity consideration, and its elastic-plastic analysis shows destabilizing response after the point of maximum postbuckling strength, also called ultimate failure point.
- Along the thickness of FGM plate with a cutout, the effect of plastic flow is observed to be more dominating in the metal rich portion of FGM plate as compared to the ceramic rich region. Accordingly, at a particular thickness, the plasticity effect is observed to be more prominent for $n = 1$ than $n = 2$ and 3.
- For all cutout shapes, the failure load of FGM plate decreases with an increase in cutout size, maximum being for A_1 cutout size. It is also observed that for smaller cutout size (A_1 and A_2 cutout size), the FGM plate with square shape cutout possesses maximum value of ultimate load carrying capacity, however, for larger cutout size (i.e., A_3), the FGM plate with diamond cutout depicts highest ultimate load carrying capacity.

CHAPTER 10

CLOSURES

10.1 Concluding Remarks

A nonlinear FEM model of FGM plate is developed to investigate the elastic and elastic-plastic buckling, postbuckling and/or failure analysis of imperforated and perforated FGM plate under thermal and/or mechanical loading conditions, with and without temperature-dependent material properties. The actual non-homogeneous (along thickness) FGM plate with continuously varying properties along thickness is modeled as a laminate composed of multiple perfectly-bonded layers of isotropic material having layer-wise constant composition. At the mid of a particular layer, thermoelastic properties and elastic-plastic strength parameters (i.e., elastic constants, thermal expansion coefficients, yield strength and plastic modulus) of FGM are calculated using theoretical and numerical micromechanics based models. The elastic-plastic behavior of FGM plate is assumed to follow J_2-plasticity with isotropic hardening, wherein the ceramic phase is considered to be elastic, whereas the metal is assumed to be elastic-plastic in accordance with the Tamura-Tomota-Ozawa model. The nonlinear temperature-dependent thermoelastic material properties are also incorporated into the model. The non-linear FEM formulation was based on the first-order shear deformation theory and the von Karman's nonlinear kinematics. The incremental solution technique based on Newton-Raphson method is adopted for the solution of non-linear algebraic equations. Various convergence and the validation studies of the present numerical model have been carried out by comparing the present results with the available results in the literature. Numerical studies are conducted on the buckling, postbuckling and failure responses of elastic and elastic-plastic FGM plates with and without perforation, considering the temperature-dependent as well as temperature-independent material properties, under thermal and/or mechanical loading condition to assess the effects of different parameters on overall structural integrity of FGM plates. Based on the present thesis work, the following important conclusions are drawn:

- **For Elastic FGM plate :**
    - Irrespective of loading conditions (i.e., for both thermal and/or mechanical loadings), the increase in the rigidity of support on the edges of FGM plate results in the increase of buckling load, postbuckling strength (at a particular value of transverse deflection), and failure load and reduces the transverse deflection; whereas simply-supported boundary conditions provide significant postbuckling reserve strength and stiffness to the FGM plate beyond buckling.
    - Under mechanical loading conditions, thin FGM plate is expected to buckle before the stresses reach to a critical level, whereas, thick FGM plate would resist buckling and fail because of large stresses developed in the FGM.
    - In the case of FGM plate with large hole-size, the rigid clamped conditions at the boundary edges of the FGM plate are found to provide the required rigidity to increase its mechanical buckling load as compared to small hole-size.
    - Increase in hole size results in monotonic decrement in the failure load and associated maximum transverse deflection as well as the postbuckling stiffness of FGM plate under mechanical loading.
    - Thermal postbuckling strength (at a particular value of deflection) of FGM plates is overestimated in the case of temperature-independent material properties when compared with the case of temperature-dependent material properties; hence, for realistic and accurate analysis of thermal postbuckling behavior of FGM plate, the temperature-dependent material properties should be considered.
    - Irrespective of type of loading, the simply-supported FGM plate does not possess bifurcation type of buckling, which is attributed to the presence of bending-extensional coupling which causes transverse deflection even in the absence of bending load.
    - Ascribed by the freely expandable movable edges, the thermal postbuckling strength of simply-supported FGM plate with movable

edges is found to be more than that of simply-supported FGM plate having immovable edges of the plate.

- For lower values of aspect ratio (i.e., a/b = 1 and 2), thermal postbuckling is preceded by the global buckling mode with one peak, whereas, for a/b = 3 and 4, the thermal postbuckling follows the local buckling of the FGM plate that causes an increase in postbuckling strength, after an initial decrease when the aspect ratio is changed from a/b = 1 to 2.
- FGM plate with a larger central cutout size possesses more resistance against thermal buckling and subsequent, thermal postbuckling phenomenon due to the increase in the domain of tensile stresses (caused by free expansion of cutout edges because of thermal load) near cutout edges as compared to the corresponding FGM plate with smaller size cutout.

- **For Elastic-Plastic FGM plate:**
  - Irrespective of loading conditions (i.e., for both thermal and/or mechanical loadings), postbuckling response of FGM plate is found to be greatly affected by the plasticity consideration. FGM plate with elastic material properties exhibits only stable equilibrium path, whereas, the elastic-plastic FGM plate shows destabilizing response after the point of maximum postbuckling strength, also called ultimate failure point.
  - Along the thickness of FGM plate, the effect of plastic flow is observed to be more dominating in the metal rich portion of FGM plate as compared to the ceramic rich region.
  - Irrespective of thermal loading conditions (i.e., thermal or thermomechanical loading condition), the effect of rise in temperature difference (i.e., ΔT) is to develop more plastic strain in FGM plate.
  - Buckling, yielding and ultimate failure loads of FGM plate under mechanical and thermomechanical loading conditions are found to decrease with the increase in aspect ratio as well as slenderness ratio of the plate. Irrespective of loading conditions, large plastic strain is

occurred in thick FGM plate at failure, whereas, thin FGM plate shows excessive out-of-plane deflection at the failure point.

- It is found that the stability and failure load of FGM plate are greatly affected by the presence of cutouts and their size and shapes. For all cutout shapes, the ultimate failure load of FGM plate under thermomechanical loading conditions is found to be decreased with an increase in cutout size.

10.2 Future Research Possibilities

- Present research work is carried out for static analysis of FGM plate and can be further extended for dynamic analysis as well.
- Continuity of the transverse shear stresses is not satisfied in present model. This point may be considered in the future studies.
- Buckling of FGM plate may be further analyzed under shear and tension-compression type of loading conditions.
- The present study assumes uni-directional gradation of FGM plate, however, based on the practical applications, multidirectional graded FGM can also be analyzed.
- Present model of FGM plate with a central cutout can also be extended to study the stability and failure response of FGM plate with eccentric cutouts.
- Optimization techniques can be applied to optimize the material gradation profile of FGMs to maximize buckling and postbuckling resistance, and failure of FGM plate.
- Molecular dynamics and micromechanics based simulations of FGMs can be performed to characterize the elastic-plastic response of FGMs.
- Certainly, the applicability of present numerical simulations can be increased by performing experimental investigations.

REFERENCES

Abolghasemi, S., Shaterzadeh, A.R., Rezaei, R., 2014. Thermo-mechanical buckling analysis of functionally graded plates with an elliptic cutout. Aerosp. Sci. Technol. 39, 250–259.

Abolghasemi, S., Shaterzadeh, A.R., Rezaei, R., 2014. Thermo-mechanical buckling analysis of functionally graded plates with an elliptic cutout. Aerosp. Sci. Technol. 39, 250–259.

Abrate, S., 2008. Functionally graded plates behave like homogeneous plates. Compos. Part B Eng. 39, 151–158.

Abrate, S., 2006. Free vibration, buckling, and static deflections of functionally graded plates. Compos. Sci. Technol. 66, 2383–2394.

Arbocz, J., Maggiori, C. italiana dei superiori, 1987. Buckling and post-buckling: four lectures in experimental, numerical, and theoretical solid mechanics based on talks given at the CISM-meeting, held in Udine, Italy, September 29-October 3, 1985. Springer-Verlag.

Asemi, K., Ashrafi, H., Salehi, M., Shariyat, M., 2013. Three-dimensional static and dynamic analysis of functionally graded elliptical plates, employing graded finite elements. Acta Mech. 224, 1849–1864.

Atmane, H.A., Bedia, E.A.A., Bouazza, M., Tounsi, A., Fekrar, A., 2016. On the thermal buckling of simply supported rectangular plates made of a sigmoid functionally graded Al/Al2O3 based material. Mech. Solids 51, 177–187.

Aydogdu, M., 2008. Conditions for functionally graded plates to remain flat under in-plane loads by classical plate theory. Compos. Struct. 82, 155–157.

Bakker, M.C.M., Rosmanit, M., Hofmeyer, H., 2009. Prediction of the elasto-plastic post-buckling strength of uniformly compressed plates from the fictitious elastic strain at failure. Thin-Walled Struct. 47, 1–13.

Bandyopadhyay, A., Atisivan, R., Kuhn, G., Yeruva, S., n.d. Mechanical Properties of Interconnected Phase Alumina-Al Composites 24–31.

Bao, G., Wang, L., 1995. Multiple cracking in functionally graded ceramic/metal coatings. Int. J. Solids Struct. 32, 2853–2871.

Bazant, Z.P., Cedolin, L., Hutchinson, J.W., 1993. Stability of Structures: Elastic, Inelastic, Fracture, and Damage Theories, Journal of Applied Mechanics.

Bellifa, H., Benrahou, K.H., Hadji, L., Houari, M.S.A., Tounsi, A., 2016. Bending and free vibration analysis of functionally graded plates using a simple shear deformation theory and the concept the neutral surface position. J. Brazilian Soc. Mech. Sci. Eng. 38, 265–275.

Benveniste, Y., 1987. A new approach to the application of Mori-Tanaka's theory in composite materials. Mech. Mater. 6, 147–157.

Bhattacharyya, M., Kapuria, S., Kumar, a. N., 2007. On the Stress to Strain Transfer Ratio and Elastic Deflection Behavior for Al/SiC Functionally Graded Material. Mech. Adv. Mater. Struct. 14, 295–302.

Bi, R., Fu, Y., Tian, Y., Jiang, C., 2014. Buckling and postbuckling analysis of elasto-plastic fiber metal laminates. Acta Mech. Solida Sin. 27, 73–84.

Birman, V., 1995. Stability of functionally graded hybrid composite plates. Compos. Eng. 5, 913–921.

Birman, V., Byrd, L.W., 2007. Modeling and Analysis of Functionally Graded Materials and Structures. Appl. Mech. Rev. 60, 195.

Bodaghi, M., Saidi, A.R., 2010. Levy-type solution for buckling analysis of thick functionally graded rectangular plates based on the higher-order shear deformation plate theory. Appl. Math. Model. 34, 3659–3673.

Bouazza, M., Tounsi, A., Adda-Bedia, E.A., Megueni, A., 2010. Thermoelastic stability analysis of functionally graded plates: An analytical approach. Comput. Mater. Sci. 49, 865–870.

Bouderba, B., Houari, M.S.A., Tounsi, A., 2013. Thermomechanical bending response of FGM thick plates resting on Winkler-Pasternak elastic foundations. Steel Compos. Struct. 14, 85–104.

Bouiadjra, R.B., Bedia, E.A., Tounsi, A., 2013. Nonlinear thermal buckling behavior of functionally graded plates using an efficient sinusoidal shear deformation theory. Struct. Eng. Mech. 48, 547–567.

Carpenter, R.D., Liang, W.W., Paulino, G.H., Gibeling, J.C., Munir, Z.A., 1999. Fracture testing and analysis of a layered functionally graded Ti/TiB beam in 3-point bending. Mater. Sci. Forum 308–311, 837–842.

Chen, C.-S., Lin, C.-Y., Chien, R.-D., 2011. Thermally induced buckling of functionally graded hybrid composite plates. Int. J. Mech. Sci. 53, 51–58.

Chen, X.L., Liew, K.M., 2004. Buckling of rectangular functionally graded material plates subjected to nonlinearly distributed in-plane edge loads. Smart Mater. Struct. 13, 1430–1437.

Chi, S.-H., Chung, Y.-L., 2006. Mechanical behavior of functionally graded material plates under transverse load—Part I: Analysis. Int. J. Solids Struct. 43, 3657–3674.

Cho, J.R., Ha, D.Y., 2001. Averaging and finite-element discretization approaches in the numerical analysis of funcionally graded materials. Mater. Sci. Eng. A 302, 187–196.

Cho, J.R., Oden, J.T., 2000. Functionally graded material: A parametric study on thermal-stress characteristics using the Crank-Nicolson-Galerkin scheme. Comput. Methods Appl. Mech. Eng. 188, 17–38.

Choi, I., Dao, M., Suresh, S., 2008. Mechanics of indentation of plastically graded materials—I: Analysis. J. Mech. Phys. Solids 56, 157–171.

Choules, B.D., Kokini, K., 1996. Architecture of functionally graded ceramic coatings against surface thermal fracture. J. Eng. Mater. Technol. 118, 522–528.

Cinefra, M., Carrera, E., Brischetto, S., Belouettar, S., 2010. Thermo-Mechanical Analysis Of Functionally Graded Shells. J. Therm. Stress. 33, 942–963.

Cinefra, M., Soave, M., 2011. Accurate Vibration Analysis of Multilayered Plates Made of Functionally Graded Materials. Mech. Adv. Mater. Struct. 18, 3–13.

Duc, N.D., Tung, H. V, 2010. Mechanical and thermal postbuckling of shear-deformable FGM plates with temperature-dependent properties. Mech. Compos. Mater. 46, 461–476.

Duc, N.D., Tung, H. Van, 2011. Mechanical and thermal postbuckling of higher order shear deformable functionally graded plates on elastic foundations. Compos. Struct. 93, 2874–2881.

Durban, D., Zuckerman, Z., 1999. Elastoplastic buckling of rectangular plates in biaxial compression/tension. Int. J. Mech. Sci. 41, 751–765.

El-Sawy, K.M., Nazmy, A.S., Martini, M.I., 2004. Elasto-plastic buckling of perforated plates under uniaxial compression. Thin-Walled Struct. 42, 1083–1101.

Eraslan, A.N., Akis, T., 2006. Plane strain analytical solutions for a functionally graded elastic-plastic pressurized tube. Int. J. Press. Vessel. Pip. 83, 635–644.

Erdogan, F., 1995. Fracture Mechanics of Functionally Graded Materials. MRS

Bull. 20, 43–44.

Estefen, S.F., Chujutalli, J.H., Soares, C.G., 2016. Influence of geometric imperfections on the ultimate strength of the double bottom of a Suezmax tanker. Eng. Struct. 127, 287–303.

Fazzolari, F.A., Carrera, E., 2014. Thermal Stability of FGM Sandwich Plates Under Various Through-the-Thickness Temperature Distributions. J. Therm. Stress. 37, 1449–1481.

Feldman, E., Aboudi, J., 1997. Buckling analysis of functionally graded plates subjected to uniaxial loading. Compos. Struct. 38, 29–36.

Finot, M., Suresh, S., Bull, C., Sampath, S., 1996. Curvature changes during thermal cycling of a compositionally graded Ni・Al2O3 multi-layered material. Mater. Sci. Eng. A 205, 59–71.

Fischmeister, H., Karlsson, B., 1977. Plastizitätseigenschaften grob-zweiphasiger Werkstoffe. Z. Met. 68.

Fu, Y., Shao, X., Chen, Y., 2014. Elasto-plastic buckling and post-buckling analysis of sandwich plates with functionally graded metal-metal face sheets and interfacial damage. Appl. Math. Mech. 35, 325–344.

Ganapathi, M., Prakash, T., 2006. Thermal buckling of simply supported functionally graded skew plates. Compos. Struct. 74, 247–250.

Ghavami, K., Khedmati, M.R., 2006. Numerical and experimental investigations on the compression behaviour of stiffened plates. J. Constr. STEEL Res.

Giannakopoulos, a. E., Suresh, S., Finot, M., Olsson, M., 1995. Elastoplastic analysis of thermal cycling: layered materials with compositional gradients. Acta Metall. Mater. 43, 1335–1354.

Gu, Y., Nakamura, T., Prchlik, L., Sampath, S., Wallace, J., 2003. Micro-indentation and inverse analysis to characterize elastic-plastic graded materials. Mater. Sci. Eng. A 345, 223–233.

Gunes, R., Aydin, M., Apalak, M.K., Reddy, J.N., 2011. The elasto-plastic impact analysis of functionally graded circular plates under low-velocities. Compos. Struct. 93, 860–869. https://doi.org/10.1016/j.compstruct.2010.07.008

Hamidi, A., Houari, M.S.A., Mahmoud, S.R., Tounsi, A., 2015. A sinusoidal plate theory with 5-unknowns and stretching effect for thermomechanical bending of functionally graded sandwich plates. Steel Compos. Struct. 18, 235–253.

Howard, S.J., Tsui, Y.C., Clyne, T.W., 1994. The effect of residual stresses on the debonding of coatings—I. A model for delamination at a bimaterial interface. Acta Metall. Mater. 42, 2823–2836.

Hu, H.T., Lin, B.H., 1995. Buckling optimization of symmetrically laminated plates with various geometries and end conditions. Compos. Sci. Technol. 55, 277–285.

Huang, H., Chen, B., Han, Q., 2014. Investigation on buckling behaviors of elastoplastic functionally graded cylindrical shells subjected to torsional loads. Compos. Struct. 118, 234–240.

Jalali, S.K., Naei, M.H., Poorsolhjouy, A., 2010. Thermal stability analysis of circular functionally graded sandwich plates of variable thickness using pseudo-spectral method. Mater. Des. 31, 4755–4763.

Javaheri, R., Eslami, M.R., 2002. Buckling of functionally graded plates under in-plane compressive loading. Math. und Mech. 82, 277–283.

Jha, D.K., Kant, T., Singh, R.K., 2013. A critical review of recent research on functionally graded plates. Compos. Struct. 96, 833–849.

Jin, Z.-H., 2002. an Asymptotic Solution of Temperature Field in a Strip a Functionally Graded Material. Int. Commun. Heat Mass Transf. 29, 887–895.

Jin, Z., Batra, R., 1996. Some basic fracture mechanics concepts in functionally graded materials. J. Mech. Phys. Solids 44, 1221–1235.

Jin, Z.H., Paulino, G.H., Dodds, R.H., 2003. Cohesive fracture modeling of elastic-plastic crack growth in functionally graded materials. Eng. Fract. Mech. 70, 1885–1912.

Kapuria, S., Bhattacharyya, M., Kumar, A.N., 2008. Bending and free vibration response of layered functionally graded beams: A theoretical model and its experimental validation. Compos. Struct. 82, 390–402.

Kesler, O., Finot, M., Suresh, S., Sampath, S., 1997. Determination of processing-induced stresses and properties of layered and graded coatings: Experimental method and results for plasma-sprayed Ni-Al2O3. Acta Mater. 45, 3123–3134.

Kiani, Y., Eslami, M.R., 2012. Thermal buckling and post-buckling response of imperfect temperature-dependent sandwich FGM plates resting on elastic foundation. Arch. Appl. Mech. 82, 891–905.

Lal, A., Neeranjan Singh, H., Shegokar, N.L., 2012. FEM model for stochastic mechanical and thermal postbuckling response of functionally graded material plates applied to panels with circular and square holes having material

randomness. Int. J. Mech. Sci. 62, 18–33.

Lanhe, W., 2004. Thermal buckling of a simply supported moderately thick rectangular FGM plate. Compos. Struct. 64, 211–218.

Lee, Y.D., Erdogan, F., 1994. Residual/thermal stresses in FGM and laminated thermal barrier coatings. Int. J. Fract. 69, 145–165.

Lee, Y.Y., Zhao, X., Reddy, J.N., 2010. Postbuckling analysis of functionally graded plates subject to compressive and thermal loads. Comput. Methods Appl. Mech. Eng. 199, 1645–1653.

Leissa, A.W., 1986. Conditions for laminated plates to remain flat under inplane loading. Compos. Struct. 6, 261–270.

Li, S.R., Zhang, J.H., Zhao, Y.G., 2007. Nonlinear thermomechanical post-buckling of circular FGM plate with geometric imperfection. Thin-Walled Struct. 45, 528–536.

Liew, K.M., Yang, J., Kitipornchai, S., 2004. Thermal Post-Buckling of Laminated Plates Comprising Functionally Graded Materials With Temperature-Dependent Properties. J. Appl. Mech. 71, 839. Liew, K.M., Yang, J., Kitipornchai, S., 2003. Postbuckling of piezoelectric FGM plates subject to thermo-electro-mechanical loading. Int. J. Solids Struct. 40, 3869–3892.

Ma, L.S., Wang, T.J., 2004. Relationships between axisymmetric bending and buckling solutions of FGM circular plates based on third-order plate theory and classical plate theory 41, 85–101.

Ma, L.S., Wang, T.J., 2003. Nonlinear bending and post-buckling of a functionally graded circular plate under mechanical and thermal loadings. Int. J. Solids Struct. 40, 3311–3330.

Mansouri, M.H., Shariyat, M., 2017. Differential quadrature thermal buckling analysis of general quadrilateral orthotropic auxetic FGM plates on elastic foundations. Thin-Walled Struct. 112, 194–207.

Matsunaga, H., 2009. Thermal buckling of functionally graded plates according to a 2D higher-order deformation theory. Compos. Struct. 90, 76–86.

Meiche, N., Tounsi, A., Ziane, N., Mechab, I., Abbes, E., Bedia, A., 2011. A new hyperbolic shear deformation theory for buckling and vibration of functionally graded sandwich plate. Int. J. Mech. Sci. 53, 237–247.

Mohammadi, M., Saidi, A.R., Jomehzadeh, E., 2010. Levy solution for buckling analysis of functionally graded rectangular plates. Appl. Compos. Mater. 17, 81–

93.

Mori, T., Tanaka, K., 1973. Average stress in matrix and average elastic energy of materials with misfitting inclusions. Acta Metall. 21, 571–574.

Morimoto, T., Tanigawa, Y., Kawamura, R., 2006. Thermal buckling of functionally graded rectangular plates subjected to partial heating. Int. J. Mech. Sci. 48, 926–937.

Na, K.-S., Kim, J.-H., 2006. Thermal postbuckling investigations of functionally graded plates using 3-D finite element method. Finite Elem. Anal. Des. 42, 749–756.

Na, K., Kim, J., 2004. Three-dimensional thermal buckling analysis of functionally graded materials. Compos. Part B Eng. 35, 429–437.

Naderi, A., Saidi, A.R., 2010. On pre-buckling configuration of functionally graded Mindlin rectangular plates. Mech. Res. Commun. 37, 535–538.

Najafizadeh, M.M., Heydari, H.R., 2004. Thermal buckling of functionally graded circular plates based on higher order shear deformation plate theory. Eur. J. Mech. A/Solids 23, 1085–1100.

Narayanan, R., Chow, F.Y., 1984. Ultimate capacity of uniaxially compressed perforated plates. Thin-Walled Struct. 2, 241–264.

Natarajan, S., Chakraborty, S., Ganapathi, M., Subramanian, M., 2014. European Journal of Mechanics A / Solids A parametric study on the buckling of functionally graded material plates with internal discontinuities using the partition of unity method. Eur. J. Mech. / A Solids 44, 136–147.

Nemat-alla, M., Ahmed, K.I.E., Hassab-allah, I., 2009. International Journal of Solids and Structures Elastic – plastic analysis of two-dimensional functionally graded materials under thermal loading. Int. J. Solids Struct. 46, 2774–2786.

Nemeth, M.P., 1996. Buckling and Postbuckling Behavior of Laminated Composite Plates With a Cutout.

Ozturk, A., Gulgec, M., 2011. Elastic-plastic stress analysis in a long functionally graded solid cylinder with fixed ends subjected to uniform heat generation. Int. J. Eng. Sci. 49, 1047–1061.

Paik, J.K., 2005. Ultimate strength of dented steel plates under edge shear loads. Thin-Walled Struct. 43, 1475–1492.

Paley, M., Aboudi, J., 1991. Plastic buckling of metal matrix laminated plates. Int. J. Solids Struct. 28, 1139–1154.

Park, J.S., Kim, J.H., 2006. Thermal postbuckling and vibration analyses of functionally graded plates. J. Sound Vib. 289, 77–93.

Prajapat, K., Ray-Chaudhuri, S., Kumar, A., 2015. Effect of in-plane boundary conditions on elastic buckling behavior of solid and perforated plates. Thin-Walled Struct. 90, 171–181.

Prakash, T., Singha, M.K., Ganapathi, M., 2009. Influence of neutral surface position on the nonlinear stability behavior of functionally graded plates. Comput. Mech. 43, 341–350.

Prakash, T., Singha, M.K., Ganapathi, M., 2008. Thermal postbuckling analysis of FGM skew plates. Eng. Struct. 30, 22–32.

Qatu, M.S., Leissa, A.W., 1993. Buckling or transverse deflections of unsymmetrically laminated plates subjected to in-plane loads. AIAA J. 31, 189–194.

Reddy, J.N., 2004. An Introduction to Nonlinear Finite Element Analysis. Oxford University Press.

Reddy, J.N., 1984. A Simple Higher-Order Theory for Laminated Composite Plates. J. Appl. Mech. 51, 745.

Reddy, J.N., Chin, C.D., 1998. Thermomechanical Analysis of Functionally Graded Cylinders and Plates. J. Therm. Stress. 21, 593–626.

Sabir, A.B., Chow, F.Y., 1986. Elastic buckling of plates containing eccentrically located circular holes. Thin-Walled Struct. 4, 135–149.

Samsam Shariat, B.A., Eslami, M.R., 2006. Thermal buckling of imperfect functionally graded plates. Int. J. Solids Struct. 43, 4082–4096.

Satyamurthy, K., Hasselman, D.P.H., Singh, J.P., Kamat, M.P., 1980. Effect of spatial variation of thermal conductivity on magnitude of tensile thermal stresses in brittle materials subjected to convective heating, in: Thermal Stresses in Severe Environments. Springer, pp. 325–342.

Shabana, Y.M., Bruck, H.A., Pines, M.L., Kruft, J.G., 2006. Modeling the evolution of stress due to differential shrinkage in powder-processed functionally graded metal–ceramic composites during pressureless sintering. Int. J. Solids Struct. 43, 7852–7868.

Shabana, Y.M., Noda, N., 2001. Thermo-elasto-plastic stresses in functionally graded materials subjected to thermal loading taking residual stresses of the fabrication process into consideration. Compos. Part B Eng. 32, 111–121.

Shakeri, M., Akhlaghi, M., Hoseini, S.M., 2006. Vibration and radial wave propagation velocity in functionally graded thick hollow cylinder. Compos. Struct. 76, 174–181.

Shakeri, M., Mirzaeifar, R., 2009. Static and Dynamic Analysis of Thick Functionally Graded Plates with Piezoelectric Layers Using Layerwise Finite Element Model. Mech. Adv. Mater. Struct. 16, 561–575.

Shanmugam, N.E., Thevendran, V., Tan, Y.H., 1999. Design formula for axially compressed perforated plates. Thin-Walled Struct. 34, 1–20.

Shao, Z.S., 2005. Mechanical and thermal stresses of a functionally graded circular hollow cylinder with finite length. Int. J. Press. Vessel. Pip. 82, 155–163.

Shariat, B.A.S., Javaheri, R., Eslami, M.R., 2005. Buckling of imperfect functionally graded plates under in-plane compressive loading. Thin-Walled Struct. 43, 1020–1036.

Shaterzadeh, A.R., Rezaei, R., Abolghasemi, S., 2015. Thermal Buckling Analysis of Perforated Functionally Graded Plates. J. Therm. Stress. 38, 1250–1268.

Shen, H.S., 2007. Thermal postbuckling behavior of shear deformable FGM plates with temperature-dependent properties. Int. J. Mech. Sci. 49, 466–478.

Shen, H.S., 2005. Postbuckling of FGM plates with piezoelectric actuators under thermo-electro-mechanical loadings. Int. J. Solids Struct. 42, 6101–6121.

Shen, H.S., Li, S.R., 2008. Postbuckling of sandwich plates with FGM face sheets and temperature-dependent properties. Compos. Part B Eng. 39, 332–344.

Shiota, I., Miyamoto, Y., 1997. Functionally graded materials 1996. Elsevier.

Simo, J.C., Taylor, R.L., 1986. A return mapping algorithm for plane stress elastoplasticity. Int. J. Numer. Methods Eng. 22, 649–670.

Singh, S.B., Kumar, A., 1999. Postbuckling response and strength of laminates under combined in-plane loads. Compos. Sci. Technol. 59, 727–736.

Soh, A.K., Bian, L.C., Chakrabarty, J., 2000. Elastic/plastic buckling of a composite flat plate subjected to uniform edge compression. Thin-Walled Struct. 38, 247–265.

Suresh, S., Mortensen, A., 1998. Fundamentals of functionally graded materials. The Institut of Materials.

Swaminathan, K., Naveenkumar, D.T., Zenkour, A.M., Carrera, E., 2015. Stress, vibration and buckling analyses of FGM plates-A state-of-the-art review. Compos. Struct. 120, 10–31.

Swaminathan, K., Sangeetha, D.M., 2017. Thermal analysis of FGM plates – A critical review of various modeling techniques and solution methods. Compos. Struct. 160, 43–60.

Tamura, I., Tomato, Y., Ozawa, H., 1973. Strength and ductility of Fe-Ni-C alloys composed of austenite and martensite with various strength. Proc. third Conf. strength Met. Alloy. vol. 1. Cambridge Inst. Met. 1, 611–616.

Thai, H.-T., Kim, S.-E., 2015. A review of theories for the modeling and analysis of functionally graded plates and shells. Compos. Struct. 128, 70–86.

Thai, H.T., Choi, D.H., 2012. An efficient and simple refined theory for buckling analysis of functionally graded plates. Appl. Math. Model. 36, 1008–1022.

Touloukian, Y.S., Center, T.P.R., 1967. Thermophysical properties of high temperature solid materials. Vol. 1. Elements.-Pt. 1. Macmillan.

Tran, L. V, Thai, C.H., Nguyen-xuan, H., 2013. An isogeometric fi nite element formulation for thermal buckling analysis of functionally graded plates. Finite Elem. Anal. Des. 73, 65–76.

Vel, S.S., Batra, R.C., 2002. Exact solution for thermoelastic deformations of functionally graded thick rectangular plates. AIAA J. 40, 1421–1433.

Wetherhold, R.C., Seelman, S., Wang, J., 1996. The use of functionally graded materials to eliminate or control thermal deformation. Compos. Sci. Technol. 56, 1099–1104.

Wilkins, M.L., 1963. Calculation of elastic-plastic flow. California Univ Livermore Radiation Lab.

Williamson, R.L., Rabin, B.H., Byerly, G.E., 1995. FEM study of the effects of interlayers and creep in reducing residual stresses and strains in ceramic-metal joints. Compos. Eng. 5, 851–863.

Williamson, R.L., Rabin, B.H., Drake, J.T., 1993. Finite element analysis of thermal residual stresses at graded ceramic-metal interfaces. Part I. Model description and geometrical effects. J. Appl. Phys. 74, 1310–1320.

Woo, J., Meguid, S.A., Stranart, J.C., Liew, K.M., 2005. Thermomechanical postbuckling analysis of moderately thick functionally graded plates and shallow shells. Int. J. Mech. Sci. 47, 1147–1171.

Wu, T.-L., Shukla, K.K., Huang, J.H., 2007. Post-buckling analysis of functionally graded rectangular plates. Compos. Struct. 81, 1–10.

Yaghoobi, H., Fereidoon, A., Khaksari Nouri, M., Mareishi, S., 2015. Thermal

Buckling Analysis of Piezoelectric Functionally Graded Plates with Temperature-Dependent Properties. Mech. Adv. Mater. Struct. 22, 864–875.

Yahia, S.A., Atmane, H.A., Houari, M.S.A., Tounsi, A., 2015. Wave propagation in functionally graded plates with porosities using various higher-order shear deformation plate theories. Struct. Eng. Mech. 53, 1143–1165.

Yamaki, N., 1961. Experiments on the Postbuckling Behavior of Square Plates Loaded in Edge Compression. J. Appl. Mech. 28, 238.

Yamaki, N., 1960. Postbuckling behavior of rectangular plates with small initial curvature loaded in edge compression—(continued). J. Appl. Mech. 27, 335–342.

Yang, J., Liew, K.M., Kitipornchai, S., 2006. Imperfection sensitivity of the post-buckling behavior of higher-order shear deformable functionally graded plates. Int. J. Solids Struct. 43, 5247–5266.

Yang, J., Shen, H.-S., 2003. Non-linear analysis of functionally graded plates under transverse and in-plane loads. Int. J. Non. Linear. Mech. 38, 467–482.

Yang, J., Shen, H.S., 2003. Nonlinear bending analysis of shear deformable functionally graded plates subjected to thermo-mechanical loads under various boundary conditions. Compos. Part B Eng. 34, 103–115.

Yin, S., Yu, T., Liu, P., 2013. Free vibration analyses of FGM thin plates by isogeometric analysis based on classical plate theory and physical neutral surface. Adv. Mech. Eng. 5, 634584.

Yu, T., Bui, T.Q., Yin, S., Doan, D.H., Wu, C.T., Do, V., Tanaka, S., Van Do, T., Tanaka, S., 2016. On the thermal buckling analysis of functionally graded plates with internal defects using extended isogeometric analysis. Compos. Struct. 136, 684–695.

Zenkour, A.M., 2005. A comprehensive analysis of functionally graded sandwich plates: Part 2—Buckling and free vibration. Int. J. Solids Struct. 42, 5243–5258.

Zenkour, a. M., Sobhy, M., 2010. Thermal buckling of various types of FGM sandwich plates. Compos. Struct. 93, 93–102.

Zhang, D.-G., 2013. Modeling and analysis of FGM rectangular plates based on physical neutral surface and high order shear deformation theory. Int. J. Mech. Sci. 68, 92–104.

Zhang, D.-G., Zhou, Y.-H., 2008. A theoretical analysis of FGM thin plates based on physical neutral surface. Comput. Mater. Sci. 44, 716–720.

Zhang, D.G., Zhou, H.M., 2015. Mechanical and thermal post-buckling analysis of

FGM rectangular plates with various supported boundaries resting on nonlinear elastic foundations. Thin-Walled Struct. 89, 142–151.

Zhang, L.W., Zhu, P., Liew, K.M., 2014. Thermal buckling of functionally graded plates using a local Kriging meshless method. Compos. Struct. 108, 472–492.

Zhang, Y., Huang, H., Han, Q., 2015. Buckling of elastoplastic functionally graded cylindrical shells under combined compression and pressure. Compos. Part B Eng. 69, 120–126.

Zhao, X., Lee, Y.Y., Liew, K.M., 2009. Mechanical and thermal buckling analysis of functionally graded plates. Compos. Struct. 90, 161–171

Appendix-I

LIST OF PUBLICATIONS

SCI

- Sharma, K., & Kumar, D. (2018). Nonlinear stability analysis of a perforated FGM plate under thermal load. *Mechanics of Advanced Materials and Structures*, *25*(2), 100-114. **(IF: 1.00).**
- Sharma, K., & Kumar, D. (2017). Elastoplastic analysis of FGM plate with a central cutout of various shapes under thermomechanical loading. *Journal of Thermal Stresses*, *40*(11), 1417-1441. **(IF: 1.21)**.
- Sharma, K., & Kumar, D. (2017). Elastoplastic Stability and Failure Analysis of FGM Plate with Temperature Dependent Material Properties under Thermomechanical Loading. *Latin American Journal of Solids and Structures*, *14*(7), 1361-1386. **(IF: 1.11)**.
- Sharma, K., & Kumar, D. (2016),"Stability and Failure Analysis of Perforated FGM Plate", *Indian Journal of Pure & Applied Physics* (IJPAP) 54, 665–675 **(IF: 0.77)**.

Non-SCI

- Sharma, K., Kumar, D., & Gite, A. (2016). Thermo-mechanical buckling analysis of FGM plate using generalized plate theory. AIP, 1728(1).
- Sharma K., & Kumar, D. (2016), "Thermo-Mechanical Analysis of FGM Plate," Adv. Sci. letters, 22 (11), 3813-3816.
- Sharma K., & Kumar, D. (2018), "Non-linear Thermal Stability of FGM Plate with Temperature-dependent Material Properties," J. Adv. Mech. Eng.

Appendix-II

BIOGRAPHICAL PROFILE OF RESEARCHERS

Dr. Dinesh Kumar (Supervisor)

Presently, **Dr. Dinesh Kumar** is working as an Assistant Professor in the Mechanical Engineering Department of Malaviya National Institute of Technology (MNIT) Jaipur. Before joining MNIT Jaipur in 2012, Dr Kumar worked for 7 years in BITS Pilani. He earned his ME in 2004 and Ph.D. in 2011 both from BITS Pilani. His teaching interests are in the areas of Mechanical Design, Solids Mechanics and Finite Element Methods. His present research group works on simulation tools based on FEM and Molecular Dynamics (MD), such ANSYS, ABAQUS, LAMMPS, Material Studio to carry out research in the areas of Mechanics of Composite, FGM, and Nanocomposites. Dr Kumar has successfully completed few research projects sponsored by CSIR and Birla Academy, and presently, work on one of the ISRO research projects entitled "Nanostructures (CNTs) Reinforced Nanocomposite Based Heat Shield System for Spacecraft Applications". He has published many research papers in national and international journals and conferences of high repute. He has guided many M.Tech. Dissertations and B.Tech Thesis, and presently, he is guiding five PhD students. He has also organized a International Conference, under the umbrella of Indian Society of Theoretical and Applied Mechanics, in 2015 (ISTAM-2015), a GIAN course on nonlinear FEM in 2016, and in addition, many other short term training programmes (STTPs) in the areas of CAD/CAE. He is also Vice-President of Indian Society of Theoretical and Applied Mechanics. Besides his professional works of teaching and research, he has interest in YOGA and reading books on “DARSHAN SHASTRA” i.e., Philosophy.

Kanishk Sharma (PhD student)

Kanishk was born in Delhi, India. He graduated from Govt. Engineering College, Bikaner and received a Bachelor of Engineering degree in Mechanical Engineering from Rajasthan University in 2007. He completed his Master of Technology in Machine Design from University College of Engineering, Kota. Before enrolling in the doctoral program in the Department of Mechanical Engineering, MNIT Jaipur in 2013, he was in USB College of Engg. & Mgt., Abu Road as Assistant Professor. The author's current research interest lies in the field of Computational Mechanics, Finite Element Methods, Mechanics of Solids and Composites, Functionally Graded Materials, Failure Analysis of Materials and Structures. He has published number of articles in international journals and conferences.